Abstract The tight coupling between the macroscopic evolution of Tokamak plasmas and the induced currents in the surrounding Vacuum Vessel (VV) and Plasma Facing Components (PFCs) has been known for decades. In the present Thesis we critically review some aspects of the electromagnetic interaction. In conditions of significant plasma-wall contact the gas mixture is generally only *partially* ionized. We try to model this situation in a consistent thermodynamic framework, allowing for ionization and the recombination phenomena, in Chapter 1. This represents the occasion to review the whole MHD theory in the wider framework of Non-equilibrium Thermodynamics, also discussing the implications of the *Curie* principle on the closure relations generally adopted. A self-consistent coupling of 3D non-linear MHD models with fully volumetric 3D structures models is still missing in the literature. We explore some possibilities in Chapter 2, hinting also the first preliminary results in the JOREK-CARIDDI coupling. Several possible formulations are discussed, together with the possible implications of halo currents in the modelling. In Chapter 3 we discuss the mass-less hypothesis and the fundamental aspects of MHD evolutionary equilibrium models. Here we also review the key aspects of the numerical model *CarMa0NL*. In the last Chapter we apply the *evolutionary equilibrium tools* previously discussed to practical problems. We first successfully cross-check analytical and numerical computation of forces during off-normal events called disruptions, providing some hints on the magnetic tensions, besides on the magnetic pressures. Further, we propose a procedure for the estimation of plasma losses during disruptions via evolutionary equilibrium models, which we apply to a simple test case. We find also in this case the fundamental role of the electromagnetic time constant, which regulates the plasma dissipated heat during the current quench phase. Further we validate *CarMa0NL* by direct comparison with JET and TCV experiments, comparing simulated and real magnetic diagnostics measurements. For JET, we find that the halo width is a crucial element for a realistic simulation. In the TCV studies we show that the disruption trajectory is dependent on the pre-disruption plasma shape.

Nicola Isernia

Electromagnetic interaction of MHD plasmas with structures. 2021 - XXXIV

Università degli Studi di Napoli Federico II

Ph.D itee information technology electrical engineering

The electromagnetic interaction of Magneto-Hydro-Dynamic plasmas with conducting structures

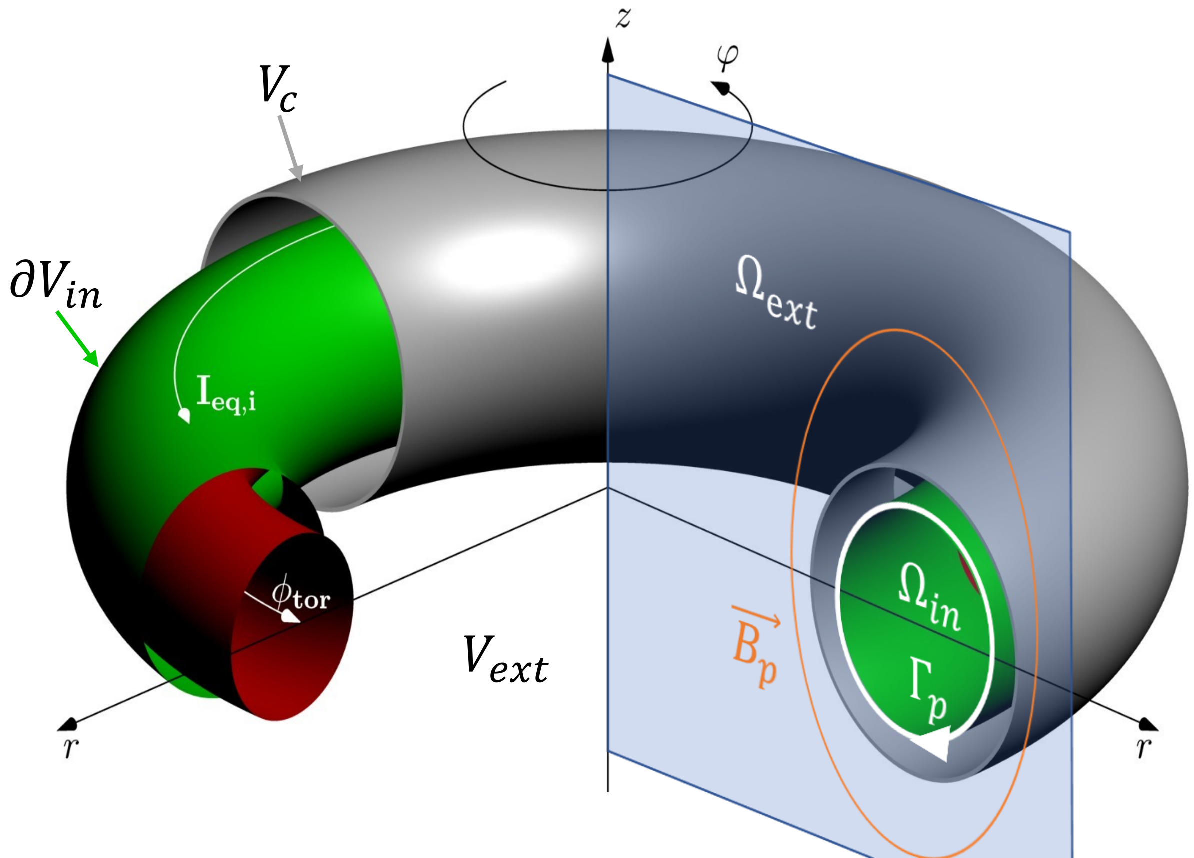

Nicola Isernia

Ph.D. in Information Technology and Electrical Engineering

UNIVERSITÀ DEGLI STUDI DI NAPOLI FEDERICO II

PH.D. THESIS
IN
INFORMATION TECHNOLOGY AND ELECTRICAL ENGINEERING

THE ELECTROMAGNETIC INTERACTION OF MAGNETO-HYDRO-DYNAMIC PLASMAS WITH CONDUCTING STRUCTURES

NICOLA ISERNIA

TUTOR: PROF. FABIO VILLONE

COORDINATOR: PROF. DANIELE RICCIO

XXXIV CICLO

SCUOLA POLITECNICA E DELLE SCIENZE DI BASE
DIPARTIMENTO DI INGEGNERIA ELETTRICA E TECNOLOGIE DELL'INFORMAZIONE

“ Ciò di cui si nutre un organismo è l’entropia negativa.
Meno paraddossalmente si può dire che l’essenziale nel metabolismo
è che l’organismo riesca a liberarsi di tutta l’entropia
che non può non produrre nel corso della vita.”

E. Schrödinger, Che cos’é la vita?

In ricordo della Professoressa Eufemia Spinosa

Acknowledgments

During these three years, I met many people which contributed to my scientific formation and excitement towards research. First, I want to thank my supervisor, Prof. F. Villone, which largely stimulated the debate about the main achievements of this work, and which has been always prone to tackle and further stimulate the discussion about my questions. Next, I want to acknowledge those persons which would immediately recognise their influence reading this manuscript: Prof. C. Serpico, Prof. V.D. Pustovitov and Ph.D. V. Yanovskiy. Moreover, I want to thank Ph.D. J. Artola and M.Sc. N. Schwarz for the intense scientific discussions we had during my stay in Garching, which provided me with further motivation towards our common research.

I want to express my sincere gratitude to the Electrical Engineering research unit and the CREATE research group here at the University of Napoli Federico II. I am in debt with them for stimulating discussions and studies on fundamental topics well beyond my research area. In particular, some students and young researchers at the Department became friends throughout these years, and I want to thank explicitly A. Castaldo, A. Cervone, A. di Pasquale, A. Iaiunese, A. Mele, A. Quercia, C. Sirico, E. Fedele, M. Pascale, P. Franzese, P. Zumbolo, R. Tricarico, S. Dubbioso, S. Perna, and V. Scalera.

Finally, beyond my daily research environment, I want to thank for their unceasing support my family, my friends, and my girlfriend Alessandra. Without their deep affection and empathy this work would not have been possible.

Nicola Isernia

Abstract

The tight coupling between the macroscopic evolution of tokamak plasmas and the induced currents in the surrounding Vacuum Vessel (VV) and Plasma Facing Components (PFCs) has been known for decades. In the present Thesis we critically review some aspects of the electromagnetic interaction. In conditions of significant plasma-wall contact the gas mixture is generally only partially ionized. We try to model this situation in a consistent thermodynamic framework, allowing for ionization and recombination phenomena, in Chapter 1. This represents the occasion to review the whole MHD theory in the wider framework of Non-equilibrium Thermodynamics, also discussing the implications of the Curie principle on the closure relations generally adopted. A self-consistent coupling of 3D non-linear MHD models with fully volumetric 3D structures models is still missing in the literature. We explore some possibilities in Chapter 2, hinting also the first preliminary results in the JOREK-CARIDDI coupling. Several possible formulations are discussed, together with the possible implications of halo currents in the modelling. In Chapter 3 we discuss the mass-less hypothesis and the fundamental aspects of MHD evolutionary equilibrium models. Here we also review the key aspects of the numerical model CarMa0NL. In the last Chapter we apply the evolutionary equilibrium tools previously discussed to practical problems. We first successfully cross-check analytical and numerical computation of forces during off-normal events called disruptions, providing some hints on the magnetic tensions, besides on the magnetic pressures. Further, we propose a procedure for the estimation of plasma losses during disruptions via evolutionary equilibrium models, which we apply to a simple test case. We find also in this case the fundamental role of the electromagnetic time constant, which regulates the plasma dissipated heat during the current quench phase. Further we validate CarMa0NL by direct comparison with JET and TCV experiments, comparing simulated and real magnetic diagnostics measurements. For JET, we find that the halo width is a crucial element for a realistic simulation. In the TCV studies we show that the disruption trajectory is dependent on the pre-disruption plasma shape.

Contents

List of Figures

Introduction

Sustainable energy production is one of the key aspects to limit global warming well below $2°C$, and possibly below $1.5°C$, objective set up by the *United Nations Framework Convention on Climate Change* (UNFCC), as a result of the 21^{st} *Conference Of Parties* (COP21), held in Paris in December 2015. The agreement became effective and binding as soon as 55 countries, responsible for more than the 55% of greenhouse gases emission ratified the agreement in 2016. The Paris agreement requires especially the committed countries to monitor and reduce their greenhouse gas emissions.

Since then, there has been debate on the effectiveness of this international contract, and several others Conference Of Parties took place. In particular, there was great expectation for the last one, the COP26, held in Glasgow in November 2021. The objectives of COP26 were quite ambitious in the beginning, among these it is worth quoting the *phase-out* of coal-fired power plants for several countries by 2040, the reduction of greenhouse gases emissions of 45% by 2030 respect to the levels of 2010, and the creation of an economic fund for most vulnerable countries already experiencing dramatic effects of the climate change. Here, it is worth mentioning that coal power plants are among the most polluting in general, even compared to other fossil fuels plants, essentially due to the lower efficiency of the plants themselves[1]. Unfortunately the initial *phase-out* objective was smoothed into a *phase-down* during the final stages of the Conference.

For what concerns my research activity, it is remarkable that for the first time a COP reserved a relatively consistent time slot to discuss about Fusion Energy. The urgency of climate actions makes fusion-fired power plants not a viable option to limit the global warming below $2°C$ on time, since the first commercial prototype will likely not be connected to grid before 2050 accord-

[1]The average efficiency of a methane-fired plant can reach the 60%, as compared to the 40% of a coal-fired plant.

Table 1: Heating energy per unit mass of reactants in fusion nuclear reactions involving Deuterium (D) and Tritium (T), compared to methane combustion.

$D-D$	$D-T$	CH_4
$78\,TJ/kg$	$338\,TJ/kg$	$40\,MJ/kg$

ing to the roadmap of the *European Fusion Development Agreement* (EFDA) [1]. Nonetheless, fusion power plants will likely have a significant impact on the energy market in the long-term [2].

Then, what is fusion energy? Why is it considered as a possible player in the future energy market? Fusion is essentially the process which feeds most of stars' energy, transforming light hydrogen isotopes into helium. In nature we find three different isotopes of hydrogen, which differ in the number of neutrons in the nucleus. Namely the Protium (H-1) has only one proton in the nucleus, the Deuterium (H-2 or D) has one proton and one neutron, while Tritium (H-3 or T) has one proton and two neutrons. As a result of *nuclear reactions*, the mass of the products is slightly less than the original mass of the reacting hydrogen isotopes, contrary to any standard *chemical reaction*. For the human-scale, the small amount of lost mass is converted into a huge amount of energy. This is of the same type of solar energy which makes life possible on earth. We compare the heating power of fusion reactions which are envisioned on earth to the heating power due to the combustion of methane in Table 1.

The 6 orders of magnitude between fusion reactions and standard fossil fuels combustion make the idea of a fusion-fired power plant at least attractive. The enormous energy release generated during a fusion reaction is related to a mass loss: in the transformation of the original hydrogen isotopes into helium and neutrons a small quantity of mass is converted into a huge quantitative of energy. This mechanism is totally different from any standard chemical reaction, which only involve the outer electrons of the atoms, and where the mass is always conserved. The incomparable specific energy of a nuclear reaction is moreover complemented by the huge reservoirs of deuterium available on earth. The deuterium is indeed available directly in ocean water, with approximately 1 atom for every 6700 atoms of hydrogen, by easy procedures of extraction. Deuterium in ocean water alone could be considered sufficient to power the earth for at least 2 billion years at the present rate of world energy consumption [2].

However, the triggering of a fusion reaction is not exactly a simple task. In order to trigger a reaction involving atoms' nuclei it is necessary to make the atoms collide with sufficient energy to win all the repulsive forces of Coulomb and atomic-scale nature. This energy is made available to the colliding atoms in the sun core by extremely high temperatures, in the order of 15 MK. Moreover the gas there is confined together by the gravitational force itself of such a massive star. Compared to the sun core, we have two quite important and correlated problems: reach temperatures higher then the sun core[2], take the hydrogen gas confined in some region of space.

As a first step towards the realization of competitive fusion energy power plants, Deuterium-Tritium reactions will be employed, since they require less energy to trigger the nuclear reaction. It is worth mentioning that Tritium is radioactive, with a very short half-life of about 12 years. Consequently, there are no natural reservoirs of Tritium on earth, and today the Tritium used in experimental devices is essentially available as a by-product of fission reactors. Anyway, it is envisaged for next generation fusion reactors to produce tritium directly via the breeding of lithium and of neutrons obtained from the nuclear reactions. Indeed, the isotope of lithium Li^6 will be injected in a blanket structure surrounding the reactor core. Neutrons, a natural by-product of fusion reactions, will impact the atoms of Li^6, triggering the reactions resulting into Tritium. The Li^6 available on earth would be sufficient for 20 thousands years of fusion-energy production [2], and hopefully technology will be able to initiate Deuterium-Deuterium reactions far earlier. The large and relatively economic reservoirs of deuterium and lithium on earth represent another key element which potentially makes fusion energy a convenient opportunity.

Let's move then to another key question: is fusion energy sustainable? The main by-products of fusion reactions are helium and high-energy neutrons. Namely the energy released in a fusion reaction is kinetic energy of these two by-products. Helium is an inert gas, hence totally harmless. On the other hand, the high energy neutrons impact the structures surrounding the gas, and are responsible for their activation. Anyway the half-life of such activated materials is estimated to be ~ 100 years, at least one order of magnitude less than by-products and activated materials of fission reactors. Significant endeavours on research for low-activation materials are taking place at the *International Fusion Materials Irradiation Facility*, in Japan.

A last advantage of a fusion power plant is its intrinsic safety, besides the technical precautions. The fusion reaction mechanisms require to continuously feed the reactor core with Deuterium and Tritium. Anyway, the tanks of these

[2]about 1 order of magnitude more, $\sim 150\ MK$

isotopes need to be completely isolated from the reactor core: only few grams of Deuterium and Tritium are inside the reaction chamber during normal operation. Therefore, there is no risk of avalanche reactions leading to catastrophic events.

Despite the large Deuterium availability, the zero net CO_2 emissions, and the intrinsic safety, a fusion reactor is nonetheless a complex and costly facility. Lots of scientific and technological challenges have to be tackled for the commissioning of a fusion power plant competitive with other energy sources. We mentioned already that to trigger fusion reactions on earth we need the hydrogen gas to reach temperatures even higher than in the sun core. How could we do that?

First one may look for an answer in the stars' processes. Due to the local conditions of density and temperature, hydrogen isotopes in stars' core present themselves in a peculiar gaseous state. The high temperatures are responsible for a substantial dissociation of the electrons from their nuclei, resulting in a cloud of positive ions and electrons. A gas of completely ionised particles is generally regarded as a state of matter on its own, and defined as a *plasma*. This term was probably firstly used by Irwing Langmuir to designate in particular a ionised gas where the local concentration of positive and negative particles was the same [3, 4]. The possibility of fusion reactions on the sun is provided by its large mass: the gravitational force brings the hydrogen atoms together, counter-balancing the pressure gradient force which tends to make the gas expand in the surrounding universe. Anyway we do not have any possibility of confining the gas with a mass comparable to that of the sun clearly. We have then to look somewhere else, and there are essentially two different strategies to confine the plasma on earth.

A first methodology is defined as *Inertial Confinement Fusion*. Here the idea is to get the particles close together by their own mechanical inertia. Then, a few mg solid Deuterium-Tritium pellet is heated via an external driver beam, *e.g.* a laser. The outer layer will ablate generating a force on the inner layers of the pellet due to the action-reaction principles, essentially as a rocket. The atoms travel towards the centre of the pellet at very high speed, gaining substantial mechanical inertia and leading to a compression of the pellet to densities far beyond that of any solid. Contextually a shock wave arriving at the centre of the pellet increases the temperature to the values necessary to trigger fusion reactions. [5]

The second methodology uses hydrogen isotopes in their plasma state. As soon as such a high temperature gas touches some solid structure, it will clearly melt the interface and contextually rapidly lose almost all of its thermal energy, preventing the possibility of nuclear reactions. Any gas naturally tends to occupy all the available space at its disposal, hence hitting the walls of any box where we store it. We have a huge problem then: we need the gas to stay confined in some physical space, without touching any solid surface. Anyway a ionised gas has some different properties from a standard neutral gas: it is electrically conductive. The idea is then to have a current distribution within the gas, supply an external magnetic field and counter-react the pressure gradient force which would make the gas expand via the Lorentz force $\mathbf{i} \times \mathbf{B}$. This is the main principle of *Magnetic Confinement Fusion*.

The present thesis is concerned with Magnetic Confinement Fusion devices, with a particular attention for those defined as *Tokamaks*, a Russian acronym to indicate “toroidal camera with magnetic coils”. Indeed this magnetic confinement concept for plasmas was first conjectured by the Soviet physicists Igor Tamm and Andrei Sakharov, during the 1950s. At those times the fusion research programmes of technologically advanced countries were still kept secret, until the 2^{nd} United Nations Conference on the Peaceful Uses of Atomic Energy, in 1958. Since then, fusion research has made great steps forward.

Many of the critical key questions in the roadmap to realization of fusion will be addressed in the internationally funded Tokamak facility ITER (International Thermonuclear Experimental Reactor). ITER has two main objectives dealing with physics. The first is to reach a stable pulsed operation with high energy gain ($Q = P_{out}/P_{in} = 10$). In a second test phase the reactor will be operated in steady state with reduced power gain ($Q \simeq 5$). Thanks to the knowledge on plasma physics and technology issues addressed through ITER, the next step in the realization of fusion energy will be the first commercial prototype, called DEMO. The engineering design of DEMO should be ready not later than 2030, according to the roadmap presented by the *EFDA* board [1]. The final aim is a successful connection of the power plant to the grid by the year 2050.

The Tokamak is of course a toroidal device: the plasma is bent in a doughnut, so that a current can be induced within the gas, even without the need for the contact of the gas with solid electrodes. The necessarily high temperatures require large plasma currents, in the order of MA, and large externally applied magnetic fields, in the order of T, so to contemporaneously heat the plasma by Joule effect and counter-react the pressure gradient. In its original version the current was solely induced like in a simple transformer, today a wider range of non-inductive mechanisms is considered, as Neutral Beam Injection and Radio-Frequency current drive [6]. Moreover a large fraction of the current is now self-induced via the achievement of large density gradients between the core and the external layers of the plasma column, via an effect known as *bootstrap current* [7].

The toroidal chamber encapsulating the plasma, the active coils necessary to generate the external magnetic field, and several additional plasma facing components necessary for the correct operation of the device are generally electrically conducting. As easily imagined, any variation in the plasma column position, or any variation of the large plasma current induces eddy currents in the surrounding conducting structures. At the same time currents circulating in the conducting structures alter the magnetic fields applied to the plasma, those responsible for the original mechanical equilibrium and stability of the plasma column. A tight electromagnetic interconnection relates the evolution of the plasma column and the evolution of the currents in the surrounding conductors. This is precisely the topic of this Thesis, and we will enter in the details of the mutual effect between tokamak plasma and external currents evolution.

The outline of the thesis is the following:

Chapter 1 presents the *Magneto-Hydro-Dynamics* (MHD) theory, generally adopted to describe astrophysical and laboratory plasmas, in a macroscopic perspective. In particular, tools of Non-Equilibrium Thermodynamics are used to show how a thermodynamically consistent three-species fluid plasma model can be set up. The possibility of ionization and recombination is accounted, giving back *Saha Equation* in the limit of Thermodynamic Equilibrium between particle concentrations. From here, the standard single fluid model is easily introduced, giving the opportunity to discuss the conceptual connections between *Ohm's law* and the hypothesis of *local neutrality*. The Thermodynamics framework allows a discussion of the spatial symmetry constraints on the actual constitutive phenomenological relations assumed for the closure of the MHD model, in presence of a magnetic field. Both the Curie symmetry principle and Onsager reciprocal relations are applied to the case of interest: the resulting coordinate-independent constitutive equations highlight the coefficients which the theory should be concerned about and are suitable to implementation. Finally the fundamental physical interaction of a fusion plasma facing a solid wall is described, introducing the Bohm criterion and the ion saturation current concepts.

In **Chapter 2** we first introduce some of the state of the art extended-MHD numerical models, focusing the attention on the electromagnetic boundary conditions required for their solution. Next we present a convenient *Magneto-Quasi-Static* numerical model for describing currents in the structures surrounding the plasma, highlighting the role of induced voltages due to plasma variations. These preliminary Sections constitute the basis to discuss how to self-consistently compute the plasma and external currents evolution. The remainder of the Chapter presents indeed several possible schemes to compute the MHD boundary condition and the plasma-induced voltages on structures, solely in terms of the external currents and the magnetic vector potential or magnetic field at the boundary. The modelling implications of shared currents flowing from plasma to structures and vice-versa are also discussed in the final Section.

Chapter 3 addresses the Theory of MHD evolutionary equilibrium. First we comment on the key role of the electromagnetic inertia in the plasma column mechanical evolution, clarifying when an evolutionary equilibrium model is effective in the description of a tokamak plasma. Subsequently, we set up the theory for a circular high-aspect-ratio tokamak, which provides insight in several aspects of the electromagnetic problem. We conclude the discussion presenting the free-boundary evolutionary equilibrium model *CarMa0NL*.

Chapter 4 applies the tools of evolutionary equilibrium theory introduced in previous Chapter to the study of hard-to-predict fast plasma transients, which generally lead to the termination of the experiment, also known as *disruptions*. We first analyse the electromagnetic forces generated on the wall surrounding the plasma during a fast plasma transient. The key role of the net poloidal current and of the pre-disruption plasma position will emerge clearly from the discussion. Following, we show how evolutionary equilibrium models, with relatively little physical details, can be used to get simple estimates of global plasma losses during *disruptions*. The other way around, the methodology presented allows to check the energetic consistency of simulation results. The discussion reveals the key role of the total current decay time as compared to the electromagnetic time constant of the surrounding wall for the overall energy dissipation. The last Sections are finally dedicated to the validation of the modelling tools, via the comparison of simulation results and real experiments at the TCV and JET Tokamaks. The qualitative, and quantitative, agreement reveals the efficacy of the proposed methods for studying real experiments.

Chapter 1

A continuum theory of fluid conductors

Magneto-Hydro-Dynamics (MHD) is the branch of physics which studies the behaviour of conducting fluids in a continuum perspective, and is an essential tool in the study of astrophysical and laboratory plasmas. Its birth is historically associated to the discovery of the *electromagnetic-hydrodynamic waves* by Hannes Alfvén in 1942 [8]. In this respect Magneto-Hydro-Dynamics may be regarded as an extension of Hydro-Dynamics, which accounts also for the interaction of the continuum medium with the electromagnetic field. It is quite common to introduce MHD simply as a fluid dynamic extension [9, 10, 11].

A further common viewpoint is to regard the *Magneto-Hydro-Dynamic* models as a mere approximation of more accurate and sophisticate kinetic models. This is due to the early work on the kinetic theory of gases of S. Chapman and T. Cowling [12] and Harold Grad [13, 14]. Especially Grad, with its *thirteen moments approximation* method [13], influenced definitively the way MHD theory was regarded and is now regarded [15, 16, 17, 18, 19, 20]. His method allows to clearly define fluid dynamics variables such as mass density, barycentric velocity, stress tensor and heat flux starting from microscopic quantities describing a single particle within the gas. On the same grounds, he provided a set of conservation Equations for the fluid variables by proper averages of the Boltzmann Equation, creating a sound link between the kinetic theory of gases and the theory of fluid dynamics. Within this framework, was even possible to estimate the transport coefficients, postulating on physical grounds the microscopic interactions between particles [16], committing definitely the problem of the closure of the MHD model to the averaging of kinetic theory models.

Anyway, this perspective on the subject suffers some weaknesses. First, the possibility for chemical reactions should be really accounted by the means of microscopic inelastic collisions within the kinetic model, a circumstance which is generally neglected, even if it may be taken into account [21, 22]. Moreover, it requires generally to make hypothesis on collisions at a microscopic level in order to evaluate the transport coefficients. Since the molecular interactions in a tokamak plasma are only approximately known, besides being very sensitive to the experimental conditions, the resulting transport coefficients are generally subject to a high degree of uncertainty. Respect to the first problem, we provide in this Chapter some method to include chemical reactions in the hydrodynamic model by the means of *Non-Equilibrium Thermodynamics* theory [23, 24]. This method will provide to be consistent in the limit of chemical equilibrium, returning the *Saha Equation*. The second problem cannot be solved instead by Non-Equilibrium Thermodynamic tools. Nonetheless this framework provides clear indications on the constraints which the transport coefficients shall satisfy in presence of a magnetic field. Chemically reacting fluid mixtures were already studied in the context of local thermodynamic equilibrium in Ref. [25]. Compared to that study, we discuss the role of the magnetic field in the theory, provide details on the electric current and its relation to electromagnetic and electrochemical potentials, besides making explicit the local equilibrium equations of state, thanks to the *ideal gas* hypothesis. Moreover, the mathematical rigour offered by Thermodynamics will allow also some critical comments on the actual form which we shall postulate for *Ohm's law*. This choice will be related to the standard hypothesis of local neutrality [11, 19], circumstance which has not been sufficiently stressed in the literature probably.

The role of the magnetic field will be discussed in detail in Section 1.7, using the tools of *invariant tensor functions* theory [26]. Hence we will extend the Curie spatial symmetry consideration to the case in which a magnetic field is present, being responsible for the space anisotropy. This will provide insight in the admissible couplings between *thermodynamic fluxes* and *forces*: even [odd] order *fluxes* may be related only with even [odd] order *forces*. We will find that the structure of the conduction tensor postulated by Braginskii [16] is a mere consequence of the symmetry constraints imposed by the presence of the magnetic field. This will give us the occasion to present the constitutive Equations in the coordinate-independent form also found in Ref. [27] for the electrical conduction, stating clearly the parity of the coefficients respect to the magnetic field. These coefficients are the ones diffusion theories should be primarily investigate. Moreover, the coordinate independent is suitable for the implementation of the anisotropic relations, without requiring ad hoc reference systems.

The Chapter is organized as follows. In the first two Sections we quickly review the key ingredients of the kinetic theory of gases, culminating in the *Boltzmann Equation*. This will be just a literature review, to actually show where is exactly the conjunction point between microscopic and macroscopic theories. We refer to standard textbooks [18, 19] for details on this link while we proceed introducing the plasma MHD model directly in a macroscopic perspective, framing the model in the context of Non-equilibrium Thermodynamics in Section 1.3.1. Straight afterwards, in Section 1.4, we discuss the equations of state locally valid in our constrained thermodynamic equilibrium conditions, also examining the limit of chemical equilibrium. In Section 1.5 we postulate the conservation equations for the mass density, the concentrations of the different fluids, the overall linear momentum and the internal energy of the plasma. At this stage, the kinetic energy of diffusion is discarded, together with the inertia of any diffusion process. This means that we will not account separately for the mechanical inertia of ions and neutrals. In principle this is an unnecessary assumption, anyway it serves to keep the discussion plain, focusing on other key aspects. On the other hand no assumption is made on the local neutrality of the plasma in the beginning. In Section 1.6 we discuss the entropy balance Equation, paying some attention to the heat flux definition and the electro-chemical potentials. Following we discuss the constitutive Equations between the thermodynamic fluxes and forces, thoroughly analysing the constraints imposed by the presence of the magnetic field in Section 1.7. We critically discuss *Ohm's law* and its relation to the quasi-neutrality assumption in Section 1.8. The standard single fluid model is finally collected together in Section 1.9. In the last Section we discuss some aspects of the plasma-wall interaction, introducing the Bohm criterion for the ion velocity and the ion saturation current.

1.1 From micro to macro, Liouville Theorem

The problem of determining the evolution of a fusion plasma could be regarded as conceptually simple. There are N material point particles, namely ions, electrons or even neutrals. Each particle has its own mass, and its internal structure is ignored. We denote the generalized coordinates of the particles by q^i and the generalized momenta by p_i, for $i = 1, \cdots, N$, where N is the total number of particles. All the particles are subject to classical Hamilton equations of motion:

$$\begin{aligned} \frac{\mathrm{d}}{\mathrm{d}t} q^i &= -\frac{\partial}{\partial p^i} \mathcal{H} \\ \frac{\mathrm{d}}{\mathrm{d}t} p^i &= +\frac{\partial}{\partial q^i} \mathcal{H} \end{aligned} \tag{1.1}$$

The Hamilton function $\mathcal{H}\left(q^i, p_i, t\right)$ can be identified with the total mechanical energy of the system. If we know the initial positions and momenta of the particles, we could in principle solve Hamilton Equations (1.1) and predict the evolution of the mechanical system. Besides not having precise information on the initial mechanical state, it would be impossible to solve such a coupled system of ordinary differential equations, considering that classical particle concentrations in a fusion plasma are about $10^{20} m^{-3}$. A great step-forward was first provided by Gibbs theory of ensembles [13], which replaces the discrete description of the point-particles with the definition of a distribution function $F(q^i, p_i, t)$ in the *phase space*, *i.e.* that space whose coordinates are given by (q^i, p_i). As a probability density, $F(q^i, p_i, t)\mathrm{d}q^i\mathrm{d}p_i$ provides the probability the mechanical system belong to the volume element $\mathrm{d}q^i\mathrm{d}p_i$ centred in (q^i, p_i), at the time instant t. Starting from (1.1), Liouville theorem provides the evolution equation for $F(q^i, p_i, t)$. The *velocity field* $\underline{V}$ in our 6N-dimensional phase space is clearly given by Hamilton Equations (1.1). Let's make this explicit

$$\underline{V} = \frac{\mathrm{d}}{\mathrm{d}t} \begin{bmatrix} q^1 \\ \vdots \\ q^N \\ p^1 \\ \vdots \\ p^N \end{bmatrix} = \begin{bmatrix} -\partial\mathcal{H}/\partial p_1 \\ \vdots \\ -\partial\mathcal{H}/\partial p_N \\ \partial\mathcal{H}/\partial q^1 \\ \vdots \\ \partial\mathcal{H}/\partial q^N \end{bmatrix}, \tag{1.2}$$

Hence, it is immediate to verify that $\underline{V}$ is divergence-free in the phase space, since $\partial^2\mathcal{H}/\partial q^i \partial p_i = \partial^2\mathcal{H}/\partial p_i \partial q^i \; \forall i = 1, \cdots, N$,

$$\nabla \cdot \underline{V} = \frac{\partial}{\partial q^1}\dot{q}^1 + \cdots + \frac{\partial}{\partial q^1}\dot{q}^{6N} + \frac{\partial}{\partial p_1}\dot{p}^1 + \cdots + \frac{\partial}{\partial p_{6N}}\dot{p}^{6N} = 0 \tag{1.3}$$

This trivial consequence of Hamilton Equations is also known as Liouville's Equation. The physical content of this Equation is easily understood. Take a volume in the phase space: each point represent a mechanical state of the system. Now let the system evolve according to Hamilton Equations of motion. After some time the original volume may be moved and deformed arbitrarily, but its actual volume will be the same. This is a mere consequence of the fact that we are excluding any dissipative phenomena: in a system of point particles with no internal degrees of freedom there is no opportunity of dissipation. The Hamiltonian of the system can also depend explicitly on time, as long as the applied forces are conservative, Liouville's Equation is satisfied. In the case of a system of charged particles we may write in particular the Hamiltonian as

$$\begin{aligned}\mathcal{H}(\mathbf{q^{(i)}}, \mathbf{p_{(i)}}, t) = &\sum_{i=1}^{N} \frac{1}{2} m_i \left(\mathbf{p_{(i)}} - \frac{e_{(i)}}{m_{(i)}} \mathbf{A}(\mathbf{q^{(i)}}, t)) \right)^2 \\ &+ \sum_{i=1}^{N} e^{(i)} \Phi(\mathbf{q^{(i)}}, t) + \mathcal{H}_c(\mathbf{q^{(i)}}, \mathbf{p_{(i)}});\end{aligned} \tag{1.4}$$

In Equation (1.4), we grouped the generalized coordinates and momenta identifying each single particle (i) via the vectors $(\mathbf{q^{(i)}}, \mathbf{p_{(i)}})$. Moreover, we introduced the electric scalar potential Φ and the magnetic vector potential $\mathbf{A}$, in such a way to have for the electric field $\mathbf{E}$ and the magnetic flux density $\mathbf{B}$ in the physical space:

$$\begin{aligned}\mathbf{E} &= -\frac{\partial \mathbf{A}}{\partial t} - \nabla \Phi \\ \mathbf{B} &= \nabla \times \mathbf{A}\end{aligned} \tag{1.5}$$

Finally the collisional term $\mathcal{H}_c$ in (1.4) does not depend explicitly on time, as it is not related to external forces or collective long-range phenomena. On the opposite electric and magnetic fields are due to external currents and collective ordered motion of charged particles in the plasma. It is worth to recall that the generalized momenta are in relation to the generalized velocities via

$$\mathbf{p_{(i)}} = m_{(i)} \dot{\mathbf{q}}^{\mathbf{(i)}} - e_{(i)} \mathbf{A}(\mathbf{q^{(i)}}, t). \tag{1.6}$$

Independently from these considerations, We can set up a continuity equation for the distribution function $F(q^i, p_i, t)$ in the $6N$-dimensional phase-space,

$$\frac{\partial F}{\partial t} + \nabla \cdot (F\underline{V}) = \left[\frac{\partial F}{\partial t}\right]_c \tag{1.7}$$

On the right hand side, we used the suffix "c" again to indicate the *collisions*. We are very trivially stating that if there are some particles entering a volume element in the phase space, this is either due to a net flux of particles through the boundary of this volume or due to collisions of the point particles which instantaneously modify the momenta of the colliding particles. In principle we could make explicit the effect of collisions in the Hamiltonian of the system, *i.e.* one can provide an operative expression for $\mathcal{H}_c\left(q^i, p_i, t\right)$ in Equation (1.4). Anyway, this would require to describe the relatively short-range interaction between particles, complicating the task [28]. It is important to notice that we attributed the long range electromagnetic interactions between particles due to charge accumulation and collective ordered motion already to the electromagnetic potentials $(\mathbf{A}, \phi)$ introduced in Equation (1.5). For completeness, it is just worth to mention here that collisions in an ionised gas can be substantially different from collisions in neutral gases. Ionised particles interact via Coulomb electrical forces, regulating the friction between the electron and ion particles and determining energy losses via *bremsstrahlung* radiation [2]. The actual Coulomb collision cross-section also determines whether the electrons really collide with the ions or if they can be accelerated up to relativistic velocities by an applied electric field. We will not need to enter these details for what we want to show. Indeed, we need just one more ingredient to the recipe, the standard vector identity:

$$\nabla \cdot (F\underline{V}) = F\nabla \cdot \underline{V} + \underline{V} \cdot \nabla F. \tag{1.8}$$

Using this vector identity in the continuity Equation (1.7), and considering that $\nabla \cdot \underline{V} = 0$ from Liouville's Equation (1.3), we finally have

$$\frac{\partial F}{\partial t} + \underline{\dot{q}} \cdot \nabla_{\underline{q}} F + \underline{\dot{p}} \cdot \nabla_{\underline{p}} F = \left[\frac{\partial F}{\partial t}\right]_c \tag{1.9}$$

Equation (1.9) is also referred to as *Liouville Theorem*. It is a simple consequence of the definition of the distribution function $F\left(q^i, p_i, t\right)$ and of the validity of Hamilton Equations of motion. It is important for us to notice that Equation (1.7) is especially valid for a limited class of close thermodynamic systems, where not only the number of particles is fixed, but each particle has no internal degree of freedom. Indeed, in this case binary collisions are necessarily elastic, and the evolution Equations take the Hamilton form (1.1).

In order to accommodate inelastic collisions one should allow the particle to have at least one internal degree of freedom, which can record the information about the "excitation" state [21]. Moreover, we did not provide any mathematical framework to allow particles to undergo chemical reactions, *i.e.* in Equation (1.7) there is not any mathematical instrument set up to change the label of each particle [22].

These aspects might reveal important for a fusion plasma, and radiative phenomena together with the interaction with solid walls make fusion plasmas neither isolated nor even close thermodynamic systems. During the start-up phase of an experiment, the deuterium is puffed into the vacuum chamber, and in case of significant plasma-wall contact, we may have a large exchange of electrons between plasma and solid structures, besides various possible chemical reactions at the plasma-solid interface. Despite this, in steady state nominal operation, it is normally assumed that the system is not exchanging mass with the environment and full ionization of the gas, which allows to neglect chemical reactions related to the internal degrees of freedom of the particles.

1.2 From Deterministic to Statistic: Boltzmann Equation

We notice explicitly as by now we could have really described any system of material point particles, eventually charged, and subject to external forces which do not compromise the indivergence of the *time evolution* vector field in phase-space. Liouville's Theorem really does not contain any information on the particular system examined. We have plenty of opportunities to start from here to make hypothesis and try a macroscopic description of any state of matter in principle. Anyway, gases exhibit one peculiarity which really provides a great chance of simplification and conscious neglect of information from the model, which was first exploited by Boltzmann [29]. First, for us macroscopic observers, the particles are undistinguishable. If we exchange coordinates and momenta of two particles, we are not really able to appreciate any difference. Further, we can introduce a statistical hypothesis, assuming *molecular chaos* [13] for the particles belonging to the plasma.

It is worth some clarification here, which is conceptually important for the applications presented later in the manuscript. Namely, Liouville's Theorem, as presented in Equation (1.9), is only valid for a fixed number of particles N. This assumption allowed both to define a 6N-dimensional phase-space and consequently a distribution function $F\left(\mathbf{q}^{(\mathbf{i})}, \mathbf{p}_{(\mathbf{i})}, t\right)$. By the way, we are rather interested in what happens to the particles inside a certain bounding box, the number of particles could really vary inside the volume considered, for example due to gas injection, or electric currents shared between solid walls and plasma. When we apply Liouville Equation we should hence refer to the whole thermodynamic universe, following all the particles which might enter in our control volume. The molecular chaos hypothesis for such a kind of open system, occupying the region V_{pl} of the physical space, reads as

$$F(\mathbf{q}^{(\mathbf{i})}, \mathbf{p}_{(\mathbf{i})}, t) = F^{out}(\mathbf{q}^{(\mathbf{k})}, \mathbf{p}_{(\mathbf{k})}, t) \cdot \prod_{\mathbf{q}^{(\ell)} \in V_{pl}} f_{\ell}(\mathbf{q}^{(\ell)}, \mathbf{p}_{(\ell)}, t). \tag{1.10}$$

Whenever a particle (i) is within the control volume, its mechanical state is statistically independent from the mechanical state of any other particle. There is no correlation between the mechanical states of distinct particles within the control volume. We can integrate Liouville Equation on all the particles coordinates and velocities, but one, and we would find this way the *Boltzmann Equation* for the *single particle distribution function* [18]:

$$\frac{\partial f^{(\ell)}}{\partial t} + \dot{\mathbf{q}}^{(\ell)} \cdot \frac{\partial f^{(\ell)}}{\partial \mathbf{q}} + \dot{\mathbf{p}}^{(\ell)} \cdot \frac{\partial f^{(\ell)}}{\partial \mathbf{p}} = \left(\frac{\partial f^{(\ell)}}{\partial t} \right)_c \tag{1.11}$$

and the time derivative $\dot{\mathbf{p}}^{(\ell)}$ is given by Hamilton Equations. In the collisional collisional term of Boltzmann Equation (1.11) we can symbolically account also for those collisions with solid walls which make the plasma an open thermodynamic system. The possibility of studying the Boltzmann equation alone and to get anyway information on the full mechanical system is strictly related to the hypothesis of statistical independence between particles made, besides the fact that particles are retained indistinguishable. In case there are particle of different *species*, *i.e.* particles which carry some label, we can write a Boltzmann Equation for each distinct group of indistinguishable particles. The resulting Boltzmann Equations are coupled via a collisional term modelling the interaction between particles of different species. It is remarkable that as long as we consider only binary elastic collisions between particles of the same species the corresponding collisional term in (1.11) is zero. The situation is different if we can distinguish at least between two groups of particles with different *labels*. In this case even elastic collisions can transfer momentum and energy from one group of particles to the other, and the collisional terms in the resulting two Boltzmann Equations are non-null.

As hinted, a standard way of introducing the plasma fluid models relies now on the calculation of proper moments of the Boltzmann Equation[1] respect to the single particle momentum [19]. In particular Grad's thirteen moments method [13] is based on the expansion of the single particle distribution function in a basis of Hermite polynomials. The coefficients of the expansion are taken as state variables, and are shown to correspond to clear macroscopic fluid quantities. Although this approach is very elegant, the actual description of inter-particle interactions at the microscopic level can be difficult and clear microscopic collisional models may be valid in practical narrow operational regimes. Hence, for what concerns us, an entirely macroscopic description will be sufficient. This is indeed what follows in next Sections.

1.3 MHD and Non Equilibrium Thermodynamics

We are going to describe *Magneto-Hydro-Dynamics* in the framework of classical Non-equilibrium Thermodynamics. This is a branch of Thermodynamics which allows to deal with physical systems which are only in local or better *constrained* Thermodynamic Equilibrium. The first comprehensive treatment on the subject was probably given by de Groot and Mazur [23]. In this framework, the arbitrary assumptions on collisions, necessary to derive the conservation laws for the fluid from Boltzmann Equations, are in a sense postponed directly to the macroscopic framework, where it is hopefully more easy to provide the missing information on a phenomenological basis.

In Non-equilibrium Thermodynamics it is generally assumed that locally to a small volume element we have conditions of thermodynamic equilibrium. Hence there are few quantities, the *thermodynamic variables*, retained to describe sufficiently well the mechanical state of the fluid element, thanks to some statistical hypothesis. In our case these quantities will be the densities and internal energies of the distinct fluid species within the considered volume element. Strictly, the equilibrium within the volume element may be assumed only for a subset of the thermodynamic variables, and for example we will not always assume that equilibrium respect to particle densities is reached. In any case, the specific entropy is a state function of these thermodynamic variables, and its knowledge allows to set up the *Equations of State*.

The conservation laws for the thermodynamic variables and for the mechanical momentum of the fluid will be postulated based on first principles.

[1] or eventually the system of Boltzmann Equations for the various groups of undistinguishable particles.

In the resulting evolution Equations some terms will appear which are further unknowns for the system, such as the reaction rates, diffusion flows, and heat fluxes. These will be defined as *thermodynamic flows* or *fluxes* in the theory, and their determination should be based on phenomenological observations.

Nonetheless, as we shall see soon, the non-conservation Equation for the entropy constrains the possible constitutive relations between the *thermodynamic flows* and the *thermodynamic forces*. The latter will be defined as those external fields or those gradients of the thermodynamic variables which are responsible for the system to be out of equilibrium. For the moment we just intuitively mention that the conjugate force to the heat flux will be the temperature gradient, as well as the conjugate force to the electric current density will be the electric field, or the conjugate force to the neutrals diffusion flow will be the gradient of its chemical potential.

The main ansatz in this framework is that *thermodynamic flows* depend linearly on *thermodynamic forces*. This way standard closure relations as Fourier's law for the heat flux, or Ohm's law for the electric current will be recovered. Whether this assumption is reasonable or not is questionable and largely depends on the phenomena we want to describe. Grad, in the framework of kinetic theory, already pointed out a long time ago [13] as there is not any linear relation between the "flows" and "forces", as postulated in non-equilibrium thermodynamics. Rigorously, any flow defined in the macroscopic theory is governed by some further evolution equation, which can be derived from the kinetic theory, when proper assumptions are made on the collisional terms. Anyway, whenever the time constant of evolution τ of a certain *thermodynamic flow* is sufficiently smaller than the time constants of evolution of the thermodynamic variables, we might take $\tau \to 0$, and recover the linear phenomenological laws between fluxes and forces postulated in the Thermodynamics framework. When this separation between time scales is not verified, one could incorporate between the thermodynamic variables the relevant "flows" which evolve on the same time-scale as mass, momentum and energy. In this way, the real notion of *thermodynamic flow* moves to higher order moments of the Boltzmann Equation. These considerations underlie the theory of *extended thermodynamics* [30], a further branch of *Thermodynamics* which shows as physical processes normally retained diffusive do hide in general a propagative nature, which is hidden by the really short propagation time constants.

As hinted, the main limit of classical non-equilibrium thermodynamics is that it does not provide any value for the coefficients that will appear in the laws relating thermodynamic *flows* and *forces*. The Thermodynamics theory offers anyway several constraints between the coefficients appearing in the linear laws, namely the *Curie symmetry principle* and *Onsager's reciprocal relations* [23].

1.3.1 Definitions

We shall consider an ideal gas mixture made out of electrons, positive ions and mono-atomic neutrals, which describes essentially a mono-atomic deuterium plasma. The ideal gas hypothesis is in general reasonably satisfied by stellar plasmas and laboratory plasmas in fusion experiments, due to the low densities of the constituents and the high temperature[2]. We shall exploit also the circumstance the gas is mono-atomic, allowing to not consider vibrational or rotational intrinsic energies for the particles, when deriving the local equilibrium equations of state [31]. Nonetheless, the method can be generalised to deal with general fluids [25], hence with non ideal or molecular ideal gases.

We shall describe our system in the framework of *Non Equilibrium Thermodynamics* [24, 23]. This is a theory of local thermodynamic equilibrium, *i.e.* in a small fluid element some condition of thermodynamic equilibrium is retained true, and irreversible phenomena are essentially attributed to inhomogeneities of thermodynamic quantities in the sample or to generalized forces which keep the system out of equilibrium.

Here and later the subscript k is used to indicate the fluid species and varies in the set of labels $\{e, i, a\}$, pointing out respectively electrons, positive ions and neutral atoms. It is possible to define a mass density ρ_k, a specific volume $v_k = 1/\rho_k$ and a particle density $n_k = \rho_k/m_k$ for each fluid in the mixture. The overall mass density for the gas mixture is clearly

$$\rho = \frac{1}{v} = \sum_k \rho_k. \tag{1.12}$$

and the mass concentrations are defined as

$$c_k = \frac{\rho_k}{\rho} \tag{1.13}$$

The relevant thermodynamic variables we will choose to describe the local thermodynamic equilibrium for a small fluid element are the specific volume v, the mass concentrations c_k and the overall specific internal energy u. The

[2] $n =\sim 10^{20} m^{-3}$ and $T \sim 150\ MK$ in average Tokamak experiments.

specific entropy shall be specified as a state function of the thermodynamic variables,

$$s = s(v, c_k, u). \tag{1.14}$$

In order to get an explicit expression for the specific entropy, hence in order to set up the equations of state, it is first worth to treat all the different fluid species as separate, virtually isolated. This is equivalent to consider an enlarged thermodynamic state space, the macroscopic system being described by the specific volumes v_k and the internal energies u_k of the different fluids. We could imagine a set of virtual constraints which prevents the different fluids to exchange internal energy or undergo chemical reactions, although they live in the same physical space region [32].

The specific entropy for the k-species ideal gas is clearly a state function of its specific volume and internal energy,

$$s_k = s_k\left(v_k, u_k\right) \tag{1.15}$$

As long as the different gases are considered as non-interacting, the overall specific entropy s is hence obtained by weighted summation of the specific entropy of each subsystem,

$$s\left(v_k, u_k\right) = \sum_k c_k s_k\left(v_k, u_k\right) \tag{1.16}$$

It is rather natural to require the overall specific entropy to be a thermodynamic function of the overall specific volume v. In this way the mechanical deformation work will be clearly distinguished from the convective energy exchange mechanisms related to the passage of particles through the boundary of the fluid element. The passage from the thermodynamic variables (v_k, u_k) to the variables (v, c_k, u_k) shall be regarded simply as a change of coordinates in the thermodynamic state space, which highlights the possible ways by which our system exchange energy with the surrounding environment, a fundamental aspect in thermodynamic theories [32],

$$s = s\left(v, c_k, u_k\right) \tag{1.17}$$

Clearly the mass concentrations are not independent variables, since $\sum_k c_k = 1$, hence the number of independent thermodynamic variables is unaltered in the two descriptions (1.16) and (1.17), moreover $v_k = v/c_k$. We will always retain thermodynamic equilibrium respect to different fluids internal energies, meaning that all the temperatures equilibrate $T_k = T \quad \forall k \in \{e, i, a\}$. This is equivalent to relax the virtual constraints imposed on the system which were preventing the exchanges of internal energies between the components of the mixture. We can hence concentrate our attention on a sub-manifold of our enlarged thermodynamic state space. In particular we may assign the internal energy of a single arbitrary component of the mixture or the overall specific internal energy $u = \sum_k c_k u_k$ indifferently, carrying the same information as if we are specifying the internal energies of all the different fluids in the mixture. Thanks to this hypothesis, we can express the specific entropy s as a state function of the specific volume v, the mass concentrations c_k and the internal energy u, as prescribed in Equation (1.14).

In order to deal with plasmas where thermal equilibration among the distinct fluid components is not achieved, it is sufficient to stop one step behind and take Equation (1.17) as state function for the specific entropy. Anyway, the state function (1.14) still allows to describe states of chemical non-equilibrium, since the mass concentrations c_k are retained as thermodynamic variables. Resuming, we will deal generally with plasmas in local thermodynamic equilibrium respect to the internal energies of the individual species within the mixture, but which are not in equilibrium with respect to the mass concentrations of the distinct fluids.

In a macroscopic context, for a mixture of N particles species there are at most $N-1$ linearly independent chemical reactions, since the overall mass conservation should be guaranteed. In our particular case, also the electric charge should be conserved, and a single macroscopic reaction may take place, *i.e.* the ionization/recombination reaction

$$\underbrace{e+i}_{reactants} \leftrightarrows \underbrace{a}_{product} \tag{1.18}$$

Now, we indicate by $\overline{\nu_k}$ the true stoichiometric coefficients of element k involved in the reaction. It is useful for the following to introduce also the normalized stoichiometric coefficients ν_k, such that the sum of the normalized stoichiometric coefficients of the reactants is -1 and the sum of the normalized stoichiometric coefficients of the products is $+1$ for each of the eventual chemical reactions of interest. In particular, having the indices of reactants from 1 to q and the indices of products from $q+1$ to N, we may define unambiguously,

$$\nu_k = \frac{m_k \overline{\nu_k}}{\sum_{j=q+1}^{N} m_j \overline{\nu_j}} \tag{1.19}$$

It is very important to notice as in presence of chemical reactions while the overall mass density (1.12) is conserved, the overall particle density $n = \sum_k n_k$ may change. This implicates that we cannot relate the mass density and the particle density by a simple constant, for example attributing all the inertia to ions, as generally done in two-fluid descriptions of the plasma. We summarize the true and normalized stoichiometric coefficients for our ionization reaction (1.18) in Table 1.1.

Table 1.1: Stoichiometric coefficients for the ionization/recombination reaction defined in Equation (1.18)

	electron	ion	atom
true ($\overline{\nu}$)	-1	-1	$+1$
normalized (ν)	$-m_e/m_a$	$-m_i/m_a$	$+1$

It is worth to include here some further definitions. The *barycentric velocity* is defined as the velocity of the mass centre of a fluid element,

$$\mathbf{v} = \frac{\sum_k \rho_k \mathbf{v_k}}{\rho} \tag{1.20}$$

The relative velocity of the fluid k respect to the barycentric velocity has some importance in the theory, and we define the diffusion flow of the species k fluid as

$$\mathbf{j_k} = \rho_k \left(\mathbf{v_k} - \mathbf{v}\right) \tag{1.21}$$

We notice explicitly as the sum of all diffusion flows is zero ($\sum_k \mathbf{j_k} = 0$), by definition of the barycentric velocity (1.20). Defined e_k as the electric charge of a single particle for the ideal gas species k, it is convenient to define the charge to mass ratio,

$$z_k = \frac{e_k}{m_k}. \tag{1.22}$$

Through this definition, we may define both the electric charge density,

$$q = \sum_k z_k \rho_k \tag{1.23}$$

and the electric current density in the fluid element reference frame as

$$\mathbf{i}^* = \sum_k z_k \mathbf{j_k} \tag{1.24}$$

The electric current density in the fluid reference is also obtained subtracting from the electric current seen in the laboratory reference frame all the convective current related to the motion of the electric charge density attached to the barycentre of the fluid element,

$$\mathbf{i}^* = \mathbf{i} - q\mathbf{v} \tag{1.25}$$

Generally, based on first principles consideration of MHD modelling [33], we assume that any ion hitting the solid surface is quickly recombined with an electron. This configures the solid wall as a sink for ions-electron couples and as a source of neutral atoms. In particular for any ion impinging the wall, there will be a neutral coming out. Moreover, we stress as there are really many other chemical reactions occurring at the solid surface, such as sputtering of impurities and emission of electrons due to Auger effect [19]. We shall always neglect such kind of reactions, together with the related presence of impurities in the plasma, besides these may have important implications also in the steady state operation of a Tokamak.

1.4 Thermodynamic Equilibrium

We shall present in this Section the *Equations of State* valid in our constrained thermodynamic equilibrium conditions, *i.e.* those relations locally valid in each fluid element due to thermodynamic equilibrium. We here use specific quantities, considering first particles of species k virtually *isolated* respect to the particles of other species. Anyway, as discussed in previous Section, we will later take as state variables the overall specific volume v, mass concentrations c_k and overall internal energy u.
All the gas species are retained to be ideal, *i.e.* the particles within the gas are non-interacting and undistinguishable. Moreover we identify for each particle a *translational* energy, associated to particle motion and an *intrinsic* energy, related to quantum-mechanical considerations [31], *e.g.* possible spin states of the particle. We consider here mono-atomic gases, so that vibrational and rotational energy contributions may be discarded. Moreover, we have for the excited states of the deuterium atom much higher energies as compared to the ground state. Hence we can consider just the fundamental state of energy $\epsilon_{0,k}$

and degeneracy G_k when computing the intrinsic canonical partition functions. If the intrinsic and translational energies of the single particle are independent, as normally retained, by means of the canonical ensemble, we can set up the *Sackur-Tetrode* formula [34]

$$s_k = \frac{k_B}{m_k} \log \left[\frac{1}{n_k \left(\Lambda_{Th,k} \right)^3} \right] + \frac{k_B}{m_k} \left(\frac{5}{2} + \log G_k \right). \tag{1.26}$$

where the *Thermal De Broglie wavelength* is introduced, indicating by h the Planck constant,

$$\Lambda_{Th,k} = \frac{h}{\sqrt{2\pi m_k k_B T_k}}. \tag{1.27}$$

In the same approximations, the internal energy for the k-species gas assumes the form

$$u_k = \frac{3}{2} \frac{k_B T_k}{m_k} + \frac{\epsilon_{0,k}}{m_k}. \tag{1.28}$$

Using the Equation of State (1.28), the definition of *thermal De Broglie wavelength* (1.27) and the identity $n_k = c_k/m_k v$, we may rewrite Sackur-Tetrode formula (1.26) in the form of an *Equation of State*,

$$\begin{aligned} s_k &= \frac{k_B}{m_k} \log \left[\frac{m_k v}{c_k} \left(u_k - \frac{\epsilon_{0,k}}{m_k} \right)^{3/2} \left(\frac{4\pi}{3} \right)^{3/2} \cdot \left(\frac{m_k}{h} \right)^3 \right] \\ &+ \frac{k_B}{m_k} \left(\frac{5}{2} + \log G_k \right). \end{aligned} \tag{1.29}$$

For a mixture in *thermal equilibrium*, each specific entropy s_k may be expressed in terms of the overall specific internal energy $u = \sum_k c_k u_k$ and the mass concentrations of all of the species in the mixture c_k. It is indeed sufficient to substitute in Equation (1.26), the expression of the thermal De Broglie wave-length (1.27) and the following the identity descending from (1.28)

$$\frac{3}{2} k_B T = \frac{u - \sum_j c_j \epsilon_{0,j}/m_j}{\sum_\ell c_\ell / m_\ell}. \tag{1.30}$$

In this way, we may use property (1.16) to get the overall specific entropy as a function of state of the specific volume v, the overall specific internal energy u and the different species mass concentrations c_k only, as postulated originally in Equation (1.14). Finally, we can write down the first principle of thermodynamics during a reversible process as

$$\mathrm{d}u = T\mathrm{d}s - p\mathrm{d}v + \sum_k \mu_k \mathrm{d}c_k \tag{1.31}$$

The relation above defines the kinetic pressure and chemical potentials as proper partial derivatives of the entropy respect to the thermodynamic variables. We first notice, by definition of kinetic pressure,

$$p = T\left(\frac{\partial s}{\partial v}\right)_{c_k,u} = \sum_k \underbrace{n_k k_B T}_{p_k}. \tag{1.32}$$

The partial pressure p_k is the pressure the gas species k would apply to the walls of the fluid element if it was alone. Moreover, using Equation (1.28), considering $u = \sum_k c_k u_k$, we may write down the internal energy per unit volume of the gas mixture as a function of the kinetic pressure and the particle densities,

$$\rho u = \frac{3}{2}p + \sum_k n_k \epsilon_{0,k}. \tag{1.33}$$

The chemical potentials are defined as

$$\mu_k = -T\left(\frac{\partial s}{\partial c_k}\right)_{u,v,c_{i\neq k}} \tag{1.34}$$

After some algebra, we consistently see that

$$s_k = -\frac{\mu_k - h_k}{T} \tag{1.35}$$

where we introduce the specific enthalpy for the k-species fluid as

$$h_k = u_k + p_k v_k = \frac{5}{2}\frac{k_B T}{m_k} + \frac{\epsilon_{0,k}}{m_k} \tag{1.36}$$

From property (1.35), the specific enthalpy definition (1.36) and the *Sackur-Tetrode* formula (1.26) we can write finally

$$\mu_k = \frac{k_B T}{m_k}\log\overline{c_k} + \underbrace{\frac{k_B T}{m_k}\log\left[\frac{p}{k_B T}\frac{(\Lambda_k)^3}{G_k}\exp\left(\frac{\varepsilon_{0,k}}{k_B T}\right)\right]}_{\zeta_k(p,T)/m_k} \tag{1.37}$$

In Equation (1.37), $\zeta_k(p, T)$ is a function of the kinetic pressure and of the temperature only, and it varies from species to species due to the different molecular masses m_k, intrinsic energies $\epsilon_{0,k}$ and degeneracies of the ground state G_k. Finally, we can take the chemical potentials to be functions $\mu_k\left(T, p, \overline{c_k}\right)$ of the temperature, the kinetic pressure (1.32) and the particles concentrations

$$\overline{c_k} = \frac{n_k}{n} = \frac{\rho_k}{m_k} \frac{1}{\rho \sum_j c_j/m_j} = \frac{c_k/m_k}{\sum_j c_j/m_j}. \tag{1.38}$$

We are done with the *Equations of State* which we retain always valid within a fluid element, we will need in particular Equations (1.32), (1.33) and (1.37).

We conclude this Section, investigating the consequences of having thermodynamic equilibrium respect to the different species mass concentrations c_k. For fixed internal energy and specific volume, these may vary in relation to the ionization/recombination chemical reaction (1.18). The variation of the number of a certain species respect to another one is regulated by the ratio between the true stoichiometric coefficients $\overline{\nu_i}$,

$$\frac{\partial n_j}{\partial n_k} = \frac{\overline{\nu_j}}{\overline{\nu_k}} \quad \Rightarrow \quad \frac{\partial c_j}{\partial c_k} = \frac{m_j}{m_k} \frac{\overline{\nu_j}}{\overline{\nu_k}} \tag{1.39}$$

The condition of thermodynamic equilibrium to be maximum has the important consequence

$$\begin{aligned} \left(\frac{\partial s}{\partial c_k}\right)_{v,u} = 0 \quad \Longrightarrow \quad & \sum_j \left(\frac{\partial s_j}{\partial c_j}\right)_{u,v} \cdot \frac{\partial c_j}{\partial c_k} = 0 \\ & -\sum_j \frac{\mu_j}{T} \frac{m_j}{m_k} \frac{\overline{\nu_j}}{\overline{\nu_k}} = 0 \end{aligned} \tag{1.40}$$

In last passage we used the chemical potentials definition (1.34). Substitution of the chemical potential expressions (1.37) into the chemical equilibrium constraint (1.40) leads to the following law of mass action,

$$\frac{n_e n_i}{n_a} = \frac{1}{(\Lambda_e)^3} \left(\frac{m_i}{m_a}\right)^{3/2} \frac{G_e G_i}{G_a} \exp\left[\frac{\varepsilon_{0,a} - \varepsilon_{0,e} - \varepsilon_{0,i}}{k_B T}\right] \tag{1.41}$$

We may take [19],

$$\frac{m_i}{m_a} \simeq 1, \; G_e = 2, \; \frac{G_i}{G_a} \simeq 1 \tag{1.42}$$

Moreover we can define the ionization energy,

$$\epsilon_i = \epsilon_{0,e} + \epsilon_{0,i} - \epsilon_{0,a} \tag{1.43}$$

Substituting (1.42) and (1.43) into (1.41), and making explicit the *thermal De Broglie wavelength* of elecrtons as a function of the temperature (1.27), we obtain the celebrated *Saha Equation* [11]

$$\frac{n_e n_i}{n_a} = \frac{(2\pi m_e k_B)^{3/2}}{h^3} T^{3/2} \exp\left(-\frac{\epsilon_i}{k_B T}\right) \tag{1.44}$$

which expresses the degree of ionization of the gas mixture in conditions of Thermodynamic Equilibrium respect to the particle concentrations. We shall see later in Section 1.6 how to describe the irreversible phenomena taking place during chemical reactions in conditions of chemical non-equilibrium, keeping the Saha Equation as limit for null reaction rate.

It is worth to stress here that the various fluid species do not necessarily are in local thermal equilibrium between each other, *i.e.* different fluid species in the same region of space can have different temperatures. This is often the case in many practical plasma applications, where the temperature of electrons T_e can differ significantly from the ion temperature T_i. In that case the specific entropy would be a function of the internal energies of each distinct fluid species. Similarly to how we found Saha Equation, we would find that in conditions of local thermodynamic equilibrium respect to the distinct fluid internal energies the temperatures equilibrate, *i.e.* $T_i = T_e = T_a$.

1.5 Conservation laws

In previous Section we provided the *Equations of State* (1.32), (1.33) and (1.37), valid in a small fluid element, due to local thermodynamic equilibrium. The next step is to postulate the conservation laws for the thermodynamic variables and the linear momentum of the fluid element [9]. We first discuss the conservation law for the overall mass density ρ and the evolution equations for mass concentrations c_k. Next, neglecting the inertia and kinetic energy of diffusion phenomena, we postulate a conservation equation for the linear momentum $\rho\mathbf{v}$ of the fluid element. To be general one should account separately for the conservation of momentum of the distinct fluid species. Anyway, as long as the collective barycentric motion carries the most of the kinetic energy, we can drop such conservation Equations and later recover information on the relative motion of the distinct fluid species respect to the barycentre via the constitutive Equations. We retain the fluid element has no intrinsic angular momentum. This circumstance, together with the symmetry of Maxwell stress tensor, reduces the conservation law for the fluid angular momentum to the requirement that the viscous stress is symmetric [23]. Finally, given that the total energy is certainly conserved[3], the evolution Equation for the internal energy is found by difference of the conservation Equation of the total energy and the evolution Equations for kinetic energy and electromagnetic energy.

1.5.1 Mass and concentrations

The time evolution for the mass density of a certain fluid component is intuitively given in the form of a conservation law as

$$\frac{\partial \rho_k}{\partial t} + \nabla \cdot (\rho_k \mathbf{v_k}) = \nu_k J_r \tag{1.45}$$

The symbol J_r denotes the reaction rate of the unique *macroscopic* reaction given in (1.18) describing ionization and recombination phenomena. Its dimensions are clearly mass per unit volume and unit time, and the normalized stoichiometric coefficients can be found in Table 1.1. Summing up the Equations of conservations for mass densities of distinct species (1.45) we get the Equation of conservation for the overall mass density of the fluid element,

$$\frac{\partial}{\partial t}\rho + \nabla \cdot \rho \mathbf{v} = 0. \tag{1.46}$$

The following conservation equations can be set up for the mass concentrations $c_k = \rho_k/\rho$ of the distinct species, considering simultaneously (1.45) and (1.46),

$$\rho \frac{\mathrm{d}}{\mathrm{d}t} c_k + \nabla \cdot \mathbf{j_k} = \nu_k J_r. \tag{1.47}$$

[3] we neglect nuclear reactions!

Manipulating Equations (1.47) we find also

$$\frac{\partial}{\partial t} q + \nabla \cdot \mathbf{i} = 0 \tag{1.48}$$

$$\rho \frac{\mathrm{d}}{\mathrm{d}t} c_q + \nabla \cdot \mathbf{i}^* = 0 \tag{1.49}$$

In the following we may choose arbitrarily three independent evolution Equations. Instead of taking the three Equations (1.45), we take the conservation Equations for the overall mass density (1.46), the concentration of neutrals [(1.47) for $k = a$], and the electric charge density (1.48).

1.5.2 Linear momentum

We assume that the inertia of diffusion phenomena, together with the kinetic energy of the diffusion flows is negligible. In this assumption, considering also the action-reaction principle of mechanics, and the overall conservation of mass property (1.46), we can set up the conservation Equation for the linear momentum of the mass centre of the fluid element as

$$\rho \frac{\mathrm{d}}{\mathrm{d}t} \mathbf{v} + \nabla \cdot \underline{\mathbf{P}} = q\mathbf{E} + \mathbf{i} \times \mathbf{B} \tag{1.50}$$

On the right hand side the Lorentz force appears clearly. At the left hand side $\underline{\mathbf{P}}$ is the pressure tensor, describing both the effect of the kinetic pressure p defined in Equation (1.32) and of the viscous stress $\underline{\mathbf{\Pi}}$,

$$\underline{\mathbf{P}} = p\underline{\mathbf{I}} + \underline{\mathbf{\Pi}} \tag{1.51}$$

Since the Maxwell stress tensor is symmetric, retaining that the fluid element has no intrinsic angular momentum, we can conclude that the antisymmetric part of the viscous stress should be zero, *i.e.* $\underline{\mathbf{\Pi}} = \underline{\mathbf{\Pi}}^{(s)}$ [23].

It is important to bear in mind that it is possible to define the velocity of each gas species. The missing evolution Equations for the linear momentum of each distinct species are replaced only in part by the overall linear momentum conservation equation (1.50) and further information will be provided by the constitutive equations. This is generally possible any time the evolution time constants governing the dynamics of the distinct fluid velocities relative to mass centre are fast as compared to the time scale of interest [30]. These assumptions are related precisely to the hypothesis of negligible inertia of diffusion phenomena. Postulating the linear momentum conservation (1.50) we consider in particular,

$$\nabla \cdot \sum_k \rho_k \left(\mathbf{v_k} - \mathbf{v}\right) \mathbf{v_k} \simeq 0 \tag{1.52}$$

This is coherent with the assumption of retaining the overall kinetic energy approximately equal to the kinetic energy related to the barycentric motion,

$$\sum_{k=1}^{3} \frac{1}{2} \rho_k \mathbf{v_k}^2 \simeq \frac{1}{2} \rho \mathbf{v}^2 \tag{1.53}$$

This is also equivalent to attribute the kinetic energy of diffusion to the internal energy sink, but then makes our Equations of State imprecise when the above hypothesis are not satisfied.

In this perspective, let us scalar multiply Equation (1.50) by the barycentric velocity $\mathbf{v}$. Simple manipulation, and the conservation of mass property (1.46), allow to write an evolution equation for the kinetic energy of the mass centre of the fluid element,

$$\begin{aligned} \frac{\partial}{\partial t}\left(\frac{1}{2}\rho \mathbf{v}^2\right) & +\nabla \cdot \left(\frac{1}{2}\rho v^2 \mathbf{v} + \underline{\mathbf{P}} \cdot \mathbf{v}\right) \\ = & \ \underline{\mathbf{P}} : \nabla \mathbf{v} + q\mathbf{E} \cdot \mathbf{v} + \mathbf{i} \times \mathbf{B} \cdot \mathbf{v} \end{aligned} \tag{1.54}$$

1.5.3 Internal energy

One interesting feature of the Non Equilibrium Thermodynamics framework is the way to introduce the internal energy. This is defined by difference of the overall specific energy within the system e and all the "external" energy sinks we retain important [23]. If we discard important energy sinks from the analysis, our thermodynamic model will be inconsistent, since we are making the hypothesis that our internal energy satisfy the Equation of State (1.33). Besides the barycentric kinetic energy, the largest "external" energy sink in a variety of plasma physics applications is generally the electro-magnetic one,

$$w_{e.m.} = \left(\frac{1}{2}\varepsilon_0 \mathbf{E}^2 + \frac{1}{2\mu_0}\mathbf{B}^2\right) \tag{1.55}$$

The electro-magnetic energy is subject to the following conservation law, also known as *Poynting Theorem*,

$$\frac{\partial}{\partial t} w_{e.m.} = -\nabla \cdot \mathbf{K_{e.m.}} - \mathbf{E} \cdot \mathbf{i}, \tag{1.56}$$

where the Poynting vector is defined as

$$\mathbf{K_{e.m.}} = \mathbf{E} \times \frac{\mathbf{B}}{\mu_0} \tag{1.57}$$

The Poynting Theorem (1.56) is a simple consequence of the validity of Maxwell Equations, for a critical discussion in the context of fusion plasmas see [35].

We can finally state that the overall energy is given by the sum of barycentric kinetic energy, electromagnetic energy and internal energy,

$$\rho e = \frac{1}{2}\rho\mathbf{v}^2 + w_{e.m.} + \rho u \tag{1.58}$$

As hinted, we considered the only relevant kinetic energy is the one related to the motion of the mass centre, hence the kinetic energy of diffusion is accounted within the internal energy. The chemical energy per unit volume is also considered a form of internal energy, hence it is also contained in ρu. We can take for granted, at least as long as nuclear reactions are negligible, that the total energy within an arbitrary volume cannot be created or destroyed,

$$\frac{\partial \rho e}{\partial t} + \nabla \cdot \mathbf{K_e} = 0 \tag{1.59}$$

where $\mathbf{K_e}$ is a total energy current density, which we postulate to be

$$\mathbf{K_e} = \rho e\mathbf{v} + \underline{\mathbf{P}} \cdot \mathbf{v} + \mathbf{K_{e.m.}} + \mathbf{K_q} \tag{1.60}$$

The vector $\mathbf{K_q}$ defines a current density of internal energy, also known as heat flux. We can now obtain a balance equation for the internal energy by the subtraction of the total energy conservation equation (1.59) and the conservation equations for the barycentric kinetic energy (1.54) and the electromagnetic energy (1.56),

$$\frac{\partial}{\partial t}(\rho u) = -\nabla \cdot (\rho u\mathbf{v} + \mathbf{K_q}) - \underline{\mathbf{P}} : \nabla\mathbf{v} + \mathbf{i}^* \cdot (\mathbf{E} + \mathbf{v} \times \mathbf{B}) \tag{1.61}$$

1.6 Entropy conservation

We have set up the conservation laws concerning the mass density (1.46), the neutrals concentration (1.47), the electric charge density (1.48), the overall linear momentum (1.50), and the internal energy (1.61) of a fluid element.

Moreover the local thermodynamic equilibrium hyptohesis provided us with Equations of State (1.32), (1.33) and (1.37). Anyway, the mathematical model is still undetermined, as we have introduced some unknowns for which we did not provide any constraint: the reaction rate J_r, the electric current in the laboratory reference frame $\mathbf{i}$, the neutrals current density $\mathbf{j_a}$, the heat flux $\mathbf{K_q}$, and finally the viscous stress tensor $\underline{\mathbf{\Pi}}$. The general assumption of classical irreversible thermodynamics is to assume that all these *thermodynamic fluxes* depend linearly on some other quantities which we are able to determine and which are either due to external constraints keeping the system out of thermodynamic equilibrium or due to the inhomogeneities of thermodynamic variables across different fluid elements.

A standard procedure is available in this context to provide a linear closure of the model [23], which we apply here to the case of interest. The first principle of thermodynamics for our multi-component fluid in a reversible process was provided in Equation (1.31). We may assume this is valid close to thermodynamic equilibrium, allowing to write in a small time interval $\mathrm{d}t$,

$$\rho\frac{\mathrm{d}s}{\mathrm{d}t} = \frac{1}{T}\rho\frac{\mathrm{d}u}{\mathrm{d}t} + \frac{p}{T}\rho\frac{\mathrm{d}\frac{1}{\rho}}{\mathrm{d}t} - \sum_k \frac{\mu_k}{T}\rho\frac{\mathrm{d}c_k}{\mathrm{d}t} \tag{1.62}$$

We may now substitute the conservations laws postulated in previous Section, for the mass density (1.46), the mass concentrations (1.47), and the internal energy (1.61) into Equation (1.62). Arranging properly the divergence terms, we are able to distinguish clearly the entropy flux $\mathbf{K_s}$ from the entropy production term σ, that is

$$\rho\frac{\mathrm{d}s}{\mathrm{d}t} = -\nabla\cdot\mathbf{K_s} + \sigma \tag{1.63}$$

Here the entropy flux density $\mathbf{K_s}$ is defined as

$$\mathbf{K_s} = \frac{\mathbf{K_q} - \sum_{k=1}^{3}\mu_k\mathbf{j_k}}{T}. \tag{1.64}$$

and the entropy production is given by Equation (1.65).

$$\sigma = \overbrace{\frac{1}{T}\mathbf{K_q}\cdot\left(-\frac{\nabla T}{T}\right) + \frac{1}{T}\sum_{k=1}^{3}\mathbf{j_k}\cdot\left[-T\nabla\left(\frac{\mu_k}{T}\right) + z_k\left(\mathbf{E}+\mathbf{v}\times\mathbf{B}\right)\right]}^{\sigma_{odd}}$$
$$\underbrace{-\frac{1}{T}\Pi : \nabla\mathbf{v} - \frac{1}{T}J_r A_r}_{\sigma_{even}} \tag{1.65}$$

Here A_r is the chemical affinity of the ionization/recombination reaction (1.18). The chemical affinity is defined, eventually for each independent chemical reaction, as

$$A_r = \sum_{j=1}^{n} \nu_j \mu_j \tag{1.66}$$

where the normalized stoichiometric coefficients were introduced already in Equation (1.19).

The split of the *r.h.s.* of Equation (1.62) into a divergence term and a production term is not arbitrary. This shall satisfy a number of requirements, in particular the Galilei invariance, and the condition of null entropy production at thermodynamic equilibrium, which determine this separation uniquely [23]. Notice also that Clausius-Carnot Theorem is satisfied when the system is not allowed to exchange mass with the surrounding environment. Definition (1.64) reflects indeed how to extend the entropy flux definition to open thermodynamic systems.

In Equation (1.65) above each thermodynamic flux scalar multiplies a further quantity, which is defined as its conjugate thermodynamic force. Nonetheless, many linear combinations of fluxes and forces may be defined which leave the entropy production term unaltered, *i.e.* we may find transformation of fluxes and forces which save the sum of scalar products in Equation (1.65). We will use only transformations which leave the spatial symmetry constraints, and Onsager's reciprocal relations unaltered. However a wider class of transformations exist which may save the entropy production but not the Onsager reciprocal relations (see Chapter VI of [23] for more details). The motivations that lead us to distinguish the entropy production due to vectorial phenomena σ_{odd} and due to scalar and second order quantities σ_{even} will be clear in next Section. In the remainder of this Section we present two entropy production expressions which will reveal to be convenient for our application.

By the *Equations of State* (1.37), we take the chemical potential μ_k to be a function of the temperature T, the kinetic pressure p and particles concentration $\overline{c_k}$. By a change of variables we may adopt different representations for the chemical potentials, but the form (1.37) is a convenient choice. We can highlight the effect of the temperature gradient on the diffusion flows by the vector identity,

$$T\nabla\left(\frac{\mu_k}{T}\right) = \nabla\mu_k\Big|_T - \frac{1}{T}\left[\mu_k - T\frac{\partial\mu_k}{\partial T}\Big|_{p,\overline{c_k}}\right]\nabla T. \tag{1.67}$$

where we indicated as a subscript the thermodynamic quantities to consider homogeneous throughout the sample when differentiating. In particular the first gradient at the right hand side is performed assuming homogeneous temperature. By the *Equation of State* (1.37) we observe

$$\nabla\mu_k\Big|_T = \frac{k_B T}{m_k}\nabla\log p_k \tag{1.68}$$

and

$$\mu_k - T\frac{\partial\mu_k}{\partial T}\Big|_{p,\overline{c_k}} = \frac{5}{2}\frac{k_B T}{m_k} + \frac{\epsilon_{0,k}}{m_k} = h_k \tag{1.69}$$

These observations lead us to reformulate the odd contribution to the entropy production in Equation (1.65) as follows,

$$\begin{aligned} \sigma'_{odd} = & \quad -\frac{1}{T^2}\mathbf{K_q}^* \cdot \nabla T \\ = & \quad -\frac{1}{T}\sum_{k=1}^{3}\mathbf{j_k}\cdot[\nabla(\mu_k)_T - z_k\left(\mathbf{E}+\mathbf{v}\times\mathbf{B}\right)]. \end{aligned} \tag{1.70}$$

where,

$$\mathbf{K}^*_\mathbf{q} = \mathbf{K_q} - \sum_k h_k\mathbf{j_k} \tag{1.71}$$

Here a sort of *decomposition* for the heat flux $\mathbf{K_q}$ was naturally introduced. This choice allows moreover to write the entropy flux density (1.64) as

$$\mathbf{K_s} = \frac{\mathbf{K}^*_\mathbf{q}}{T} - \sum_k\frac{\mu_k - h_k}{T}\mathbf{j_k} \tag{1.72}$$

Property (1.36) leads to

$$\mathbf{K_s} = \frac{\mathbf{K_q^*}}{T} + \sum_k s_k \mathbf{j_k} \tag{1.73}$$

Equations (1.71)-(1.73) provide a clear interpretation of the additional entropy flux contribution for open thermodynamic system, allowing to identify the entropy fluxes related to the exchanges of matter. Notice in particular that for a close thermodynamic system $\mathbf{K_q} = \mathbf{K_q^*}$ at the boundary.

Finally, for our application it is certainly convenient to exploit the linear dependence of the diffusion flows $\sum_k \mathbf{j_k} = 0$. We use this constraint, and take as diffusion flows the electric current in the fluid reference frame $\mathbf{i}^*$ and the neutral diffusion flow $\mathbf{j_a}$. Proper transformation of the thermodynamic forces, and expressing the electromagnetic fields by the electromagnetic potentials, allows finally to write the odd contribution to the entropy production in the following equivalent forms,

$$\begin{aligned}
(a) \qquad \sigma^*_{odd} &= \mathbf{K_s} \cdot \left(-\frac{\nabla T}{T}\right) + \frac{1}{T}\mathbf{j_a} \cdot (-\nabla \mu_a^*) \\
&+ \frac{1}{T}\mathbf{i}^* \cdot \left[-\nabla\left(\phi + \phi_\mu^*\right) - \frac{\partial \mathbf{A}}{\partial t} + \mathbf{v} \times \nabla \times \mathbf{A}\right] \\
(b) \qquad \sigma^*_{odd} &= \frac{\mathbf{K_q^*}}{T} \cdot \left(-\frac{\nabla T}{T}\right) + \frac{1}{T}\mathbf{j_a} \cdot (-\nabla \mu_a^*)_T \\
&+ \frac{1}{T}\mathbf{i}^* \cdot \left[-\nabla\left(\phi + \phi_\mu^*\right)_T - \frac{\partial \mathbf{A}}{\partial t} + \mathbf{v} \times \nabla \times \mathbf{A}\right]
\end{aligned} \tag{1.74}$$

In Equations (1.74) we used the electric scalar potential and the magnetic vector potential introduced in Equation (1.5). Moreover we introduced the modified chemical potential μ_a^* and the electro-chemical potential ϕ_μ^*, defined as

$$\begin{aligned}
(a) \quad \phi_\mu^* &= \frac{m_{e,i}}{e}\left(\mu_i - \mu_e\right), \\
(b) \quad \mu_a^* &= \mu_a + \frac{m_{ei}}{m_e}\mu_i - \frac{m_{e,i}}{m_i}\mu_e \simeq \mu_a + \mu_i.
\end{aligned} \tag{1.75}$$

where

$$m_{e,i} = \frac{m_e m_i}{m_e + m_i} \tag{1.76}$$

is the reduced electron mass. It is important to stress these are still to consider functions of the temperature T, the pressure p and the particles concentrations $\overline{c_k}$.

The $\mathbf{K}_{\mathbf{q}}^*$ contribution to the heat flux finds the expression,

$$\mathbf{K}_{\mathbf{q}}^* = \mathbf{K}_{\mathbf{q}} - \xi_h^* \mathbf{i}^* - h_a^* \mathbf{j}_{\mathbf{a}} \tag{1.77}$$

where we adopted the following definitions,

$$\begin{aligned} (a) \quad & \xi_h^* = \frac{m_{ei}}{e} \left(h_i - h_e \right) \\ (b) \quad & h_a^* = h_a + \frac{m_{ei}}{m_e} h_i - \frac{m_{ei}}{m_i} h_e \end{aligned} \tag{1.78}$$

It is important to notice that the entropy production is by definition a non-negative quantity. This circumstance and the inner product structure of the entropy production (1.65) suggest to set a linear relationship between fluxes and forces: in this way the entropy production term σ, in any of its forms (1.65), (1.70) or (1.74), is a bilinear form in the thermodynamic forces. Hence, it is relatively simple to force the entropy production be positive-definite, via simple constraints on the coefficients of the phenomenological relations. Moreover the entropy production will be related solely to those external forces keeping the system out of equilibrium or to inhomogeneities of the physical system. This can be considered an optimal approximation for a wide category of transport phenomena, such as electric current and heat conduction.

At this stage any thermodynamic flux might depend linearly on any thermodynamic force, even the coupling between fluxes and forces of different tensor order is in principle allowed. For example, without further knowledge of the physical system, we may consider the possibility for a chemical affinity to originate a viscous stress, or for a temperature gradient to cause a reaction rate. Moreover, even for fluxes and forces of the same tensorial order, the linear relation is usually not provided by a scalar: the x- component of the temperature gradient might be responsible for an y-component of the heat flux for example. Clearly not all of these linear relations are really physical and allowed. The Curie symmetry principle and Onsager's reciprocal relations greatly reduce the allowed linear relations between fluxes and forces and determine the structure of the tensors representing the linear constitutive relations. We shall explore these constraints in the next Section. It is important to stress that different "representations" for the entropy production, such as (1.74a) and (1.74b), lead to completely equivalent closure relations. There will exist indeed some transformations between the linear coefficients of the constitutive equations obtained from the different representations.

Besides the linear closure is efficient in describing heat conduction and diffusion phenomena, the approximation of chemical reactions by linear laws is generally too far from real experimental conditions for most applications. Hence, it is necessary to take here some results from chemical kinetics, in order to introduce a realistic closure equation for the reaction rate of recombination J_r [23]. We first assume that chemical reactions are not directly related to other dissipative phenomena through constitutive Equations and vice-versa. Further, indicating by k_f and k_r the forward and reverse reaction rate coefficients, we require

$$\frac{J_r}{m_a} = k_f n_a - k_r n_e n_i = k_r n_a \left(\frac{k_f}{k_r} \frac{n_e n_i}{n_a} - 1 \right) \tag{1.79}$$

The physical ground for the above relation are intuitive. The forward reaction rate is proportional to the product of the particle densities of electrons and positive ions (reactants) while the reverse reaction rate is proportional to the particle density of the neutral atoms (product). We now focus the attention on the ratio between particle densities at the right hand side of Equation (1.79). Expressing particle densities as a function of the chemical potentials (1.37), and highlighting the functions $\zeta_k(p,T)$, leads to

$$\frac{n_e n_i}{n_a} = n \exp \left[\frac{-m_a A_r - (\zeta_e + \zeta_i - \zeta_a)}{k_B T} \right] \tag{1.80}$$

At thermodynamic and chemical equilibrium the chemical affinity is null, $A_r = 0$, and Equation (1.80) reduces to Saha Equation (1.44). In the same conditions, the reaction rate J_r in Equation (1.79) should be null, leading to conclude

$$\frac{k_f}{k_r} = \frac{1}{n} \exp \left[\frac{(-\zeta_a + \zeta_e + \zeta_i)}{k_B T} \right] \tag{1.81}$$

Substituting Equations (1.80) and (1.81) into (1.79) we finally obtain

$$J_r = k_r m_a n_a \left[\exp \left(-\frac{m_a A_r}{k_B T} \right) - 1 \right] \tag{1.82}$$

It is interesting to observe as for $m_a A_r \ll k_B T$ we could establish a linear relationship between the reaction rate and the chemical affinity.

1.7 Magnetic field anisotropy

A mixture of charged ideal gases would be an isotropic system in absence of an externally applied magnetic field. Indeed, we may argue that there is a *spher-*

ical symmetry for the medium considered as a continuum, and all proper and improper rotations of any material element should not affect the constitutive equations. In this situation, we say that the *symmetry group* for the constitutive equations of our system is the full orthogonal group $O(3)$. We provide some details about symmetry groups and the theory of invariant tensor functions in Appendix A.

Our first aim is to identify the symmetry group for our multi-component mixture of ideal gases, when a magnetic field is present. Following Ref. [23], we may well be tempted to claim that our linear constitutive Equations should be solely invariant respect to rotations about the magnetic field lines. This is almost true, as we shall see briefly. Indeed, proceeding rigorously, we can state that any orthogonal transformation of the fluid element which does not alter the magnetic field perceived by the fluid element itself shall not be responsible for a modification of the constitutive equations. In this context it is important to figure out that the magnetic field is not a standard *polar* vector field. Indeed, in any point of the Euclidean space, the magnetic field is a second order skew-symmetric tensor. Second order skew-symmetric tensors in three dimensions have exactly three degrees of freedom as standard polar vectors, hence they are usually represented as vectors through the inverse volume form $\overline{\omega}$,

$$\tilde{B} \doteq \begin{bmatrix} 0 & B_z & -B_y \\ -B_z & 0 & B_x \\ B_y & -B_x & 0 \end{bmatrix} \xRightarrow{\overline{\omega}} \mathbf{B} \doteq \begin{bmatrix} B_x \\ B_y \\ B_z \end{bmatrix} \tag{1.83}$$

and defined as *pseudo* or *axial* vectors. Hence, we can conclude that the *structural tensor* [36, 37] which characterize the symmetry group of our constitutive Equations is the second order skew-symmetric tensor $\tilde{B}$. The subgroup of $O(3)$ corresponding to this structural tensor is a transverse isotropy group often denoted by the symbol $C_{\infty,h}$ [26]. Transformations in this group are given by any combination of rotations of the fluid element about the magnetic field lines and by the inversion of the material element. The presence of the inversion transformation within the symmetry transformations is intimately related to the pseudo-vector nature of the magnetic field. Indeed, pseudo-vectors, compared to standard polar vectors, undergo an additional sign-flip of the components for an inversion of the basis vectors. As a result, the material element, after an inversion, keep to perceive the same magnetic field as before. Comparatively, if the magnetic field was to consider a standard *polar* vector field, an element inversion would have caused a sign flip of the perceived magnetic field.

Now that the symmetry group for our constitutive equations is clear, we may use some standard results of the theory of invariants for tensor functions, commented in Appendix A, to provide the constitutive Equations for our system consistently with the spatial symmetry constraints. The first important consequence of the isotropization theorem [37] and the irreducible and complete representations for tensor functions in isotropic systems synthesized in Table 11 and Table 12, is that a linear tensor function of an even order tensor cannot return an odd-order tensor, and vice versa, even in presence of a magnetic field. This is an extension of the *Curie symmetry principle* from isotropic conditions to the case of interest. In particular this guarantees that a vectorial thermodynamic flux may be linearly related solely to vectorial thermodynamic forces, while scalar and second order tensors thermodynamic fluxes may be related both to scalars and second order tensors thermodynamic forces. This implicates that the entropy production term may be split as indicated in Equation 1.65. The two contributions σ_{odd} and σ_{even} should be separately positive semi-definite.

The results of tables 11 and 12, together with the isotropization Theorem [37] allow moreover to give an invariant representation for all the constitutive equations allowed, *i.e.* vector-valued functions of vectors, second-order symmetric tensor-valued functions of scalars and second-order tensors, and scalar-valued functions of scalars and second-order symmetric tensors.

Let us start from the linear constitutive equation relating a vector thermodynamic flux $\mathbf{u}$ and a vector thermodynamic force $\mathbf{v}$.

$$\mathbf{u} = L\left(\mathbf{v}\right) = \beta_0 \mathbf{v} + \beta_1 \tilde{B}\mathbf{v} + \beta_2 \tilde{B}^2 \mathbf{v} \tag{1.84}$$

where the scalar coefficients β_k are eventually scalar functions of the unique invariant $\mathrm{tr}\left(\tilde{B}^2\right)$. In our case, the vector $\mathbf{u}$ may represent either the heat flux $\mathbf{K}^*_{\mathbf{q}}$ or the electric current density in the fluid reference frame $\mathbf{i}^*$, while the vector $\mathbf{v}$ is either the electric field $\left[\mathbf{E} + \mathbf{v} \times \mathbf{B} - \nabla\left(\phi^*_\mu\right)_T\right]$ or the relative temperature gradient $-\frac{\nabla T}{T}$. In standard vector notation we may write

$$\mathbf{u} = \beta_0 \mathbf{v} + \beta_1 \mathbf{v} \times \mathbf{B} + \beta_2 \mathbf{v} \times \mathbf{B} \times \mathbf{B} \tag{1.85}$$

Let us represent this constitutive Equation also in a Cartesian coordinate system, with the z-axis aligned along the magnetic field direction. Constitutive Equations (1.84) and (1.85) may be represented as,

$$\begin{bmatrix} u_x \\ u_y \\ u_z \end{bmatrix} = \begin{bmatrix} \beta_0 - \beta_2 B^2 & -\beta_1 B & 0 \\ \beta_1 B & \beta_0 - \beta_2 B^2 & 0 \\ 0 & 0 & \beta_0 \end{bmatrix} \begin{bmatrix} v_x \\ v_y \\ v_z \end{bmatrix} \tag{1.86}$$

From these representations we may take β_0 as significant of the *isotropic* relation between the input and output vector. The coefficient β_1 regulates the Hall effect, being orthogonal both to the input vector and the magnetic vector field. The coefficient β_2 is responsible for a modification of the conductivity orthogonal to the magnetic field direction. We may assume that the isotropic relation is not influenced by the application of the magnetic field, hence retaining β_0 independent from $\mathrm{tr}\left(\tilde{B}^2\right)$. The Hall effect is usually retained linear in the magnetic field, hence we may argue that also β_1 is a coefficient independent from the magnetic field. Finally, the variation of conductivity transverse to the magnetic field may be taken to be quadratic in the magnetic field magnitude, as observed in experiments on metals at low temperature [38]. This requires β_2 to not depend directly on the magnetic field. In any case the coefficients β_k are even functions of the magnetic field, hence the parity of the coefficients with respect to the magnetic field in the Cartesian representation can be easily read from Equation (1.86). This highlights as the symmetric part of the tensor $L(\cdot)$ representing the constitutive Equation is even in the magnetic field, while the antisymmetric part, related solely to the Hall effect, is odd in the magnetic field. Synthetically,

$$L(\mathbf{B}) = L^T(-\mathbf{B}) \tag{1.87}$$

Let us consider the possible scalar effects s_o due to a second order symmetric trace-less tensor $\mathbf{T}$. The only possible scalar invariant linear in $\mathbf{T}$ is $\mathrm{tr}\,(\mathbf{T}\tilde{B}^2)$, hence

$$s_o = L(\mathbf{T}) = \gamma\ \mathrm{tr}\,(\mathbf{T}\tilde{B}^2) \tag{1.88}$$

As usual $\gamma = \gamma\left(\mathrm{tr}(\tilde{B}^2)\right)$. In the case under exam the scalar quantity may be the trace of viscous stress $\mathrm{tr}(\Pi)$ or eventually the reaction rate J_r, while the traceless second order tensor T can be only the traceless part of $\Pi^{(s)}$. In a Cartesian coordinate system with the z-axis oriented along the magnetic field equals

$$s_o = L(\mathbf{T}) = -\gamma B^2\,(T_{x,x} + T_{y,y}) \tag{1.89}$$

Since $\mathrm{tr}\,(\mathbf{T}) = 0 \leftrightarrow T_{x,x} + T_{y,y} + T_{z,z} = 0$ and we may write equivalently,

$$s_o = L(\mathbf{T}) = \gamma B^2 \left(T_{x,x} + T_{y,y} - 2T_{z,z}\right) \tag{1.90}$$

Further, we may study whether a scalar solicitation s_i can be responsible for a second order symmetric trace-less tensor $\mathbf{U}$. The only possibility is the following

$$\mathbf{U} = L(s) = \zeta s \left(\tilde{B}^2 - \mathrm{tr}\,(\tilde{B}^2) I\right) \tag{1.91}$$

where ζ is as usual a function of $\mathrm{tr}\left(\tilde{B}^2\right)$. In a coordinate system with the z-axis along the magnetic field direction, the above expression looks like

$$L(s) = \zeta s \begin{bmatrix} B^2 & 0 & 0 \\ 0 & B^2 & 0 \\ 0 & 0 & -2B^2 \end{bmatrix} \tag{1.92}$$

Consider finally two second order symmetric tensors, the thermodynamic flux $\mathbf{U}$ and the thermodynamic force $\mathbf{T}$. The constant γ regulate how the traceless part of $\mathbf{T}$ influences the trace of $\mathbf{U}$. Similarly the constant ζ regulate the effect of the trace of $\mathbf{T}$ on the traceless part of $\mathbf{U}$. Both are even functions of the magnetic field, resulting in particular to be functions of $\mathrm{tr}\,(\tilde{B}^2)$. These constants are equal due to Onsager reciprocal relations, *i.e.* $\gamma = \zeta$ [23].

Thanks, as usual, to the *isotropization theorem* [37], and having $\tilde{B}$ as structural tensor for the system symmetry, we find the following coordinate-free form for the linear constitutive relation between the traceless part of the two second order symmetric tensors,

$$\begin{aligned} \mathring{\mathbf{U}} =& \eta_0 \mathring{\mathbf{T}} + \eta_1 \left(\mathring{\mathbf{T}}\tilde{B} - \tilde{B}\mathring{\mathbf{T}}\right) + \eta_2 \left(\mathring{\mathbf{T}}\tilde{B}^2 + \tilde{B}^2\mathring{\mathbf{T}}\right) \\ &+ \eta_3 \left(\tilde{B}\mathring{\mathbf{T}}\tilde{B}^2 - \tilde{B}\mathring{\mathbf{T}}\tilde{B}^2\right) \\ &+ \eta_4 \,\mathrm{tr}\,(\mathring{\mathbf{T}}\tilde{B}^2) \left(\tilde{B}^2 - \mathrm{tr}\,(\tilde{B}^2) I\right) \end{aligned} \tag{1.93}$$

We indicate here the traceless part of the tensor with a circle accent. All of the constants η_k might depend on $\mathrm{tr}\left(\tilde{B}^2\right)$, hence are always even in the magnetic field. Let us consider explicitly $\mathbf{T} = (\nabla \mathbf{v})^{(s)}$ and $\mathbf{U} = \underline{\mathbf{\Pi}^{(\mathbf{s})}}$. These tensors, besides being symmetric, admit in general a non-null trace. If we take a Cartesian coordinate system with the z-axis along the magnetic field direction, we can merge previous results synthetically in Table 1.7. We notice explicitly as the scalar η_0 carries the information of the isotropic relation we would obtain in absence of magnetic field, and is usually defined as shear viscosity in fluid dynamics. The volume viscosity η_v defines the trace of the viscous stress originating by the barycentric velocity divergence. Each coefficient η_k in Table 1.7 multiplies B^k, giving information on the parity of the coefficients of the constitutive relation respect to the magnetic field. We claim again that the coefficients η_v, ζ and η_k might be considered independent from the magnetic field in first approximation. Transport theory experts are in charge of determining the coordinate-independent coefficients η_v, η_k, ζ based on experiments or microscopic models. It is worth to notice that the constitutive Equation relating the viscous stress to the symmetric part of the velocity gradient is arbitrarily retained isotropic even in presence of a magnetic field in fusion plasma applications [39, 40], meaning that only the shear viscosity η_0 and the volumetric viscosity η_v are taken to be non-null.

Table 1.2: Synthetic scheme of the constitutive relation between viscous pressure and symmetric part of velocity gradient, with magnetic field aligned in the positive z-direction.

	$(\overset{\circ}{\nabla}\mathbf{v})^{(s)}xx$	$(\overset{\circ}{\nabla}\mathbf{v})^{(s)}yy$	$(\overset{\circ}{\nabla}\mathbf{v})^{(s)}zz$	$(\overset{\circ}{\nabla}\mathbf{v})^{(s)}xy$	$(\overset{\circ}{\nabla}\mathbf{v})^{(s)}yz$	$(\overset{\circ}{\nabla}\mathbf{v})^{(s)}xz$	$\nabla\cdot\mathbf{v}$
$\mathring{\Pi}_{xx}$	$\eta_0 - 2\eta_2 B^2 - \eta_4 B^4$	$-\eta_4 B^4$	0	$-2\eta_1 B - 2\eta_3 B^3$	0	0	ζB^2
$\mathring{\Pi}_{yy}$	$-\eta_4 B^4$	$\eta_0 - 2\eta_2 B^2 - \eta_4 B^4$	0	$2\eta_1 B + 2\eta_3 B^3$	0	0	ζB^2
$\mathring{\Pi}_{zz}$	$-2\eta_4 B^4$	$-2\eta_4 B^4$	η_0	0	0	0	$-2\zeta B^2$
$\mathring{\Pi}_{xy}$	$\eta_1 B + \eta_3 B^3$	$-\eta_1 B - \eta_3 B^3$	0	$\eta_0 - 2\eta_2 B^2$	0	0	0
$\mathring{\Pi}_{yz}$	0	0	0	0	$\eta_0 - 2\eta_2 B^2$	$\eta_1 B$	0
$\mathring{\Pi}_{xz}$	0	0	0	0	$-\eta_1 B$	$\eta_0 - 2\eta_2 B^2$	0
$\mathrm{tr}\,\Pi$	ζB^2	ζB^2	$-2\zeta B^2$	0	0	0	$-\eta_v$

We conclude this Section showing how Onsager's reciprocal relations apply in this context to the constitutive equations between thermodynamic fluxes and forces. We assign a label k to each pair of conjugate thermodynamic fluxes and forces. The constitutive equation between the thermodynamic flux of label i and the thermodynamic force of label j is provided by the T_1^1 tensor $L_{i,j}$. The subscripts are here necessary to identify the tensor function, and do not refer to components in a Cartesian reference frame. Due to the microscopic reversibility of the laws of motion, the following Onsager's reciprocal relations are valid [23],

$$L_{i,j}(\mathbf{B}) = L_{j,i}(-\mathbf{B})^T \tag{1.94}$$

These reciprocal relations do not add any new information respect to the spatial symmetry constraint (1.87) for conjugate thermodynamic fluxes and forces pairs. On the other hand, the simultaneous consideration of the spatial symmetry constraint (1.87) and Onsager's reciprocal relations (1.94) leads to

$$L_{i,j}(\mathbf{B}) = L_{j,i}(\mathbf{B}) \tag{1.95}$$

also for $i \neq j$. Onsager reciprocal relations hence allow to greatly reduce the number of independent coefficients to determine in order to assign the constitutive Equations which close the MHD problem. It is worth to notice as these relations have a precise effect on the entropy production. Namely, the Hall effect relating non-conjugate fluxes and forces is not responsible for a net entropy production. The same was clearly true for conjugate fluxes and forces, and Onsager reciprocal relations extend this property to non-conjugate fluxes and forces.

In our study we are concerned with three pairs of conjugate vector thermodynamic fluxes and forces. Taking the entropy production representation for vector phenomena (1.74b), we have the conjugate flux-force pairs reported in Table 1.3, in particular there are three vector fluxes and three vector forces, for a total of 9 possible couples. The spatial symmetry constraints reduce the number of independent coefficients to assign from 9 for each possible flux-force pair, hence 81, to 3 per constitutive Equation, hence 27. Further, Onsager reciprocal relations allow to identify coefficients regulating cross-effects, requiring finally to assign only 18 coefficients to determine uniquely the linear constitutive Equations. It is common in fusion applications to neglect the cross-effects between heat flux and electromagnetic field and between the electric current and temperature gradient. The cross effects between different diffusion phenomena may be expected to be particularly important, since collisions

Table 1.3: Resume of the conjugate thermodynamic fluxes and forces according to the entropy production form (1.74b).

Order	Fluxes	Forces
Even	J_r	A_r
	$\mathrm{tr}(\Pi)$	$\nabla \cdot \mathbf{v}$
	$\mathring{\Pi}^{(s)}$	$\mathring{\nabla \mathbf{v}}^{(s)}$
Odd	$\mathbf{K}_{\mathbf{q}}^{*}$	$-\nabla T/T$
	$\mathbf{i}^{*}$	$-\partial \mathbf{A}/\partial T + \mathbf{v} \times \nabla \times \mathbf{A} - \nabla \left(\phi + \phi_{\mu}^{*}\right)_T$

between the distinct fluid particles take place. It is not important which particular representation is chosen, hence the actual choice of the forces and fluxes, provided that all the choices preserve Onsager reciprocal relations.

As an example we report the constitutive Equation for the electric current density in the fluid reference frame $\mathbf{i}^*$ when the plasma is fully ionized, hence $c_a = 0$ and we may neglect neutrals diffusion, with the above mentioned choice of conjugate flux-force pairs,

$$\mathbf{i}^* = \underline{\sigma} \left(\mathbf{E} + \mathbf{v} \times \mathbf{B} - \nabla \phi_{\mu}^{*}|_T\right) + \underline{\sigma_{\mathbf{TH}}} \left(-\frac{\nabla T}{T}\right) \tag{1.96}$$

With the entropy production representation (1.74a) the constitutive equation would be,

$$\mathbf{i}^* = \underline{\sigma}' \left(\mathbf{E} + \mathbf{v} \times \mathbf{B} - \nabla \phi_{\mu}^{*}\right) + \underline{\sigma_{\mathbf{TH}}}' \left(-\frac{\nabla T}{T}\right) \tag{1.97}$$

Clearly, in order for the two constitutive equations to be equivalent,

$$\underline{\sigma}' = \underline{\sigma}, \quad \underline{\sigma_{\mathbf{TH}}}' = \underline{\sigma_{\mathbf{TH}}} - T s_q \underline{\sigma} \tag{1.98}$$

where

$$s_q = \frac{m_{e,i}}{e} \left(s_i - s_e\right). \tag{1.99}$$

1.8 Local Neutrality

The hypothesis of local neutrality is of central importance in nearly all plasma MHD theories, and most of the literature, following the definition of Langmuir

[3, 4, 11], define a plasma as a locally neutral ionized gas. The justification of this property for the space and time scales of interest is related to the *Debye shielding* theory [11, 19]. The plasma is assumed to be in local thermodynamic equilibrium, so that partial pressures, particle densities and temperature are well defined quantities, moreover the temperature and the ion density are taken to be homogeneous in the sample, *i.e.* $T(\mathbf{x}) = T_0$, $n_i(\mathbf{x}) = n_0$. No magnetic field is present, so that we can take $\mathbf{E} = -\nabla\phi$. The electron inertia is neglected, so that electrons are always in mechanical equilibrium under the action of the electron pressure gradient $-\nabla p_e$ and the Lorentz force $en_e\nabla\phi$,

$$\nabla\left(\phi - \frac{k_B T}{e}\log n_e\right) = 0. \tag{1.100}$$

The above equilibrium constraint, together with the conditions of regularity at infinity for the scalar potential, suggests to take $n_e = n_0\mathrm{exp}(e\phi/k_B T)$. Gauss law then takes the form:

$$\nabla^2\phi = -\frac{n_0 e}{\varepsilon_0}\left[1 - \exp\left(\frac{e\phi}{k_B T}\right)\right] - \frac{q_{ext}}{\varepsilon_0} \tag{1.101}$$

In the hypothesis $e\phi/k_B T \ll 1$, the above Equation reduces to

$$\nabla^2\phi - \left(\frac{1}{\lambda_D}\right)^2\phi = -\frac{q_{ext}}{\varepsilon_0} \tag{1.102}$$

where we have introduced the *Debye length*,

$$\lambda_D = \sqrt{\frac{\varepsilon_0 k_B T}{n_0 e^2}}, \tag{1.103}$$

If we take the external charge distribution to be a localized point charge placed in the origin of our reference system, *i.e.* $q_{ext} = Q\delta(\mathbf{r})$, we easily obtain the Green function for the electrostatic potential [11, 19]:

$$\phi(r) = \frac{Q}{4\pi\varepsilon_0 r}\exp\left(-\frac{r}{\lambda_D}\right) \tag{1.104}$$

The Green function (1.104) indicates as the electrostatic potential of a any point charge is shielded within few Debye lengths. Hence when the space scale of interest is much greater than the Debye length the plasma can be regarded as locally neutral. This is generally the case of fluid models for tokamak plasmas, where the typical temperature and densities are responsible for a Debye length quite smaller than the typical dimension of the fluid element.

Once the hypothesis of local neutrality is accepted, quite much of the model set up is automatically solved. Indeed, we can set $q = 0$, while up to now q was a state variable to determine self-consistently, in the same stream as the plasma mass density ρ. Now that the electric charge density does not vary in time, the electric current density is divergence-free, *i.e.* $\nabla \cdot \mathbf{i} = 0$. Clearly, this also implies that displacement current are dropped for consistency, hence the validity of Ampère's law $\nabla \times \mathbf{B} = \mu_0 \mathbf{i}$. The electric field disappears structurally from the problem, as the only source of electric field is given now by magnetic flux variations. Most importantly, Poisson Equation is dropped from the model. Finally, we are discarding quite much information within Ohm's law. This is slightly subtle: plug *Ohm's law* (1.96), where we multiplied both therms by the resistivity $\underline{\eta}$, within Faraday's law. This way we provide an evolution equation for the magnetic field, where the electric field disappears,

$$\nabla \times (\underline{\eta} \mathbf{i}) = -\frac{\partial \mathbf{B}}{\partial t} + \nabla \times (\mathbf{v} \times \mathbf{B}) \tag{1.105}$$

The conservative electromotive force $\nabla \phi_\mu^*$ does not play any role in this respect, and clearly only the rotational part of the electric field is involved in this relation (*i.e.* $-\partial \mathbf{A}/\partial t$ in the Coulomb gauge).

We now discuss how the Debye theory is recovered in the framework of the thermodynamic model developed so far. Besides being a consistency check, this discussion provides indications on why the local neutrality hypothesis keeps to be well satisfied on the space scale of interest for a larger set of operating conditions than the ones assumed to obtain (1.100).

We adopt the Coulomb gauge, and consider a plasma at rest (*i.e.* $\mathbf{v} = 0$) with a uniform conductivity $\underline{\sigma}$. In these conditions, if we take the divergence of Ohm's law, and consider the continuity Equation for the electric charge, we get

$$\frac{\varepsilon_0}{\sigma} \frac{\partial q}{\partial t} = \varepsilon_0 \cdot \left(\nabla^2 \phi + \nabla^2 \phi_\mu^* \right) \tag{1.106}$$

Due the high conductivity of a ionised gas, the time of relaxation of the electric charge is extremely small, *i.e.* $\tau = \varepsilon_0/\sigma \to 0$. Hence, we get $\nabla^2 \phi = -\nabla^2 \phi_\mu^*$. This is not dissimilar to what we found earlier, indeed for uniform temperature and ion density:

$$\nabla \phi_\mu^* = -\frac{k_B T}{e} \nabla \log n_e \tag{1.107}$$

Hence, we recover exactly the Debye theory formulated at the beginning of this Section, even in presence of a stationary current density. Let us go through the immediately successive non-trivial example. This time we suppose directly to have a steady state divergence-free current density. Suppose now there is a discontinuity of the conductivity in the direction of the current density flow. Due to the continuity of the normal component of the current density, a discontinuity in the normal component of the electric field would exist in a standard Ohmic conductor. Here part of this discontinuity can be accommodated in a discontinuity for $\nabla\phi^*_\mu$. Moreover we expect an eventual accumulation of charge to be shielded within few Debye lengths.

Let's go further and consider still a different situation: the conductivity and the temperature are still homogeneous but the barycentric velocity is allowed to vary. The magnetic field is certainly present due to the presence of a plasma current and eventual external currents. Again we take $\varepsilon_0/\sigma \to 0$, so that by means of Gauss law, we get

$$\frac{q}{\varepsilon_0} = \nabla^2\phi^*_\mu + \nabla\cdot(\mathbf{v}\times\mathbf{B}) \tag{1.108}$$

The electric charge density that would have appeared in absence of $\nabla\phi^*_\mu$ is clearly given by

$$\varepsilon_0\left(\mathbf{B}\cdot\omega - \mu_0\mathbf{i}\cdot\mathbf{v}\right), \tag{1.109}$$

where we indicated by $\omega = \nabla\times\mathbf{v}$ the fluid velocity vorticity. If we consider this as an applied external charge, we again expect that the force $\nabla\phi^*_\mu$ is responsible for its shielding in few Debye lengths. Theoretically, one may pretend that the separation of charge is in instantaneous phenomenon. The static relation between the electric charge and other fields would be offered in particular by

$$\varepsilon_0\nabla\cdot\left[\underline{\sigma}\ \left(\mathbf{E}+\mathbf{v}\times\mathbf{B}-\nabla\phi^*_\mu\right)\right] = 0 \tag{1.110}$$

which we may decide to use, in lieu of $q = 0$. In general it is retained that the electromotive forces and the conductivity inhomogeneities do not alter really much the result $q = 0$, which is then used greatly simplifying the model.

Not surprisingly at this point, the actual form postulated for Ohm's law is not standard in the tokamak literature. Any electromotive force which is conservative in the plasma, does not really alter the results as illustrated in (1.105), since $q = 0$ is rather imposed than obtained self-consistently. In principle, the local neutrality should be found solving the electric charge conservation equation (1.48) or, still quite precisely, imposing the electric current to be divergence-free. In Ref. [40] the generalized force is taken to be $\mathbf{E} + \mathbf{v} \times \mathbf{B}$. In the same work, they have $\mathbf{E} = -\frac{\partial \mathbf{A}}{\partial t}$, considering the gauge condition of Weyl, hence eventually $\nabla \cdot \mathbf{A} \neq 0$. In numerical implementations of Refs. [41, 39], the conjugate force to the electric current is rather taken from the entropy production representation (1.74b). The gradient component of the generalized force is retained in the model, and further corrective terms appear, including those related to viscosity. In these models they only neglect the term proportional to the ion pressure gradient, since it is of order $m_{e,i}/m_i$ respect to the electron pressure gradient. Finally they do not provide a coupling of the electric current with the temperature gradient, hence retaining the entropy production form (1.74b) "diagonalizes" the constitutive equations. In any of these cases, the curl-free part of the force driving the current will somehow disappear from the model, due to the assumed local neutrality.

1.9 The standard single fluid model

In many practical applications enough physics to describe the phenomena of interest is still captured by the following assumptions:

- The temperature is high enough to retain that the neutral fluid concentration is negligible as compared to the concentration of positive ions and free electrons, according to Saha Equation (1.44), *i.e.* $c_a = 0$;

- Inhomogeneities of the conductivity and magnetic effects do not alter very much the thermodynamic equilibrium situation described in previous Section, making the ionised gas locally neutral on the space scale of interest, *i.e.* $q = 0$ ($\overline{c_i} = \overline{c_e} = 1/2$);

- As already assumed, the various gas species within our mixture are altogether in local thermal equilibrium, allowing to define a unique temperature, *i.e.* $T_i = T_e = T$.

Under these circumstances we can take as state variables the mass density ρ, the barycentric velocity $\mathbf{v}$, the temperature T, and the magnetic flux density $\mathbf{B}$. The conservation laws assume the form:

$$
\begin{aligned}
&(a) \quad \frac{\partial \rho}{\partial t} + \nabla \cdot (\rho \mathbf{v}) = S_\rho \\
&(b) \quad \rho \frac{\mathrm{d}}{\mathrm{d}t}\mathbf{v} + S_\rho \mathbf{v} = -\nabla p - \nabla \cdot \Pi^{(s)} + \mathbf{i} \times \mathbf{B} + S_{\rho \mathbf{v}} \\
&(c) \quad \rho \frac{\mathrm{d}}{\mathrm{d}t} u + S_\rho u = \\
&\qquad - \nabla \cdot \mathbf{K_q} - p \nabla \cdot \mathbf{v} - \underline{\mathbf{\Pi^{(s)}}} : \nabla \mathbf{v} + \mathbf{i} \cdot (\mathbf{E} + \mathbf{v} \times \mathbf{B}) + S_{\rho u}
\end{aligned}
\tag{1.111}
$$

For completeness we included here some production terms, related to physical phenomena which we are not describing self-consistently but rather providing as forcing terms. The hypothesis of local thermodynamic equilibrium allows to enforce the Equation of State, hence relating the internal energy and kinetic pressure to the fluid temperature:

$$
(d) \quad \rho u = \frac{3}{2} p = \frac{3}{2} \frac{\rho}{m_a} k_B T \quad \rightarrow \quad u = \frac{3}{2} \frac{k_B T}{m_a} \tag{1.112}
$$

Maxwell Equations in the Magneto-Quasi-Static limit provide the evolution equations for the magnetic field:

$$
\begin{aligned}
&(e) \quad \frac{\partial \mathbf{B}}{\partial t} = -\nabla \times \mathbf{E} \\
&(f) \quad \nabla \times \mathbf{B} = \mu_0 \mathbf{i} \\
&(g) \quad \nabla \cdot \mathbf{B} = 0
\end{aligned}
\tag{1.113}
$$

The closure for the system of Equations (a)-(g) is now provided by the Non-equilibrium Thermodynamics considerations discussed in this Chapter. In particular we claim the entropy production expression (1.74b) "decouples" the linear closure Equations, *i.e.*

$$
\begin{aligned}
&(h) \quad \mathbf{K_q} = -\underline{\gamma} \cdot \nabla T - \frac{5}{2} \frac{k_B T}{e} \mathbf{i} \\
&(i) \quad \mathbf{i} = \underline{\sigma} \left[\mathbf{E} + \mathbf{v} \times \mathbf{B} \right] \\
&(l) \quad \underline{\mathbf{\Pi^{(s)}}} = \underline{\underline{\eta}} \cdot \nabla \mathbf{v}
\end{aligned}
\tag{1.114}
$$

In order to set up the constitutive Equation (h) we exploited the circumstance $m_e \ll m_i$, besides the assumed local electrical neutrality of the fluid, $q = 0$. The constitutive Equation (i) is Ohm's law, where $\mathbf{E} + \mathbf{v} \times \mathbf{B}$ is the electric field felt by the the fluid element in its motion. It was found here taking

$\nabla \left(\phi + \phi^*_\mu\right)_T = 0$, since we observed that the curl-free part of the force is unimportant in the hypothesis $q = 0$. Moreover $q = 0$ was found in thermodynamic equilibrium as approximate consequence of this force balance. All the tensor fields above $\{\underline{\gamma},\ \underline{\sigma}, \underline{\underline{\eta}}\}$ are functions of the thermodynamic variables $\{\rho, T\}$ besides of the magnetic field, which also determines the structure of such tensors, as illustrated in Section 1.7. We notice that constitutive relation (1.114h) extends classical Fourier's law to account for the internal energy brought by diffusion phenomena within the gas mixture.

The system of Equations (a)-(l) describes already a quite wide range of phenomena of interest, and in next Chapter we will describe some state of the art numerical models to solve similar sets of Equations for simulating tokamak plasmas.

1.10 The plasma-wall interface

In the study of plasmas, a certain interest was always devoted to those *electric circuits* constituted at the same time by the ionised gas and the surrounding solid conductors. It is the case for example of an Argon lamp discharge, where a voltage is applied to the gas through electrodes. In the tokamak literature, the shared electric currents between plasma and solid walls are defined as *halo currents* [42, 43]. Their formation is a threat to the integrity of the device: their presence is generally responsible for dangerous electromagnetic forces on structures [44]. It is clear that *halo currents* in tokamaks, as well as shared plasma-wall currents in general, have a key role in the electromagnetic coupling of fluid and solid conductors, hence it is worth to report briefly the key physics at the plasma-wall interface, which also explain the possible boundary conditions to use in the MHD plasma model.

We notice immediately, on fundamental physical grounds, that the gas cannot penetrate the solid wall surface, unless peculiar absorption properties are accounted. This provides with the widely used boundary condition:

$$\rho \mathbf{v} \cdot \hat{\mathbf{n}} = 0 \tag{1.115}$$

at the interface between the plasma and solid structures. The further fundamental consideration is that, on the scale length of interest, the electric current density should be solenoidal, in accordance with the *Magneto Quasi Static* (MQS) approximation,

$$\mathbf{i} \cdot \hat{\mathbf{n}}\Big|_{pl} - \mathbf{i} \cdot \hat{\mathbf{n}}\Big|_{w} = 0 \tag{1.116}$$

This is true even in the general case where ionization and recombination phenomena take place, as there is no macroscopic charge accumulation. A further boundary condition is anyway still missing, as there are three gas species in the mixture: electrons, positive ions and neutrals.

1.10.1 Bohm Criterion

The remaining boundary condition is deduced from more subtle considerations, which are beyond the hypothesis of local neutrality and local thermodynamic equilibrium. In order to grasp the key aspects it is convenient to first consider a cold-ion plasma, where $T_i = 0$. On the other hand, electrons have their own approximately thermal motion, which we may define as "fractional"-Maxwellian [33]. Indeed thermal electrons moving towards the wall surface are captured by the wall, and hence not scattered back into the plasma. At the wall surface we may consider exactly *half* of the Maxwellian distribution of electron velocities as cut-off due to this mechanism. Moreover the mean velocity of the underlying Maxwellian is retained null at the wall surface. The wall surface charges negatively, as a consequence of the incident electrons, and a positive space charge region develops in the nearby plasma. The result is a space charge layer which tends to repel the plasma thermal electrons. The plasma-wall interface region where quasi-neutrality is broken and large variations of the electric charge density takes place is defined as *plasma sheath* [33, 45]. We shall see that the characteristic length of this region is indeed the *Debye* length. In the perspective of an MHD scientist, this region is infinitesimally thin in extent, at least until the Debye length is small compared to the characteristic dimensions defining the fluid element (*e.g.* the Larmor radius or the mean free paths for the different collisions taking place [46]). The description of the plasma-wall interface is hence beyond the *locally-neutral* MHD modelling capabilities. Accurate account of the electric charge distribution at the interface is needed to provide a further boundary boundary condition to the MHD problem.

The dynamics of formation of the space charge layer can be retained essentially instantaneous from the MHD perspective. In order to find the most important implication of the sheath formation, let us assume that the electron temperature can be retained homogeneous throughout our sample. We moreover retain the sheath essentially collision-less, this hypothesis will reveal valid any time the *Debye length* is sufficiently shorter than the mean free path between collisions. We now consider a simplified 1D problem where a quasi-neutral plasma face an infinitely extended solid wall. The plasma quantities area allowed to vary only along the x direction, perpendicular to the wall. We may well describe the situation via the simple model proposed in [45]:

$$\begin{aligned}
&(a) \quad n_i v_i = n_{i,0} v_{i,0} \\
&(b) \quad m_i v_i \frac{\partial v_i}{\partial x} = -e \frac{\partial V}{\partial x} \\
&(c) \quad \frac{k_B T_e}{n_e} \frac{\partial n_e}{\partial x} = +e \frac{\partial V}{\partial x} \\
&(d) \quad \frac{\partial^2 V}{\partial x^2} = -\frac{q}{\varepsilon_0} = \frac{e}{\varepsilon_0} (n_e - n_i)
\end{aligned} \tag{1.117}$$

In this context the eventual net current density in the plasma does not play a role, *i.e.* its role is fully accounted at the MHD scale. At the *plasma-sheath* scale the electrostatic effects are predominant. The set of Equations above is complemented by the boundary conditions at the plasma side:

$$\begin{aligned}
&(\alpha) \quad n_e = n_i = n_0 \\
&(\beta) \quad V = 0 \\
&(\gamma) \quad \frac{\partial V}{\partial x} = \frac{\partial n_e}{\partial x} = \frac{\partial n_i}{\partial x} = 0
\end{aligned} \tag{1.118}$$

It is convenient to normalize the set of Equations (1.117-1.118), defining

$$\eta = -\frac{eV}{k_B T_e}, \quad N_e = \frac{n_e}{n_0}, \quad N_i = \frac{n_i}{n_0}, \quad u_i = \frac{v_i}{c_s} \tag{1.119}$$

where we introduced the *single fluid sound speed*

$$c_s = \sqrt{\frac{k_B T_e}{m_i}} \tag{1.120}$$

After some algebra, Equations (1.117-1.118) are transformed into

$$\frac{\mathrm{d}^2 \eta}{\mathrm{d}x^2} = \frac{1}{\lambda_D^2} \left[\frac{1}{\sqrt{1 + \frac{2\eta}{u_{i,0}^2}}} - e^{-\eta} \right] \tag{1.121}$$

Here λ_D is the Debye length obtained for the electron density and temperature at the sheath entrance. In the limit $\eta \ll 1$ Equation (1.121) is approximated as

$$\frac{\mathrm{d}^2\eta}{\mathrm{d}x^2} = \frac{1}{\lambda_D^2}\left(1 - \frac{1}{u_{i,0}^2}\right)\eta \tag{1.122}$$

The electric potential distribution within the sheath is monotonic, and non-oscillating, solely in the hypothesis

$$u_{i,0} \geq 1 \quad \leftrightarrow \quad v_{i,0} \geq c_s \tag{1.123}$$

The latter is the *Bohm* criterion for the ion velocity. This constraint guarantees in particular that the electron density decrease towards the wall faster than the ion density [47, 46]. In normal situation the above criterion is *marginally* satisfied, *i.e.* is satisfied with the equality sign [48, 46]. Correctly considering the ion temperature, keeping the hypothesis of isothermal flow, the fluid sound speed is corrected to [49, 46]:

$$c_s = \sqrt{\frac{k_B\left(T_i + T_e\right)}{m_i}} \tag{1.124}$$

From the above discussion we may conclude that a valid candidate boundary condition for the MHD problem is represented by

$$\mathbf{v_i} \cdot \mathbf{n} = c_s \tag{1.125}$$

The non-penetration condition (1.115), implies clearly that for any ion impinging the wall there will be a released neutral particle, *i.e.* $\mathbf{v_a} \cdot \hat{\mathbf{n}} = -\mathbf{v_i} \cdot \hat{\mathbf{n}}$. Since the fluid velocity normal to the boundary is null, while the ion and neutral velocities are as large as the ion acoustic speed, it is quite more robust to retain in the model at least the ionised fluid and the neutral fluid inertia, as done for example in [50].

1.10.2 The pre-sheath

Condition (1.125) requires nonetheless some mechanism within the plasma capable to accelerate ions to this acoustic sound speed. Most importantly, at the sheath edge the actual particle density may differ from the one of the *undisturbed plasma*. This is defined in standard sheath physics literature as that region where we do not observe variations in the particle densities, and the plasma can be retained in thermodynamic equilibrium. A *pre-sheath* region is generally retained to exist where an electric field is still associated to the gradient of particle densities. The actual dimensions of such a layer depends on the actual physical mechanism driving the ions to the Bohm velocity at the sheath entrance. The pre-sheath width can be related for example to some geometrical factor, to the ion mean free path, to the ionization length or to the ion gyroradius [46]. A variety of pre-sheath models is available according to the dominant effect, anyway the essential ingredients of all the models are:

- the pre-sheath is retained a quasi-neutral region;
- the collisionality of electrons is discarded;
- The electron directed velocity is far smaller than the electron thermal velocity.

As a consequence of the last two assumptions, Chodura [51] proposed to discard the $\mathbf{v_e} \times \mathbf{B}$ term in the electron momentum balance Equation, which leads to a Boltzmann relation between electron density and electric potential in the pre-sheath [52]. For example, assuming the acceleration of ions is essentially due to magnetic fields, besides the electric field close to the boundary, the MHD code JOREK [50] impose boundary conditions for the ion velocity at a magnetic pre-sheath entrance [52].

Anyway in our case the definition of *undisturbed plasma* loses some of its features. In a working tokamak, the plasma is purposely out of equilibrium. Thanks to the language set up in previous Sections, we can see that the pre-sheath region could be in principle accounted directly within the fluid model. The low collisionality of electrons in the pre-sheath corresponds to set an infinite conductivity in Ohm's law (1.114i). This suggests that the electric field felt by the ionised fluid in its motion is $\frac{k_B T}{e}\nabla \ln n_e$. Anyway, this is inessential in the momentum transfer Equation for the ionised gas (1.50), since $q = 0$. The fluid acceleration, $\frac{\mathrm{d}\mathbf{v}}{\mathrm{d}t}$ scales already as $\nabla p/\rho \simeq \frac{k_B T}{m_i}\nabla \ln n_e$. Hence, the classic interpretation that ions are accelerated by an electrostatic field is found even in our simple single fluid MHD model[4]. The real definition of "undisturbed" or "bulk" plasma could be then provided as that portion of the plasma where the Bohm condition has no more influence on the pressure gradient.

The consequence of this discussion is that in principle the MHD model contains all the fundamental ingredients to describe the pre-sheath region on the same grounds as the background plasma. The only apparent structural difference is in the collisionality of electrons, which is retained null in the pre-sheath modelling. Observe anyway that this is rather an assumption, and

[4]We are attributing here the inertia of the ionised fluid to ions

we can just be more general and tune correctly the collisionality in proximity of the sheath entrance via the electric resistivity. Clearly enough resolution should be provided in order to correctly represent the eventually steep variations of particle density and ion velocity in a thin region close to the sheath. It is indeed important to figure out that the particle density at the sheath and at the pre-sheath entrance may be different, and this difference can be crucial to the correct modelling.

1.10.3 Ion and electron current to the wall

The velocity distribution of electrons in front of the wall is an *half-Maxwellian*: there are no electrons moving from the wall surface to the plasma if electron emission is excluded. Moreover the *foreword-going* distribution of velocity is Maxwellian. The electrons crossing the wall surface are hence given by [45, 33]

$$\Gamma_{e,w} = \frac{1}{4} n_{e,w} v_{th,e}, \tag{1.126}$$

where the thermal speed of electrons is given by

$$v_{th,e} = \sqrt{\frac{8k_B T_e}{\pi m_e}}. \tag{1.127}$$

As we move further and further from the wall towards the plasma the *backward-going* tail of the Maxwellian distribution is gradually recovered. Contextually the electron flux should be kept and the "fractional" Maxwellian has to be shifted. At some point we will recover a full *drifted* Maxwellian distribution, with some mean velocity v_e. In particular the electron flux we have at the sheath entrance $n_0 v_e$ should equal the electron flux we have at the wall, given by (1.126). The actual electron density at the wall is given by the Boltzmann factor, hence we find

$$\Gamma_{e,w} = n_0 \mathrm{e}^{\frac{e\Delta V_w}{k_B T_e}} v_{th,e} \tag{1.128}$$

Here ΔV_w is the voltage difference between the wall and the plasma sheath entrance, and is to be determined by considering the overall experimental situation (*i.e.* the applied voltage differences due to bulk plasma and external conductors). At the same time, the inflow of ions at the sheath entrance provides the ion current density, due to the continuity relation (1.117a),

$$\Gamma_{i,w} = n_0 c_s \tag{1.129}$$

If the wall is a perfect insulator the electron and ion flux should be equal to each other, $\Gamma_{e,w} = \Gamma_{i,w}$, so that the net electric current vanishes. Using expressions (1.128, 1.129) for the fluxes and (1.124, 1.127) for the velocities we can calculate the voltage at such a sheath interface:

$$\frac{e\Delta V_i}{k_B T_e} = \frac{1}{2} \ln \left[\left(2\pi \frac{m_e}{m_i} \right) \left(1 + \frac{T_i}{T_e} \right) \right] \tag{1.130}$$

With this definition we may express the electric current to the wall as

$$j_{w,n} = n_0 c_s \left(1 - \mathrm{e}^{\frac{\Delta V_w - \Delta V_i}{k_B T_e}} \right) \tag{1.131}$$

Equation (1.131) is the desired result: it provides a relation between the voltage drop across the sheath and the actual current flowing from the plasma to the wall. For $\Delta V_w \rightarrow -\infty$ the current saturates to the *ion current saturation value*. In general ΔV_w will be an unknown of the plasma-wall interaction problem. For a straight plasma column, confined within two equal electrodes, the application of a voltage will result in an electric current whose magnitude is always less than the ion saturation value [33]. In this respect the application of a voltage to the sheath modifies the electron flux to the wall. The ion flux is not modified, the Bohm criterion keeping its validity. The overall current density crossing the sheath is hence evidently limited by the ion saturation current. This circumstance should likely be considered in the modelling of *halo currents* in Tokamak devices, and we shall comment a bit more about this point at the end of the next Chapter.

Chapter 2

Interaction of MHD Plasmas and MQS Conductors

In the previous Chapter we presented a sound Thermodynamics framework to build close Magneto-Hydro-Dynamic models. Nonetheless the practical implementation and solution of such a model requires still quite many steps:

- Setting up a functional relation for the coefficients of phenomenological laws in terms of thermodynamic and internal variables, besides of the magnetic field. These relations may depend on the type of experiment and on the operational regime;

- providing proper boundary and initial conditions, significant for the experiment under exam;

- Building a sound numerical approximation for the problem, which allows to deal with all the space and time scales of interest, still using a tractable number of degrees of freedom;

The conductivity parameters for diffusion phenomena and heat fluxes, as well as the viscosities, are normally set up on a phenomenological basis, and they are not object of this Thesis. Instead we are going to present few fundamental ideas of some state of the art *extended* MHD numerical models for tokamak studies. Such models are in the stream of those presented in previous Chapter, and include the energy evolution equation, besides the momentum balance equation, the evolution equation for the mass density, and Faraday's equation in presence of a finite resistivity. The local neutrality hypothesis is still retained satisfied, and in the majority of implemented models the neutral gas is discarded from the analysis. Anyway, further hypothesis are relaxed compared to what illustrated in previous Chapter. For example the inertia and the temperature of the different fluid species are accounted separately in some of the implementations, so to study the relaxation of temperature or the effect of electron inertia on the plasma evolution. Further, the closure relations are postulated relying on different physical models and observations, not necessarily of thermodynamic nature. Namely we will describe the code M3D-C1 [39, 41, 53] in Section 2.1 and the code JOREK [54, 55, 40, 56] in Section 2.2. These Sections will provide an idea on how to fill the gap between models as the one presented in Section 1.9 and their actual solution. The attention is focused on the electromagnetic boundary conditions needed by the MHD models. We will find that the tangential component of the magnetic flux density at the boundary of the computational domain $\mathbf{B} \times \hat{\mathbf{n}}$ needs to be provided at any time instant of the simulation.

Following, in Section 2.4 we describe a convenient integral formulation for solving the eddy current problem in conducting structures, based on the introduction of an electric vector potential and the use of edge shape functions [57]. There we highlight as the magnetic vector potential due to plasma currents should be provided as a forcing term for this model. These preliminary Sections constitute the fundamentals to discuss the possible coupling strategies between extended MHD models and conducting structures models in the remainder of the Chapter.

From that point onwards, the attention will be devoted to the two fundamental aspects of a self-consistent coupling:

- The computation of the correct boundary condition $\mathbf{B} \times \hat{\mathbf{n}}$ at the boundary of the MHD computational domain;

- The evaluation of the magnetic vector potential due to plasma currents in the conducting domain

In order to describe clearly these two aspects, it is convenient to regard the space as essentially split into the *interior* or *inner* domain V_{in} and the *exterior* or *outer* domain $V_{ext} = \mathbb{E}_3 \backslash V_{in}$. Here, the interior domain is essentially the computational domain for the MHD problem, while the exterior domain is the remainder physical space. In the exterior domain we will find the conducting structure domain V_c, where active and passive currents are allowed to circulate. We define the interface which separates the inner and the outer region as *Coupling Surface* and we denote it by $+\partial V_{in}$, since it is the boundary of the MHD

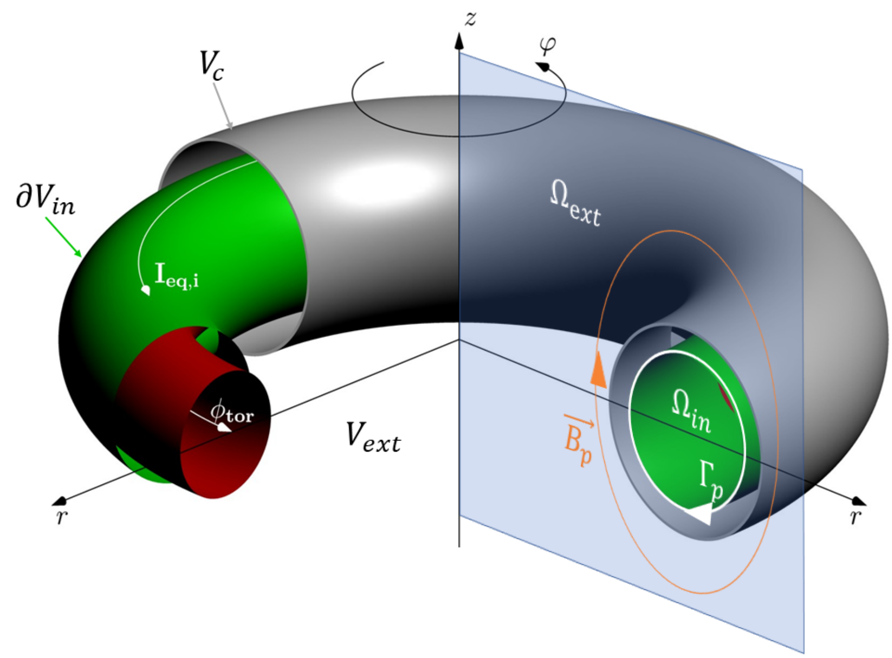

Figure 2.1: Example Geometry for the Coupling problem. The Coupling Surface ∂V_{in} is indicated in Green and bounds the inner domain V_{in}. The remainder space is the exterior domain $V_{ext} = \mathbb{E}_3 \backslash V_{in}$. We indicate also the trace in the poloidal cross-section at $\varphi = 0$ of the inner domain Ω_{in} and of the outer domain Ω_{ext}. The line separating these traces run clock-wise in the direction $\hat{\mathbf{i}}_{\mathbf{u}} = \hat{\mathbf{i}}_{\varphi} \times \hat{\mathbf{n}}$.

computational domain. Some of the notation we will use in the whole Chapter is collected in Figure 2.1. We indicate the trace of the Coupling Surface in the poloidal half-plane $\varphi = 0$, oriented clock-wise, as $+\Gamma_p$. This closed line separates the cross sectional areas of the inner domain Ω_{in} from the cross-sectional area of the outer domain Ω_{ext}. Much of our discussion does not need assumptions about the axisymmetry of the *Coupling Surface*, anyway we will see that this is the case at least for the JOREK and M3D-C1 codes, hence these definitions will prove to be useful.

In the context of tokamak plasmas, the problem of assigning $\mathbf{B} \times \hat{\mathbf{n}}$ at the boundary of the interior domain is generally met when computing the MHD equilibrium configuration. Several strategies are possible to couple a Finite Element formulation of the MHD equilibrium problem within the Coupling Surface, to the solution of the magnetostatic problem in the *exterior* domain [58]. The natural framework in this context is that of *Boundary Element Methods* (BEMs). Essentially, the magnetostatic field problem in the exterior domain is reduced to an integral equation which needs to be satisfied at the boundary of the domain. The possibility to set up such formulas is offered by Green function theorems, as we shall see briefly. The boundary conditions for the exterior problem will appear naturally in the boundary integral equation (either $\mathbf{B}\cdot\hat{\mathbf{n}}$ or $\mathbf{A}\times\hat{\mathbf{n}}$ at the boundary have to be supplied). Similarly, the information about electric currents in the outer domain will be condensed in the magnetic fields and potentials these currents generate at the Coupling Surface. BEMs have the great advantage of not requiring any discretization of the vacuum domain to provide the necessary boundary condition on $\mathbf{B}\times\hat{\mathbf{n}}$. Completely different strategies to describe the electromagnetic coupling with structures are also present in the literature, for example M3D-C1 models both the conductors and the outer vacuum domain within its FEM formulation, up to some point where homogeneous boundary conditions can be retained [59]. This methodology is justified there stressing the non-locality of BEMs, leading to fully populated response matrices, *i.e.* $\mathbf{B}\times\hat{\mathbf{n}}$ at some location of the boundary can be linearly related to $\mathbf{B}\cdot\hat{\mathbf{n}}$ completely elsewhere along the boundary.

In this Chapter, we shall always move in the context of *Boundary Element Methods*. Although most of the concepts presented are general, we will consider as reference models for the coupling JOREK for the plasma and CARIDDI for the structures. Indeed the JOREK-CARIDDI coupling has been the subject of a recent collaboration of my research group with the *fast particles and MHD group* at the *Max-Planck Institute for Plasma Physics* situated in Garching. The first coupling strategy we describe is based on the Virtual Casing Principle, and it is described in Section 2.5. This is in particular the methodology already used for the JOREK-STARWALL coupling [60, 61], and the main alternative currently programmed for the JOREK-CARIDDI coupling. As we shall discuss in some detail in next Chapter, this is also the methodology used in the evolutionary equilibrium MHD model CarMa0NL [62]. The idea is to represent the magnetic vector potential due to plasma currents in the exterior domain via an equivalent surface current distribution at the Coupling Surface. In the context of Boundary Element Methods, this can be retained an *indirect* or *Bielak-MacCamy* method [58]. At the moment, I was involved in the implementation of the relevant routines to extrapolate the equivalent currents to the plasma at the Coupling Surface and in the validation of the magnetic field produced by such equivalent currents in the outer domain. In Section 2.6, two possible *direct* or *Johnson-Nedeléc* BEM formulations are presented [58, 63, 64], respectively in terms of magnetic vector potential and magnetic field[1]. For the magnetic vector potential formulation, the possible implications of the adopted gauge are discussed. We will see that the gauge choice is irrelevant for the computation of the poloidal magnetic field in the axisymmetric case, but generates sensible complications in a fully 3D problem. Anyway, as important by-product of this discussion, we will find a relation between electromagnetic quantities at the Coupling Surface and plasma-induced voltages in conducting structures. Since the wide variety of gauges adopted in extended MHD codes, a whole magnetic field formulation is discussed straight afterwards. We will show that the possibility of inversion of the resulting boundary integral Equation is subject to the topology of the computational domain. The singularity of the related linear system will be associated to the homology group of curves wrapping around the torus, via considerations about the uniqueness of the magnetostatic problem. We discuss there how to make the system invertible, and we show that the topological problem is essentially related to the axisymmetric component of the magnetic field.

The last Section explores the implications of shared injected currents between plasma and structures on the coupling strategies presented. In these scenarios, direct magnetic field formulations keep the feature of not requiring fictitious conducting shells. A critical discussion of the potential advantages and disadvantages of this circumstance concludes the Chapter.

2.1 M3D-C1

The *M3D-C1* form of the resistive MHD single fluid Equations is illustrated in [39], and it is of course quite similar to what we have presented in Section 1.9. There is a difference solely in the relation between viscous stress and gradient of the velocity, which is retained to be isotropic there. Moreover an adiabatic situation is described, hence the heat flux does not play a role.

A more general model within the *M3D-C1* formulation was described in [41]. There the ion and electron fluids are not considered in local thermodynamic equilibrium between each other, meaning they are locally at eventually different temperatures $T_i \neq T_e$. Nonetheless the local electrical neutrality is

[1] I would like to acknowledge N. Schwarz and F. J. Artola for the intense discussions which originated these two formulations during my stay in Garching.

assumed, allowing to consider a single continuity law for the particle density. Moreover electron inertia is neglected, allowing to derive a Generalised Ohm's law from the momentum transfer equation for electrons. Clearly two evolution equations for the internal energies of the two non-isothermal but co-existing fluids should be integrated. An exchange term tends to equalize the temperatures of the two co-existing gas species, consistently with the thermodynamic picture illustrated in Chapter 1. The viscous stresses for electrons and ions needs to be defined separately in such a framework, and in particular $\underline{\Pi_e} \propto \nabla \mathbf{i}$ is retained. Some correction terms for the viscous effects are also considered coming from gyrokinetic models.

In Subsection 2.1.1 we illustrate how the unknown vector fields are represented in terms of stream functions and we define the complete set of projection operators which is used to provide the evolution Equations for the stream functions describing the magnetic field. We will take care of the weak formulation of the problem, in order to evidence how the electromagnetic boundary conditions emerge in the task. This aspect of the M3D-C1 formulation was not illustrated for convenience in [39], although the possibility of using BEMs for coupling the MHD model with the exterior magnetostatic problem was certainly explored with the predecessor M3D [65]. The projection operators used for the momentum balance Equation were presented both in [39] and in [66]. In the latter reference, the partial decoupling of the different MHD dynamics provided by these projection operators is commented, together with the *split-implicit* method used for time-integration. The latter method allows to decouple the time evolution of some of the unknowns of the problem at the expenses of the introduction of higher order spatial derivatives. Details about this integration procedure were discussed in [41, 67].

It is just worth to mention here that M3D-C1 uses a C1-finite element space for the representation of the unknown stream functions. The discretization of the domain is provided by the Cartesian product of triangles in the poloidal plane and segments of toroidal lines along the toroidal angle. The space of solutions is contextually approximated by the tensor product of *reduced-quintic* polynomials in the poloidal plane triangles and *cubic Hermite* functions along the toroidal lines. The *reduced-quintic polynomials* used for representing the stream functions in the poloidal plane were discussed in [53]. The introduction of such elements was motivated there based on the flexibility of triangles in representing complex geometries, and the inherent simplicity of mesh refinement, in conjunction with the expected desirable properties of C1 elements. If we expect the solution to be $C1$-continuous we can immediately discard the non-relevant lower order continuous solutions from our space of test functions. Moreover the $C1$-elements allows to deal directly with weak formulation of partial differential Equations up to the fourth-order, convenient circumstance in view of using the *split-implicit* time integration method.

For the reduced quintic polynomial representation adopted the interpolation error is estimated to be of the order $O(h^5)$, as compared to the $O(h^2)$ of standard linear Lagrange elements[2]. Compared to a full fifth-order polynomial description of some functions ϕ within the triangle element, three degrees of freedom are eliminated enforcing the continuity of the normal derivative of ϕ across triangle edges. This reduces the number of degrees of freedom from 21 to 18 per triangle, besides enforcing the desired $C1$-continuity in the poloidal plane. Six degrees of freedom are associated to each node of the triangle: $(\phi, \partial_r\phi, \partial_z\phi, \partial^2_{r^2}\phi, \partial^2_{z^2}\phi, \partial^2_{r,z}\phi)$. Further 3 degrees of freedom per node will appear due to the tensor product with the cubic Hermite functions along the toroidal angle. The resulting mass-matrices, after the application of the Galerkin method, will have in general a block three-diagonal structure, due to the coupling between adjacent poloidal planes. This symmetry is exploited with proper block Jacobi pre-conditioners before the eventual matrix inversions, as described in detail in [66].

2.1.1 Representation and Projection Operators

The unknown vector fields are taken to be the barycentric velocity $\mathbf{v}$ and the magnetic vector potential $\mathbf{A}$. In a cylindrical coordinate reference system (r, φ, z) these are represented in the following form:

$$\mathbf{v} = r^2\nabla u \times \nabla\varphi + \omega r^2\nabla\varphi + \frac{1}{r^2}\nabla_\perp\chi \tag{2.1}$$

$$\mathbf{A} = r^2\nabla\varphi \times \nabla f + \psi\nabla\varphi - F_0 \ln r\, \hat{\mathbf{i}}_\mathbf{z} \tag{2.2}$$

For the definition of the nabla operator in the poloidal plane $\nabla_\perp$, we refer to Appendix B. The last choice is compatible with the gauge condition $\nabla \cdot \left(\mathbf{A}/r^2\right) = 0$ and implies, by consecutive application of the curl operator, the following representation for the magnetic flux density and electric current density:

[2] h is the typical linear dimension of mesh edges.

$$\begin{aligned} \mathbf{B} &= \nabla\psi \times \nabla\varphi + F^* \nabla\varphi \\ \mathbf{i} &= \nabla F^* \times \nabla\varphi + \frac{1}{r^2}\nabla_\perp \frac{\partial\psi}{\partial\varphi} - \Delta^*\psi\nabla\varphi \end{aligned} \tag{2.3}$$

where

$$F^* = F_0 + r^2 \nabla\cdot\nabla_\perp f + \frac{\partial^2 f}{\partial\varphi^2} \tag{2.4}$$

Such expressions for the magnetic field, electric current density and flow velocity can now be replaced in the single fluid MHD Equations. In particular we provide as an example here solely the evolution Equation for the magnetic flux density, obtained plugging Ohm's law in Faraday's Equation:

$$\frac{\partial\mathbf{B}}{\partial t} = -\nabla\times\left(\underline{\eta}\mathbf{i}\right) + \nabla\times(\mathbf{v}\times\mathbf{B}) \tag{2.5}$$

Before going through a weak formulation for the coupled system of Partial Differential Equations, each of the vector field evolution Equations is projected on three orthogonal subspaces. These projections, together with the adopted representations (2.1)-(2.3a), allow to isolate the evolution Equations for each stream function. The projection operators adopted for the magnetic flux density evolution Equation are:

$$\begin{aligned} &(a) \quad \nabla\varphi\cdot\nabla_\perp\times[(\mathrm{Eq.})] \\ &(b) \quad \nabla\varphi\cdot(\mathrm{Eq.}) \\ &(c) \quad \nabla\cdot[(\mathrm{Eq.})] \end{aligned} \tag{2.6}$$

In particular the last projection (2.6c) is unnecessary since the indivergence of $\mathbf{B}$ is automatically satisfied due to the chosen representation. The projection operators used for the momentum transfer Equation and further details can be found in [39].

A Galerkin method can then be applied, taking the weak form of the projected evolution equations. Hence, these evolution equations for the stream functions are first multiplied by a test function $\nu_i(r,\varphi,z)$ and then integrated over the computational volume. Each test function determines an algebraic Equation. The axisymmetry of the computational domain allows to first integrate over a poloidal plane, and later along the toroidal angle. It is worth stressing that besides the domain is axisymmetric, scalar and vector fields are allowed to be fully three-dimensional. Quite much details of this procedure were discussed in [39], although an important step was omitted there[3]: the rigorous consideration of surface terms coming out from the Galerkin method. Indeed such surface terms were considered to vanish. We show here how this approximation is precisely enforcing some boundary condition, for the PDE problem. The discussion reveals how to extend that picture to consider different boundary conditions.

In particular, the neglect of such surface terms forces M3D-C1 to either treat the conducting wall as ideal or to encapsulate the conducting and vacuum domain within the computational domain [59].
Here we project via the operator (2.6a) the magnetic field evolution Equation (2.5) and consider the weak form of such projected Equation. In order to focus the attention on key aspects, we consider the resistivity to be isotropic and assigned, and the fluid velocity to be zero.Leaving the toroidal angle integration as a successive step, after some algebra we get the evolution equation ($\mathrm{d}^3\mathbf{r} = r\,\mathrm{d}^2\mathbf{r} = r\,\mathrm{d}r\,\mathrm{d}z$):

$$
\begin{aligned}
&-\int_{\Omega_{in}} \frac{1}{r^2}\left(\nu_i,\dot{\psi}\right) r\,\mathrm{d}^2\mathbf{r} + \int_{\Gamma_p} \frac{\nu_i}{r}\frac{\partial\dot{\psi}}{\partial n}\,\mathrm{d}\ell = \\
&+\int_{\Omega_{in}} \frac{\eta}{r^2}\Delta^*\nu_i\Delta^*\psi r\,\mathrm{d}^2\mathbf{r} \\
&-\int_{\Omega_{in}} \frac{\eta}{r^2}\left\{\nu_i,\frac{\partial F^*}{\partial\varphi}\right\} r\,\mathrm{d}^2\mathbf{r} - \int_{S_{fw}} \frac{1}{r^2}\frac{\partial\eta}{\partial\varphi}\left\{\nu_i,F^*\right\} r\,\mathrm{d}^2\mathbf{r} \\
&-\int_{\Omega_{in}} \frac{\eta}{r^4}\left(\nu_i,\frac{\partial^2\psi}{\partial\varphi^2}\right) r\,\mathrm{d}^2\mathbf{r} - \int_{S_{fw}} \frac{1}{r^4}\frac{\partial\eta}{\partial\varphi}\left(\nu_i,\frac{\partial\psi}{\partial\varphi}\right) r\,\mathrm{d}^2\mathbf{r} \\
&-\int_{\Gamma_p} \frac{\nu_i}{r}\frac{\partial}{\partial n}\left(\eta\Delta^*\psi\right) - \eta\frac{\Delta^*\psi}{r}\frac{\partial\nu_i}{\partial n}\,\mathrm{d}\ell \\
&+\int_{\Gamma_p} \frac{\nu_i}{r}\frac{\partial}{\partial\varphi}\left(\eta\nabla F^*\times\nabla\varphi\right)\cdot\mathbf{n}\,\mathrm{d}\ell \\
&+\int_{\Gamma_p} \frac{\nu_i}{r}\frac{\partial}{\partial\varphi}\left(\frac{\eta}{r^2}\nabla_\perp\frac{\partial\psi}{\partial\varphi}\right)\cdot\mathbf{n}\,\mathrm{d}\ell
\end{aligned}
\tag{2.7}
$$

It is interesting to notice that the last three terms at the right hand side are certainly null whenever the current is not allowed to circulate on the boundary of our axisymmetric domain. Even in this case at the left hand side, we find a boundary term involving the time derivative of $(1/r)\partial\psi/\partial n$ at the boundary,

[3] since it was not important for that discussion

which is related with the tangential component of the magnetic field. This is not a coincidence: the magnetic flux density tangent to the boundary should be provided as a boundary condition to the MHD problem. Nonetheless, if we take a boundary far enough from the plasma we may impose homogeneous Dirichlet boundary conditions and neglect also such a term. This was the strategy adopted for simulating the mutual plasma-structure interaction in [59], where the structures and the vacuum domain are modelled within the M3D-C1 computational boundary.

2.2 JOREK

The extended MHD code JOREK solves a variety of MHD physical models in toroidal geometry, based on different approximations or studies objectives [56]. Within the JOREK code we may solve models which eventually include a description of neutrals [68], ablation models for pellet injection [69, 70], fluid models for runaway electrons [71, 72], separate description of ion and electron temperatures [73], just to quote a few non-trivial extensions. The code was anyway initially thought for simulating Edge Localized Modes [55, 61] and the main *reduced* and *full* MHD models were described in some detail respectively in [74] and [40, 75].

The fundamentals of the finite element space implemented were presented in [54]: while a Fourier decomposition is adopted along the toroidal angle, the poloidal cross-section is discretized via Bézier surfaces. Bernstein polynomials are used as test functions to implement an iso-parametric C1 finite element space. Between the advantages of using such an isoparametric approach there is the possibility to fit the curved elements to the initial magnetic flux map. We will describe briefly Beziér finite element space in subsection 2.2.2.

It is certainly worth mentioning that main JOREK models for the plasma were also coupled to the eddy current code STARWALL [60, 61]. The coupling allows for free-boundary plasma simulations, which greatly extended the prediction capabilities of simulations. We will widely comment about the JOREK-STARWALL coupling in later Sections, as the electromagnetic interaction of the tokamak plasma with the conducting structures is the real focus of this Chapter. The main limitation of the STARWALL code is that only includes the possibility of modelling thin conductors. Recently endeavours for the self consistent coupling of JOREK with the fully volumetric 3D eddy current code CARIDDI are ongoing, and we shall comment the first steps in this direction.

Different time integration schemes are allowed for advancing the stream functions and potentials in time. In particular two numerical parameters are introduced, which allow to choose between the implicit-Euler, the Crank-Nicholson and the Gears time integration schemes, besides all the combinations in between. Details on the time discretization will be presented later when discussing the JOREK-CARIDDI coupling via the Virtual Casing Principle approach.

2.2.1 Models and representations

In Tokamaks the toroidal magnetic fields applied by external coils is generally much larger than the toroidal magnetic field generated by plasma currents. In first approximation, hence we may retain the toroidal field to be constant in time and varying as $1/r$ within the first wall,

$$\mathbf{B} = F_0 \nabla\varphi + \nabla\psi \times \nabla\varphi \tag{2.8}$$

Here F_0 is constant, and we may define the stream function ψ as poloidal flux. It is worth noticing that ψ is not necessarily axisymmetric, *i.e.* $\psi = \psi(r, \varphi, z)$. Moreover, the *reduced MHD* representation (2.8) makes the poloidal magnetic field divergence-free on its own, which is a rigorously true feature of axisymmetric problems. One may correctly argue that this representation does not allow for the circulation of poloidal currents, however these are recovered assuming that the poloidal currents needs to provide the MHD equilibrium at each time step (*i.e.* the inertial force is replaced by the $\mathbf{j_{pol}} \times \mathbf{B}_\varphi$ force). In this *reduced-MHD* framework the velocity field is represented by [74, 61]

$$\mathbf{v} = v_\parallel \mathbf{B} + r^2 \nabla u \times \nabla\varphi \tag{2.9}$$

If compared with the M3D-C1 representation reported in (2.1) you see immediately that the toroidal flow and the curl$_\perp$-free $(r^2\mathbf{v})$ contribution to the poloidal flow are essentially attributed to the flow along magnetic field lines. The term $r^2\nabla u \times \nabla\varphi$ is instead normally attributed to the $\mathbf{E}\times\mathbf{B}$ velocity [61]. Representation (2.9) allows to greatly simplify the solution of the MHD problem, eliminating fast magneto-sonic dynamics from the description and one of the stream functions for the velocity. Further details on this ansatz are given in reference [56].

Equations (2.8)-(2.9) define the JOREK reduced MHD model vector representations for the unknown vector fields. A careful derivation of the reduced MHD Equations based on the ansatz (2.8)-(2.9) has been given in [74], where the terms neglected in the formulation are also commented. For the purpose of the present Thesis, it is just worth to mention about the electromagnetic Equations

$$\begin{aligned} &(a) \quad \frac{\partial \psi}{\partial t} = r^2 \{\psi, u\} - F_0 \frac{\partial u}{\partial \varphi} + \frac{\eta}{r^2} \frac{\partial^2 \psi}{\partial \varphi^2} + \eta (j - j_0) \\ &(b) \quad j = \Delta^* \psi \end{aligned} \tag{2.10}$$

Equation (2.10a) is obtained by Faraday's law, and Ohm's law in the form $\mathbf{E} + \mathbf{v} \times \mathbf{B} = \eta \mathbf{i}$, with the provided representation for the magnetic flux density (2.8) and fluid velocity (2.9). The variable j is directly related to the toroidal current density, *i.e.* $j = -r j_\varphi$, hence Equation (2.10b). The standard reduced JOREK model, implements a forcing term j_0 and drops the term $(\eta/r^2)\partial^2_{\varphi^2}\psi$. Equations (2.10) are first scaled by $1/r^2$ before a Galerkin method is implemented on the space of Bézier-trigonometric test functions. For the toroidal current j we find in particular:

$$\begin{aligned} \int_0^{2\pi} \int_{\Omega_{in}} \frac{\nu_i}{r} j \, \mathrm{d}\mathbf{r} \mathrm{d}\varphi = &\int_0^{2\pi} \int_{\Gamma_p} \frac{\nu_i}{\mu_0} \frac{1}{r} \frac{\partial \psi}{\partial n} \, \mathrm{d}\ell \mathrm{d}\varphi \\ &- \int_0^{2\pi} \int_{\Omega_{in}} r \nabla_\perp \left(\frac{\psi}{\mu_0 r^2} \right) \cdot \nabla_\perp (\nu_i) \, \mathrm{d}\mathbf{r} \mathrm{d}\varphi \end{aligned} \tag{2.11}$$

Again we find that the tangential component of the magnetic field at the Coupling Surface has to be provided as an input for the solution of the MHD problem. The correct imposition of such a boundary condition necessarily goes through the solution of the magnetostatic problem straight outside of the MHD computational domain.

The representation of vector fields for the *full MHD* JOREK models is directly in terms of their cylindrical components. The magnetic field is represented as the curl of the magnetic vector potential

$$\mathbf{A} = A_r \nabla r + \psi \nabla \varphi + A_z \nabla z \tag{2.12}$$

The freedom in the gauge is eliminated considering the Weyl gauge, *i.e.* $\mathbf{E} = -\frac{\partial \mathbf{A}}{\partial t}$.

2.2.2 Bézier Finite Elements space

For the sake of completeness it is worth to report briefly on the finite element space adopted to solve the extended MHD JOREK models. As hinted already the evolution Equations for the vector potential, the barycentric velocity, the plasma density and the internal energy, complemented by suitable closure relations are solved in an axisymmetric domain. The dependence of physical quantities on the toroidal angle can be then accounted via a simple Fourier decomposition. The discretization of the poloidal cross-section of the JOREK domain is then performed via *Bézier* patches. These elements carry the name of the engineer *Pierre Bézier*, which developed a novel way to describe curves in a language easily comprehensible for a computer during the 60s. Bézier objects are today found in most drawing software packages. The motivations which lead to this choice were essentially three [54]:

- The possibility of simple mesh refinement
- The possibility to align the grid on the MHD equilibrium flux map, which requires curved elements
- As evidenced already for M3D-C1, the use of $C1$ elements has several other advantages in terms of convergence.

The possibility of discretizing the domain via curved patches is given by the choice of an isoparametric method: the mapping from the reference element to the mesh element uses the same test functions as the unknown variables. In particular the test functions used in JOREK are cubic Bernstein polynomials, defined as follows,

$$B_i(s) = \frac{6}{i!\,(3-i)!} s^i \,(1-s)^{3-i} \quad \forall i \in \{0,1,2,3\} \tag{2.13}$$

which represents a basis for polynomials of degree ≤ 3. The test functions defined in (2.13) define a partition of unity, *i.e.* they sum to 1 for any value of $s \in [0,1]$. We can easily use such polynomials to build a curve in the euclidean space, defining four reference points $P_i = (x_i, y_i, z_i)$ and considering the mapping:

$$\begin{aligned} [0,1] \in \mathbb{R} &\rightarrow \mathbb{E}_3 \\ s &\mapsto \sum_{i=0}^{4} P_i B_i(s) \end{aligned}$$

Quite similarly we can build a patch considering the Cartesian product between the cubic Bernstein polynomials. In this case the mapping looks like

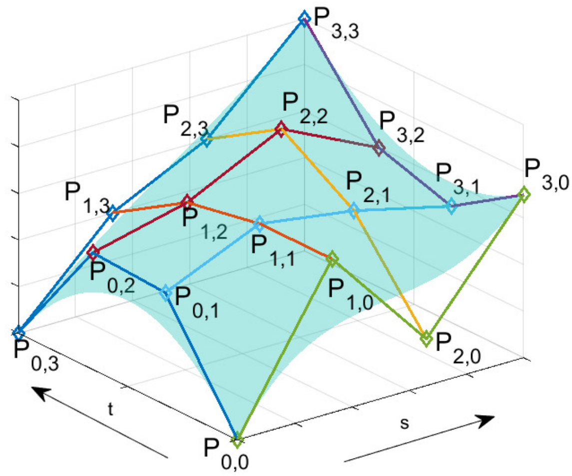

Figure 2.2: Example of Bézier patch, used in the JOREK numerical formulation.

$$
\begin{aligned}
[0,1]\times[0,1] \in \mathbb{R}^2 &\rightarrow \mathbb{E}_3 \\
(s,t) &\mapsto \sum_{i=0}^{4}\sum_{j=0}^{4} P_{i,j}B_i(s)B_j(t)
\end{aligned}
$$

Hence, 16 points are necessary to define a Bézier patch. Keep in mind that in the case of JOREK we are interested in points $P_{i,j}$ which have the real poloidal coordinates of the mesh control points as first two coordinates and the unknown stream function under exam as the third one, *e.g.* $P_{i,j} = (r_{i,j}, z_{i,j}, \psi_{i,j})$. Hence for each Bézier patch we have 16 degrees of freedom. We can associate 4 d.o.f. to each of the corner nodes of the patch, which are in particular related to the actual value of the unknown function, the first order derivatives along the directions defined by the *tangent* control points and the mixed second order derivative identified by the *twist* point. The details are illustrated in [54], we just provide an example of a Bézier element which provide an intuition of such property in Figure 2.2.

Requiring the control points between two consecutive patches to coincide, we enforce both the $C0$-continuity and the continuity of first order derivatives along the tangential direction to the edge separating the two patches. Further, we just need to enforce the continuity of the normal derivatives across patches, which is easily accomplished observing that the two *twist* points associated to two adjacent Bézier patches in correspondence of a corner point have to be aligned with the tangent control point right in the middle. In this way, the 4 degrees of freedom previously associated to a corner node are indeed the same for all the patches sharing that corner point. This means also that the 9 control points associated to a corner node between 4 Beziér patches are completely specified by the 4 degrees of freedom associated to that corner point.

2.3 Vector Green's Theorem

This mathematical interlude is solely intended to introduce the notation we use in the remainder of the Chapter, the content herein being well-known for a long time. Nonetheless the necessity of taking care about the gauge used in extended MHD models, compared to the Coulomb gauge generally used in eddy current codes, makes this Section useful for the following. It is just for completeness that we derive the Green's Theorem at the grounds of nearly any BEM formulation. This identity will show that all the information we will need about the plasma produced magnetic vector potential in the outer domain is contained in the magnetic vector potential, and its normal spatial derivatives, at the Coupling Surface. The Green's function for the Laplace operator, *i.e.* the solution of

$$\nabla^2 G(\mathbf{r}, \mathbf{r}') = -4\pi\delta(\mathbf{r} - \mathbf{r}') \tag{2.14}$$

is

$$G(\mathbf{r}, \mathbf{r}') = \frac{1}{|\mathbf{r} - \mathbf{r}'|} \tag{2.15}$$

From now on, in order to simplify the notation, we will denote the Green function $G = G(\mathbf{r}, \mathbf{r}')$ omitting its explicit dependence on the coordinates of the source and field point. In order to distinguish whether a vector vector fields depends on the source or field coordinate, we will use a prime, *i.e.* $\mathbf{A}' = \mathbf{A}(r')$. We will use the same notation for the nabla operator, *i.e.* $\nabla' = \nabla_{\mathbf{r}'}$. As well known, the fact that (2.15) is a solution of (2.14) means that the convolution operator obtained with the above kernel is actually the inverse of the the Laplacian operator:

$$f(\mathbf{r}) = -\frac{1}{4\pi} \int_{\mathbb{E}_3} G \nabla'^2 f' \, \mathrm{d}\mathbf{r}' \tag{2.16}$$

This is the basic ingredient to build generic Biot-Savart formulas, in arbitrary bounded and unbounded domains. The consideration of finite boundaries is of particular concern for us, as we want to determine the vector potential in the exterior domain to a torus. Direct application of (2.16) allows to write

$$\mathbf{A} = -\frac{1}{4\pi} \int_{\mathbb{E}_3} G \nabla^{2'} \mathbf{A}' \, \mathrm{d}\mathbf{r}' \tag{2.17}$$

We define now, in an arbitrary gauge, the magnetic vector potential associated to the *inner* domain as

$$\mathbf{A_{in}} = -\frac{1}{4\pi} \int_{V_{in}} G \nabla^{2'} \mathbf{A}' \, \mathrm{d}\mathbf{r}' \tag{2.18}$$

Contextually we define the magnetic vector potential due to interior currents as

$$\mathbf{A^*_{in}} = +\frac{1}{4\pi} \int_{V_{in}} G \nabla' \times \nabla' \times \mathbf{A}' \, \mathrm{d}\mathbf{r}' \tag{2.19}$$

Of course $\nabla \times \nabla \times \mathbf{A} = \mu_0 \mathbf{i}$. In particular the electric current density in the inner domain is solely related to plasma currents by construction of the Coupling Surface. The two definitions (2.18) and (2.19) overlap exactly only when the Coulomb gauge is adopted, otherwise they are related by

$$\mathbf{A^*_{in}} = \mathbf{A_{in}} + \int_{V_{in}} G \, \nabla' \left(\nabla' \cdot \mathbf{A}' \right) \mathrm{d}\mathbf{r}' \tag{2.20}$$

Similar vector fields $\mathbf{A_{ext}}$ and $\mathbf{A^*_{ext}}$ are defined when the integration is performed on the exterior domain V_{ext}. In particular the currents in the exterior domain are solely the ones in the conducting domain V_c.

We now show how to completely describe the vector potential associated to the interior domain $\mathbf{A_{in}}$ in the outer domain based only on information about the vector potential and its spatial derivatives at the Coupling Surface. First, using $\nabla \cdot \left(f \overline{\mathbf{T}} \right) = f \nabla \cdot \overline{\mathbf{T}} + \nabla f \cdot \overline{\mathbf{T}}$, we transform (2.18) into

$$\mathbf{A_{in}} = -\frac{1}{4\pi} \int_{V_{in}} \nabla' \cdot G \nabla' \mathbf{A}' \, \mathrm{d}\mathbf{r}' + \frac{1}{4\pi} \int_{V_{in}} \nabla' G \cdot \nabla' \mathbf{A}' \, \mathrm{d}\mathbf{r}' \tag{2.21}$$

According to the vector identity for dyadic products $\nabla \cdot (\mathbf{v} \otimes \mathbf{w}) = (\nabla \cdot \mathbf{v})\mathbf{w} + (\mathbf{v} \cdot \nabla)\, \mathbf{w}$, we can further transform the second term at the right hand side of Equation (2.21) into:

$$\nabla' G \cdot \nabla' \mathbf{A}' = \nabla' \cdot \left[\nabla' G \otimes \mathbf{A}' \right] - \nabla'^2 G \mathbf{A}' \tag{2.22}$$

Considering the definition of the Green function (2.14) and the last vector identity (2.22) and using the divergence Theorem for tensor fields, we finally can write (2.21) as:

$$\mathbf{A_{in}} = -\frac{1}{4\pi} \int_{+\partial V_{in}} \left[G\big(\hat{\mathbf{n}}' \cdot \nabla' \mathbf{A}'\big) + \big(\hat{\mathbf{n}}' \cdot \nabla' G\big) \mathbf{A}' \right] \mathrm{d}\mathbf{r}' + \nu \mathbf{A} \tag{2.23}$$

where

$$\nu(\mathbf{r}) = \begin{cases} 1 & \mathbf{r} \in V_{pl} \\ 0.5 & \mathbf{r} \in \partial V_{pl} \\ 0 & \mathbf{r} \notin V_{pl} \end{cases} \tag{2.24}$$

Of course we can rewrite (2.23) also as

$$\mathbf{A_{in}} = -\frac{1}{4\pi} \int_{+\partial V_{in}} \left[G \frac{\partial \mathbf{A}'}{\partial n'} - \frac{\partial G}{\partial n'} \mathbf{A}' \right] \mathrm{d}\mathbf{r}' + \nu \mathbf{A} \tag{2.25}$$

It is important to recognise that Equations (2.23)-(2.25) are nothing else than the vector version of classical Green's second identity. Indeed, given a vector field $\mathbf{v}$ and a function G we have implicitly shown:

$$\int_V \left[\mathbf{v}' \nabla'^2 G - G \nabla'^2 \mathbf{v}' \right] \mathrm{d}^3\mathbf{r}' = \int_{\partial V} \left[\left(\hat{\mathbf{n}}' \cdot \nabla' G \right) \mathbf{v}' - G \left(\hat{\mathbf{n}}' \cdot \nabla' \mathbf{v}' \right) \right] \mathrm{d}^2\mathbf{r}' \tag{2.26}$$

2.4 MQS models for conducting structures

The description of eddy currents in bulk volumetric structures is conveniently tackled via integral formulations, exploiting the Biot-Savart law [76]. Essentially this requires to enforce Ohm's law in weak form on a suitable set of test functions in the conducting domain,

$$\int_{V_c} \mathbf{w} \cdot \eta \mathbf{i} \, \mathrm{d}\mathbf{r}' = \int_{V_c} \mathbf{w} \cdot \left(-\frac{\partial \mathbf{A}}{\partial t} - \nabla \phi \right) \mathrm{d}\mathbf{r}' \tag{2.27}$$

The Coulomb gauge is generally adopted, so that the magnetic vector potential, is conveniently split a contribution due to plasma currents and a portion associated to currents in external conductors, *i.e.*

$$\mathbf{A} = \mathbf{A}^* = \underbrace{\frac{\mu_0}{4\pi}\int_{V_{in}} G\mathbf{i}'\,\mathrm{d}\mathbf{r}'}_{A^*_{in}} + \underbrace{\frac{\mu_0}{4\pi}\int_{V_{ext}} G\mathbf{i}'\,\mathrm{d}\mathbf{r}'}_{A^*_{ext}} \tag{2.28}$$

The only currents circulating in the exterior domain are those in active and passive conductors, hence we can reduce the integration volume from V_{ext} to V_c, while in the inner domain only the plasma fluid conductor is present in our applications. In view of using a Galerkin method, contextually with the fact the current density is divergence-free, we can take as space of test functions to enforce (2.27) a subspace of $\ker(div(V_c))$. The actual discretization of (2.27) on a set of test functions $\{\mathbf{w_k} : \nabla \cdot \mathbf{w_k} = 0\}$ leads to the algebraic linear ordinary differential equation system

$$\underline{\underline{L_w}}\,\frac{\mathrm{d}}{\mathrm{d}t}\underline{I_w} + \underline{\underline{R_w}}\,\underline{I_w} + \underline{V_{pl}} + \underline{\underline{F_w}}\,\underline{V_{w,e}} = \underline{0} \tag{2.29}$$

where $\underline{I_w}$ is the vector of degrees of freedom for the current density.Since in applications one is generally concerned mostly about the conducting *wall* surrounding the plasma we indicate more generally all the d.o.f. for external currents by the subscript "w". The further subscript "e" indicates the eventual equipotential electrodes present at some boundary face. The matrices above are simply defined in terms of the test functions:

$$\begin{aligned} (a) \quad (L_w)_{i,j} &= \frac{\mu_0}{4\pi}\int_{V_c} \mathbf{w_i}\cdot\int_{V_c} G\mathbf{w_k}'\,\mathrm{d}\mathbf{r}'\,\mathrm{d}\mathbf{r} \\ (b) \quad (R_w)_{i,j} &= \int_{V_c} \mathbf{w_i}\cdot\underline{\eta}\cdot\mathbf{w_k}\,\mathrm{d}\mathbf{r} \\ (c) \quad (F_w)_{i,j} &= \int_{S_j} \mathbf{w_i}\cdot\hat{\mathbf{n}}\,\mathrm{d}\mathbf{r}' \end{aligned} \tag{2.30}$$

In Equation (2.30c) we denoted by S_j an equipotential electrode surface on the boundary of the conducting domain, so that V_k is essentially the potential at that electrode. The remaining source term, related to the induction effect of plasma currents is given by

$$V_{pl,k} = \frac{\mathrm{d}}{\mathrm{d}t}\int_{V_c} \mathbf{w_k}\cdot\mathbf{A}^*_{\mathbf{in}}\,\mathrm{d}\mathbf{r}' \tag{2.31}$$

Much of the effort in later Sections will be to understand the possible ways to correctly evaluate $\mathbf{A}^*_{\mathbf{in}}$ in the conducting domain in terms of the vector potential or magnetic field at the Coupling Surface. At the moment we can consider it as a source term. Also the vector $\underline{V_{w,e}}$ is clearly the vector of the applied voltages to the electrodes. If at the electrodes we know the injected currents, rather then the applied voltages, we can treat the voltages $\underline{V_{w,e}}$ as unknowns, and enforce Kirchoff current law at such equipotential electrodes:

$$\underline{\underline{F}}^T\, \underline{I_w} = \underline{I_{w,e}} \tag{2.32}$$

A variety of possible representations for the electric current density and of finite element spaces is available to tackle the problem [77]. In the remainder of this Section we shall review the fundamental ingredients of the eddy current code CARIDDI [76, 57, 78, 79]. In some aspects we may regard the eddy current code STARWALL [80, 81] as the thin structures version of CARIDDI. Besides eliminating the unnecessary degrees of freedom related to the description of divergent vector fields, this code has some others highly desirable features for modelling the large conducting structures of a tokamak device:

- Further degrees of freedom are automatically eliminated considering only those divergence-free basis vectors which are independent in the definition of a solenoidal current density
- It allows the current density across elements to be discontinuous in the tangential direction, so to accommodate the possibility of a finite current density at the interface between the conducting and the vacuum domain, besides the possibility of correctly describing the tangent discontinuity of the current density between elements with different resistivities

The code has been extensively used for the simulation of eddy currents in tokamak devices [82, 83], also thanks to its essential integration in the evolutionary equilibrium model CarMa0NL [62, 84, 85]. It implements some specific features in order to exploit the symmetries of the toroidal device [86]. Moreover, provided the actual injected currents from the plasma, CARIDDI has been used to evaluate the resistive current path in structures due to halo currents in realistic 3D geometries [87, 88].

2.4.1 The Electric Vector Potential

Mathematically, the fundamental idea behind the eddy current code CARIDDI, is to enforce the solenoidality of the unknown current density $\mathbf{i}$, via an *electric* *vector potential*,

$$\mathbf{i} = \nabla \times \mathbf{T} \tag{2.33}$$

Due to Ampére's law this electric potential differs from the magnetic field for the gradient of a scalar function,

$$\mathbf{H} = \mathbf{T} - \nabla\Omega \tag{2.34}$$

where $\mathbf{T} \in \mathrm{grad}(H^1)^\perp$. Of course the electric currents in the conducting domain is fully described by the curl of $\mathbf{T}$, while in vacuum the magnetic field is solely provided by $-\nabla\Omega$. While the Magneto-Quasi-Static problem in the whole space for linear conductors has a unique solution in terms of $\mathbf{H}$, the solution in terms of the potentials $(\mathbf{T}, \Omega)$ is not unique. Indeed, provided a possible solution $(\mathbf{T_1}, \Omega_1)$ we have that $(\mathbf{T_1} - \nabla f, \Omega_1 + f)$, with f arbitrary scalar function, generates exactly the same magnetic field. Hence, there is some freedom to determine $\mathbf{T}$, and we shall impose a proper gauge condition.

The classical Coulomb or Lorentz gauges can be assigned, together with proper boundary conditions at the conducting-vacuum interface to provide separately uniqueness both for $\mathbf{T}$ and Ω [77]. A more convenient choice is the two-component gauge described in [76, 89, 90], briefly discussed here. Essentially we consider a vector field $\mathbf{v}$, which has no close field lines in the conducting domain, more precisely $\mathbf{v} \in \mathrm{curl}(H^1(V_c))^\perp$. In particular from a certain point P_0 it is possible to reach any point of the conducting domain moving along the lines of the vector $\mathbf{v}$, without closing any loop. The desired gauge is finally

$$\mathbf{T} \cdot \mathbf{v} = 0 \tag{2.35}$$

Besides it is possible to prove the uniqueness of $\mathbf{T}$ for the MQS problem in this gauge [77], we will see clearly why it is like that in the discrete version of the problem, hence let's move to the finite element space employed.

2.4.2 The Edge Shape Functions

It is clear that we are going to represent the vector field $\mathbf{i}$ as the curl of the electric vector potential $\mathbf{T}$, and that the formulation will be rigorously in the degrees of freedom for the electric vector potential. In order to enforce the continuity of $\mathbf{i} \cdot \hat{\mathbf{n}}$ across elements, we need to enforce the continuity across elements' facets of $\hat{\mathbf{n}} \times \mathbf{T}$. On the other hand, we would like to describe currents whose tangential component is eventually discontinuous across elements and across the interface with the vacuum domain, which requires the discontinuity of the normal component of $\mathbf{T}$ across elements facets. It is convenient then to introduce basis functions which automatically enforce this property. A suitable choice is found within the vector basis functions $\mathbf{T_e}$, associated to the edges of the mesh discretizing the conducting domain. Rigorously, an isoparametric finite element space is implemented, where the scalar test functions are the usual piece-wise linear function N_k. Given a certain element V_d

$$\begin{gathered} N_j(\mathbf{x_m}) = \delta_{j,m} \\ \sum_{j=1}^{N_{nodes}} N_j(\mathbf{x}) = 1 \; \forall \mathbf{x} \in V_d \end{gathered} \tag{2.36}$$

where j and m run through the indices of the element nodes. Now we can associate to each oriented edge e identified by the starting and ending nodes (i, j) a vector basis function associated to edge [91]. In case of tetrahedral elements these vector basis functions can be defined as [57]

$$\mathbf{T_e} = \mathbf{T_{(i,j)}} = N_i \nabla N_j - N_j \nabla N_i \tag{2.37}$$

It is not hard to show that the edge shape functions (2.37) satisfy the desired continuity properties, defining vector fields whose tangential component to elements' faces are continuous across different elements. Vice-versa the normal component to elements' facets can be discontinuous. The edge shape functions defined in (2.37), and all the corresponding ones defined for different element shapes, satisfy the following property:

$$\int_{(\pm)e_j} \mathbf{T_{e_k}} \cdot \mathbf{t} \, \mathrm{d}\ell = (\pm)\delta_{e_j,e_k} \tag{2.38}$$

i.e. the line integral of the edge basis function $\mathbf{T_{e_k}}$ is unitary on the edge e_k itself, and null along any other edge $e_{j \neq k}$. Notice again that the edges are oriented, hence the $\pm$ sign. This property provides us with the great effectiveness of this representation for describing currents. Consider indeed the electric vector potential approximated via edge shape functions,

$$\mathbf{T} = \sum_{e=1}^{N_e} I_e \mathbf{T_e} \tag{2.39}$$

where we defined the degrees of freedom I_e associated to each edge. Let's try to compute the electric current flowing through some face of the discretized conducting domain. Thanks to Stoke's Theorem we get

$$I_{S_f} = \int_{S_f} \mathbf{i} \cdot \hat{\mathbf{n}} \, \mathrm{d}\mathbf{r} = \int_{+\partial S_f} \mathbf{T} \cdot \mathbf{t} \, \mathrm{d}\ell. \tag{2.40}$$

We can subdivide the boundary of the surface S_f into the actual different mesh edges constituting it. Using (2.38), we finally get

$$I_{S_f} = \sum_{e \in \partial S_f} (\pm) I_e \tag{2.41}$$

The current flowing through some face of the domain is given by the summation of the degrees of freedom of the electric potential associated to each edge of the surface boundary. In principle it is sufficient a single *active* edge to define the currents flowing through a face of the discretized domain. Not coincidentally, we have still to apply the gauge condition (2.35). The discrete version of such a constraint essentially requires to find a tree of the mesh, and set to zero the corresponding degrees of freedom. The edges of the co-tree alone are necessary and sufficient to determine a unique solution of the eddy current problem. Further degrees of freedom are eliminated when there are no current flows across the boundary of the conducting domain, hence we can set to zero all the degrees of freedom associated to cotree boundary edges.

Anyway, in presence of non-simply connected conductors, this procedure would automatically exclude the possibility of having net currents flowing around the handles of the domain. Each handle requires for an additional degree of freedom, the dimension of the closed curves homology group of the domain being defined also as *genus* of the domain. Hence, suitable automatic procedures were identified to correctly re-activate a single degree of freedom per handle. Each additional degree of freedom is a suitable linear combination of the degrees of freedom associated to tree boundary edges [92, 93].

It is easily understood, that the electric vector potential and the electric current density share the same degrees of freedom, the electric current density being represented by

$$\mathbf{i} = \sum_{k=1}^{n_c} I_k \underbrace{\nabla \times \mathbf{T_k}}_{\mathbf{w_k}} \tag{2.42}$$

2.5 Virtual Casing Principle Approach

In this section, we consider both the fundamentals aspects and the pragmatic steps of the coupling between models of plasma and conducting structures via the *Virtual Casing* principle, originally proposed by Shafranov and Zakharov to the magnetic fusion devices community [94, 95]. The fundamental idea of the *Virtual Casing* is very simple to explain via the following imaginary experiment. We consider the Coupling Surface as virtually made of some superconducting material. Any current we drive within the the interior domain is structurally shielded from a corresponding surface current on the superconducting sheet: an observer in the outer domain would not experience any magnetic field related to that current. This provide us with the sound intuition that we can define an equivalent surface current at the Coupling Surface which perfectly reproduce the magnetic fields due to plasma currents in the outer domain.

In this Section we shall clarify how to find this equivalent surface current for an arbitrary current distribution within the plasma, and how this information can be potentially exploited for simulating the self-consistent evolution of the plasma and the surrounding eddy currents. For fixing the ideas we take as specific example the MHD code JOREK, and the eddy current code CARIDDI. The coupling strategy we are going to present is quite general and it is essentially the same employed in the JOREK-STARWALL coupling [60, 61].

Before going further it is useful to prove the following uniqueness Theorem, which provide us with the certainty that all the information we need to solve the outer magnetostatic problem is actually contained within the tangential component of the magnetic vector potential at the MHD computational boundary, and in external currents.

Theorem 1 *Given the electric current density* $\mathbf{i}$ *in* V_{ext}*, and the tangential component of the magnetic vector potential* $\mathbf{a_t}$ *at* $+\partial V_{in}$*, the magnetostatic problem*

$$\nabla \times \mathbf{B} = \mu_0 \mathbf{i} \quad \mathrm{in} \Omega_e$$

$$\mathbf{B} = \nabla \times \mathbf{A} \quad \mathrm{in} \Omega_e$$

$$\hat{\mathbf{n}} \times \mathbf{A} = \mathbf{a_t} \quad \mathrm{on} \partial\Omega_e$$

has a unique solution, provided $\mathbf{B}$ *is regular at infinity.*

Proof: Suppose that two different solutions of the above problem exist, and define their difference as $\delta\mathbf{B} = \mathbf{B_1} - \mathbf{B_2}$. Due to linearity, clearly $\delta\mathbf{B}$ has to satisfy the associated homogeneous problem. Let us evaluate the L^2-norm of $\delta\mathbf{B}$:

$$\|\delta\mathbf{B}\|_{L^2}^2 = \int_{V_{ext}} |\delta\mathbf{B}|^2 \,\mathrm{d}V = \int_{V_{ext}} \delta\mathbf{B} \cdot \nabla \times \delta\mathbf{A} \,\mathrm{d}V$$

which, by standard vector identities, gets the form:

$$\|\delta\mathbf{B}\|_{L^2}^2 = \int_{V_{ext}} \delta\mathbf{A} \cdot \underbrace{\nabla \times \delta\mathbf{B}}_{=0} \mathrm{d}V + \int_{-\partial V_{in}} \underbrace{\hat{\mathbf{n}} \times \delta\mathbf{A}}_{=0} \cdot \delta\mathbf{B} \,\mathrm{d}S$$

Since the L^2-norm of the difference magnetic field needs to be zero, we conclude that the solution is really unique: $\mathbf{B_1} = \mathbf{B_2}$. □

This theorem clearly shows that the magnetostatic problem in the *outer* domain is well-posed if we specify:

- the electric current density in the whole Ω_e
- the tangential component of the magnetic vector potential at the interface with the inner domain
- suitable regularity conditions at infinity

Notice moreover that the tangential component of the magnetic vector potential can be provided in any gauge, the magnetostatic problem will still have unique solution. In this case the difference vector potential is the gradient of a scalar function $\delta\mathbf{A} = \nabla\delta\phi$, while the curl of $\delta\mathbf{B}$ is still null. The surface term in the last passage of our proof gets the form:

$$\begin{aligned}
\int_{-\partial V_{in}} (\hat{\mathbf{n}} \times \nabla\delta\phi) \cdot \delta\mathbf{B} \,\mathrm{d}S &= \int_{V_{ext}} \nabla \cdot [\nabla\delta\phi \times \delta\mathbf{B}] \,\mathrm{d}V = \\
&= \int_{V_{ext}} \underbrace{\nabla \times \nabla\delta\phi}_{\text{always } 0} \cdot \delta\mathbf{B} - \nabla\phi \cdot \underbrace{\nabla \times \delta\mathbf{B}}_{=0} \mathrm{d}V \\
&= 0
\end{aligned} \tag{2.43}$$

2.5.1 The equivalent surface current

Either an equivalent surface current or the tangential component of the magnetic vector potential completely specify the outer magnetostatic problem. Hence a relation between the two exists, eventually involving the currents in the exterior domain. According to the notation introduced in Section 2.3, this relation is provided in particular by:

$$\begin{aligned}(1-\nu)\,\mathbf{A} = {} & \frac{\mu_0}{4\pi}\int_{\partial V_{in}} G\,\mathbf{k_{eq}}'\,\mathrm{d}\mathbf{r}' \\ & + \frac{\mu_0}{4\pi}\int_{V_c} G\,\mathbf{i}'\,\mathrm{d}\mathbf{r}' \\ & - \frac{1}{4\pi}\nabla\int_{V} G\left(\nabla'\cdot\mathbf{A}'\right) \quad \text{on } \partial V_{in}\end{aligned} \tag{2.44}$$

The currents in the exterior domain $\mathbf{i}$ are assigned, and the vector potential $\mathbf{A}$ is known at the Coupling surface. Essentially we pretend that the actual information on the vector potential associated to currents in the interior domain is given by the equivalent surface current $\mathbf{k_{eq}}$ at the Coupling Surface. It is important to account for the gauge immediately, to ensure our problem is not affected by this choice. We see that in Equation (2.44) there is anyway a further unknown term, related precisely to the gauge choice. Anyway this is the gradient of a scalar function, and is not too much problematic[4]. We recognise indeed, for a plasma current distribution which is solenoidal in the interior domain ($\mathbf{i} \in [\mathrm{grad}\left(H^1(V_{in})\right)]^{\perp}$), that the only information we need about $\mathbf{A}$ at the boundary is found in its tangent divergence-free component to the boundary. Indeed, all the information about magnetic fluxes at the Coupling Surface is therein. Moreover $\mathbf{k_{eq}}$ is a divergence-free vector field tangent to the boundary. Finally we can enforce the weak form of (2.44) at the Coupling Surface on the space of divergence-free vector fields there $\ker[\mathrm{div}(\partial V_{in})]$, or a suitable subspace. Let us indicate for convenience by $\mathbf{A_{pl}}$ the difference between the overall magnetic vector potential $\mathbf{A}$, in its arbitrary gauge, and the magnetic vector potential associated to the currents in external conductors $\mathbf{A}^*_{\mathbf{w}}$, shortly:

$$\mathbf{A_{pl}} = \mathbf{A} - \mathbf{A}^*_{\mathbf{w}} \tag{2.45}$$

With this notation, the weak form of Equation (2.44) is

[4] at least as long as there are no currents crossing the Coupling Surface

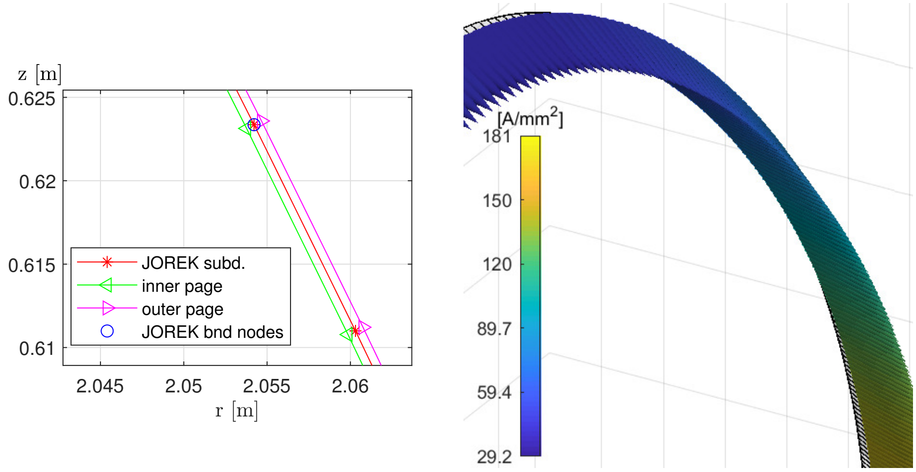

(a) (b)

Figure 2.3: (a) Example of the discretization of the JOREK boundary for preparation of the CARIDDI equivalent shell; (b) example of the CARIDDI shell with some equivalent current to the plasma.

$$\int_{\partial V_{in}} \mathbf{w} \cdot \mathbf{A_{pl}} \, \mathrm{d}\mathbf{r} = \int_{\partial V_{in}} \mathbf{w} \cdot \frac{\mu_0}{4\pi} \int_{\partial V_{in}} G \, \mathbf{k_{eq}}' \, \mathrm{d}\mathbf{r}' \, \mathrm{d}\mathbf{r} \qquad \forall \, \mathbf{w} \in \, \ker[\mathrm{div}(\partial V_{in})] \tag{2.46}$$

The possible implications of a current which is not solenoidal in V_{in}, but only in the overall volume V, are commented later in Section 2.7. We approximate the Coupling Surface ∂V_{in} with an infinitesimally thick volumetric shell V_{eq}, discretized via hexahedral CARIDDI elements. In particular, provided some points along the JOREK boundary, we can first move along the normal direction to the JOREK boundary, providing some reference poloidal coordinates, and then move along the toroidal angle via straight segments. Other constructions are possible, however this looks robust in the set-up of automatic procedures respect to the eventual presence of sharp corners in the Coupling Surface, compared to other eventual barycentric alternatives. An example for the equivalent shell built on the top of the JOREK boundary for ASDEX-Upgrade simulations is given in Figure 2.3.

The corresponding CARIDDI basis vectors within this fictitious shell, provided the further constraint $\mathbf{w_k} \cdot \hat{\mathbf{n}} = 0$ on ∂V_{eq}, represent exactly a finite subset of the vector space $\ker[\mathrm{div}(\partial V_{in})]$ we need. Equation (2.46) gets the form

$$\int_{V_{eq}} \mathbf{w_k} \cdot \mathbf{A_{pl}} \, \mathrm{d}\mathbf{V} = \sum_{j=1}^{n_C} I_{eq,j} \int_{V_{eq}} \mathbf{w_k} \cdot \frac{\mu_0}{4\pi} \int_{V_{eq}} G \mathbf{w_j}' \, \mathrm{d}\mathbf{r}' \, \mathrm{d}\mathbf{r} \tag{2.47}$$

Here $\mathbf{w_k}$ are the standard CARIDDI basis functions for the electric current density, $\{\mathbf{w_k} = \nabla \times \mathbf{T_k} \; \forall k = 1, \cdots, n_{eq}\}$. We indicated by n_{eq} the total number of degrees of freedom for the equivalent current in the CARIDDI representation. Now we come back to our definition of $\mathbf{A_{pl}}$ (2.45), which we plug into (2.46):

$$\begin{aligned} &\int_{\Omega_{eq}} \mathbf{w_k} \cdot (\mathbf{A} - \mathbf{A_w^*}) \, \mathrm{d}V = \\ &\quad = \sum_{j=1}^{n_C} I_{eq,j} \int_{V_{eq}} \mathbf{w_k} \cdot \frac{\mu_0}{4\pi} \int_{V_{eq}} G \mathbf{w_j}' \, \mathrm{d}\mathbf{r}' \, \mathrm{d}\mathbf{r} \\ &\quad \forall \, k \in \; \{1, \cdots, n_{eq}\} \end{aligned} \tag{2.48}$$

While $\mathbf{A_w^*}$ is calculated completely within CARIDDI as a function of the wall currents, the overall vector potential at the interface surface $\mathbf{A}$ is provided by JOREK in terms of its boundary basis functions. In general we may write:

$$\mathbf{A} = \sum_{j=1}^{n_J} A_j \mathbf{u_j} \tag{2.49}$$

where n_J is the overall number of degrees of freedom for the boundary vector basis functions of JOREK $\mathbf{u_j}$. Equation (2.48) takes finally the algebraic form:

$$\underline{\underline{H}} \, \underline{A_j} - \underline{\underline{M_{eq,w}}} \, \underline{I_w} = \underline{\underline{L_{eq}}} \, \underline{I_{eq}} \tag{2.50}$$

where,

$$H_{k,j} = \int_{V_{eq}} \mathbf{w_k} \cdot \mathbf{u_j} \, \mathrm{d}V \tag{2.51}$$

$$(M_{eq,w})_{k,j} = \int_{V_{eq}} \mathbf{w_k} \cdot \frac{\mu_0}{4\pi} \int_{V_c} G \, \mathbf{w_j}(\mathbf{r}') \, \mathrm{d}\mathbf{r}' \, \mathrm{d}\mathbf{r} \tag{2.52}$$

$$(L_{eq})_{k,j} = \int_{V_{eq}} \mathbf{w_k} \cdot \frac{\mu_0}{4\pi} \int_{V_{eq}} G \, \mathbf{w_j}' \, \mathrm{d}\mathbf{r}' \, \mathrm{d}\mathbf{r} \tag{2.53}$$

The projection of JOREK basis functions to CARIDDI basis functions described in Equation (2.51) is performed by the means of a Gauss integration. For example, in the reduced MHD model, Equation (2.51) writes down

$$\int_{V_{eq}} \psi_j \nabla\varphi \cdot \mathbf{w_k} \, \mathrm{d}S \tag{2.54}$$

Where ψ_j is a scalar basis function for the JOREK representation of the vector potential. Hence, within one CARIDDI element, Gauss quadrature formulas look like

$$\sum_{i=1}^{N_G} detJ(i) \cdot \frac{\psi_j(\mathbf{r_i})}{r_i} \mathbf{w_k} \cdot \mathbf{i}_\varphi(\mathbf{r_i}) \tag{2.55}$$

The inherent difficulty now is that the point $\mathbf{r_i}$, which is a Gauss point of the straight CARIDDI element, does not necessarily belong to the JOREK boundary (*i.e.* the Coupling Surface). Hence, the CARIDDI Gauss point is approximated to be the same as the nearest point on the real JOREK boundary in order to evaluate ψ_j:

$$\psi_j(\mathbf{r_i}) \simeq \psi_j(\mathbf{r_{i,projected}}) \tag{2.56}$$

In principle, one can find proper 1:1 mappings between the mid-plane of each CARIDDI straight element parallel to the Coupling Surface and a real patch covering the JOREK boundary, given by the tensor product of a Beziér and a toroidal segment. This way one could pull back and push forward scalar and vector fields accurately. Anyway this would greatly complicate the task, in practice requiring to set up curved elements in CARIDDI, and not necessarily bringing much more accuracy: the idea is that we are piece-wise linearizing the Coupling Surface. In this respect, if the toroidal or poloidal discretization of the equivalent shell is not sufficient the CARIDDI equivalent current may not well represent the plasma current in the proximity of the shell. We show some preliminary results obtained for the geometry of ASDEX-Upgrade, and for an axisymmetric plasma, in Figure 2.4. The equivalent reference poloidal flux ψ_{pl} employed is the same used for calculating the equivalent current in Figure 2.3b.

Test results shown in Figure 2.4 take $\mathbf{A_{pl}}$, as defined in (2.45) as a precomputed input where $\mathbf{A}$ is the real JOREK vector potential and $\mathbf{A_w^*}$ is computed by STARWALL. The equivalent currents are then calculated via the relation

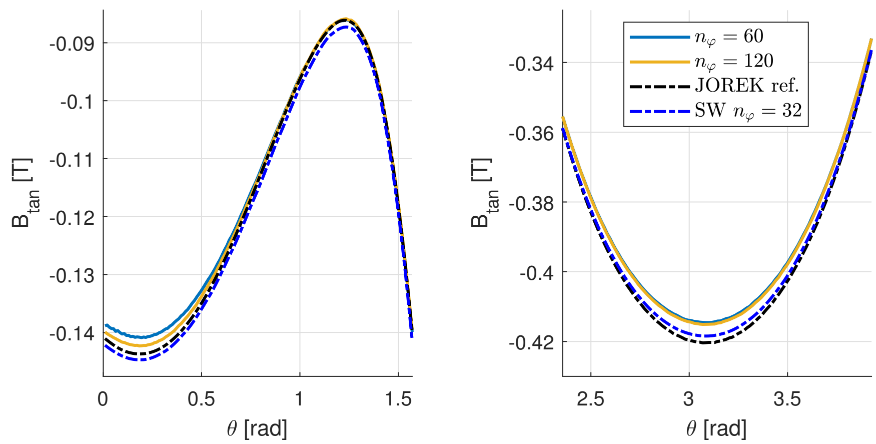

Figure 2.4: Tangent poloidal magnetic field at a surface shifted of $1\ mm$ respect to the JOREK boundary, as given by the CARIDDI equivalent current for two different discretizations along the toroidal angle, by JOREK via a toroidal filament representation, and by the equivalent current in STARWALL. 10 subdivisions per JOREK boundary element along the poloidal angle are adopted, the shell thickness is $1\ mm$ in this numerical experiment.

$$\underline{I_{eq}} = \left(\underline{\underline{L_{eq}}}^{-1}\,\underline{\underline{H}}\right)\,\underline{A_{pl,j}} \tag{2.57}$$

where $\underline{A_{pl}}$ is clearly the vector specifying the plasma magnetic vector potential in the JOREK representation, according to the above assumption. In this sense the results reported in Figure 2.4 do not represent a full CARIDDI test where $\mathbf{A}^*_\mathbf{w}$ is represented coherently to the other CARIDDI variables. Nonetheless the qualitative agreement is good, and both the root mean square error and the maximum error on the computation of the tangent magnetic field, taking the JOREK-computed quantities as reference, is less than $1.2\ \%$.

2.5.2 Evolution Equations for the eddy currents: decoupling plasma and wall vector potential

Within the CARIDDI integral formulation the evolution Equation for the external currents (2.29) now looks like:

$$\underline{\underline{L_w}}\,\frac{\mathrm{d}}{\mathrm{d}t}\underline{I_w} + \underline{\underline{R_w}}\underline{I_w} + \underline{\underline{M_{w,eq}}}\frac{\mathrm{d}}{\mathrm{d}t}\underline{I_{eq}} = \underline{0} \tag{2.58}$$

Here $\underline{\underline{M_{w,eq}}} = \underline{\underline{M_{eq,w}}}^T$. We can use Equation (2.50) to make explicit the dependence of the equivalent currents on the wall currents and on the overall vector potential, since these are the real unknowns for the system:

$$\left(\underline{\underline{L_w}} - \underline{\underline{M_{w,eq}}}\,\underline{\underline{L_{eq}}}^{-1}\,\underline{\underline{M_{eq,w}}}\right)\frac{\mathrm{d}}{\mathrm{d}t}\underline{I_w} + \left(\underline{\underline{M_{w,eq}}}\,\underline{\underline{L_{eq}}}^{-1}\,\underline{\underline{H}}\right)\frac{\mathrm{d}}{\mathrm{d}t}\underline{A} + \underline{\underline{R_w}}\,\underline{I_w} = 0 \tag{2.59}$$

We notice the immediately that

$$\underline{\underline{L^*_w}} = \underline{\underline{L_w}} - \underline{\underline{M_{w,eq}}}\,\underline{\underline{L_{eq}}}^{-1}\,\underline{\underline{M_{eq,w}}} \tag{2.60}$$

is the modified inductance matrix we would have in presence of the conductive structures and a superconducting shell at the Coupling Surface. Depending on the JOREK model we may have degrees of freedom for the magnetic vector potential $\underline{A}$ which have the dimensions of a vector potential or of a magnetic flux. We indicate shortly:

$$\underline{\underline{N}} = \underline{\underline{M_{w,eq}}}\,\underline{\underline{L_{eq}}}^{-1}\,\underline{\underline{H}} \tag{2.61}$$

It is convenient for the following to rewrite the time evolution Equation (2.59) in view of the last two definitions:

$$\underline{\underline{L_w^*}}\frac{\mathrm{d}}{\mathrm{d}t}\underline{I_w} + \underline{\underline{N}}\frac{\mathrm{d}}{\mathrm{d}t}\underline{A} + \underline{\underline{R_w}}\,\underline{I_w} = \underline{0} \tag{2.62}$$

Before going further to the time discretization, we change the vector basis respect to which we represent wall currents. The convenience of this transformation will be apparent at the end of the Section. In particular we solve the generalized eigenvalue problem:

$$\underline{\underline{L_w^*}}\,\underline{I_w} = \lambda\underline{\underline{R_w}}\,\underline{I_w} \tag{2.63}$$

The modified inductance matrix $\underline{\underline{L_w^*}}$ and the resistance matrix $\underline{\underline{R_w}}$ are symmetric and of dimension $n_w \times n_w$, indicating by n_w the number of degrees of freedom for the representation of currents in external conductors. A discrete set $\{\lambda_k\}$ of n_w generalized eigenvalues exists which makes the solution of the linear system (2.63) non-trivial. The eigenvector corresponding to λ_k is denoted here by $\underline{I_{\lambda_k}}$. The transformation matrix for the components of a vector from the canonical basis to this new eigenvector basis is built simply by taking the eigenvectors as the columns of a matrix $\underline{\underline{S}}$:

$$\underline{\underline{S}} = \begin{bmatrix} \vdots & & \vdots \\ \underline{I_{\lambda_1}} & \cdots & \underline{I_{\lambda_{n_c}}} \\ \vdots & & \vdots \end{bmatrix} \tag{2.64}$$

We rewrite the time evolution Equation (2.59), multiplying from the left both sides by $\underline{\underline{S}}^T$. Moreover we express the components of the wall currents in the new eigenvector basis:

$$\underline{\underline{\tilde{L}_w^*}}\frac{\mathrm{d}}{\mathrm{d}t}\underline{\tilde{I}_w} + \underline{\underline{\tilde{R}_w}}\underline{\tilde{I}_w} + \underline{\underline{S}}^T\,\underline{\underline{N}}\frac{\mathrm{d}}{\mathrm{d}t}\underline{A} = 0 \tag{2.65}$$

where

$$\underline{\underline{\tilde{L}_w^*}} = \underline{\underline{S}}^T\,\underline{\underline{L_w^*}}\,\underline{\underline{S}} \tag{2.66}$$

$$\underline{\underline{\tilde{R}_w}} = \underline{\underline{S}}^T\,\underline{\underline{R_w}}\,\underline{\underline{S}} \tag{2.67}$$

$$\tag{2.68}$$

are the modified inductance matrix and the resistance matrix in the new reference system. Here the inductance matrix $\underline{\underline{\tilde{L}_w^*}}$ results to be a diagonal matrix containing the above-mentioned eigenvalues $\{\lambda_k\}$, while $\underline{\underline{\tilde{R}_w}}$ results to be the identity matrix.

The time integration of above Equations will be performed within JOREK, advancing the structures degrees of freedom $\underline{I_w}$ together with the JOREK variables. It is then important to have a look on how their time discretization scheme applies to Equation (2.65):

$$\begin{aligned}(1+\xi)\,\underline{\underline{\tilde{L}_w^*}}\,\underline{\delta\tilde{I}_w^{(n)}} + \Delta t\theta\underline{\underline{\tilde{R}_w}}\,\underline{\delta\tilde{I}_w^{(n)}} + (1+\xi)\,\underline{\underline{S}}^T\,\underline{\underline{N}}\,\underline{\delta A^{(n)}} = \\ = -\,\Delta t\theta\underline{\underline{\tilde{R}_w}}\,\underline{\tilde{I}_w^{(n)}} + \xi\underline{\underline{\tilde{L}_w^*}}\,\underline{\delta\tilde{I}_w^{(n-1)}} + \xi\underline{\underline{S}}^T\,\underline{\underline{N}}\,\underline{\delta A^{(n-1)}}\end{aligned} \tag{2.69}$$

where we have defined the difference of a vector:

$$\underline{\delta v^{(k)}} = \underline{v^{(k+1)}} - \underline{v^{(k)}} \tag{2.70}$$

and we have introduced the numerical parameters

$$(\xi,\ \theta) \quad \in \quad [0,1]\times[0,1] \tag{2.71}$$

It is easy to see, that setting the couple of numerical parameters (θ, ξ) appropriately we can choose between different time integration schemes:

- $(1/2, 0) \rightarrow$ Crank-Nicholson
- $(1, 0) \quad\ \rightarrow$ implicit Euler
- $(1, 1/2) \rightarrow$ Gears

We have anyway to consider (2.69) in its generality, *i.e.* for any admissible value of θ and ξ. In particular we find that

$$\underline{\delta\tilde{I}_w^{(n)}} = \left[(1+\xi)\,\underline{\underline{\tilde{L}_w^*}} + \Delta t\theta\underline{\underline{\tilde{R}_w}}\right]^{-1}\left(\underline{b} - \left(\underline{\underline{S}}^T\,\underline{\underline{N}}\right)\delta\underline{A^{(n)}}\right) \tag{2.72}$$

where, the vector $\underline{b}$ is known from previous time steps, being essentially the r.h.s. of Equation (2.69),

$$\underline{b} = \underline{b}\left(\underline{\tilde{I}_w^{(n)}}, \underline{A^{(n)}}, \underline{\tilde{I}_w^{(n-1)}}, \underline{A^{(n-1)}}, \xi, \theta, \Delta t\right) \tag{2.73}$$

The inversion of the term in square bracket is immediate thanks to the change of basis described by the transformation matrix (2.64). Indeed the modified inductance matrix $\underline{\underline{\tilde{L}_w^*}}$ is the diagonal matrix of the generalized eigenvalues for the linear system (2.63) and $\underline{\underline{\tilde{R}_w}}$ is the identity matrix.

Finally we are ready to provide the boundary conditions, *i.e.* to provide an operative expression for $\hat{\mathbf{n}} \times \mathbf{B}$ at the boundary in the JOREK representation. By a Biot-Savart integral and a proper Gauss projection we provide indeed in the JOREK representation:

$$\delta \underline{B_{tan}^{(n)}} = \underline{\underline{Q_{eq}}}\, \delta \underline{I_{eq}^{(n)}} + \left(\underline{\underline{Q_w}}\, \underline{\underline{S}}\right) \delta \underline{\tilde{I}_w^{(n)}} \tag{2.74}$$

As intermediate step in the calculation of $\underline{\underline{Q_{eq}}}$ one has to calculate the tangent magnetic field produced by the equivalent current in appropriate JOREK field points. These were illustrated in the example of Figure 2.4. Relation (2.50) for the vector potential at the interface surface leads then to

$$\delta \underline{B_{tan}^{(n)}} = \underbrace{\left(\underline{\underline{Q_{eq}}}\, \underline{\underline{L_{eq}}}^{-1}\, \underline{\underline{H}}\right)}_{\underline{\underline{Q_A^*}}} \delta \underline{A^{(n)}} + \left[\underbrace{\left(\underline{\underline{Q_w}} - \underline{\underline{Q_{eq}}}\, \underline{\underline{L_{eq}}}^{-1}\, \underline{\underline{M_{eq,w}}}\right)}_{\underline{\underline{Q_w^*}}} \underline{\underline{S}}\right] \delta \underline{\tilde{I}_w^{(n)}} \tag{2.75}$$

We notice that $\underline{\underline{Q_w^*}}\, \underline{\underline{S}}\, \underline{\tilde{I}_w^{(n+1)}}$ is that tangential magnetic field we would find keeping the currents in the conductors as they are and considering the interface itself made by a superconducting material. The matrix $\underline{\underline{Q_A^*}}$ was tested for the calculation of free-boundary equilibria, in lieu of the corresponding STARWALL matrix with preliminary good results, which will be published during the year. Finally, by Equation (2.72), we find

$$\begin{aligned}\delta \underline{B_{tan}^{(n)}} = &\left\{ \left(\underline{\underline{Q_{eq}}}\, \underline{\underline{L_{eq}}}^{-1}\, \underline{\underline{H}}\right) - \left(\underline{\underline{Q_w^*}}\, \underline{\underline{S}}\right) \left[(1+\xi)\, \underline{\underline{\tilde{L}_w^*}} + \Delta t \theta \underline{\underline{\tilde{R}_w}}\right]^{-1} \left(\underline{\underline{S}}^T\, \underline{\underline{N}}\right) \right\} \delta \underline{A^{(n)}} \\ &+ \left[\underline{\underline{Q_w^*}}\underline{\underline{S}}\right] \underline{b}\end{aligned} \tag{2.76}$$

The "forcing" term $\underline{b}$ was already defined in (2.73) and depends solely on the numerical parameters $\{\xi, \theta, \Delta t\}$, besides the electromagnetic variables at previous time steps.

2.6 Direct Boundary Element Approach

Coupling strategies based on the virtual casing principle have been implemented and proved to be efficient in many applications, as we have seen for the JOREK-STARWALL coupling [60, 61], and as we shall see for the evolutionary equilibrium code CarMa0NL [62]. Anyway this is not the only opportunity, and we shall comment on two further possible coupling strategies in this Section.

We are going to present a magnetic vector potential formulation in subsection 2.6.1, which is in principle the real Johnson-Nédélec formulation [58, 63, 64]. We will see anyway that the different gauge choice between the formulation of the extended MHD problem and the formulation of the MQS problem for conducting structures will in general make this strategy inapplicable. We shall see anyway, that the gauge choice does not affect the problem of the poloidal magnetic field in the axisymmetric case. The boundary integral Equation in that case will correspond to the one already found in [96], presenting tokamak magnetic diagnostics. Moreover, as a by-product of this formulation, we will find a valid direct formula to compute the magnetic vector potential due to plasma currents in the exterior domain as a function of the tangential component of the overall magnetic field and vector potential at the Coupling Surface, independently of the gauge choice in extended MHD model. The computed $\mathbf{A_{in}}$ will differ by the one in the Coulomb gauge only for the gradient of a scalar function, being irrelevant in the determination of applied voltages to structures.

Further, we present a magnetic field formulation in subsection 2.6.2. The corresponding boundary integral Equation was used in [97] to show that we can't get real informations about the actual plasma current distribution within the plasma from external magnetic measurements, since the tangential magnetic flux density at the plasma boundary determines alone the actual measurements, and many different current density distributions can reproduce the same tangential field at the boundary. This was in a sense already found in practice computing MHD equilibria and comparing them to the simulated measurements in [98]. In the last reference, it was evidenced that few parameters for tuning the plasma current distribution[5], clearly not enough to reproduce the details of the current distribution within the plasma, were instead sufficient to reproduce the correct magnetic measurements around the plasma.

[5] the overall current J, the poloidal beta β_p, and the internal inductance ℓ_i. We shall come back to these definitions and the definition of plasma boundary in next Chapter.

2.6.1 Vector Potential Formulation

A pure Johnson-Nédélec formulation can be set up if we are in the Coulomb gauge. Indeed in this case, the Laplace problem for the magnetic vector potential

$$\begin{aligned} &\nabla^2 \mathbf{A}^* = -\mu_0 \mathbf{i} \quad \text{in } V_{ext} \\ &\mathbf{A}^* = \mathbf{A}_0 \quad \text{on } \partial V_{ext} \end{aligned} \tag{2.77}$$

has unique solution provided the electric currents in external conductors $\mathbf{i}$ and Dirichlet boundary conditions $\mathbf{A_0}$. Now consider our general Green's identity (2.25) and add to both sides the vector potential associated to the exterior domain (which is both due to currents $\mathbf{i}$ and eventually due to the Gauge $\nabla(\nabla \cdot \mathbf{A})$)

$$(1-\nu)\,\mathbf{A} = -\frac{1}{4\pi}\int_{+\partial V_{in}} \left[G\frac{\partial \mathbf{A}'}{\partial n'} - \frac{\partial G}{\partial n'}\mathbf{A}' \right] \mathrm{d}\mathbf{r}' + \mathbf{A_w} \tag{2.78}$$

In general, we would like to invert the above boundary Equation respect to $\partial \mathbf{A}/\partial n$, since therein we have all the information about the tangential component of the magnetic field. Anyway are not really able to calculate $\mathbf{A_w}$ at the Coupling Surface, unless we are in the gauge of Coulomb. In this case indeed the magnetic vector potential is solely due to the electric currents, and both CARIDDI and STARWALL can easily compute the Biot-Savart integral to calculate $\mathbf{A}^*_\mathbf{w}$ as a function of the external currents $\mathbf{i}$. Unfortunately the extended MHD models considered all use different gauges. In particular we have that

$$\mathbf{A_w} = \mathbf{A}^*_\mathbf{w} + \int_{V_{ext}} G\nabla' \left(\nabla' \cdot \mathbf{A}'\right) \mathrm{d}\mathbf{r}' \tag{2.79}$$

and the second term at the right-hand-side is exactly what we are not able to evaluate, preventing the possibility of a solution for $\partial \mathbf{A}/\partial n$. Besides this inherent difficulty, it is worth to still explore some property of this integral Equation.

In particular in the next paragraph we illustrate how (2.25) can be used to calculate the plasma induced voltages in conducting structures, independently of the gauge. In the last paragraph of this subsection we illustrate that we may still use this direct formulation for computing the poloidal field related to the axisymmetric mode.

The plasma-induced Voltages

Here we first find a convenient expression for the magnetic vector potential associated to electric currents in the inner domain, as a function of the external currents and of the vector potential at the Coupling Surface. We can start directly from (2.20). Notice that the plasma vector potential due to currents in the interior domain $\mathbf{A}^*_{\mathbf{in}}$ is effectively the plasma currents generated vector potential in the Coulomb gauge. Using the vector identities $\nabla(gf) = g\nabla f + f\nabla g$, $\int_V \nabla f \,\mathrm{d}\mathbf{r} = \int_{+\partial V} f\hat{\mathbf{n}}\,\mathrm{d}\mathbf{r}$ and $\nabla' G = -\nabla G$, we get:

$$\mathbf{A}^*_{\mathbf{in}} = \mathbf{A}_{\mathbf{in}} + \int_{+\partial V_{in}} G(\nabla' \cdot \mathbf{A}')\hat{\mathbf{n}}'\,\mathrm{d}\mathbf{r}' - \nabla \underbrace{\left[\int_{V_{in}} (\nabla' \cdot \mathbf{A}') G\,\mathrm{d}\mathbf{r}'\right]}_{\chi_{in}} \quad (2.80)$$

Here we could get the derivative out of the integral, thanks to the fact that $\nabla G = -\nabla' G$, and by analogy with electrostatic problems. The last term at the r.h.s. appears really as the electric field generated by a charge distribution $\nabla \cdot \mathbf{A}$. We rigorously show in Appendix C, that Equation (2.80) above, thanks to Green's vector identity (2.23), can be rewritten in the more convenient form:

$$\begin{aligned} \mathbf{A}^*_{\mathbf{in}} &= \nu \mathbf{A} - \nabla \chi_{in} \\ &- \frac{1}{4\pi}\int_{\partial V_{in}} \left[G\left(\mathbf{B}' \times \hat{\mathbf{n}}'\right) + \left(\mathbf{A}' \times \hat{\mathbf{n}}'\right) \times \nabla' G - \left(\mathbf{A}' \cdot \hat{\mathbf{n}}'\right)\nabla' G\right]\mathrm{d}\mathbf{r}' \end{aligned} \quad (2.81)$$

For $\nabla \chi_{in} = 0$ (*i.e.* in the Coulomb Gauge) this is essentially the same form as provided in Stratton's textbook [99].

In case we want to evaluate $\mathbf{A}^*_{\mathbf{in}}$ for points $\mathbf{r}$ in the outer domain V_{ext}, then we have certainly $\nu = 0$. Moreover, the gradient terms, which involve the volume integral and the surface integral of $G(\mathbf{A} \cdot \hat{\mathbf{n}})$ are also unimportant, since they will not have any effect on induced voltages. This makes clear that we can easily evaluate induced voltages due to plasma currents if we know about the tangential magnetic field and the tangential vector potential at a surface enclosing the plasma, whatever is the gauge actually used. The fact that $\mathbf{A} \cdot \hat{\mathbf{n}}$ is unimportant is physically consistent with the fact that it does not specify anything about magnetic fluxes linked to curves on the interface between the two domains. Finally the electromagnetic effect of the plasma currents on the outer domain is correctly represented by the equivalent surface current distribution

$$\mathbf{k_{eq}} = -\frac{1}{\mu_0}\mathbf{B} \times \mathbf{n} \tag{2.82}$$

and the equivalent surface distribution of magnetic moment

$$\mathbf{M_{eq}} = -\frac{1}{\mu_0}\mathbf{A} \times \mathbf{n} \tag{2.83}$$

so that

$$\begin{aligned} \mathbf{A}^*_{\mathbf{in}} + \nabla f =& \frac{\mu_0}{4\pi}\int_{\partial V_{in}} G\,\mathbf{k}'_{\mathbf{eq}}\,\mathrm{d}\mathbf{r}' \\ &+ \frac{\mu_0}{4\pi}\int_{\partial V_{in}} \mathbf{M}'_{\mathbf{eq}} \times \nabla' G\,\mathrm{d}\mathbf{r}' + \nu\mathbf{A} \end{aligned} \tag{2.84}$$

which implies, since $\mathbf{M_{eq}} \cdot \hat{\mathbf{n}} = 0$,

$$\begin{aligned} \mathbf{B_{in}} =& \frac{\mu_0}{4\pi}\int_{\partial V_{in}} \mathbf{k}'_{\mathbf{eq}} \times \nabla' G\,\mathrm{d}\mathbf{r}' \\ &+ \frac{\mu_0}{4\pi}\int_{\partial V_{in}} \nabla'_{\parallel} \cdot \mathbf{M}'_{\mathbf{eq}} \nabla' G\,\mathrm{d}\mathbf{r}' + \nu\mathbf{B} \end{aligned} \tag{2.85}$$

Using definition (2.83), it is possible to show $\mu_0\nabla_{\parallel} \cdot \mathbf{M_{eq}} = B_n$. Hence finally we can express (2.85) in terms of magnetic flux density:

$$\begin{aligned} \mathbf{B_{in}} =& \frac{1}{4\pi}\int_{\partial V_{in}} \left(\mathbf{B}' \times \hat{\mathbf{n}}'\right) \times \nabla' G\,\mathrm{d}\mathbf{r}' \\ &+ \frac{1}{4\pi}\int_{\partial V_{in}} B'_n \nabla' G\,\mathrm{d}\mathbf{r}' + \nu\mathbf{B} \end{aligned} \tag{2.86}$$

Implications for the MHD Boundary Conditions

Let's look again to the problem of the calculation of $\hat{\mathbf{n}} \times \mathbf{B}$, now that this term appears explicitly in our boundary integral Equations. Thanks to definition (2.79) and our result (2.81), we can rewrite (2.78) as

$$
\begin{aligned}
(1-\nu)\,\mathbf{A} = &-\frac{1}{4\pi}\int_{\partial V_{in}}\left[G\left(\mathbf{B}'\times\hat{\mathbf{n}}'\right)\right]\mathrm{d}\mathbf{r}' \\
&-\frac{1}{4\pi}\int_{\partial V_{in}}\left[\left(\mathbf{A}'\times\hat{\mathbf{n}}'\right)\times\nabla' G-\left(\mathbf{A}'\cdot\hat{\mathbf{n}}'\right)\nabla' G\right]\mathrm{d}\mathbf{r}' \\
&+\mathbf{A}^{*}_{\mathbf{ext}}+\nabla\underbrace{\int_{V_{ext}}G\left(\nabla'\cdot\mathbf{A}'\right)\mathrm{d}\mathbf{r}'}_{\chi_{ext}}
\end{aligned}
\tag{2.87}
$$

Again, we face the problem of the apparently unknown term related to the gauge choice. Also in this case, relying on physical considerations, we may probably restrict our attention to the subspace of vector fields whose tangent component to the boundary to the boundary is divergence-free. Anyway, the real idea which lead us to the formulation of such *direct* method was to avoid the construction of ad hoc subspaces on the Coupling Surface for getting information on $\mathbf{B}\times\hat{\mathbf{n}}$. Whenever this is not the case, we may well stay with the Virtual Casing formulation. Hence, we do not explore this opportunity.

We just want to explore here some interesting features of the axisymmetric case. For completeness, let us arrive to describe this case via a Fourier decomposition of the problem along to the toroidal angle, we will need such kind of expansions also later. For clarity we keep an exponential notation here:

$$
\begin{aligned}
(a)\quad \hat{\mathbf{B}} &= \sum_{k=-\infty}^{+\infty}\hat{\mathbf{B}}_{\mathbf{k}}\mathrm{e}^{jk(\varphi-\varphi')} \\
(b)\quad \hat{\mathbf{A}} &= \sum_{k=-\infty}^{+\infty}\hat{\mathbf{A}}_{\mathbf{k}}\mathrm{e}^{jk(\varphi-\varphi')}
\end{aligned}
\tag{2.88}
$$

In this notation, we use an hat to denote the complex quantities in the Fourier space, relative to the spatial coordinate φ. We need at this stage to expand the Green function $G(\mathbf{r},\mathbf{r}')$ defined by (2.15) similarly [100]:

$$
G=\frac{1}{|\mathbf{r}-\mathbf{r}'|}=\frac{1}{\pi\sqrt{rr'}}\sum_{k=-\infty}^{\infty}e^{i\,k(\varphi-\varphi')}Q_{k-1/2}(\chi) \tag{2.89}
$$

where $Q_{k-1/2}(\chi)$ are half-integer Legendre functions of the second kind:

$$
Q_{k-1/2}(\chi)=\frac{1}{2\sqrt{2}}\int_0^{2\pi}\frac{\cos ku}{\sqrt{\chi-\cos u}}\,\mathrm{d}u \tag{2.90}
$$

and

$$\chi = \frac{2}{k^2} - 1 \quad \text{with} \quad k^2 = \frac{4rr'}{(r+r')^2 + (z-z')^2} \tag{2.91}$$

It is evident that we can study the problem harmonic by harmonic. Let us introduce some short-hands for convenience and clarity. We denote $\mathbf{B_{tan}} = \mathbf{B} \times \hat{\mathbf{n}}$, $\mathbf{A_{tan}} = \mathbf{A} \times \hat{\mathbf{n}}$, and clearly $A_n = \mathbf{A} \cdot \hat{\mathbf{n}}$ in (2.87). Moreover we define:

$$G_k = Q_{k-1/2} \frac{\sqrt{rr'}}{2\pi} \tag{2.92}$$

With this notation, we finally expand (2.87) in toroidal harmonics. Equating each term with the same dependence on φ, we get

$$\begin{aligned}(1-\nu)\, \hat{\mathbf{A}}_{\mathbf{k}} - \left(\hat{\nabla}\chi_{ext}\right)_k = & \hat{\mathbf{A}}^*_{\mathbf{w,k}} \\ & - \frac{1}{r} \int_{\Gamma_p} G_k \hat{\mathbf{B}}'_{\mathbf{tan,k}} \,\mathrm{d}\ell' \\ & - \frac{1}{r} \int_{\Gamma_p} \hat{\mathbf{A}}'_{\mathbf{tan,k}} \times \left[r' \nabla' \frac{G_k}{r'} - jkG_k \mathbf{i}'_\varphi \right] \mathrm{d}\ell' \\ & - \frac{1}{r} \int_{\Gamma_p} \hat{A}'_{n,k} \left[r' \nabla' \frac{G_k}{r'} - jkG_k \mathbf{i}'_\varphi \right] \mathrm{d}\ell' \end{aligned} \tag{2.93}$$

In general, we are not able to evaluate $(\hat{\nabla}\chi_{ext})_k$, except eventually at the expenses of very large volume integrals. However, consider the axisymmetric mode $n = 0$. In this case the toroidal component of the magnetic vector potential is solely related to the poloidal component of the magnetic field and vice-versa. We can hence focus our attention to the axisymmetric toroidal component of the magnetic vector potential, $\psi_0 \nabla\varphi$, which generates the axisymmetric poloidal field $\nabla\psi_0 \times \nabla\varphi$. In the projection of (2.93) along the toroidal angle the gradient term $\left(\hat{\nabla}\chi_{ext}\right)_0$ drops out. Indeed a the gradient of a scalar single valued function cannot have an axisymmetric component in the toroidal direction. Hence, after some algebra[6], the toroidal projection of (2.93) for $k = 0$ takes the form:

$$(1-\nu)\,\psi_0 = \psi^*_{ext,0} - \int_{\Gamma_{p,in}} G_0 \frac{1}{r'} \frac{\partial \psi'_0}{\partial n'} \,\mathrm{d}\ell' + \int_{\Gamma_{p,in}} \psi'_0 \frac{1}{r'} \frac{\partial G_0}{\partial n'} \,\mathrm{d}\ell' \tag{2.94}$$

[6]In particular, using the property $\nabla\left(G_0/r'\right) = -\nabla'\left(G_0/r'\right)$.

where G_0 is given by (2.92), and is the standard Green function for the poloidal flux produced by a toroidal filament. In [96] the factor $(1 - \nu)$ is better specified in terms of solid angles, so to account for eventual singularities of the surface ∂V_{in}. We see that Equation (2.94) is valid in any gauge, and we may use it for getting information on the tangential component of the axisymmetric poloidal field at the Coupling Surface. The necessary and sufficient information to determine the outer magnetostatic problem is contained respectively in ψ_0 (tangential component of the vector potential at the boundary) and in $\psi^*_{ext,0}$ (information about currents in the exterior domain). The fact that the axisymmetric version of the problem is gauge independent, at least as far as the poloidal magnetic field is concerned, should not be surprising. Indeed, in the axisymmetric case, $\psi(r, z)$ assumes the real meaning of the flux of magnetic field linked to the loop whose trace in the poloidal half-plane $\varphi = 0$ is given by the coordinates (r, z).

The discussion would be instead quite more intricate for what concerns the poloidal component of the magnetic vector potential, hence the toroidal magnetic field, and we prefer to postpone this problem directly to the magnetic field formulation presented in next Section. Here it is just worth recalling that in normal situations there are no poloidal currents crossing the physical boundary ∂V_{in}, and the toroidal field can be substantially attributed to the external conductors. The topology of the problem itself, together with Ampère's law suggest then to write the toroidal magnetic field at the boundary as

$$B_\varphi = \frac{F_{act} + F_{eddy}}{r} \tag{2.95}$$

To conclude, the boundary integral Equation (2.94) is suitable to find the the axisymmetric poloidal magnetic field component tangent to the boundary. On the other hand, this method suffers the gauge choice for higher order harmonics.

2.6.2 Magnetic Field Formulation

The inherent difficulties related to the gauge in the vector potential formulation, lead us to go toward a pure magnetic field formulation. The fundamental Equation was already provided as a by-product of the previous discussion, see Equation (2.86). It is convenient to rewrite it again here, adding directly the contribution of the active and wall currents:

$$(1-\nu)\,\mathbf{B} = \mathbf{B_{ext}} - \frac{1}{4\pi}\int_{\partial V_{in}} \left[\left(\mathbf{B}'\times\hat{\mathbf{n}}'\right)\times\nabla' G - B_n'\nabla' G\right]\mathrm{d}\mathbf{r}' \quad (2.96)$$

For points on the Coupling Surface, we may enforce (2.96) in weak form, using JOREK boundary basis vectors as space of test functions. This would lead to the algebraic problem

$$\underline{B_{tan}} = \underline{B_{ext,tan}} + \underline{\underline{M_{t,t}}}\,\underline{B_{tan}} + \underline{\underline{M_{t,n}}}\,\underline{B_n} \quad (2.97)$$

where the vector of external magnetic fields $\underline{B_{ext,tan}}$ and the vector of the normal component of the overall magnetic field $\underline{B_n}$ are assigned. The question arises whether (2.96) is suitable for the calculation of the tangential magnetic field, *i.e.* whether the linear system (2.97) is invertible respect to $\underline{B_{tan}}$. Observe immediately that $\mathbf{B}\cdot\hat{\mathbf{n}}$ brings an information "almost" equivalent to the one contained in $\mathbf{A}\times\hat{\mathbf{n}}$. The information lost, passing from the tangential component of the vector potential to the normal component of the magnetic field is precisely related to the flux linked by a curve wrapping around the hole of our toroidal Coupling Surface. Given this information, $\mathbf{B}\cdot\mathbf{n}$ allows in principle to reconstruct the information of $\mathbf{A}\times\hat{\mathbf{n}}$.

Is this *lost* information important? Consider a simple case where there are no currents in the outer domain. Think of a non-null toroidal current density distribution within the inner domain which makes the Coupling Surface itself a flux surface, *i.e.* $\mathbf{B}\cdot\hat{\mathbf{n}} = 0$ on ∂V_{in}. The linear system (2.97) would be homogeneous, but we know that a tangent magnetic vector field exists. In order to persuade ourselves that the system is undetermined, we consider two more uniqueness Theorems for the magneto-static field.

Theorem 2 *In the outer domain V_{ext}, the electric current density* $\mathbf{i}$*, the normal component of the magnetic flux density at the Coupling Surface $\mathbf{B}\cdot\hat{\mathbf{n}} = f$, and the circulation $\mu_0 I_\varphi$ of $\mathbf{B}$ linked to a curve $[\Gamma_p]$, representative for the homology group of curves wrapping around the torus, are assigned. Then, the magnetostatic problem*

$$\nabla\times\mathbf{B} = \mu_0\mathbf{i} \quad \text{in}\Omega_e$$

$$\nabla\cdot\mathbf{B} = 0 \quad \text{in}\Omega_e$$

$$\mathbf{B}\cdot\hat{\mathbf{n}} = f \quad \text{on}\partial\Omega_e$$

$$\int_{\Gamma_p} \mathbf{B} \cdot \mathbf{t} \, \mathrm{d}\ell = \mu_0 I_\varphi$$

has a unique solution, provided $\mathbf{B}$ *is regular at infinity.*

Proof: Suppose that two different solutions of the above problem exist, and define their difference as $\delta\mathbf{B} = \mathbf{B_1} - \mathbf{B_2}$. Due to linearity, clearly $\delta\mathbf{B}$ has to satisfy the associated homogeneous problem. Let us evaluate the L^2-norm of $\delta\mathbf{B}$. Considering together the indivergence of $\delta\mathbf{B}$ and the fact that $\delta\mathbf{B} \cdot \mathbf{n} = 0$ on the boundary of the domain, we can conclude that $\delta\mathbf{B}$ is orthogonal to the gradient of any scalar function in V_{ext}:

$$\int_{V_{ext}} \delta\mathbf{B} \cdot \nabla\varphi \, \mathrm{d}^3\mathbf{r} = \int_{+\partial V_{ext}} \varphi \underbrace{\delta\mathbf{B} \cdot \mathbf{n}}_{=0} \mathrm{d}^2\mathbf{r} - \int_{V_{ext}} \varphi \underbrace{\nabla \cdot \delta\mathbf{B}}_{=0} \mathrm{d}^3\mathbf{r} = 0 \quad (2.98)$$

Besides curl-free, the difference field $\delta\mathbf{B}$ is also conservative if and only if its circulation along Γ_p is zero. We notice explicitly that only in this case the circulation of $\delta\mathbf{B}$ along any close line will be zero. □

Theorem 3 *In the outer domain V_{ext}, the electric current density* $\mathbf{i}$*, the normal component of the magnetic flux density at the Coupling Surface* $\mathbf{B} \cdot \hat{\mathbf{n}} = f$*, and the flux* ψ_t *of* $\mathbf{B}$ *linked to a curve* $[\Gamma_t]$*, representative for the homology group of curves wrapping around the hole of the torus, are assigned. Then, the magnetostatic problem*

$$\nabla \times \mathbf{B} = \mu_0 \mathbf{i} \quad \mathrm{in} \Omega_e$$

$$\nabla \cdot \mathbf{B} = 0 \quad \mathrm{in} \Omega_e$$

$$\mathbf{B} \cdot \hat{\mathbf{n}} = f \quad \mathrm{on} \partial\Omega_e$$

$$\int_{\Sigma_{\Gamma_t}} \mathbf{B} \cdot \hat{\mathbf{n}} \, \mathrm{d}\mathbf{r} = \psi_{\Gamma_t}$$

has a unique solution, provided $\mathbf{B}$ *is regular at infinity.*

Proof: As before, we want the difference problem to define $\delta\mathbf{B}$ to be orthogonal to itself in $L^2(V_{ext})$. We already know that $\delta\mathbf{B} \in \ker(\mathrm{div}(V_{ext}))$, we need to prove it is also in $\mathrm{grad}[H^1(V_{ext})]$. Since $\delta\mathbf{B} \cdot \hat{\mathbf{n}} = 0$ and $\delta\mathbf{i} = 0$, the magnetic flux linked to any curve in the homology group of Γ_t is the same.

This is in a $1:1$ correspondence to the circulation of $\delta\mathbf{B}$ around the torus, via the external inductance of the toroidal surface,

$$\delta\psi = L\,\delta I_\varphi$$

Since $\delta\psi = 0$, then $\delta I_\varphi = 0$ and the circulation of $\delta\mathbf{B}$ along any close line is zero. □

The discussion makes clear that we need to re-integrate some information in (2.97) to make it invertible, since $\mathbf{B}\cdot\hat{\mathbf{n}}$ alone is not sufficient. In particular, if the plasma current is known, we can really enforce the discrete version of the circulation constraint:

$$\underline{\Lambda}\cdot\underline{B_{tan}} = \mu_0 I_p \tag{2.99}$$

The constraint can be imposed via an eigenvector decomposition. In particular we can take:

$$\underline{\underline{1}} - \underline{\underline{\underline{M_{t,t}}}} = \underline{\underline{T}}^{-1}\,\underline{\underline{\Sigma}}\,\underline{\underline{T}} \tag{2.100}$$

where $\underline{\underline{T}}$ is the matrix whose columns are the eigenvectors of the linear operator $\underline{\underline{1}} - \underline{\underline{\underline{M_{t,t}}}}$, and $\underline{\underline{\Sigma}}$ is the diagonal matrix containing the eigenvalues. We find numerically that the above matrix is indeed singular, having a null eigenvalue. We order the eigenvalues so that the null one is also the last. Now, we consider the linear system (2.97), and the topological constraint (2.100) in the basis of eigenvectors,

$$\begin{aligned} (a) \quad & \underline{\underline{\Sigma}}\,\underline{\tilde{B}_{tan}} = \underline{\underline{\tilde{M}_n}}\,\underline{B_n} + \underline{\tilde{B}_{ext,tan}} \\ (b) \quad & \underline{\tilde{\Lambda}}\cdot\underline{\tilde{B_{tan}}} = \mu_0 I_\varphi . \end{aligned} \tag{2.101}$$

The tilde denotes here vectors and matrices as represented in the eigenvector basis. We need just to add the constraint (b) to the last Equation of the linear system (a). The result, moving back to the original representation is:

$$\left(1 - \underline{\underline{M_{B_t,B_t}}} + \underline{\underline{M_\Lambda}}\right)\underline{B_{tan}} = \underline{\underline{M_{B_t,B_n}}}\,\underline{B_n} + \mu_0 I_\varphi \underline{B_{tan,0}} + \underline{B_{ext,tan}} \tag{2.102}$$

where $\underline{B_{tan,0}}$ is the eigenvector associated to the originally null eigenvalue and

$$\underline{\underline{M_\Lambda}} = \underline{B_{tan,0}} \otimes \underline{\Lambda} \tag{2.103}$$

Equation (2.102) provides an example of magnetic field formulation, properly fixed to account for the topological singularity. It is worth stressing that the plasma current is not always an input of the model (it is actually not in general, and it is really computed as the circulation of $\mathbf{B}$ indeed). Hence, proper techniques should be set up if one wants to enforce the constraint in this way.

The Toroidal Geometry

Expansion in the toroidal angle makes the magnetic field formulation very convenient, besides providing some insight about the topological constraint applied to the problem. Let us then apply the toroidal expansion of $\mathbf{B}$ and of the Green function G, already described in (2.88) and (2.89), to the boundary Equation (2.96):

$$\begin{aligned}(1-\nu)\,\hat{\mathbf{B}}_{\mathbf{k}} = \hat{\mathbf{B}}_{\mathbf{ext},\mathbf{k}} \\ -\frac{1}{r}\int_{\Gamma_p} \hat{\mathbf{B}}'_{\mathbf{tan},\mathbf{k}} \times \left[r'\nabla' G_k - jkG_k\mathbf{i}'_{\varphi}\right] \mathrm{d}\ell' \\ +\frac{1}{r}\int_{\Gamma_p} \hat{B}'_{n,k}\nabla' \left[r'\nabla' G_k - jkG_k\mathbf{i}'_{\varphi}\right] \mathrm{d}\ell'\end{aligned} \tag{2.104}$$

where the Green functions G_k were defined in (2.92).

Let us consider now (2.104) for a generic toroidal harmonic $k \geq 1$. Clearly, a magnetic field with such a periodicity in the toroidal angle can't give any finite flux through a surface linked to Γ_t. This is a structural feature of the toroidal harmonic decomposition, and suggests that the system (2.104) is invertible for any $k \geq 1$. This is further confirmed considering the circulation along a poloidal curve such as the Γ_p defined in Figure 2.1. The information contained in $\int_{\Gamma_p} \hat{\mathbf{B}}_{\mathbf{k}} \cdot \hat{\mathbf{t}}\,\mathrm{d}\ell$ is indeed information on the actual currents flowing inside and outside the domain with toroidal frequency $k/2\pi$. This information is however already contained in the external currents to the MHD computational domain (since the jump of $\mathbf{i}\cdot\hat{\mathbf{n}}$ across the Coupling Surface has to be null). There are enough arguments to claim that the topological constraint needs hence to be applied to the problem solely for the $n=0$ mode. Limiting our attention to the axi-symmetric case, of course we have again the poloidal/toroidal decomposition of the problem, and Equation (2.104) takes the form ($\hat{\mathbf{i}}_{\varphi} \times \hat{\mathbf{n}} = \hat{\mathbf{i}}_{\mathbf{u}}$):

$$
\begin{aligned}
(a) \quad (1-\nu)\left(-\frac{1}{r}\frac{\partial\psi}{\partial n}\right) = \quad & \frac{1}{r}\frac{\partial}{\partial n}\left[\int_{\Gamma_p}\frac{1}{r'}\frac{\partial\psi'}{\partial n'}G_0\,\mathrm{d}\ell'\right] \\
& +\frac{1}{r}\frac{\partial}{\partial u}\left[\int_{\Gamma_p}\frac{1}{r}\frac{\partial\psi'}{\partial u'}G_0\,\mathrm{d}\ell'\right] \\
(b) \quad (1-\nu)\frac{F}{r} = \quad & \frac{F_{ext}}{r} - \frac{1}{r}\int_{\Gamma_p}F'\frac{\partial G_0}{\partial n'}\,\mathrm{d}\ell'
\end{aligned}
\tag{2.105}
$$

As discussed, Equation (2.105a) is not invertible. Indeed the information on the plasma current or equivalently on the poloidal flux regards solely this field component. On the other hand the axisymmetric toroidal field at the boundary is solved solely in terms of the external currents. Indeed when there are no currents in external circuits $F = 0$.

2.7 The role of Halo Currents

Up to this point, we scarcely commented on the possibility of shared currents between plasma and structures, which are instead a major concern of the tokamak community, and generally defined as *halo currents* [101, 102, 103]. Although they are negligible in the normal operation of the device, fast transients may be responsible for a significant contact of the plasma column with the solid structures, and in turn of a significant plasma current injected into structures. Especially the axisymmetric poloidal halo current, in its interaction with the toroidal magnetic field applied by the external Toroidal Field coils, can generate severe forces on structures [44].

We commented in previous Sections that the essential information we need about $\mathbf{A_{tan}}$, is essentially the one related to the magnetic fluxes, linked to any possible close line laying on the boundary. This lead us to consider the portion of $\mathbf{A}$ tangent to the Coupling Surface and divergence-free therein. Those considerations are still valid, anyway it is the case now of providing information on the actual currents crossing the Coupling Surface. Earlier, when discussing the Virtual Casing Principle, we assumed that the electric current density within the inner domain was on its own solenoidal ($\mathbf{i} \in \mathrm{grad}[H^1(V_{in})]$), circumstance which is not valid in presence of halo currents. What does happen if we apply Equation (2.50) to find the equivalent current in presence of halo currents?

Our current distribution $\mathbf{i}$ is not anymore solenoidal separately in both domains V_{in} and V_{ext}, but solely in the whole domain V. We can anyway imagine to add and subtract to the current $\mathbf{i}$ a surface current distribution $\mathbf{k_{halo}}$ located at the Coupling Surface. In particular we can imagine that $\mathbf{k_{halo}}$, on the inner page of the Coupling Surface, makes close the plasma current paths within the inner domain. On the outer page $-\mathbf{k_{halo}}$ makes close instead the current paths of external conductors which terminate at the Coupling Surface. Certainly $\mathbf{k_{halo}}$ belongs to the space $(\ker[\mathrm{div}(\partial V_{in})])^{\perp}$. Indeed, in absence of halo currents we don't need such a current sheet, while in order to provide a closure of the plasma current paths it is certainly:

$$\nabla_{\parallel} \cdot \mathbf{k_{halo}} = \mathbf{i} \cdot \hat{\mathbf{n}} \tag{2.106}$$

The fact that $\mathbf{k_{halo}}$ is orthogonal to div-free vector fields in the Coupling Surface, means that we can write it as the surface gradient of some scalar function $\mathbf{k_{halo}} = -\nabla_{\parallel}\phi_{halo}$. The current $\mathbf{i} + \mathbf{k_{halo}}$ is on its own solenoidal in the inner domain. Hence we can retain that this current contribution is correctly reproduced by the equivalent current as previously computed via (2.50). Anyway we left out a further contribution $-\mathbf{k_{halo}}$. Let's have a look whether this is accounted in our equivalent current:

$$\begin{aligned}\int_{\partial V_{in}} \mathbf{w} \cdot \int_{\partial V_{in}} G\mu_0 \nabla'_{\parallel}{\phi_{halo}}' \,\mathrm{d}\mathbf{r}\,\mathrm{d}\mathbf{r} = \\ = -\int_{\partial V_{in}} \mathbf{w} \cdot \nabla_{\parallel} \int_{\partial V_{in}} G\mu_0 {\phi_{halo}}' \,\mathrm{d}\mathbf{r}\,\mathrm{d}\mathbf{r} = 0\end{aligned} \tag{2.107}$$

We see that $-\mathbf{k_{halo}}$ the current density distribution which would make the currents in the exterior domain solenoidal within V_{ext}, is not contained within the equivalent current $\mathbf{k_{eq}}$ we calculate. This is clear, as we are considering an divergence-free current on the Coupling Surface, contrary to the nature of $\mathbf{k_{halo}}$ as we defined it. One may think then to consider a complementary set of basis functions in $\mathrm{grad}\left[H^1(\partial V_{in})\right]$, to represent the effect of currents crossing the interface. Anyway, the projection of (2.44) on such a subspace, would not set to zero the gauge-related terms. This aspect, together with the actual properties of CARIDDI basis vectors, makes this way not very practical in view of the plasma-structures electromagnetic coupling. Nonetheless, as long as the injected currents are provided, $-\mathbf{k_{halo}}$ can be easily reconstructed. In particular we can define electrodes on the outer page of the equivalent shell. The halo current injected into the conducting structures has to be drained from the equivalent shell and vice versa. This way we recover all the remainder previously discarded information.

In this respect, while we may still keep the virtual casing formulation to model the solenoidal eddy currents, we found a special treatment for the halo currents. In particular, when injecting halo currents in structures, we should always be careful to make the currents in the outer domain solenoidal on their own, implementing a surface current distribution which makes the outer domain current paths close. This is in a sense the approach used in the axisymmetric evolutionary equilibrium model *CarMa0NL* [84, 104]. There, equivalent currents are only able to catch the information on the toroidal plasma current, the poloidal currents within the first wall being synthetically described by a plasma toroidal flux variable. In order to inject currents in the wall, a fictitious shell is implemented which allows for the currents in the exterior domain to be solenoidal in V_{ext}. A divergence-free poloidal equivalent surface current at the Coupling Surface, could only account for the overall toroidal flux information. The neglect of other information virtually coincides with the set-up of a poloidal surface current distribution on the inner page of ∂V_{in} which makes the plasma currents solenoidal on their own, and whose undesired effect in terms of magnetic field is annihilated precisely by the corresponding fictitious poloidal currents in the outer domain.

On the other hand, the magnetic field formulation proposed in Section 2.6.2, does not need particular care in this respect, as the boundary conditions set up for the magnetic fields at the computational MHD boundary are independent from the eventual passage of currents across the Coupling Surface. Consider the case of an axisymmetric plasma hitting the wall, generating this way a shared axisymmetric poloidal current between plasma and structures. The governing Equation for the boundary condition on the toroidal magnetic field is provided by (2.105). We may rewrite that Equation in the more physically intuitive form:

$$(1-\nu)\,\frac{\mu_0 I_{pol}}{2\pi r} = \frac{\mu_0}{4\pi}\int_{V_{ext}} \mathbf{i}\times\nabla' G\,\mathrm{d}\mathbf{r}' - \int_{\partial V_{in}} \frac{\mu_0 I'_{pol}}{2\pi r'}\hat{\mathbf{i}}'_{\mathbf{u}}\times\nabla' G\,\mathrm{d}\mathbf{r}' \tag{2.108}$$

The surface integral is exactly the magnetic field produced by a poloidal current distribution at ∂V_{in} of density $\mu_0 I_{pol}/2\pi r$. Consider first a situation when there are no halo currents, and the external toroidal field is clearly given by $\mu_0 I_{ext}/2\pi r$. Then equation above is trivially satisfied by $I_{pol} = I_{ext}$ at the boundary of the domain. Similarly when we have a current crossing ∂V_{in}, the last surface term configures a current distribution which makes solenoidal the current distribution $\mathbf{i}$ within structures. At the boundary between inner and outer domain this overall solenoidal current distribution produce a discontinuous toroidal field which is given essentially by one half of the toroidal field in the perfect toroidal solenoid constituted by the real currents flowing in external conductors and the fictitious current circulating on ∂V_{in}. Not by coincidence at the boundary $(1-\nu) = 1/2$, and the boundary conditions are again provided correctly. Hence this formulation maintains the potential advantage of non-discretizing the MHD computational boundary accordingly with the MQS numerical model of the external structures, even in presence of halo currents. This same fact could be seen eventually also as a possible disadvantage: the eventual mismatch between the effective toroidal and curved Coupling Surface ∂V_{in} and the straight electrodes of conducting structures, can configure a current density which is quite "imprecisely solenoidal" (*e.g.* the surface current may vanish in vacuum at some point and appear again at some conducting structures' electrode).

The uniqueness of the overall coupled problem is subject to the condition of having an overall solenoidal current density. Notice that in principle the current density has not to be solenoidal separately in the two domains, but just in the whole domain. Then we need to enforce the continuity of the normal component of the current density, which configures itself as a Kirchoff Current Law at the structures *electrodes* facing the plasma in the CARIDDI formulation. In this respect, the injected currents into CARIDDI electrodes could be assigned, while electrodes potentials could be treated as further unknowns. This way we would have an equal number of Equations and unknowns in the CARIDDI formulation, see Equations (2.29) and (2.32). Take in mind moreover that the actual current density crossing the boundary is given by the line integrals along the boundary of the tangent magnetic field. In both the approaches presented the tangent magnetic field is obtained as the solution of the outer magnetostatic field problem, and we may well argue that $I_{halo} = f(B_{tan})$.

It remains an open question whether the sheath physics models described in the previous Chapter can be conveniently coupled in this framework. A recent attempt to include the effect of the ion saturation current was made in [50]. First notice that at the present we retain that there are no surface current densities tangent to the boundary, so that the tangential magnetic field is essentially the same at the boundary of the MHD computational domain and at the sheath entrance. In any case the halo current flowing across the computational domain is given by the coupled solution of the inner and outer problems to the Coupling Surface. In this framework is not simple to imagine how the current-voltage characteristics of the sheath can be taken into account in the interaction scheme. The discussion of Section 1.10 would suggest to model the actual sheath as a set of non-linear resistors connecting the inner and the outer domain. These resistors would have a shared terminal in the bulk plasma, which is retained equipotential, plus a further terminal at the conducting structures' electrodes. The highly non-linear characteristic (i, v) already discussed is moreover determined by the actual value of the electron temperature. How can we frame those considerations in this context? The answer does not seem simple, and will be object of future research.

Chapter 3

Theory of MHD Evolutionary Equilibrium

The birth of Magneto-Hydro-Dynamics as a physics subject on itself is largely due to the seminal paper of H. Alfvén "Existence of Electromagnetic-Hydrodynamic Waves" [8]. Probably for the first time, it was evidenced as a wave Equation can result from the coupling of purely mechanical and electromagnetic quasi-static phenomena. The characteristic velocity for the propagation of a magnetic field perturbation in a plasma with assigned current density is today indicated in literature as "Alfvén velocity" and defined as:

$$v_A = \frac{B}{\sqrt{\mu_0 \rho}} \rightarrow \tau_A = \frac{L}{v_A} \tag{3.1}$$

For typical tokamak plasma densities and magnetic fields, considered a characteristic length $L = 1$ m, the Alfvén time falls generally within the range 1-10 μs[1]. The electromagnetic interaction of the MHD plasma with the surrounding environment adds anyway an important ingredient to the Alfvén recipe.

In particular, for typical tokamak devices, where many conducting structures surround the plasma, the real inertia to the plasma motion is mostly provided by the eddy currents around the plasma, rather than by the mass density of the plasma itself. When this is the case, the mechanical motion will evolve on the relatively long electromagnetic time-scale (*i.e.* $\sim$ 1-10 ms for

[1]For a tokamak plasma we consider as reference magnetic flux density the **poloidal** magnetic flux density.

medium size devices). In these conditions, further physical phenomena taking place on the Alfvénic time-scale can be retained essentially instantaneous when studying plasma displacements. It makes sense in such situations to use *MHD evolutionary equilibrium models*, where the mass of the plasma is discarded completely. The electro-mechanical analogue of such a situation is that of an electrical motor driving an arbitrary machinery, the whole system having null mechanical inertia. The electromagnetic torque provided by the motor would adapt at any time to fit the load torque of the machinery. The velocity of the motor-machine drive would then result from this *mechanical equilibrium constraint* at any time instant[2].

In **Section 3.1** we show when the *evolutionary equilibrium* hypothesis makes sense in the study of rigid Vertical Displacement Events (VDEs) of the plasma column. This problem is considered here mainly to motivate the convenience and possible efficacy of evolutionary equilibrium MHD models for the coherent study of plasma mechanical evolution. Anyway the problem of the vertical motion of a tokamak plasma column plays a crucial role on its own in present tokamaks. Indeed, it is well recognised that a plasma with a vertically elongated cross section presents better performances in terms of *poloidal beta* and *energy confinement time* [105]. We shall come back to the definition of poloidal beta in this Chapter, this is a figure of merit which quantifies the achieved plasma kinetic pressure as compared to the magnetic pressure. The *energy confinement time* can be defined simply as the ratio of the plasma thermal energy and the plasma power losses and quantifies the capability of operating a tokamak in steady state [106]. The actual realization of vertically elongated plasma cross-sections, in MHD mechanical equilibrium, requires the application of quite large quadrupole magnetic fields, which in turn determines a mechanical instability respect to vertical displacements [107, 108]. As soon as the plasma displaces vertically it will find a radial field which further pushes the plasma in the direction of the motion. In Section 3.1 we will discriminate in which conditions this instability is *Alfvénic* and when instead the vertical motion evolves on the electromagnetic time-scale, introducing the a figure of merit known as *stability margin* [108, 109, 110, 111].

Motivated by the former discussion, we first introduce the MHD evolutionary equilibrium model for a simple high-aspect-ratio circular tokamak in **Section 3.2**. The discussion will reveal some key aspects of the MHD equilibrium

[2]This would be equivalent to consider the electrical drive system evolving through points of the steady state torque-velocity characteristic of the motor, instead of properly considering the angular momentum balance equation for the electrical drive.

problem, such as the necessity of a vertical field to provide the radial mechanical equilibrium, and its relation to the plasma internal parameters. Moreover this will be the occasion to derive some analytical formulas we will use in next Chapter for providing simple estimates of wall forces and energy exchanges. The approximations are introduced in successive steps, so to understand what key features remain valid in general. The discussion largely follows the work of V. D. Pustovitov [112, 113, 114].

Straight afterwards, in **Section 3.3** we provide a classification of MHD Equilibrium problems, mainly to introduce the concept of free-boundary MHD simulation. With these concepts set-up, we will be ready to describe in **Section 3.4** to introduce the free-boundary MHD evolutionary equilibrium model *CarMa0NL* [62]. Here, a free-boundary MHD equilibrium solver interacts self-consistently with the 3D model for conducting structures CARIDDI already described in Section 2.4. Hence, we will first review the key aspects of the free-boundary MHD equilibrium solver, which closely resembles the one presented in [115]. Following we will evidence how the *Virtual Casing Principle* is applied here for the self-consistent simulation of the plasma motion subject to the inertia of the external passive currents. Applications of this tool are postponed to the next Chapter.

3.1 Electro-mechanical semi-rigid Model

In this section we show the efficacy and comment on the range of validity of the plasma mass-less approximation when studying mechanical instabilities of a tokamak plasma column. In order to understand this key aspect we refer to a very simplified model of the single fluid MHD Equations. In particular, we consider an axisymmetric plasma column with a given cross-section. The only motions we allow for the plasma column are the rigid vertical motion and the radial motion. Moreover, also the plasma current distribution within this cross-section is assigned, so that we can describe the plasma ring simply in terms of a self-inductance and mutual inductances with the other circuits, variable only in relation to the position of the column in the poloidal plane (r, z).

In subsection 3.1.1 we provide the Equations of motion for a tokamak plasma under these constraints, using a Lagrangian formulation. It is worth stressing that a radial motion is not a rigid displacement: any time the major radius of the plasma changes the actual volume of the plasma column changes consequently. An overall radial mehcanical momentum balance hence involves internal forces to the plasma column, as we shall see soon. That's the motivation lead us to define the following model as "semi-rigid".

Strictly, for what we want to demonstrate, it is not even necessary to consider radial motions of the column: this general viewpoint is presented rather to allow for possible theoretical future extensions. In subsection 3.1.2 we indeed focus the attention solely on the rigid vertical displacements. Here we show that the neglect of plasma mass, besides being a singular perturbation, leads to meaningful results, at least as long as some figure of merit, which quantifies the *stabilizing force* provided by external passive currents is sufficiently larger than the *de-stabilizing force*.

3.1.1 Equations of Motion

The assumptions introduced, allow to study the plasma in interaction with the surrounding structures by the classical tools of Electrical Engineering. In particular the evolution equations for the electro-mechanical system introduced by these assumptions can be set up via a Lagrangian formulation [116].

All the conductors are fixed in the laboratory reference frame, except the plasma ring, which is allowed to rigidly displace vertically and to compress/extend along the radial direction. In our study we are interested solely in the self and mutual inductances between circuits, besides the eventual resistive dissipation there. We can neglect from the beginning the parasitic capacitances and capacitors within the external circuits, as they will not play a role in the subsequent study. The average kinetic pressure within the plasma is assumed to be assigned within each cross section, and is denoted by $\langle p \rangle$.

The generalized Lagrangian coordinates for such a system include:

- The generalized electric charges for each independent loop
$$q_k(t) = \int_{t_0}^{t} i_k(\tau)\,\mathrm{d}\tau \tag{3.2}$$
where the i_k are the electric currents for each independent loop in the external conductors;

- The generalized electric charge for the net toroidal and poloidal current within the plasma
$$\begin{aligned} (a) \quad & Q_\varphi(t) = \int_{t_0}^{t} I_\varphi(\tau)\,\mathrm{d}\tau \\ (b) \quad & Q_{pol}(t) = \int_{t_0}^{t} I_{pol}(\tau)\,\mathrm{d}\tau \end{aligned} \tag{3.3}$$

where I_φ is the overall toroidal plasma current and I_{pol} is the net poloidal current within the plasma. We stress that the current distributions are here considered to be always the same within the plasma poloidal cross-section.

- The radial and vertical position of the plasma cross-section within the poloidal plane, $r_p(t)$ and $z_p(t)$ respectively

The Lagrangian function describing such a system is

$$\begin{aligned}\mathcal{L} = &\frac{1}{2}\underline{i}\,\underline{\underline{L_{e,e}}}\,\underline{i} + \frac{1}{2}L_\varphi I_\varphi^2 + \frac{1}{2}L_{pol}I_{pol}^2 \\ &+ \underline{i}\cdot\underline{L_{e,\varphi}}\,I_\varphi + \underline{i}\cdot\underline{L_{e,pol}}\,I_{pol} \\ &+ \frac{1}{2}m_p\dot{r}^2 + \frac{1}{2}m_p\dot{z}^2 \\ &- \underline{V}\cdot\underline{q} - V_\varphi Q_\varphi - V_{pol}Q_{pol} - 2\pi r_p S_p\langle p\rangle\end{aligned} \tag{3.4}$$

Here the magnetic energy is described by the first five terms. As intuitively recognised $\underline{\underline{L_{e,e}}}$ is the mutual inductance matrix between external conductors, independent of the plasma position. The self inductance terms for plasma toroidal and poloidal currents are L_φ and L_{pol} respectively. The other mutual inductance terms are similarly defined. We notice explicitly that the self-inductance for these two plasma currents is insensitive to the vertical motion of the plasma itself, *i.e.* $L_\varphi = L_\varphi(r_p)$ and $L_{pol} = L_{pol}(r_p)$. Moreover, the net poloidal and toroidal plasma currents originate orthogonal magnetic fields, hence there is no mutual inductance between I_φ and I_{pol}. Since the poloidal current paths originate perfect toroidal solenoids the inductance terms $\underline{L_{e,pol}}$ are null for toroidal filament conductors and in any case depend solely on the radial position of the plasma r_p. In the remainder of the Lagrangian we notice the kinetic energy for the plasma cross-section, and the potential energy terms. In particular the last one synthetically accounts for the exchange term between mechanical energy and internal energy of the plasma and it is related to the deformation of the plasma ring. Further, we introduce linear dissipative terms for the various circuits by the means of a dissipation function

$$F_k = -\frac{\partial}{\partial i_k}D(i_1,\cdots,i_N)\,;\quad D = \underline{i}\cdot\underline{\underline{R}}\cdot\underline{i} \tag{3.5}$$

The Euler-Lagrange Equations for this electro-mechanical system are in principle:

$$
\begin{aligned}
(a)\quad & \underline{\underline{L}}\frac{\mathrm{d}}{\mathrm{d}t}\underline{i} + \underline{\underline{R}}\,\underline{i} + \underline{L_{e,\varphi}}\frac{\mathrm{d}}{\mathrm{d}t}I_\varphi + \underline{L_{e,pol}}\frac{\mathrm{d}}{\mathrm{d}t}I_{pol} \\
& + \frac{\partial \underline{L_{e,\varphi}}}{\partial r_p}\dot{r_p}I_\varphi + \frac{\partial \underline{L_{e,\varphi}}}{\partial z_p}\dot{z_p}I_\varphi + \frac{\partial \underline{L_{e,pol}}}{\partial r_p}\dot{r_p}I_{pol} + \underline{V} = \underline{0} \\
(b)\quad & L_\varphi\frac{\mathrm{d}}{\mathrm{d}t}I_\varphi + R_\varphi\, I_\varphi + \underline{L_{e,\varphi}}\frac{\mathrm{d}}{\mathrm{d}t}\underline{i} \\
& + \frac{\partial \underline{L_{e,\varphi}}}{\partial r_p}\dot{r_p}\cdot\underline{i} + \frac{\partial \underline{L_{e,\varphi}}}{\partial z_p}\dot{z_p}\cdot\underline{i} + \frac{\partial L_\varphi}{\partial r_p}\dot{r_p}\cdot I_\varphi + V_\varphi = 0 \\
(c)\quad & L_{pol}\frac{\mathrm{d}}{\mathrm{d}t}I_{pol} + R_{pol}\, I_{pol} + \underline{L_{e,pol}}\frac{\mathrm{d}}{\mathrm{d}t}\underline{i} \\
& + \frac{\partial \underline{L_{e,pol}}}{\partial r_p}\dot{r_p}\cdot\underline{i} + \frac{\partial L_{pol}}{\partial r_p}\dot{r_p}\cdot I_{pol} + V_{pol} = 0 \\
(d)\quad & m_p\frac{\mathrm{d}}{\mathrm{d}t}\dot{r_p} - \frac{1}{2}\frac{\partial L_\varphi}{\partial r_p}I_\varphi^2 - \frac{1}{2}\frac{\partial L_{pol}}{\partial r_p}I_{pol}^2 \\
& - \frac{\partial \underline{L_{e,\varphi}}}{\partial r_p}\cdot\underline{i}I_\varphi - \frac{\partial \underline{L_{e,pol}}}{\partial r_p}\cdot\underline{i}I_{pol} + 2\pi S_p\langle p\rangle = 0 \\
(e)\quad & m_p\frac{\mathrm{d}}{\mathrm{d}t}\dot{z_p} - \frac{\partial \underline{L_{e,\varphi}}}{\partial z_p}\cdot\underline{i}I_\varphi = 0
\end{aligned}
\tag{3.6}
$$

Various approximations of the dynamical system above are possible. In particular, as hinted, we consider the toroidal plasma current I_φ and the poloidal plasma current I_{pol} as assigned in the following discussion, so to neglect the Euler Lagrange equations (b) and (c) above. In the same stream, instead of feeding active coils via the corresponding voltages in the vector $\underline{V}$ we assume the active currents as known in advance.

3.1.2 Rigid Vertical Displacements

The only admissible rigid displacement for an axisymmetric system is the one along the vertical direction. Hence, we further assume here that the plasma column can only move vertically, via a rigid displacement. Moreover a single active circuit and a single eigenmode for the electric currents in passive structures is retained important. The plasma currents and active coil currents are assigned and constant through time. In these further approximations, Euler Equations (3.6) simplify to:

$$
\begin{aligned}
(a) \quad & L_w \dot{I}_w + R_w I_w + I_\varphi \frac{\partial M_{w,p}}{\partial z_p} \dot{z}_p = 0 \\
(b) \quad & m_p \ddot{z}_p - \frac{\partial M_{p,w}}{\partial z_p} I_w \, I_\varphi - \frac{\partial M_{p,PF}}{\partial z_p} I_{PF} \, I_\varphi = 0
\end{aligned}
\tag{3.7}
$$

Here the suffix "PF" is used to indicate the active "Poloidal Field" coil, and the suffix "w" is used to indicate the "wall" current. Whenever the toroidal plasma current is assumed to be concentrated in a toroidal filament of coordinates (r_p, z_p) in the poloidal plane, direct computation of the Lorentz force provides:

$$
\frac{\partial M_{p,w}}{\partial z_p} = -2\pi r_p \tilde{B}_{r,w}, \quad \frac{\partial M_{p,PF}}{\partial z_p} = -2\pi r_p \tilde{B}_{r,PF} \tag{3.8}
$$

where $\tilde{B}_{r,w}$ and $\tilde{B}_{r,PF}$ are the radial magnetic flux densities at (r_p, z_p) produced by a unitary current in the *wall* and *Poloidal Field* circuit respectively.

The dynamical system (3.7) is still non-linear as the spatial derivatives of the various mutual inductances are still arbitrary functions of the vertical position. It is convenient to linearise about a position of mechanical equilibrium,

$$
m_p \delta \dddot{z}_p + m_p \frac{1}{\tau_w} \delta \ddot{z}_p + \left(\frac{\partial F_{ST}}{\partial z_p} - \frac{\partial F_{PF}}{\partial z_p} \right)_{z_{eq}} \delta \dot{z}_p - \frac{1}{\tau_w} \frac{\partial F_{PF}}{\partial z_p} \bigg|_{z_{eq}} \delta z = 0 \tag{3.9}
$$

Here we consistently considered that at MHD equilibrium, there are no induced currents in passive structures, *i.e.* $I_w(t_0) = 0$. Moreover we defined the *stabilizing* force due to passive currents and the *destabilizing* force due to the active coil currents as

$$
\begin{aligned}
(a) \quad & \delta F_{ST} = \left(\frac{\partial M_{p,w}}{\partial z_p} \right)_{z_{eq}} I_\varphi \frac{\delta M_{p,w} \, I_\varphi}{L_w} \\
(b) \quad & \delta F_{PF} = \delta \left(\frac{\partial M_{p,PF}}{\partial z_p} \right)_{z_{eq}} I_\varphi I_{PF}
\end{aligned}
\tag{3.10}
$$

Notice that the stabilizing force δF_{ST} is the restoring force acting on the plasma column due to the action of wall currents in the limit case $R_w \to 0$, so that the current in passive conductors is purely inductive. In order to highlight the different time-scales involved, it is convenient to normalize Equation (3.9) so that the coefficient multiplying the higher order derivative multiplies an dimensionless term,

$$\left(\frac{\tau_A}{\tau_w}\right)^2\left[\delta\dddot{z}_p+\frac{1}{\tau_w}\delta\ddot{z}_p\right]+\left(\frac{1}{\tau_w}\right)^2\cdot\overbrace{\left[\frac{\mu_0}{B_0^2\,L}\cdot\left(\frac{\partial F_{ST}}{\partial z_p}-\frac{\partial F_{PF}}{\partial z_p}\right)_{z_{eq}}\right]}^{\hat{k}_1}\delta\dot{z}$$
$$-\left(\frac{1}{\tau_w}\right)^3\underbrace{\left[\frac{\mu_0}{B_0^2\,L}\cdot\left.\frac{\partial F_{PF}}{\partial z_p}\right|_{z_{eq}}\right]}_{\hat{k}_2}\delta z=0 \tag{3.11}$$

Here, provided the reference length L and the reference magnetic flux density B_0, the Alfvénic time was defined as

$$\tau_A=\frac{L\sqrt{\mu_0\frac{m_p}{L^3}}}{B_0} \tag{3.12}$$

and the coefficient $\hat{k}_1$ is defined as *stability margin* in the literature [108, 109, 110], although using a different normalization. This parameter provides an indication on how the stabilizing and destabilizing forces acting on the plasma vary in the direction of motion, although in the *ideal wall* limit (*i.e.* $R_w \to 0$). It is interesting to notice that the stability margin solely depends on the geometry of the problem, and the plasma and active coil currents. Explicitly considering the definitions of stabilizing and destabilizing forces (3.10) into the definition of stability margin provided in (3.11), we find

$$\hat{k}_1=\frac{\mu_0}{B_0^2L}\cdot\left[\left(\frac{\partial M_{p,w}}{\partial z_p}\right)^2_{z_{eq}}\frac{I_\varphi^2}{L_w}-\left(\frac{\partial^2 M_{p,PF}}{\partial z_p^2}\right)_{z_{eq}}I_{PF}I_\varphi\right] \tag{3.13}$$

Notice in particular that the stabilizing force depends on the square of the plasma current, while the destabilizing force depends linearly on it. Hence for an assigned normalized plasma current distribution, and given active currents, we shall expect that the stability margin decreases when the plasma current decreases [117]. We will see shortly that the actual dynamics of the plasma column evolution are essentially determined from this parameter: if the stabilizing force due to passive currents grows faster in the direction of the motion than the destabilizing force, the plasma column will move vertically on the electromagnetic time-scale. On the contrary the vertical instability will be Alvénic.

Hence, besides the ratio between the Alfvénic time scale and the electromagnetic time scale of external conductors is in general very small, *i.e.*

$$\varepsilon = \frac{\tau_A}{\tau_w} \to 0 \tag{3.14}$$

due to the presence of an eventually positive real eigenvalue, we should be very careful in discarding the higher order terms in the linear system (3.11), which would be the same as to neglect the plasma mass in the original dynamical system (3.7). More generally, such type of “perturbations” are singular, changing clearly the actual dynamical order of the system itself and eventually hiding some important dynamics. Hence we provide in next paragraph an asymptotic solution for the linear system (3.11), properly accounting for the mass of the plasma column. The asymptotic solution will confirm our claims and highlight the dependencies, showing in which conditions the plasma is unstable respect to the vertical motion and the key role of the *stability margin* in determining whether the instability is on the Alfvénic or electromagnetic time scale. In last paragraph we provide some further comments on the possibility of neglecting the mass of the plasma, showing that Tikhonov’s Theorem is inapplicable to the case of interest, unless explicitly accounting for the viscous phenomena.

Asymptotic Solution for Small Perturbations

In this paragraph, using Perturbation Theory tools for multiple time-scale systems [118], we provide an asymptotic solution of the linear system (3.9). The solution of the linear system is thought as an expansion in the small parameter $\varepsilon = \tau_A/\tau_w$:

$$\delta z_p\left(t\right) = \delta z_0\left(t\right) + \varepsilon \delta z_1\left(t\right) + \cdots \tag{3.15}$$

In particular, we will discard all correction terms, retaining $\delta z_p \simeq \delta z_0$. The idea is now to explicitly introduce two distinct time variables, one for the slow dynamics and another one for the fast dynamics [118]. This possibility can be understood going back to the phase-space description of the dynamical system. We think the “Hamiltonian” vector field $\frac{\mathrm{d}}{\mathrm{d}t}$ as a linear combination of two new vector fields $\frac{\partial}{\partial t_1}$ and $\frac{\partial}{\partial t_2}$, in particular

$$\frac{\mathrm{d}}{\mathrm{d}t} \mapsto \frac{1}{\varepsilon}\frac{\partial}{\partial t_1} + \frac{\partial}{\partial t_2} \tag{3.16}$$

These phase-space vector fields ∂_{t_1} and ∂_{t_2} commute with each other, so that it is the same whether we move first along a field line of ∂_{t_1} of some parameter

Δt_1 and then along a field line of ∂_{t_2} of some parameter Δt_2 or vice-versa. Neglecting dissipative terms for the moment, this means that a single surface is spanned by the field lines of ∂_{t_1} and ∂_{t_2} passing by a certain point of the phase-space P, exactly in the same way as in a conservative system a single field line of $\frac{\mathrm{d}}{\mathrm{d}t}$ passes through P. The evolution of the mechanical system is then parametrized in terms of the two variables (t_1, t_2) rather than in terms of a single time t.

The benefit of this new view-point will be apparent in few lines. In particular, substituting (3.16) into the ordinary differential Equation (3.9), and explictly considering the pertubative expansion for the solution (3.15), we get the following "partial" evolution Equation for $\delta z_0\,(t_1, t_2)$:

$$\frac{\partial^3}{\partial t_1^3}\delta z_0\,(t_1, t_2) + \frac{\hat{k}_1}{\tau_w^2}\frac{\partial}{\partial t_1}\delta z_0\,(t_1, t_2) = 0 \tag{3.17}$$

There are two types of general solution for the above dynamical system, depending on the sign of $\tilde{k}_1$. For $\tilde{k}_1 > 0$, the general integral of Equation (3.17) is

$$\delta z_0\,(t_1, t_2) = a_0\,(t_2)\,\cos\left(\frac{\sqrt{\hat{k}_1}}{\tau_w}t_1\right) + b_0\,(t_2)\,\sin\left(\frac{\sqrt{\hat{k}_1}}{\tau_w}t_1\right) + c_0\,(t_2) \tag{3.18}$$

For $\tilde{k}_1 < 0$ we would have had an instability on the fast time scale t_1, indeed:

$$\delta z_0\,(t_1, t_2) = d_0\,(t_2)\,\exp\left(\frac{\sqrt{|\hat{k}_1|}}{\tau_w}t_1\right) + e_0\,(t_2)\,\exp\left(-\frac{\sqrt{|\hat{k}_1|}}{\tau_w}t_2\right) + f_0\,(t_2) \tag{3.19}$$

If we go back to the definition of $\hat{k}_1$, see Equation (3.11), we understand that as long as the stabilizing force F_{ST} grows along the vertical direction more than the destabilizing force F_{PF}, than the fast dynamics reduce to oscillations. Anyway, whenever the destabilizing force grows faster an Alfvénic instability is generated. In this respect, the parameter $\hat{k}_1$ exactly quantifies whether the "electromagnetic inertia" offered from surrounding structures reduce the fast dynamics to be solely oscillations in the plasma position or not.

Let us now compute the slow dynamics, in the case $\hat{k}_1 > 0$: we again make explicit the operator (3.16) and the expansion (3.15) into the ordinary differential Equation (3.9), this time considering the first order correction terms in ε:

$$\begin{aligned}
&\frac{\partial^3}{\partial t_1^3}\delta z_0\left(t_1,t_2\right)+\frac{\hat{k}_1}{\tau_w^2}\frac{\partial}{\partial t_1}\delta z_0\left(t_1,t_2\right)=\\
&+\frac{1}{\tau_w^2}\cos\left(\frac{\sqrt{\hat{k}_1}}{\tau_w}t_1\right)\left[2\hat{k}_1a_0'+\frac{\hat{k}_1+\hat{k}_2}{\tau_w}a_0\right]\\
&+\frac{1}{\tau_w^2}\sin\left(\frac{\sqrt{\hat{k}_1}}{\tau_w}t_1\right)\left[2\hat{k}_1b_0'+\frac{\hat{k}_1+\hat{k}_2}{\tau_w}b_0\right]\\
&+\frac{1}{\tau_w^2}\left[\hat{k}_1c_0'-\frac{\hat{k}_2}{\tau_w}\right]
\end{aligned} \tag{3.20}$$

We require the above "partial" evolution equation to be homogeneous, in order for $\delta z_0(t_1,t_2)$ to be the best possible approximation of $\delta z_p(t)$ [118]. This requirement is equivalent to the requirement that the terms in square brackets above are null, providing the evolution Equations for $a_0(t_2)$, $b_0(t_2)$, and $c_0(t_2)$. The general form for such "slow-time" quantities is:

$$\begin{aligned}
a_0\left(t_2\right)&=A_0\exp\left[-\left(\frac{\hat{k}_1+\hat{k}_2}{\hat{k}_1}\right)\frac{t_2}{\tau_w}\right]\\
b_0\left(t_2\right)&=B_0\exp\left[-\left(\frac{\hat{k}_1+\hat{k}_2}{\hat{k}_1}\right)\frac{t_2}{\tau_w}\right]\\
c_0\left(t_2\right)&=C_0\exp\left[\left(\frac{\hat{k}_2}{\hat{k}_1}\right)\frac{t_2}{\tau_w}\right]
\end{aligned} \tag{3.21}$$

Finally A_0, B_0 and C_0 are scalar constants to determine enforcing the initial conditions at $t_1=t_2=0$. The actual mechanical state parametrized via the parameter t along the integral line of $\frac{\mathrm{d}}{\mathrm{d}t}$ is identified along the integral lines of ∂_{t_1} and ∂_{t_2} via the parameters

$$t_1=\frac{t}{\varepsilon},\quad t_2=t \tag{3.22}$$

Hence our asymptotic solution for the linear system (3.9), in the limit $\tau_A/\tau_w\to 0$ and in case $\hat{k}_1>0$, is finally

$$\delta z_p\left(t\right) \simeq \left[\Delta z_0 + \varepsilon^2 \frac{\tau_w^2}{\hat{k}_1}\Delta \ddot{z}_0\right] e^{\frac{\hat{k}_2}{\hat{k}_1}\frac{t}{\tau_w}}$$
$$- \left[\varepsilon^2 \frac{\tau_w^2}{\hat{k}_1}\Delta \ddot{z}_0 \cos\left(\frac{\sqrt{\hat{k}_1}}{\tau_A}t\right) - \varepsilon \frac{\tau_w}{\sqrt{\hat{k}_1}}\Delta \dot{z}_0 \sin\left(\frac{\sqrt{\hat{k}_1}}{\tau_A}t\right)\right] e^{-\frac{\hat{k}_1+\hat{k}_2}{\hat{k}_1}\frac{t}{\tau_w}} \tag{3.23}$$

Here the symbols Δz_0, $\Delta \dot{z}_0$, and $\Delta \ddot{z}_0$ were used to indicate the initial perturbation on the plasma position, velocity and acceleration. Remember that $\hat{k}_1$ and $\hat{k}_2$ are dimensionless quantities close to unity in magnitude. In particular we obtained the asymptotic solution (3.23) for $\hat{k}_1 > 0$. We see that in this case the Alfvénic motion reduces to an oscillation which decays on the longer electromagnetic time-scale. The unstable mode is generated on the electromagnetic time-scale any time that $\hat{k}_2 > 0$, *i.e.* any time that the destabilizing force grows along the direction of the plasma column motion. It is instructive to make explicit $\hat{k}_2$, as defined via Equations (3.10-3.11), in case the plasma column can be schematically regarded as a toroidal current-carrying filament, making valid expressions (3.8),

$$\hat{k}_2 = -\frac{\mu_0}{B_0^2 L} 2\pi r_p \frac{\partial \tilde{B}_{r,PF}}{\partial z_p} I_{PF} I_\varphi \tag{3.24}$$

Inside the plasma chamber, the magnetic field produced by the external conductors is curl-free, meaning that $\frac{\partial \tilde{B}_{r,PF}}{\partial z_p} = -\frac{\partial \tilde{B}_{z,PF}}{\partial r_p}$. Hence we can rewrite (3.24) as

$$\hat{k}_2 = \frac{\mu_0}{B_0^2 L}\, 2\pi \tilde{B}_{z,PF} I_{PF} I_\varphi \underbrace{\left[-\frac{r}{\tilde{B}_{z,PF}}\frac{\partial \tilde{B}_{z,PF}}{\partial r_p}\right]}_{n} \tag{3.25}$$

The term in square bracket, denoted by n, is also defined as *decay index* [107, 108]. As we shall see, for a positive plasma current ($I_\varphi > 0$) the conditions of radial mechanical equilibrium will require the external coils to provide a negative vertical field ($I_{PF}\tilde{B}_{z,PF} < 0$). Vice-versa a negative toroidal current will require to supply a positive vertical field. Hence, the vertical instability will be generated for a negative decay index, $n < 0$. This means that the filamentary plasma will be unstable with respect to the vertical motion whenever the magnitude of the vertical field increases along the radial direction. Probably more intuitively, for a positive plasma current I_φ, hence a negative vertical field $I_{PF}\tilde{B}_{z,PF}$, the plasma is vertically unstable for negative values $\partial\tilde{B}_{r,PF}/\partial z_p$. In this case indeed, as soon as the plasma filament moves vertically it will meet a radial field which tends to further displace the filament from its initial MHD Equilibrium position.

From the asymptotic solution (3.23), and for $\hat{k}_2 > 0$, we see that a vertical instability is triggered by an initial plasma displacement or acceleration. This zero order approximation suggests that an initial perturbation of the velocity, keeping null the initial displacement and acceleration, does not trigger the unstable mode. Moreover a perturbation of the plasma position, keeping null this time the initial velocity and acceleration, does not stimulate the Alfvénic oscillations.

The asymptotic solution (3.23) suggests that we may disregard the fast Alfvén dynamics in first approximation for $\varepsilon \to 0$, as these appears as corrections of order ε and ε^2, which are moreover damped in few electromagnetic time-scales. Anyway this is true solely for $\hat{k}_1 > 0$.

Tikhonov's Theorem

In the framework of Perturbation Theory, there are few tools to conveniently deal with multiple time-scale systems [119]. In particular, *Tikhonov's Theorem* provides some sufficient conditions to state that the solution of a dynamical system in the form

$$\begin{aligned} \dot{\underline{x}} &= f\left(\underline{x}, \underline{y}, t\right) + \varepsilon \cdots \quad \underline{x(t_0)} = \underline{x_0} \\ \varepsilon\dot{\underline{y}} &= g\left(\underline{x}, \underline{y}, t\right) + \varepsilon \cdots \quad \underline{y(t_0)} = \underline{y_0} \end{aligned} \tag{3.26}$$

in the limit $\varepsilon \to 0$ tends to the solution of the *reduced problem*

$$\begin{aligned} &\dot{\underline{x}} = f\left(\underline{x}, \underline{y}, t\right) \quad \underline{x(t_0)} = \underline{x_0} \\ &0 = g\left(\underline{x}, \underline{y}, t\right) \end{aligned} \tag{3.27}$$

In our simple model, the state variables $\underline{x}$ is precisely given by the wall current, and the vertical position of the plasma column in the poloidal plane, $\underline{x} = (\delta I_w, \delta z_p)$, while the state variable y is given by the toroidal filament vertical velocity $y = \delta\dot{z}_p$, see Equation (3.7). Hence we would greatly benefit of this result, in order to state with mathematical rigour that we can indeed neglect the mass.

Within the sufficient conditions however we find that the static part of the reduced problem, $g\left(\delta I_w, \delta z_p, \delta\dot{z}_p\right) = 0$, has to be solved by an isolated root

$\overline{\delta\dot{z}_p} = \phi(\delta I_w, \delta z_p)$ (which has to be continuous). Moreover $\overline{\delta\dot{z}_p}$ has to be an asymptotically stable solution of the problem

$$\frac{\mathrm{d}}{\mathrm{d}t}\delta\dot{z}_p = g(\delta I_w, \delta z_p, \delta\dot{z}_p) \tag{3.28}$$

for assigned δI_w and δz_p. Further, it is required that the initial conditions on the velocity are in the domain of attraction of the reduced solution.

Unfortunately, we are not even in the conditions to satisfy the first hypothesis: the force balance equation does not involve even the velocity, hence an isolated root $\overline{\delta\dot{z}_p}$ does not exist, and virtually the force balance can be satisfied for any value of the velocity.

As frequent, the introduction of even a small friction term sorts out most of the undesirable mathematical features. Besides a fusion plasma may be considered substantially a non-viscous fluid, due to its relatively low density, it is convenient to account even for the eventually very small viscosity which is present, as this changes the mathematical structure of the dynamical system. Let us introduce a friction term in the linearised version of the momentum balance Equation (3.7b), where we set $m_p = 0$,

$$\left(-\frac{\partial M_{p,w}}{\partial z_p}\Big|_{z_{eq}}\right) I_\varphi \delta I_w + \left(-\frac{\partial^2 M_{p,PF}}{\partial z_p^2}\Big|_{z_{eq}} I_{PF}\, I_\varphi\right)\delta z_p + \eta_z \delta\dot{z}_p = 0 \tag{3.29}$$

It is seen immediately that a unique solution $\overline{\delta\dot{z}_p}$ can be identified, and that this is an asymptotically stable solution of (3.28).

3.2 Fundamentals of Evolutionary Equilibrium

The discussion of Section 3.1 provide us with some confidence about the actual possibility of retaining the macroscopic plasma motions *quasi-static*, *i.e.* evolving through mechanical equilibrium states. We illustrated indeed that in some conditions, the Alfvénic dynamics determine solely local oscillations, which have no influence on the actual macroscopic motion of the column. Besides Tikhonov Theorem does not apply immediately, it is generally possible to retain in a wide variety of experiments that in the limit $\tau_A/\tau_w \to 0$ the true solution of the massive problem converges towards the solution of the massless model. Discarding viscous phenomena, it is hence possible to retain in each time instant of the plasma evolution

$$\mathbf{i} \times \mathbf{B} = \nabla p \tag{3.30}$$

Here p is the local thermodynamic equilibrium pressure, governed by the Equations of State for ideal gases. Accordingly, the field lines for the magnetic flux density and the electric current density will be tangent to pressure equi-level surfaces ($\mathbf{B} \cdot \nabla p = 0$, and $\mathbf{j} \cdot \nabla p = 0$). In tokamak experiments, these equi-pressure surfaces are generally nested tori [120], although of course more complicate situations could exist in presence of singularities. The fact that the magnetic field lines lay on toroidal equi-pressure surfaces allow to conclude that two magnetic flux labels can be associated to each isobaric surface. In particular on a toroidal surface there are two homology groups of close lines, which are not reducible to points by continuous deformation. One is the group of curves wrapping around the hole of the torus, in the almost-toroidal direction, $[\Gamma_t]$ (we are not yet assuming axisymmetry here). Since $\mathbf{B} \cdot \hat{\mathbf{n}} = 0$, all the curves in this group share the same linked magnetic flux, generally indicated as *poloidal flux*. Similarly the group of curves wrapping around the torus in the almost-poloidal direction will all link the same magnetic flux, this time denoted as *toroidal flux*. These definitions are borrowed clearly from the purely axisymmetric case.

In a dynamic situation, such the one we are examining, one may want to account for the small friction the plasma come across during its motion. This could be beneficial rather for questions of mathematical convergence, as commented in last Section. In this case the dynamic equilibrium constraint above should be generalize to

$$\mathbf{i} \times \mathbf{B} = \nabla \cdot \underline{\mathbf{P}} \quad \text{where } \underline{\mathbf{P}} = p\underline{\mathbf{I}} + \underline{\mathbf{\Pi}^{(\mathbf{s})}} \tag{3.31}$$

Here we indicated by $\underline{\mathbf{I}}$ the Euclidean metric tensor. For this viscous situation, the magnetic flux density and electric current density field lines shall lay on those stress-free surfaces, where the projection of $\nabla \cdot \underline{\mathbf{P}}$ is null.

Here, we will always retain the viscosity of the plasma negligible, besides its mechanical inertia, hence enforcing the equilibrium constraint in its classical form (3.30). In this context, we define *plasma boundary* the last magnetic flux surface encompassing finite plasma currents, together with the eventual wall interface which is "wet" by these currents. The implicit assumption is that there is a well defined topology for the magnetic surfaces, *i.e.* the magnetic field lines ergodically define surfaces and there is no magnetic chaos.

In general we will consider in this Chapter exclusively situations where the plasma only faces the vacuum, without any current shared between the plasma and the wall. In this respect the plasma boundary is generally retained to be the Last Closed magnetic Flux Surface (LCFS), not intersecting any solid structure. When this surface is tangent to the wall interface in one single point, we define the plasma as *limiter*. Further it is possible to break the topology of field lines within the reactor chamber with a proper set-up of the externally applied magnetic fields. In this case the LCFS is completely separated from the solid structures, at the expenses of a singular point for the magnetic flux, where the magnetic field is null. Such MHD equilibrium configurations are defined as *divertor*, and the point of null magnetic field along the plasma boundary is defined as *X-point*.

In the present Section, the important aspect we will stress several times is that the equilibrium constraint forces $\mathbf{B} \cdot \hat{\mathbf{n}} = 0$ everywhere at the plasma boundary (even at the X-point, where the normal to the boundary is undefined, $\mathbf{B} = 0$). This condition will be exploited to investigate, by the means of a very simplified quasi-cylindrical model, the actual relation between the evolution of the plasma boundary and the evolution of currents in external conductors.

Let's start immediately noting that provided the following information:

- Net plasma toroidal current
- Geometry of the plasma boundary
- Currents in external conductors

we could really set up a complete electromagnetic model of the outer domain to the plasma boundary. Indeed, since $\mathbf{B}\cdot\hat{\mathbf{n}} = 0$ at the plasma boundary, Theorem 2 of previous Chapter applies immediately. It is just sufficient to work out the mathematics. In the language set up in previous Section, one could try to adopt an integral formulation for the currents in passive conductors, and condense the information about $\mathbf{A_{pl}}$ outside the plasma in a surface integral. In particular, we may represent the magnetic vector potential $\mathbf{A}$ within the plasma, up to its boundary, as [121]

$$\mathbf{A} = \psi \nabla \varphi^* + \phi \nabla \theta^* \tag{3.32}$$

where the toroidal flux is a function of the poloidal flux, *i.e.* $\phi = \phi(\psi)$.The functions (θ^*, φ^*) are hence the curvilinear coordinates placed on any magnetic toroidal surface, in order to identify a specific point there. The plasma boundary is identified by some "label" ψ_b or $\phi_b = \phi(\psi_b)$. This representation consistently guarantees that the magnetic flux density is tangent to the plasma boundary ($\mathbf{B} \cdot \hat{\mathbf{n}} = 0$), moreover highlights that a finite magnetic flux exists for each of the two homology groups of close curves laying boundary. The general vector identity (2.81), at the plasma boundary, takes the simple form:

$$\mathbf{A_{pl}} = -\frac{1}{4\pi} \int_{\partial\Omega_{pl}} G\left(\mathbf{B} \times \hat{\mathbf{n}}\right) \mathrm{d}^2 r - \phi_b \int_{\partial\Omega_{pl}} \left(\nabla\theta^* \times \hat{\mathbf{n}}\right) \times \nabla G \, \mathrm{d}^2 r \quad (3.33)$$

All the information about $\mathbf{A_{pl}}$ outside of the plasma boundary is contained within the tangential component to the plasma boundary of the total magnetic flux density and in the toroidal flux. Anyway, in a dynamic situation the actual integration domain would be variable in time. Precise information on $\mathbf{B} \times \hat{\mathbf{n}}$ should be determined at each time as a function of the net toroidal plasma current and of the external currents, see Equation (2.102) where all the matrices are now function of the geometry of the plasma boundary, hence variable in time. Clearly, this way does not appear very convenient numerically. Moreover, the actual information available in terms of plasma boundary evolution is in general poor and we would prefer to know the plasma boundary as a result of simulations, rather than providing it as an input.

With this consciousness, in the last paragraph of this Section, we will try to find the actual magnetic field tangent to the plasma boundary based on totally different considerations, and in particular relating this quantity to the solution of the MHD problem within the plasma column itself. We will find that few information about the current density within the plasma column will be sufficient to determine $\mathbf{B} \times \mathbf{n}$ at the plasma boundary, meaning that few moments of the actual current distribution are actually important for the determination of the inductive coupling with structures.

We can finally start to derive our high-aspect-ratio circular tokamak model, valuable in capturing many key features of MHD evolutionary equilibrium models. We will introduce the assumptions step-by-step, mainly following References [113, 114].

(a) Axisymmetry

We already explored how an axially symmetric magnetic field can be represented in cylindrical coordinates in the previous paragraph, we shall say something more here. Exploiting the axisymmetry hypothesis, we can focus on an arbitrary poloidal half-plane (r, z) with $r \geq 0$. In this respect, each pair (r^*, z^*) is representative for the circumference of radius r^*, laying on the plane $z = z^*$ and centred on the z-axis. We already defined $\psi(r, z) = rA_\zeta$ as the poloidal flux of $\mathbf{B}$ across such a circle, normalized by 2π. Similarly we define the poloidal current per radian as $I = rB_\zeta/\mu_0$. These two scalar functions contain all the information about the magnetic field and current density:

$$\mathbf{B} = \nabla\psi \times \nabla\varphi + \mu_0 I \nabla\varphi, \tag{3.34}$$

$$\mathbf{j} = \nabla I \times \nabla\varphi - r^2 \left(\nabla \cdot \frac{\nabla\psi}{\mu_0 r^2}\right) \nabla\varphi. \tag{3.35}$$

The above representation, makes moreover quite clear that the poloidal component of the magnetic field is solely related to the toroidal component of the magnetic vector potential, and vice-versa. Let us now define the trace in the poloidal plane of the plasma boundary as *separatrix line*, we will denote it with Γ_{pl}, similarly to what we did in Figure 2.1 for the trace of the Coupling Surface. In particular we define the tangential direction to the separatrix as $\hat{\mathbf{i}}_{\mathbf{tan}} = \mathbf{i}_\varphi \times \hat{n}$, where $\hat{\mathbf{n}}$ is the normal to the plasma boundary pointing outwards. With this notation, we notice explicitly that

$$B_{tan} = -\frac{1}{r}\frac{\partial\psi}{\partial n} \tag{3.36}$$

Application of (2.94) to the case of interest, taking the plasma boundary in lieu of the Coupling Surface, leads then immediately to

$$(1-\nu)\,\psi = \psi_{ext} + \psi_{pl} \tag{3.37}$$

where

$$\psi_{pl} = \oint_{\Gamma_{pl}} G_0\left(r, r', z, z'\right) B_{tan}(r', z')\,\mathrm{d}\ell' \tag{3.38}$$

The integral in ψ disappeared, thanks to the fact that the plasma boundary is a flux surface. The axisymmetric Green function G_0 was already defined in (2.92), we here provide it more explicitly in terms of elliptic integrals:

$$G_0\left(r, r', z, z'\right) = \frac{\sqrt{rr'}}{\pi k}\left[\left(1 - \frac{k^2}{2}\right) K(k) - E(k)\right] \tag{3.39}$$

Here, $K(k)$ and $E(k)$ are complete elliptic integrals of the first and second kind respectively and k was already defined in Equation (2.91). In particular, G_0 is the Green function expressing the poloidal flux generated at the poloidal plane location (r, z) by a unit current ring whose trace in the poloidal plane is given by (r', z'). Indeed we can express the poloidal flux generated by the axisymmetric toroidal currents circulating in the wall as

$$\psi_w = \int_{S_w} G_0\left(r, r', z, z'\right) \mu_0 j_{w,\varphi}\left(r', z'\right) \mathrm{d}r' \, \mathrm{d}z'. \tag{3.40}$$

(b) Thin Wall

Later, we will consider a geometrically thin wall for the tokamak, *i.e.* $d_w \ll b_w$. In order to calculate the potentials generated by such current, we can lump the volumetric current density distribution circulating in such a conductor into a thin layer placed at the wall mean surface $k_{w,\varphi}$,

$$k_{\varphi,w} = \int_{\ell_\perp} j_{w,\varphi} \, \mathrm{d}\ell \tag{3.41}$$

With this definition the poloidal flux due to eddy currents in the wall is efficiently described by

$$\psi_w = \oint_{\Gamma_w} G_0\left(r, r', z, z'\right) \mu_0 k_{w,\varphi}\left(r', z'\right) \mathrm{d}\ell' \tag{3.42}$$

(c) large aspect-ratio

We introduce here the *large aspect-ratio* hypothesis. We can introduce an arbitrary quasi-cylindrical reference system $(\rho_v,\ u_v, \varphi)$, centred at the poloidal position $(R_v, 0)$. Soon, we will be interested either to the "plasma" quasi-cylindrical reference frame (ℓ, α, φ), centred in $R_v = R_{pl}$, or to the "wall" quasi-cylindrical frame (ρ, u, φ), centred in $R_v = R_w$. See Figure 3.1 for a synthetic scheme of the conventions adopted.

The idea here is to expand the Green function G_0 for our axisymmetric problem in the inverse aspect ratio of the tokamak. It is convenient in particular to define as small parameter the *half* inverse aspect ratio

$$\varepsilon_\nu = \frac{\rho}{2R_\nu}. \tag{3.43}$$

The requirement $\varepsilon_\nu \ll 1$ in the region of interest will allow us to truncate the Green function retaining only first order toroidal corrections. Here ν is again a place-holder either to indicate the plasma reference frame $\nu = pl$ or the wall reference frame $\nu = w$ [113, 122]. The complete elliptic integrals can be represented via the asymptotic expansion:

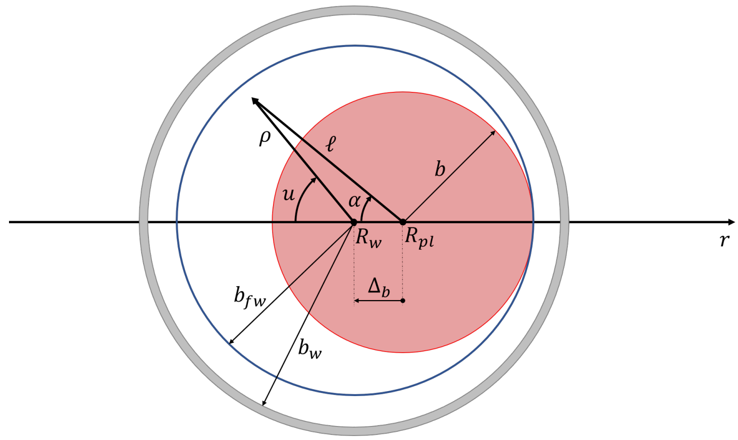

Figure 3.1: Reference Geometry for an high-aspect ratio tokamak with circular plasma and circular thin wall.

$$
\begin{aligned}
K &= \lambda + \frac{\lambda - 1}{4} k^{*2} + \cdots \\
E &= 1 + (\lambda - 0.5)\, k^{*2} + \cdots
\end{aligned}
\tag{3.44}
$$

where

$$
k^{*2} = 1 - k^2 \quad \text{and} \quad \lambda = \ln \frac{4}{k^*} \tag{3.45}
$$

and $k(r, r', z, z')$ was defined in Equation (2.91). It is convenient to refer to a Cartesian coordinate system in the poloidal plane $(\bar{x}, \bar{z})$ local to the quasi-cylindrical reference frame origin, *i.e.* whose origin is in $(R_\nu, 0)$. The following transformations are valid

$$
\bar{x} = R_w - r, \quad \bar{z} = z \tag{3.46}
$$

It is convenient to introduce the following small parameters of order ε_v:

$$\begin{aligned}(a)\delta\tilde{x} &= \frac{x+x'}{2R_v} \\ (b)\delta\tilde{z} &= \frac{z-z'}{2R_v} \\ (c)\delta\tilde{d} &= \frac{\sqrt{(x-x')^2+(z-z')^2}}{2R_v}\end{aligned} \tag{3.47}$$

The last one is carrying the information on the distance in the poloidal plane between "source" and "field" points, and it will carry the information about the singularity of our Green function (3.39). Indeed, using definitions (2.91) and (3.47) into (3.45) we have

$$k^{*2} = \delta\tilde{d}^2 \frac{1}{(1-\delta\tilde{x})^2+\delta\tilde{z}^2} \tag{3.48}$$

Hence $k^{*2} \propto \varepsilon_v^2$, and we may disregard all higher order terms in the expansions (3.44) of the elliptic integrals, as they would appear as second or higher order toroidal corrections. We can finally start to approximate our Green function as

$$G_0 \simeq \frac{\sqrt{rr'}}{2\pi k}\left[\lambda - 2\right] \tag{3.49}$$

Anyway, all of the terms in Equation (3.49) should be approximated for consistency considering only toroidal corrections up to the first order. We continue then by expanding λ, as defined in Equation (3.45), in the small parameters $\delta\tilde{x}$, $\delta\tilde{z}$ and $\delta\tilde{d}$, leading to

$$\lambda \simeq \lambda_1 = \ln\left(\frac{4}{\delta\tilde{d}}\right) - \delta\tilde{x} \tag{3.50}$$

We finally truncate also the remainder term of the Green function (3.49) to the first order toroidal correction:

$$\frac{\sqrt{rr'}}{2\pi k} \simeq R_v\left(1-\delta\tilde{x}\right) \tag{3.51}$$

Substitution of Equations (3.50) and (3.51) into (3.49), neglecting second order toroidal corrections, leads finally to

$$G \simeq \frac{R_v}{2\pi}\left[(\lambda_0 - 2) + (\lambda_0 - 1)\,\delta\tilde{x}\right] \tag{3.52}$$

where

$$\lambda_0 = \ln\left(\frac{4}{\delta\tilde{d}}\right) = \ln\left(\frac{8R_v}{\sqrt{(x-x')^2+(z-z')^2}}\right) \tag{3.53}$$

For the following discussion, it is convenient to re-write at this stage the approximate Green function (3.52) explicitly in terms of the quasi-cylindrical coordinates (ρ_ν, u_ν) and (ρ'_ν, u'_ν). In particular the quantity λ_0 defined above can be expressed as

$$\lambda_0 = \ln\frac{8R_v}{\rho_{v,max}} + \ln\frac{1}{\sqrt{1+2\xi cos(u_\nu - u'_\nu)+\xi^2}} \tag{3.54}$$

where

$$\xi = \frac{\rho_{v,min}}{\rho_{v,max}}, \quad \rho_{v,min} = \text{argmin}\{\rho_v, \rho'_v\}, \quad \rho_{v,max} = \text{argmax}\{\rho_v, \rho'_v\} \tag{3.55}$$

The second term at the r.h.s. of Equation (3.54) is a generating function for Chebyshev polynomials of the first kind. Indeed, introducing the symbol $t = \cos(u_\nu - u'_\nu)$,

$$\ln\frac{1}{\sqrt{1-2\xi t+\xi^2}} = \sum_{m=1}^{\infty}\frac{\xi^m T_m(t)}{m} \tag{3.56}$$

where:

$$T_0(t) = 1\ ,\ T_1(t) = t\ T_{m+1}(t) = 2tT_m(t) - T_{m-1}(t) \tag{3.57}$$

Considering $t = cosu' - u$ and standard trigonometric properties it is also possible to prove:

$$\ln\frac{1}{\sqrt{1-2\xi t+\xi^2}} = \sum_{m=1}^{\infty}\frac{\xi^m}{m}\cos m(u'_\nu - u_\nu) \tag{3.58}$$

In general all of the terms in Equation (3.58) must be retained as ξ, besides being less than unity, is not necessarily a small parameter. Hence, we can finally write:

$$
\begin{aligned}
G_1 = \frac{R_v}{2\pi}\Bigg\{ & \left[\ln\left(\frac{8R_v}{\rho_{v,MAX}}\right) - 2 + \sum_{m=1}^{\infty}\frac{\xi^m}{m}\cos m(u'-u)\right] \\
& - \frac{\rho_v \cos v + \rho_v' \cos v'}{2R_v} \cdot \left[\ln\left(\frac{8R_v}{\rho_{v,MAX}}\right) - 1 + \sum_{m=1}^{\infty}\frac{\xi^m}{m}\cos m(u'-u)\right]\Bigg\}
\end{aligned}
\tag{3.59}
$$

(d) Circular plasma cross-section

For an high-aspect-ratio tokamak plasma of circular cross section the application of Equation (3.38) via the approximate Green's function (3.59) is particularly simple. Indeed, taking a quasi cylindrical reference frame (ℓ, α, φ) centred at $R_v = R_{pl}$, all the "source" points are located at the plasma minor radius $\ell' = b$, and for all the field points exterior to the plasma $\xi = \ell/b$. Considering the asymptotic solutions of the outer magnetostatic problem, it could be possible to motivate the following widely used expansion of B_{tan} in the inverse aspect ratio of the plasma [107, 123]:

$$
B_{tan} = B_J\left(1 - \frac{b}{R_{pl}}\Lambda\cos\alpha\right) \tag{3.60}
$$

Using approximations (3.59)-(3.60) into the convolution product (3.38) we finally obtain:

$$
\psi_{pl} = \psi_{pl,0}(\ell) + \psi_{pl,1}(\ell)\cos\alpha \tag{3.61}
$$

where :

$$
\begin{aligned}
(a) \quad & \psi_{pl,0}(\ell) = \frac{\mu_0 R_{pl}}{2\pi} J \left(\ln\left(\frac{8R_{pl}}{\ell}\right) - 2\right) \\
(b) \quad & \psi_{pl,1}(\ell) = -\frac{\mu_0 R_{pl}}{2\pi} J \frac{\ell}{2R_{pl}} \cdot \left[\frac{b^2}{\ell^2}\cdot\left(\Lambda + \frac{1}{2}\right) + \ln\left(\frac{8R_{pl}}{\ell}\right) - 1\right]
\end{aligned}
\tag{3.62}
$$

It is worth stressing here that we discarded in the result any second order toroidal correction, as this would be inconsistent with the approximations adopted for the Green function and the magnetic flux density. Notice that $\psi_{pl,1}$ is a first order toroidal correction as compared to $\psi_{pl,0}$

(e) Circular crown wall cross-section

We consider the vacuum vessel surrounding the circular plasma to have a circular crown cross section. We assume that such a current distribution is well approximated via the representation:

$$k_{\varphi,w} = \frac{J_w}{2\pi b_w} + \frac{J_w^c}{2\pi b_w}\cos u \tag{3.63}$$

The Biot-Savart law (3.42) for such a current distribution, together with the high-aspect-ratio hypothesis for the Green function (3.59), leads to

$$\psi_w = \psi_{w,0} + \psi_{w,1}\cos u \tag{3.64}$$

In particular, the following inductance coefficient matrix can be defined as a function of ρ:

$$\begin{bmatrix} \psi_{0,w} \\ \psi_{1,w} \end{bmatrix} = \underbrace{\begin{bmatrix} L_{0,0}(\rho) & L_{0,1}(\rho) \\ L_{1,0}(\rho) & L_{1,1}(\rho) \end{bmatrix}}_{\underline{\underline{L}}(\rho)} \cdot \begin{bmatrix} J_w \\ J_w^c \end{bmatrix} \tag{3.65}$$

where:

$$\underline{\underline{L}}(\rho) = \begin{bmatrix} \frac{\mu_0 R_w}{2\pi}\left[\ln\frac{8R_w}{\rho_{max}} - 2\right] & -\frac{\mu_0 b_w}{8\pi}\left[\ln\frac{8R_w}{\rho_{max}} - 1 + \frac{1}{2}\left(\frac{\rho}{b_w}\right)^2\right] \\ -\frac{\mu_0 \rho}{4\pi}\left[\ln\frac{8R_w}{\rho_{max}} - 1 + \frac{1}{2}\frac{b_w}{\rho}\xi\right] & \frac{\mu_0 R_w}{2\pi}\frac{\xi}{2} \end{bmatrix} \tag{3.66}$$

Here ρ_{max} is the biggest between the wall minor radius b_w and the field point at the minor radius ρ. Hence, inside the plasma-wall gap $\rho_{max} = b_w$. Moreover, $\xi = \rho_{min}/\rho_{max}$ equals ρ/b_w inside the gap. It is interesting to note as the inductance matrix $\underline{\underline{L}}$ is consistently symmetric for $\rho = b_w$.

Before enforcing the weak form of Ohm's law, providing an integral formulation in the same stream of what discussed in Section 2.4, it is convenient to express the plasma poloidal flux in the quasi-cylindrical reference frame of the wall. We indicate the same quantity, expressed in (ρ, u) coordinates by an hat,

$$\hat{\psi}_{pl}(\rho, u) = \hat{\psi}_{pl,0} + \hat{\psi}_{pl,1}\cos u + \hat{\psi}_{pl,2}\cos 2u \tag{3.67}$$

where, with the short-hand $\psi_J = \mu_0 R_w J/2\pi$

$$
\begin{aligned}
&(a)\ \hat{\psi}_{pl,0} = +\psi_J \left\{ \left[\ln \frac{8R_w}{\rho} - 2 \right] + \frac{\Delta_b}{2R_w} \left[\ln \frac{8R_w}{\rho} - \frac{1}{2} \right] \right\} \\
&(b)\ \hat{\psi}_{pl,1} = -\psi_J \left\{ \frac{\rho}{2R_w} \left[\left(\frac{b}{\rho} \right)^2 \left(\Lambda + \frac{1}{2} \right) + \ln \frac{8R_w}{\rho} - 1 \right] + \frac{\Delta_b}{\rho} \right\} \\
&(c)\ \hat{\psi}_{pl,2} = +\psi_J \left\{ \left(\frac{\Delta_b}{\rho} \right)^2 \frac{1}{2} + \frac{\Delta_b}{2R_w} \frac{1}{2} \left[1 + 2 \left(\frac{b}{\rho} \right)^2 \left(\Lambda + \frac{1}{2} \right) \right] \right\}
\end{aligned}
\tag{3.68}
$$

We can enforce finally Ohm's law in the conducting thin wall in its weak form, using as test functions the same we used to represent the current density. Indicating with σ the conductivity, and with d_w the wall thickness, considering moreover the relation between wall fluxes and currents (3.65), we find

$$
\begin{aligned}
&(a) J_w = -\frac{2\pi\sigma b_w d_w}{R_w} \left[\frac{\mathrm{d}}{\mathrm{d}t} \hat{\psi}_{pl,0} + L_{0,0} \frac{\mathrm{d}}{\mathrm{d}t} J_w + L_{0,1} \frac{\mathrm{d}}{\mathrm{d}t} J_w^c \right] \\
&(b) J_w^c = -\frac{2\pi\sigma b_w d_w}{R_w} \left[\frac{\mathrm{d}}{\mathrm{d}t} \hat{\psi}_{pl,1} + L_{1,0} \frac{\mathrm{d}}{\mathrm{d}t} J_w + L_{1,1} \frac{\mathrm{d}}{\mathrm{d}t} J_w^c \right]
\end{aligned}
\tag{3.69}
$$

where the inductances (3.66) are all evaluated for $\rho = b_w$, and we omitted this explicit dependence in the notation.

(f) The Equilibrium constraint

In order for the plasma boundary to be effectively a flux surface, the α-varying term in the plasma poloidal flux expression (3.61) has to be exactly compensated by the poloidal flux applied by the external conductors. Luckily, the u-varying external poloidal flux can be readily expressed as

$$
\psi_{ext,1} = \left(\frac{\psi_{a,1}(\rho) + \psi_{w,1}(\rho)}{\rho} \right) \cdot \rho \cos u \tag{3.70}
$$

where the term in brackets is ρ-independent and $\rho \cos u = \ell \cos \alpha - \Delta_b$. Hence the equilibrium condition is easily enforced requiring

$$\begin{aligned}\frac{\psi_{a,1}(\rho)+\psi_{w,1}(\rho)}{\rho} &= -\left.\frac{\psi_{1,pl}(\ell)}{\ell}\right|_{\ell=b} \\ &= R_{pl}\underbrace{\frac{\mu_0 J}{2\pi b}\frac{b}{2R_{pl}}\left[\left(\Lambda+\frac{1}{2}\right)+\ln\frac{8R_{pl}}{b}-1\right]}_{B_{\perp,ext}}\end{aligned} \tag{3.71}$$

We highlighted in this expression the vertical magnetic flux density $B_{z,ext} = -B_{\perp,ext}$, provided by external currents to guarantee the plasma boundary to be a flux surface:

$$B_{\perp,ext} = \frac{\mu_0 J}{2\pi b}\frac{b}{2R_{pl}}\left[\left(\Lambda+\frac{1}{2}\right)+\ln\frac{8R_{pl}}{b}-1\right] \tag{3.72}$$

We indicate by the symbol Δ_t the time variations of a physical quantity between the initial equilibrium time instant t_0, where all eddy currents in the vessel are null, and the generic time instant t. With this notation, the equilibrium constraint (3.71), together with the inductance definitions (3.64)-(3.66), leads to the relation

$$L_{1,0}(b_w)J_w + L_{1,1}(b_w)J_w^c = -b_w\Delta_t\left(R_{pl}B_{\perp,ext}\right) \tag{3.73}$$

The equilibrium constraint hence enforces

$$L_{1,0}(b_w)\frac{\mathrm{d}}{\mathrm{d}t}J_w + L_{1,1}(b_w)\frac{\mathrm{d}}{\mathrm{d}t}J_w^c = -b_w\frac{\mathrm{d}}{\mathrm{d}t}\frac{\hat{\psi}_{1,pl}(b)}{b} \tag{3.74}$$

which substituted in (3.69b) provides

$$J_w^c = -\tau_w\frac{\mathrm{d}}{\mathrm{d}t}\left[J\frac{\Delta_{iw}-\Delta_b}{b_w}\right] \tag{3.75}$$

where we defined the *wall time constant*

$$\tau_w = \mu_0\sigma b_w d_w \tag{3.76}$$

and the *ideal wall shift*

$$\Delta_{iw} = b_w\cdot\frac{b_w}{2R_w}\left[\left(1-\frac{b^2}{b_w^2}\right)\left(\Lambda+\frac{1}{2}\right)+\ln\frac{b_w}{b}\right] \tag{3.77}$$

The latter is the plasma shift necessary for the wall to be a flux surface, at least up to first order toroidal corrections in ϵ_w and to first order column shift corrections in Δ_b/b_w (*i.e.* neglecting corrections of order Δ_b/R_w, and second and higher order corrections both in ϵ_w and Δ_b/b_w).

The actual physical meaning of (3.77) is easily understood in the ideal wall limit, *i.e.* $\tau_w \to \infty$. A super-conducting wall freezes the normal component to the wall of the magnetic flux density. Moreover, the overall poloidal flux cannot vary outside the wall in reason of even rapid variations in the plasma current or geometry. For a constant plasma current, Equation (3.75) reveals that the actual distance between the plasma geometrical centre and the *ideal wall* geometrical centre is fixed. This guarantees that the normal component of the magnetic flux density at the wall is indeed fixed. Whenever the plasma current varies, the normal component of the magnetic flux density can be preserved solely varying the distance between the actual geometrical centre and the ideal one. This information is still correctly reproduced by Equation (3.75). The consequences of Equation (3.75) in the ideal wall case will be gain discussed later, when we provide an explicit expression of Λ, hence of Δ_{iw} in terms of plasma internal parameters.

We conclude this paragraph showing how the evolution Equation (3.69) looks like disregarding second order toroidal corrections:

$$J_w = -\tau_{0,w}\frac{\mathrm{d}}{\mathrm{d}t}\left(J + J_w\right) \tag{3.78}$$

where

$$\tau_{0,w} = \tau_w\left(\ln\frac{8R_w}{b_w} - 2\right) \tag{3.79}$$

This makes clear that in the ideal wall case all of the net toroidal plasma current variations will be found as net toroidal current variations in the wall. This correctly represents the poloidal flux conservation in the outer domain in our high aspect-ratio framework.

(g) ψ and $\mathrm{B_{pol}}$ in the plasma-wall gap

Here we merge together the results of this section to provide the general expression of the poloidal flux in the plasma-wall gap as a function B_J, Λ and J_w, besides of the geometrical parameters which identify the plasma boundary, b and Δ_b. The parameters B_J and Λ describe the tangential component of the poloidal magnetic field at the plasma boundary, while J_w is the net toroidal current in our thin, high-aspect-ratio, circular wall. We assume then that J_w^c is automatically compatible with the equilibrium constraint, provided the above quantities.

We will write down the poloidal flux in the *wall* quasi-cylindrical reference frame. Formulas presented will be valid in points of the poloidal plane internal to the wall and external to the plasma boundary. We just need to sum up Equations (3.67)-(3.68) for the plasma poloidal flux and Equations (3.64)-(3.66) for the wall poloidal flux, considering the Equilibrium constraint (3.71) is satisfied. We have

$$\psi(\rho, u) = \psi_0(\rho) + \psi_1(\rho)\cos u + \psi_2(\rho)\cos 2u \tag{3.80}$$

where

$$\begin{aligned}
&(a)\ \psi_0 = \psi_{0,a} + \tilde{L}_w J_w + \frac{\mu_0 R_w}{2\pi}\left[\ln\frac{8R_w}{\rho} - 2\right] J + \\
&\qquad \frac{\mu_0 R_w}{2\pi}\frac{\Delta_b}{2R_w}\left[\ln\frac{8R_w}{\rho} - \frac{1}{2}\right] J \\
&(b)\ \psi_1 = \frac{\mu_0 R_w}{2\pi}\left(\frac{\Delta(\rho) - \Delta_b}{\rho}\right) J \\
&(c)\ \psi_2 = +\frac{\mu_0 R_w}{2\pi}\left\{\left(\frac{\Delta_b}{\rho}\right)^2 \frac{1}{2} + \frac{\Delta_b}{2R_w}\frac{1}{2}\left[1 + 2\left(\frac{b}{\rho}\right)^2\left(\Lambda + \frac{1}{2}\right)\right]\right\} J
\end{aligned} \tag{3.81}$$

where in Equation (3.81b) we defined

$$\Delta(\rho) = \rho \cdot \frac{\rho}{2R_w}\left[\left(1 - \frac{b^2}{\rho^2}\right)\left(\Lambda + \frac{1}{2}\right) + \ln\frac{\rho}{b}\right] \tag{3.82}$$

such that $\Delta(b_w) = \Delta_{iw}$ as defined in Equation (3.77). Indeed, from (3.81b), whenever $\Delta_b = \Delta(\rho^*)$ the corresponding $\rho = \rho*$ surface is a magnetic flux surface. Moreover we defined

$$\tilde{L}_w = L_{0,0}(b_w) = \frac{\mu_0 R_w}{2\pi}\left(\ln\frac{8R_w}{b_w} - 2\right) \tag{3.83}$$

The higher order correction terms in Δ_b/R_w and $(\Delta_b/\rho)^2$ may be discarded in first analysis. The magnetic flux density in (ρ, u) components is given by

$$
\begin{aligned}
&(a)\ B_\rho = \frac{1}{R_w}\left(1+\frac{\rho}{R_w}\right)\frac{1}{\rho}\frac{\partial\psi}{\partial u} = B_{\rho,0} + B_{\rho,1}\sin u + B_{\rho,2}\sin 2u \\
&(b)\ B_u = \frac{1}{R_w}\left(1+\frac{\rho}{R_w}\right)\quad\frac{\partial\psi}{\partial\rho} = B_{u,0} + B_{u,1}\cos u + B_{u,2}\cos 2u
\end{aligned} \tag{3.84}
$$

By definitions above and the overall poloidal flux expression in the plasma-wall gap (3.80)-(3.81), we get for B_ρ

$$
\begin{aligned}
&(a) && B_{\rho,0} = 0 \\
&(b) && B_{\rho,1} = -\tfrac{\psi_1}{\rho R_w} = B_J\tfrac{b}{\rho}\cdot\tfrac{\Delta_b-\Delta(\rho)}{\rho} \\
&(c) && B_{\rho,2} = -\tfrac{\psi_2}{\rho R_w} = -\tfrac{1}{2}B_J\tfrac{b}{\rho}\left[\left(\tfrac{\Delta_b}{\rho}\right)^2 + \left(\tfrac{\Delta_b}{2R_w}\right)\cdot\left\{1+2\left(\tfrac{b}{\rho}\right)^2\left(\Lambda+\tfrac{1}{2}\right)\right]\right\}
\end{aligned} \tag{3.85}
$$

Notice that $B_{\rho,0} = 0$, consistently with the solenoidality of the magnetic field. Further, we get for B_u

$$
\begin{aligned}
&(a) && B_{u,0} = -B_J\tfrac{b}{\rho} \\
&(b) && B_{u,1} = -B_J\tfrac{b}{\rho}\left[\tfrac{\Delta_b-\Delta(\rho)}{\rho} + \tfrac{\rho}{R_w}\left(\Lambda+\ln\tfrac{\rho}{b}\right)\right] \\
&(c) && B_{u,2} = B_J\tfrac{b}{\rho}\left[\left(\tfrac{\Delta_b}{\rho}\right)^2 + \left(\tfrac{\Delta_b}{2R_w}\right)\cdot 2\tfrac{b^2}{\rho^2}\left(\Lambda+\tfrac{1}{2}\right)\right]
\end{aligned} \tag{3.86}
$$

These results will serve as a basis to derive handy formulas describing ideal wall forces and energy fluxes during plasma transients in the following Sections.

(h) Solutions for Btan via inner problem

As hinted, we want now to evaluate the magnetic flux density at the plasma boundary exploiting the equilibrium constraint within the plasma. The general procedure which allows to extrapolate certain moment of B_{tan} in terms of some other moment of the plasma current distribution is based on a weighted residual method. The equilibrium constraint within the plasma is imposed in weak form, by appropriate choice of test basis functions. Now, we apply the method to our high aspect ratio circular plasma. The large aspect-ratio hypothesis, allowing the magnetic field representation (3.60) at the plasma boundary, will be the key assumption to determine Λ, as defined in Equation (3.60), in terms of few internal plasma quantities: the average kinetic pressure and the average poloidal magnetic energy density within the plasma cross-section.

As a first step, we rewrite our MHD mechanical equilibrium constraint (3.30) in a more convenient form, which will highlight in particular the role of the magnetic flux density at the plasma boundary in the equilibrium problem. The following manipulation is based on the vector identities:

$$\begin{aligned}
&(a)\nabla\left(\mathbf{v}\cdot\mathbf{w}\right)=\mathbf{v}\times\left(\nabla\times\mathbf{w}\right)+\mathbf{w}\times\left(\nabla\times\mathbf{v}\right)+\left(\mathbf{v}\cdot\nabla\right)\mathbf{w}+\left(\mathbf{w}\cdot\nabla\right)\mathbf{v}.\\
&(b)\nabla\cdot\left(\mathbf{v}\otimes\mathbf{w}\right)=\left(\nabla\cdot\mathbf{v}\right)\mathbf{w}+\left(\mathbf{v}\cdot\nabla\right)\mathbf{w}.\\
&(c)\nabla\cdot f\mathbf{v}=f\nabla\cdot\mathbf{v}+\mathbf{v}\cdot\nabla f
\end{aligned} \tag{3.87}$$

Using Ampere's law ($\nabla\times\mathbf{B}=\mu_0\mathbf{j}$) and the vector identity (3.87a), the *left hand side* of the MHD equilibrium Equation (3.30) can be written as

$$\frac{\left(\nabla\times\mathbf{B}\right)}{\mu_0}\times\mathbf{B}=-\nabla\left(\frac{B^2}{2\mu_0}\right)+\left(\mathbf{B}\cdot\nabla\right)\left(\frac{\mathbf{B}}{\mu_0}\right) \tag{3.88}$$

hence the equilibrium requirement becomes

$$\nabla\left[p+\frac{B^2}{2\mu_0}\right]-\frac{\mathbf{B}}{\mu_0}\cdot\nabla\mathbf{B}=0 \tag{3.89}$$

For the sake of completeness, it is worth mentioning that, exploiting the vector identity (3.87b) and the indivergence of the induction magnetic field, we can express the MHD equilibrium constraint also in terms of the Maxwell stress tensor:

$$\nabla\cdot\overline{\mathbf{T}}=0, \tag{3.90}$$

where

$$\overline{\mathbf{T}}=\left(p+\frac{B^2}{2\mu_0}\right)\bar{\mathbf{I}}-\frac{\mathbf{B}\mathbf{B}}{\mu_0}. \tag{3.91}$$

However we here enforce (3.89) in weak form, *i.e.* we multiply Equation (3.89) by an arbitrary test vector field $\mathbf{q}$ and integrate over the plasma volume. For independent vector fields $\mathbf{q}$, defined in the plasma region, we can this way study different integral consequences of the equilibrium constraint within the plasma. Let us first scalar multiply (3.89) by $\mathbf{q}$,

$$\mathbf{q} \cdot \nabla \left[p + \frac{B^2}{2\mu_0} \right] = \mathbf{q} \cdot (\mathbf{B} \cdot \nabla) \mathbf{B} \tag{3.92}$$

Using the vector identity (3.87c) and the Leibniz rule for directional derivatives, we get

$$\begin{aligned} \nabla \cdot \left[\left(p + \frac{B^2}{2\mu_0} \mathbf{q} \right) \right] - \left(p + \frac{B^2}{2\mu_0} \right) \nabla \cdot \mathbf{q} &= (\mathbf{B} \cdot \nabla) (\mathbf{B} \cdot \mathbf{q}) - \mathbf{B} \cdot (\mathbf{B} \cdot \nabla) \mathbf{q} \\ &= \nabla \cdot (\mathbf{B} \cdot \mathbf{q}) \mathbf{B} - \mathbf{B} \cdot (\mathbf{B} \cdot \nabla) \mathbf{q} \end{aligned} \tag{3.93}$$

Hence finally,

$$\nabla \cdot \left[\left(p + \frac{B^2}{2\mu_0} \right) \mathbf{q} + (\mathbf{B} \cdot \mathbf{q}) \mathbf{B} \right] = \left(p + \frac{B^2}{2\mu_0} \right) \nabla \cdot \mathbf{q} - \mathbf{B} \cdot (\mathbf{B} \cdot \nabla) \mathbf{q} \tag{3.94}$$

We are rather interested in the radial force balance of the plasma column. Hence, we first take $\mathbf{q} = \mathbf{i}_r$, that is the unitary vector indicating the radial direction in the cylindrical reference frame (r, φ, z). Clearly, we have

$$\nabla \cdot \mathbf{i}_r = \frac{1}{r} \frac{\partial}{\partial r} r = \frac{1}{r}, \;\; (\mathbf{B} \cdot \nabla) \mathbf{i}_r = \frac{B_\zeta}{r} \frac{\partial}{\partial \zeta} \mathbf{i}_r = \frac{B_\zeta}{r} \mathbf{i}_\zeta \tag{3.95}$$

Using (3.95) in the equilibrium constraint (3.94) we recover Equation (6.3) in Chapter 2 of Reference [123], despite a misprint there,

$$\int_{+\partial V_p} \left[\left(p + \frac{B^2}{2\mu_0} \right) \mathbf{i}_r + (\mathbf{B} \cdot \mathbf{i}_r) \mathbf{B} \right] \cdot \mathrm{d}\mathbf{S} = 2\pi \int_{\Omega_p} \left(p + \frac{B^2}{2\mu_0} - \frac{B_\zeta^2}{\mu_0} \right) \mathrm{d}S \tag{3.96}$$

The first integral is defined along the plasma boundary, where moreover we have $\mathbf{B} \cdot \mathrm{d}\mathbf{S} = 0$.

Following we consider the test vector field $\mathbf{q} = \mathbf{r}$, which is the vector from the origin of the reference system to any point of the space. We notice explicitly as in the cylindrical basis (r, φ, z) the components of such a vector are $(r, 0, z)$, hence

$$\nabla \cdot \mathbf{r} = \frac{1}{r} \left(\frac{\partial}{\partial r} r^2 + \frac{\partial}{\partial z} z \right) = 3, \;\; (\mathbf{B} \cdot \nabla) \mathbf{r} = \mathbf{B} \cdot \mathbf{I} = \mathbf{B} \tag{3.97}$$

Hence, the weak form of the MHD Equilibrium constraint (3.94) with $\mathbf{q} = \mathbf{r}$ finally take the form of Equation (6.1) in Chapter 2 of Reference [123]:

$$\int_{+\partial V_p} \left[\left(p + \frac{B^2}{2\mu_0} \right) \mathbf{r} + \frac{(\mathbf{B}\cdot\mathbf{r})\,\mathbf{B}}{\mu_0} \right] \cdot \mathrm{d}\mathbf{S} = 2\pi \int_{S_p} \left(3p + \frac{B^2}{2\mu_0} \right) \mathrm{d}S \quad (3.98)$$

Equations like (3.96) and (3.98) can be used to estimate a certain moment of the distribution of the magnetic flux density at the boundary. In particular, for the high aspect ratio circular tokamak, we can assume the poloidal magnetic flux density tangent to the plasma boundary to have the form (3.60) and the toroidal magnetic flux density to have the form

$$B_\varphi = \frac{\mu_0 I}{r} \simeq \frac{\mu_0 I}{R_{pl}} \left(1 + \epsilon_{pl} cos\alpha \right) \quad (3.99)$$

where I is the poloidal current per radian as already defined in Equations (3.34)-(3.35). Plugging the magnetic field representations (3.60) and (3.99) into the MHD Equilibrium constraints (3.96)-(3.98) we obtain

$$\begin{array}{llcl} (a) & -\frac{\langle B_\varphi \rangle^2_{\partial V_{pl}}}{2\mu_0} + \frac{B_J^2}{2\mu_0}(1+2\Lambda) = & \langle p \rangle_{S_{pl}} + \left\langle \frac{B_p^2}{2\mu_0} \right\rangle_{S_{pl}} - \left\langle \frac{B_\varphi^2}{2\mu_0} \right\rangle_{S_{pl}} & (3.100) \\ (b) & \frac{\langle B_\varphi \rangle^2_{\partial V_{pl}}}{2\mu_0} + \frac{B_J^2}{2\mu_0}(3+2\Lambda) = & 3\langle p \rangle_{S_{pl}} + \left\langle \frac{B_p^2}{2\mu_0} \right\rangle_{S_{pl}} + \left\langle \frac{B_\varphi^2}{2\mu_0} \right\rangle_{S_{pl}} & \end{array}$$

Here second order toroidal corrections have been discarded for consistency with the flux density representations. By difference of the two Equations above, we get the pressure balance equation:

$$\langle p \rangle_{S_{pl}} + \frac{\left\langle B_\varphi^2 \right\rangle_{S_{pl}} - \langle B_\varphi \rangle^2_{\partial V_{pl}}}{2\mu_0} = \frac{B_J^2}{2\mu_0} \quad (3.101)$$

Normalizing Equation (3.101) by the magnetic energy density $B_J^2/2\mu_0$, we get moreover

$$\frac{\left\langle B_\varphi^2 \right\rangle_{S_{pl}} - \langle B_\varphi \rangle^2_{\partial V_{pl}}}{B_J^2} = 1 - \underbrace{\frac{\langle p \rangle_{S_{pl}}}{B_J^2/2\mu_0}}_{\beta_p} \quad (3.102)$$

We introduced here a formal definition for the "poloidal beta" β_p, which is the average pressure in the plasma cross-section normalized by the average poloidal magnetic energy density at the plasma boundary we would have in the purely cylindrical case $B_J^2/2\mu_0$. This is an important figure of merit for tokamak plasmas: the higher β_p the higher the kinetic pressure (hence the temperature) we are able to reach for a given plasma current. Equation (3.102) allows to discriminate the actual orientation of poloidal currents within the plasma [124]. For $\beta_p < 1$ the toroidal field within the plasma on average is higher than the toroidal field at the plasma boundary, hence poloidal plasma currents flow in the same direction as currents in Toroidal Field coils. For $\beta_p = 1$ we do not predict poloidal currents, or at least an overall net poloidal current (current densities in the poloidal direction can still exist locally, and compensate each other in the integral relation (3.102)). For $\beta_p > 1$ we expect instead a net poloidal plasma current which counter-react the TF coils currents.

Summing up the constraints (3.101a) and (3.101b) we finally obtain an expression for the parameter Λ of the poloidal field representation (3.60) in terms of internal plasma parameters:

$$\Lambda = \underbrace{\frac{\langle p \rangle_{S_{pl}}}{B_J^2/2\mu_0}}_{\beta_p} + \frac{1}{2} \underbrace{\frac{\langle \bar{B}_p^2 \rangle_{S_{pl}}}{B_J^2}}_{\ell_i} - 1 \tag{3.103}$$

Similarly to β_p, we defined here the "internal inductance" as the the average magnetic energy density within the plasma cross section normalized by $B_J^2/2\mu_0$. This is an indicator on the distribution of electric current density within the cross-section: low values of ℓ_i indicate a rather flat profile of the toroidal current density distribution, while high values of ℓ_i indicate that the toroidal current density is very much peaked towards the centre of the plasma cross-section.

3.3 Classification of Equilibrium Problems

Now that the basics conceptual ingredients are set up, we can provide an intuitive classification of the MHD equilibrium problems one may want to solve. Moreover we can grasp the problem of the coupling with external conductors in a very concise way.

Fixed boundary - Forward problem We already stressed that if we know the actual plasma boundary and all of the external currents (say the active currents, we suppose the eddy currents to be zero) we are able to solve the magnetic field problem in the whole exterior domain to the plasma, up to the plasma boundary. In particular, for the high-aspect ratio circular tokamak, providing the plasma shift Δ_b and minor radius b, the plasma current J and the magnetic field due to external currents $B_{\perp,ext}$, we uniquely determine B_J:

$$B_J = \frac{\mu_0 J}{2\pi b} \tag{3.104}$$

and Λ

$$\Lambda = -\frac{B_{\perp,ext}}{B_J} \cdot \frac{2R_{pl}}{b} - \ln \frac{8R_{pl}}{b} + \frac{1}{2} \tag{3.105}$$

The parameters B_J and Λ completely determine the magnetic field tangent to the boundary for the high-aspect-ratio circular tokamak. The problem of the determination of B_{tan} at the plasma boundary, for assigned plasma boundary, plasma current and external magnetic fields may be correctly defined as the *MHD fixed boundary equilibrium* ***forward*** *problem*. Once B_{tan} is known at the plasma boundary, the equilibrium constraint can be used to solve the MHD Equilibrium problem within the plasma, as a Neumann problem.

Fixed boundary - backward problem In previous Section, when providing the expressions for the overall poloidal flux in the plasma-wall gap, we assumed in some sense to have a complete knowledge about the plasma boundary geometry, and the tangential component of the magnetic field. Moreover we took as known also the net current in the thin wall J_w. We observed that J_w^c was then automatically assigned, so for the equilibrium constraint to be valid. This apparently innocent procedure hides a quite different way of using the MHD equilibrium model.

We may correctly define the problem of determining external currents for assigned plasma shape, plasma current and tangential magnetic field to the boundary as the *MHD fixed boundary equilibrium* ***backward*** *problem*. For the sake of understanding imagine now the wall currents J_w and J_w^c as if they are really active currents, we shall come back to the dynamic problem in few paragraphs. Notice that, prescribed the plasma boundary geometry, and the tangential component of the magnetic field, the problem of the contemporary determination of J_w and J_w^c would be undetermined. The only well determined quantity is the vertical field to provide to keep the plasma in that particular equilibrium configuration $B_{\perp,ext}$. How this externally applied vertical field is produced by the currents J_w and J_w^c is to some extent arbitrary, since they both produce a vertical field in the tokamak. More generally we may imagine then to substitute our wall with some other conductor, which is not capable of generating a vertical field. In this case, rather than having infinite solutions, we would not have even a single one.

We are simply stating that the problem of the determination of currents which provide the magnetic field necessary to keep an MHD plasma in Equilibrium with some prescribed plasma boundary is ill-posed in the sense of Hadamard [125].

Free-boundary There is a last opportunity: we may decide to assign all the external currents[3], the overall plasma current, and information on the tangential field, assigning B_J and Λ. This represents enough information to determine the plasma minor radius b and the plasma shift Δ_b. Indeed, from J and B_J we immediately obtain the plasma minor radius:

$$b = \frac{\mu_0 J}{2\pi B_J} \tag{3.106}$$

and finally R_{pl} is easily obtained considering also the externally applied vertical field $B_{\perp,ext}$ and the value of Λ:

$$R_{pl} = -\frac{B_J}{B_{\perp,ext}} \cdot \frac{b}{2}\left[\Lambda + \ln\frac{8R_{pl}}{b} - \frac{1}{2}\right] \tag{3.107}$$

This last possibility represents the most embryonic example of a *free-boundary MHD equilibrium problem*. Notice that B_J and Λ are assigned besides we do not know about the actual location and minor radius of the circular plasma boundary. This is one of the key ingredient of free-boundary equilibrium as seen from the exterior domain: we have actually to assign some information on the magnetic field tangent to the plasma boundary, besides we do not know neither the shape nor the location of this surface.

The next ingredient in setting up a free-boundary equilibrium problem is then some machinery which allows to relate B_J and Λ to the geometrical parameters b, R_{pl}, the plasma current J and the external fields. Intuitively, if we are able to assign a current density distribution for any arbitrary plasma boundary, then we are in the position to relate the tangential field to the plasma boundary to the actual geometry of the boundary itself. Hence, the machinery we are looking for is precisely the solution of the MHD equilibrium problem

[3] again we consider a static situation where also the wall currents are assigned, the role of induction is discussed later.

within the plasma. As we shall see, the MHD Equilibrium condition constrains indeed the possible ways in which we can choose such a current distribution.

Evolutionary Equilibrium Before going further and enter the rather technical aspects of the MHD equilibrium problem within the plasma itself, let us explain which is then the role of eddy currents, and how we move from *static* MHD equilibrium to *evolutionary* MHD equilibrium problems. For our simple high-aspect-ratio circular test case, we shall admit that the vertical field provided by external conductors can be in part produced by the unknown wall currents J_w and J_w^c defined in Equation (3.63). Vessel currents have their own dynamics (3.69a, 3.75), given in first approximation by

$$\begin{aligned} &(a) \quad J_w = \tau_{0,w} \frac{\mathrm{d}}{\mathrm{d}t} (J_w + J) \\ &(b) \quad J_w^c = \tau_w \frac{\mathrm{d}}{\mathrm{d}t} \left[J \frac{\Delta_b - \Delta_{iw}}{b_w} \right] \end{aligned} \tag{3.108}$$

These are accompanied by the equilibrium constraint (3.71), where wall currents are made explicit via (3.65)-(3.66):

$$-\left[\frac{\mu_0}{4\pi}\left(\ln\frac{8R_w}{b_w} - \frac{1}{2}\right)\right] J_w + \left[\frac{\mu_0}{4\pi}\frac{R_w}{b_w}\right] J_w^c = -R_{pl}\left(B_{\perp,ext} - B_{\perp,act}\right) \tag{3.109}$$

Here $B_{\perp,ext} = B_{\perp,ext}(B_J, \Lambda, b, R_{pl})$ is the vertical field necessary to keep the plasma column in equilibrium and provided by (3.72). The vertical field provided by external active coils is assigned and indicated by $B_{\perp,act}$. At the initial time instant the wall currents are assigned to be null, *i.e.* $J_w(t_0) = J_w^c(t_0) = 0$.

Now, depending on the type of problem, different quantities can be assigned. We may assign the plasma boundary evolution, *i.e.* $\Delta_b(t)$ and $b(t)$, besides the plasma current $J(t)$, obtaining a *forward* fixed boundary evolutionary equilibrium problem. This may be used for estimating eddy currents when the plasma boundary evolution is known precisely. Moreover the tangential field to the boundary is an output of such procedure, which can be used in some time instant to compute the poloidal flux map within the boundary.

Imagine now to be able to control perfectly one of the two degrees of freedom of the current in the wall, say J_w^c, hence dropping its evolution Equation from (3.108). We may want to prescribe some desired evolution for the plasma boundary geometry, and for the tangential magnetic field to the boundary (*i.e.*

for the current density distribution inside the plasma). Then one can formulate the control problem of what is the best J_w^c to enforce this evolution. The equilibrium problem this time is *evolutionary, fixed-boundary* and *backward*.

Finally prescribing $B_J(t)$ and $\Lambda(t)$, and as usual the plasma current $J(t)$, we can contemporaneously determine the evolution of the plasma boundary and of the wall currents. In principle, this is already a *free-boundary evolutionary equilibrium* problem. However, in more general situations, it can be difficult to prescribe information about B_{tan} without knowing the actual plasma boundary, and we will need to solve the MHD equilibrium problem within the plasma precisely to add some constraint between plasma geometry, external currents and magnetic field at the plasma boundary. This is further commented in next Section.

3.4 CarMa0NL

CarMa0NL is a free-boundary evolutionary equilibrium model, first introduced in [62], later used for a variety of a tasks, ranging from the analysis of forces generated on wall structures during fast plasma transients [126, 127, 128, 85], estimation of plasma energy losses [35] and analysis of disruption events in existing devices [84, 129].

In this Section we provide the essential structure of the numerical model, explaining how to couple an axisymmetric free-boundary MHD Equilibrium solver with the fully 3D volumetric model of external conductors, already described in Section 2.4. A suitable *Coupling Surface*, located outside and in the immediate proximity of the first-wall, bounds the computational domain of the MHD equilibrium problem, as indicated in Figure 2.1. The first-wall delimits the portion of the MHD computational domain where the plasma can actually live.

The Coupling Surface is assumed to be axisymmetric, and more generally all the physical quantities within the MHD Equilibrium problem are retained independent of the toroidal angle. A differential formulation is set up for the solution of the free-boundary MHD Equilibrium problem within the Coupling Surface, described in detail in subsection 3.4.1.

We will see that the boundary conditions for the MHD equilibrium problem will require to evaluate the poloidal flux due to the external currents, both active and passive, at the Coupling Surface. The formulation has some similarity with the one presented in [115], indeed the two models adopt also the same finite elements, *i.e.* second order Lagrangian triangles, for the description of the poloidal flux in the *inner domain* Ω_{in}. In this respect, it is worth noticing that the magnetic field is determined by the superposition of the plasma and external currents produced magnetic fields. The solution of the *vacuum* outer magnetic problem can be determined separately, considering the plasma as the only magnetic field source. The solution of such problem is clearly axisymmetric and is found considering an enlarged semi-circle domain, encapsulating Ω_{in} [115]. Anyway this "plasma-only" problem is solved once for all before the simulation, providing the relation between plasma currents within Ω_{in} and plasma poloidal flux at the boundary $\partial\Omega_{in}$. Later, when discussing applications, we will see that CREATE-L represents a convenient tool for providing the initial flux map to start a CarMa0NL simulation.

The poloidal flux produced by the wall 3D currents at the Coupling Surface will be easily computed via Biot-Savart integrals, we need just to average $\psi_{ext} = rA_{\varphi,ext}$ along the toroidal angle, configuring this way a real poloidal flux. The additional non-trivial passage is how to correctly reproduce the induced voltages due to plasma variations on structures. The basic idea is to use the Virtual Casing Principle and describe the plasma produced poloidal flux ψ_p via a suitable set of equivalent filamentary toroidal currents placed in the nodes of the Coupling Surface. In subsection 3.4.2 we describe how these equivalent currents are found in terms of the plasma poloidal flux.

The overall evolutionary equilibrium model is finally summarized at the end of this Section, providing few comments on its numerical solution.

3.4.1 The Grad-Shafranov Solver

We already observed that for a plasma in MHD equilibrium, equi-pressure surfaces are also magnetic flux surfaces: current and magnetic flux density field lines are tangent to them. These equi-pressure surfaces are nested tori in case the magnetic fields are regular enough [120]. Up to know, we did not comment much on the consequences of MHD equilibrium within the plasma itself, except for the key role of figures of merit as the poloidal beta β_p and the internal inductance ℓ_i. It is worth here a short comment, in order to understand how an evolutionary equilibrium free-boundary model can be set up.

Observe in particular, from the current density representation in terms of poloidal flux ψ and poloidal current I (3.114), that the toroidal current density in axisymmetric geometry is expressed as

$$j_\varphi = -r\nabla \cdot \frac{\nabla\psi}{\mu_0 r^2} = L^*\psi \tag{3.110}$$

The elliptic operator acting on ψ at the r.h.s. is defined as the *Shafranov operator*, and sometimes indicated by the symbol L^* [130]. This is just a representation for the toroidal current density coherent with the magnetic flux density representation given in (3.34). Now, while in vacuum we have $j_\varphi = 0$, within the plasma the equilibrium constraint implies, for this axisymmetric case, that $p = p(\psi)$, $I = I(\psi)$ and

$$j_\varphi = r\frac{\mathrm{d}p}{\mathrm{d}\psi} + \frac{\mu_0}{8\pi^2 r}\frac{\mathrm{d}I^2}{\mathrm{d}\psi} \tag{3.111}$$

Here the function $\mathrm{d}p/\,\mathrm{d}\psi$ and $\mathrm{d}I^2/\,\mathrm{d}\psi$ should be specified based on the real toroidal current distribution within the palsma, which generally means on calculations of transport codes. From the point of view of MHD equilibrium these are *free-functions* which need to be specified in order to provide a closure to the Grad-Shafranov Equation resulting from the contemporary consideration of Equations (3.110) and (3.111):

$$L^*\psi = 2\pi r\frac{\mathrm{d}p}{\mathrm{d}\psi}(\psi) + \frac{\mu_0}{4\pi r}\frac{\mathrm{d}I^2}{\mathrm{d}\psi}(\psi) \tag{3.112}$$

The idea is now to solve Equation (3.112) within the domain Ω_{in}, prescribing coherently the electric current density to be null outside the plasma boundary. The free-functions $\mathrm{d}p/\,\mathrm{d}\psi$ and $\mathrm{d}I^2/\,\mathrm{d}\psi$ shall accommodate this feature. Anyway the plasma boundary is determined by the unknown flux map itself. For this reason the free functions are specified in terms of a normalized poloidal flux:

$$\bar{\psi} = \frac{\psi - \psi_a}{\psi_b - \psi_a}, \tag{3.113}$$

where we have introduced the new unknowns ψ_a, poloidal flux value at the magnetic axis, and ψ_b, poloidal flux value at the plasma boundary. The free functions can be then specified as

$$\begin{aligned} (a) \quad & \frac{\mathrm{d}p}{\mathrm{d}\psi} = \lambda\frac{\beta_0}{R_0}\left(1 - \bar{\psi}^{\alpha_{m,p}}\right)^{\alpha_{n,p}} \\ (b) \quad & \frac{\mathrm{d}I^2}{\mathrm{d}\psi} = \frac{8\pi^2}{\mu_0}\lambda R_0\left(1 - \beta_0\right)\left(1 - \bar{\psi}^{\alpha_{m,I}}\right)^{\alpha_{n,I}} \end{aligned}$$

so that the overall expression for the current density is

$$
\begin{aligned}
j_\zeta = \lambda\, \beta_0 \cdot \frac{r}{R_0} \left(1 - \bar{\psi}^{\alpha_{m,p}}\right)^{\alpha_{n,p}} \\
+ \lambda(1-\beta_0) \cdot \frac{R_0}{r} \left(1 - \bar{\psi}^{\alpha_{m,I}}\right)^{\alpha_{n,I}}
\end{aligned}
\tag{3.114}
$$

Here the input parameters to vary the toroidal current density distribution are $(\beta_0, \alpha_{m,p}, \alpha_{n,p}, \alpha_{m,I}, \alpha_{n,I})$, while R_0 is a reference major radius, generally taken to be the major radius of the vacuum vessel, *i.e.* $R_0 = R_w$. The values of ψ_a and ψ_b have to be determined self-consistently, and in particular ψ_b specifies the plasma boundary. For this reason the following constraints are enforced:

$$
\begin{aligned}
(a) \quad \psi_a = \psi(P_A) \\
(b) \quad \psi_b = \psi(P_B).
\end{aligned}
\tag{3.115}
$$

We hence need to specify, given a flux map, the locations of the magnetic axis and of the point defining the plasma boundary. This can be a non-trivial task, and represents an important feature of the solver. The boundary point P_B, in absence of halo currents or scrape-off layers, is always taken to be either the limiter point where the Last Close Flux Surface intersect solid walls, or the X-point for diverted configurations. The position of the magnetic axis is a singular point for the flux map, where the nested toroidal surfaces degenerate to a toroidal line. We need finally a constraint in order to specify λ, which is purposely introduced in the parametrization above to allow for the imposition of the net toroidal current, which is an input for the model:

$$
\int_{\Omega_{pl}} j_\varphi \,\mathrm{d}S = J \tag{3.116}
$$

The weak form for the Grad-Shafranov equation (3.112) is enforced via a Galerkin Finite Element Method, using 2D lagrangian elements [115, 62],

$$
\underline{\underline{A}}\, \underline{\psi} = \underline{g}(\underline{\psi}, \underline{s}, \underline{u}) - \underline{\underline{\hat{A}}}\, \underline{\hat{\psi}} \tag{3.117}
$$

here $\underline{\psi}$ is the vector containing the degrees of freedom for the poloidal flux in the internal nodes of the discrete domain. Similarly, the vector $\underline{\hat{\psi}}$ contains the degrees of freedom of the poloidal flux in the boundary nodes. The vector $\underline{w}$ contains the plasma profile input parameters $\underline{u} = [\beta_0, \alpha_{m,p}, \alpha_{n,p}, \alpha_{m,I}, \alpha_{n,I}]$, and the vector $\underline{s}$ contains the further unknowns which regulate the extent of the plasma region $\underline{s} = [\psi_a, \psi_b, \lambda]$. The definition of the matrices is as follows:

$$
\begin{aligned}
&(a) \quad A_{i,j} = -\int_{\Omega_{in}} \frac{\nabla w_i \cdot \nabla w_j}{r} \,\mathrm{d}\mathbf{r} \quad \forall i, j \in N_i \\
&(b) \quad \hat{A}_{i,j} = -\int_{\Omega_{in}} \frac{\nabla w_i \cdot \nabla w_j}{r} \,\mathrm{d}\mathbf{r} \quad \forall i \in N_i \quad \text{and } \forall j \in N_b \\
&(c) \quad g_j = \int_{\Omega_{in}} \mu_0 j_\varphi(\underline{\psi}, \underline{s}, \underline{u}) w_j \,\mathrm{d}\mathbf{r}
\end{aligned}
\tag{3.118}
$$

Here by w_k the Lagrange test function on triangular element; N_i is the set of indices related to d.o.f. internal to the domain; and N_b is the set of indices for the boundary degrees of freedom. The poloidal flux at the boundary $\partial\Omega_{in}$ is really given by two different sources: namely the external sources $\hat{\psi}_{ext}$ and the plasma source $\hat{\psi}_p$. At this stage we can regard $\hat{\psi}_{ext}$ as an input for the MHD equilibrium model. On the other hand, the actual value of $\hat{psi}_p$ depends on the plasma current distribution. In order to provide $\hat{\psi}_p$, the outer *vacuum* axisymmetric magnetostatic problem needs to be solved. This is done efficiently, using the same Galerkin formulation and discretizing the outer poloidal plane up to a semi-circle sufficiently far from the plasma, which allows to set up analytical Robin-like boundary conditions [131]. The Galerkin formulation for this problem looks similar to the one proposed above, although no boundary terms appear now:

$$
\underline{A^*}\ \underline{\psi_p^*} = \underline{g^*}(\underline{\psi}, \underline{s}, \underline{u}) \tag{3.119}
$$

Here the subscript "p" denotes the plasma source, while the asterisk superscript denotes that vectors and matrices are defined both in the internal and external domain to the Coupling Surface (virtually all of the poloidal plane). The forcing term $\underline{g^*}$ representing the plasma currents is the same as before, although it is defined on a wider mesh. The d.o.f. which do not correspond to nodes internal to the Coupling Surface shall be padded by zeros,

$$
(g^*)_j = \begin{cases} g_j & j \in N_i \\ 0 & \text{otherwise} \end{cases} \tag{3.120}
$$

Hence we can define a rectangular matrix $\underline{\underline{E_1}}$, which is always null except for those internal nodes to the Coupling Surface, such that $\underline{g_p} = \underline{\underline{E_1}}\ \underline{g}$. Clearly we have $\underline{\psi_p} = \underline{\underline{A^*}}^{-1}\ \underline{\underline{E_1}}\ \underline{g}$. Considering that we are only interested to the poloidal flux at the Coupling Surface, we can select the corresponding nodes via a further rectangular matrix $\underline{\underline{E_2}}$, resulting in

$$\underline{\hat{\psi}_p} = \underbrace{\underline{\underline{E_2}}\,\underline{\underline{A^{*-1}}}\,\underline{\underline{E_1}}}_{\underline{\underline{K}}}\,\underline{g}(\underline{\psi},\underline{s},\underline{u}) \tag{3.121}$$

Finally the MHD equilibrium problem is transformed to

$$\underline{\underline{A}}\,\underline{\hat{\psi}} = \left(\underline{\underline{1}} - \underline{\underline{\hat{A}}}\,\underline{\underline{K}}\right)\underline{g}(\underline{\psi},\underline{s},\underline{u}) - \underline{\underline{\hat{A}}}\,\underline{\hat{\psi}_{ext}} \tag{3.122}$$

The system of Equations above, provided the flux from external conductors $\underline{\hat{\psi}_e}$ and the input profile parameters $\underline{u}$, should be solved together with the contraints (3.115)-(3.116) for the remaining unknowns $\underline{s}$.

3.4.2 Coupling with external conductors

As hinted, the evolution of currents in the passive structures is here provided in terms of the integral formulation discussed in the previous Chapter. The actual poloidal flux $\psi_e = rA_\varphi$ which these 3D currents produce at the coupling surface points is in principle 3D, *i.e.* $\psi_e = \psi_e(r,\varphi,z)$. Nonetheless we can average the poloidal flux along the toroidal angle. The poloidal flux due to external currents is then easily computed via a Biot-Savart integration,

$$\underline{\hat{\psi}_e} = \underline{\underline{Q}}\underline{I_w} \tag{3.123}$$

where $\underline{I_w}$ is the vector of degrees of freedom for the external currents. A convenient way of providing the plasma magnetic field outside of its boundary is given by the virtual-casing principle [94], as widely discussed in previous Chapter. In particular, thanks to the assumed axisymmetry of the plasma, CarMa0NL considers a set of equivalent currents circulating in toroidal filaments placed exactly at the Coupling Surface nodes of the MHD equilibrium problem. These currents produce exactly the poloidal magnetic field of the plasma outside of the domain delimited by the Coupling Surface itself. It is then simple to represent the plasma-induced voltages in conducting structures via a simple mutual inductance matrix $\underline{\underline{M_{eq}}}$.

In order to determine the equivalent currents at the Coupling Surface nodes, we come back to the magnetostatic problem in the whole poloidal plane, for assigned plasma currents, given in Equation (3.119). Its solution provided the poloidal flux due to plasma currents in the whole poloidal plane, hence in particular $\hat{\psi}_p$ at the Coupling Surface. We adopt now the Virtual Casing principle discussed in previous Chapter. We consider a distribution of filamentary currents placed at the mesh nodes of $\partial\Omega_{in}$. We pretend these currents correctly reproduce the poloidal flux at $\partial\Omega_{in}$ in our second order Lagrangian finite element space, *i.e.*

$$\int_{\partial\Omega_{in}} G_0 \sum_{k=1}^{N_b} I_{eq,k}\delta(r'-r_k, z'-z_k)\,\mathrm{d}\ell' = \hat{\psi}_p(r,z) \quad \forall\,(r,z)\in\partial\Omega_{in} \tag{3.124}$$

Here the Green function for the poloidal flux produced by a toroidal filament was provided in Equation (3.39). We enforce (3.124) in weak form using as basis functions the 2D lagrangian basis functions associated to Coupling Surface nodes:

$$\underline{\underline{L_0}}\,\underline{I_{eq}} = \underline{\underline{H_0}}\,\underline{\psi} \tag{3.125}$$

where we defined

$$\begin{aligned} (a) \quad (L_0)_{j,k} &= \int_{\partial\Omega_{in}} w_j \int_{\partial\Omega_{in}} G_0\delta(r'-r_k, z'-z_k)\,\mathrm{d}\ell'\,\mathrm{d}\ell \\ (b) \quad (H_0)_{j,k} &= \int_{\partial\Omega_{in}} w_j \cdot w_k\,\mathrm{d}\ell \end{aligned} \tag{3.126}$$

Hence the equivalent currents are found immediately by

$$\underline{\hat{g}_{eq}} = \underline{\underline{L_0}}^{-1}\,\underline{\underline{H_0}}\,\underline{\hat{\psi}_p} \tag{3.127}$$

Of course, $\underline{\hat{\psi}_p}$ is proportional to the original vector $\underline{g}$, via the matrix $\underline{\underline{A^*}}^{-1}\underline{\underline{E_1}}$. Finally, considering definition of $\underline{\underline{K}}$ (3.121), we obtain:

$$\underline{\hat{I}_{eq}} = \underbrace{\underline{\underline{L_0}}^{-1}\,\underline{\underline{H_0}}\,\underline{\underline{K}}}_{\underline{\underline{S}}}\;\underline{g}(\underline{\psi},\underline{s},\underline{u}) \tag{3.128}$$

Once the equivalent currents are found in the 2D finite element representation calculation of the mutual inductance with structures is easily performed in CARIDDI, thanks to the standard axi-symmetric Green function G_0.

A last aspect important aspect concerns the plasma toroidal flux variations, which do induce voltages in external conductors, without actually modifying the magnetic field outside. Indeed, plasma poloidal currents configure perfect toroidal solenoids, which do not produce magnetic field outside of the plasma. The plasma toroidal flux is defined, thanks to Ampère's law,

$$\Psi_p(\underline{\psi}, \underline{s}, \underline{w}) = \frac{\mu_0}{2\pi} \int_{\Omega_{in}} \frac{I - I_0}{r} \,\mathrm{d}\mathbf{r} \tag{3.129}$$

where I is the poloidal plasma current, and I_0 is the poloidal current of external conductors, essentially the one due to Toroidal Field Coils. By a formal analogy with magnetostatic problems, we can calculate a vector potential in the exterior domain which correctly reproduces the electric field due to plasma toroidal flux variations, when considering its time variations.

In particular we can consider the toroidal flux as concentrated in a toroidal filament placed at the centre of the plasma domain, *i.e.* placed at the centre of V_{fw}. The vector potential produced by such a singular toroidal flux distribution, expressed in the Coulomb gauge, is mathematically analogous to the magnetic field produced by a current circulating in the same toroidal filament. Exploiting this analogy, we can therefore easily compute a *number of turns* vector which relates plasma toroidal flux variations to induced voltages in passive structures,

$$\underline{V_{pl,tor}} = \underline{N} \,\frac{\mathrm{d}}{\mathrm{d}t} \Psi_p(\underline{\psi}, \underline{s}, \underline{u}) \tag{3.130}$$

3.4.3 Resume

Finally the CarMa0NL evolutionary equilibrium problem looks like:

$$\begin{aligned} (a) \quad & \underline{\underline{L}} \frac{\mathrm{d}}{\mathrm{d}t} \underline{I} + \underline{\underline{R}}\, \underline{I} + M_{eq} \frac{\mathrm{d}}{\mathrm{d}t} \underline{I_{eq}} + \underline{N} \frac{\mathrm{d}}{\mathrm{d}t} \Psi_p = \underline{V} \\ (b) \quad & \underline{\underline{A}}\, \underline{\hat{\psi}} = \left(\underline{\underline{1}} - \underline{\underline{\hat{A}}}\, \underline{\underline{K}} \right) \underline{g}(\underline{\psi}, \underline{s}, \underline{u}) - \underline{\underline{\hat{A}}}\, \underline{\hat{\psi}_e} \end{aligned} \tag{3.131}$$

and complemented by the constraints (3.115) for ψ_a, ψ_b and (3.116) for λ [115]. The two systems of Equations (a) and (b) are coupled via:

$$\begin{aligned} \underline{I_{eq}} &= \underline{\underline{S}}\, \underline{g}(\underline{\psi}, \underline{s}, \underline{u}) \\ \hat{\psi}_e &= \underline{\underline{Q}}\, \underline{I} \end{aligned}$$

The meaning of each matrix was commented in previous subsections. The algebraic system of Ordinary Differential Equations above is solved via an implicit Euler scheme, which guarantees the possibility of using appropriately large time steps. While the model for the structures is fully 3D and linear, the plasma equilibrium model is 2D and fully non-linear. A great degree of non-linearity is in particular introduced by the fact that the equilibrium problem is free-boundary, hence even a linear relation between $j_{varphi}(\psi, r)$ and ψ would produce a non-linear problem. In next Chapter we will illustrate applications of CarMa0NL to physics problems and analysis of experiments.

Chapter 4

Applications to the study of Tokamak Disruptions

Hard to predict fast transient events often lead to the sudden termination of experiments in nearly all existing tokamak devices, see for example the statistical studies available for JET [132, 133, 134], and COMPASS [135]. Nearly 1 every 10 experiments is estimated to accidentally disrupt, even if this is largely related to the research character of the experiments, which push the devices to their performance limits [44]. These *disruptions* are a major threat for the integrity of tokamaks, due to different motivations. According to the *ITER Physics Basis* [44, 136], the major concerns are related to the energy deposition on the wall and plasma facing components surrounding the plasma, the electro-magnetic forces generated during the quench of the plasma current, and the generation of runaway electrons beams.

Early studies of tokamak experiments allowed to set up three essential operational bounds which almost certainly lead to an abrupt termination of the experiment [132, 137]. The *density* limit bounds the maximum achievable particle density, and roughly scales with the elongation and the plasma average current density $n \sim kJ[MA]/S[m^2]$ [138]. The *current* limit is set up by MHD instabilities occurring when the plasma boundary becomes a rational surface at $q = 2$. The *safety factor* q is a measure of the average toroidal excursion of a magnetic field line within a single poloidal transit [139]. Stable operation requires $q \geq 2$. For an assigned toroidal magnetic field, an increase in the plasma current is responsible of course also for an increase in the poloidal magnetic field, hence a degradation of the safety factor q. Finally the experimentally-found *pressure* limit indicates a maximum achievable toroidal beta which scales roughly as $\beta_t \sim 3 \cdot J[MA]/B_0 b$ [137]. Overcoming any of these operational limits, a *disruption* will likely occur, conversely the operational area identified by these bounds is not definitive. Indeed disruptions are triggered by a variety of MHD instabilities, and we lack a complete understanding of all the possible triggering mechanisms. Nonetheless statistical studies provide sufficient confidence that disruptions do not occur randomly, hence we should aim at their comprehension, classification and avoidance. The necessity for safe ITER operation led anyway to the design, test and optimization of disruption mitigation systems [140, 141, 142].

A quite general phenomenology of *disruptions* in tokamaks was described in [44]:

- due to the overcome of some operational limit, a large thermal energy loss takes place (*Thermal Quench*, TQ), on a time scale which ranges from $10\mu s$ for small devices to $100\mu s$ for Medium Size Tokamaks, up to few ms in JET;
- The current distribution within the plasma flattens, in reason of the more homogeneous temperature profile ($\lessapprox 1\ ms$);
- The overall resistivity of the plasma increase, due to the lower temperature, and consequently the toroidal plasma current drops very rapidly (*Current Quench*, CQ). The current decay rates vary for each machine, depending on several aspects like the aspect ratio and the average toroidal current density. For the sake of example, we may consider the overall area normalized current quench time for typical JET pulses. The shortest CQ fall in the 2-5 ms/m^2 range, extrapolating linearly from the 100%-40% decay time [44]. Considering an average plasma area of $3.5\ m^2$ and currents in the order of $2\ MA$, we immediately find CQ decay rates in the range 100-250 kA/ms.

In any of these steps the plasma may suffer a vertical instability, which can be even the driver for the TQ. A loss of the vertical control can indeed be responsible also for the motion of the plasma column at substantially unaltered plasma current and temperature. When plasma comes in close contact to the solid interface, the cross-sectional area shrinks rapidly, decreasing the edge safety factor q to values about 1.5-2. At this point some MHD instability is again triggered, as for the *current limit*. This type of event is sometimes indicated as hot *Vertical Displacement Event* (VDE).

This phenomenology highlights already some of the possible threats. In typical JET discharges, the thermal energy is in the order of $\sim 12\ MJ$, and in ITER this will climb up to $\sim 350\ MJ$. The sudden release of this energy, mainly by radiation, can be responsible for a severe thermal energy deposit on structures. Further, even during the Current Quench, when the thermal energy of the plasma is substantially negligible, the poloidal magnetic energy is continuously converted within the plasma into heat conducted or radiated to the surrounding plasma facing components [143, 144]. We shall explore this circumstance, by the tools discussed in previous Chapter, in Section 4.2.

Anyway, the major concern during the Current Quench in present tokamaks is related to the large Lorentz forces generated in the surrounding wall and plasma facing components. Not surprisingly electromagnetic force calculations are always necessary in the design of fusion devices, see for example computations for the future tokamak COMPASS-U [128, 85]. The electromagnetic forces are in part related to the induced currents in external conductors, and in part related to the *halo* currents shared between plasma and structures. The latter are predominantly poloidal and interact with the large toroidal field applied by TF coils, generating significant mechanical stresses. We shall study in detail eddy current-related disruption forces in Section 4.1.

It is worth to mention that in ITER a further major concern during the CQ phase is represented by the *runaway electrons* [44]. There the nominal plasma current $J \sim 15\ MA$ is estimated to decay in a time $t_{CQ} \sim 35\ ms$, the plasma major radius being $\sim 6\ m$. The resulting electric fields will be large enough to accelerate a large fraction of the electrons within the plasma up to relativistic velocities, in a runaway-like mechanism (the Coulomb collision cross-section decreases with the velocity of the particles, which become more and more collision-less as they gain velocity). The kinetic energy gained by these relativistic particles can be an important fraction of the poloidal magnetic energy, and the inherent risk is a local release of such energy when the runaway beam hits some solid surface [145].

This last Chapter is dedicated to applications of the *evolutionary equilibrium models* presented earlier, to the analysis and modelling of tokamak disruptions. This is mainly in order to demonstrate the efficacy of the developed models and their significance both for the design of fusion devices and for the analysis of tokamak experiments. In **Section 4.1** we study the forces exerted on the vacuum vessel surrounding the plasma during these fast transients. We will see, in agreement with recent literature, that the effect of net poloidal currents in the wall, and of plasma pre-disruption position is crucial on the forces estimation [127, 146, 147].

In **Section 4.2** we show how evolutionary equilibrium models can be used to estimate the plasma losses during a disruption, or equivalently how to test an evolutionary equilibrium simulation for being energetically consistent. Interestingly we will find that the amount of possibly dissipated energy during the CQ strongly depends on the electromagnetic time constant of the wall.

Finally, in **Section 4.3** and **Section 4.4** we compare CarMa0NL simulations respectively for JET and TCV experiments, benchmarking via simulated and real magnetic diagnostics measurements. We will use a simplified model for the JET conducting structures, leading to an overstimate of the growth rate of the vertical displacement, as expected from [148]. We will overcome this problem with a fictitious down-scaling of the disruption trigger, to focus our attention to the latest phase of the disruption, when the plasma comes in close contact to the solid surface and an halo region develops. The simulation results, in good agreement with the experimental measurements, will show the development of a relatively wide halo region, carrying a significant portion of the overall plasma current.

For TCV we will report on simulation results dedicated to the study of plasma trajectories during disruptions, aiming to interpret a recent experimental campaign on this topic. to show main dependencies. We will see that the radial motion is greatly affected by the pre-disruption plasma shape, and we will propose an interpretation of this behaviour.

4.1 Electromagnetic Forces

In this Section discuss the electromagnetic forces generated on conducting structures during disruptions, in order to provide design indications and understand the magnitude of electromagnetic local and integral forces generated on surrounding structures by fast variations of the plasma current J, internal inductance ℓ_i or poloidal beta β_p.

In subsection 4.1.1 we develop handy analytical formulas to estimate local and integral forces for an high-aspect-ratio circular tokamak, in the ideal wall hypothesis. These are compared with CarMa0NL simulation results in the following subsection, for a cross validation of analytical and numerical models.

4.1.1 Ideal Wall Forces

Here we provide some analytical formulas for the estimation of electromagnetic local and integral forces generated during disruptions in an high-aspect-ratio, circular tokamak, with thin wall. The analysis will follow easily from the discussion provided in Section 3.2, and it is based on references [149, 127, 147].

The plasma transient is assumed to be fast enough to consider the wall as ideal with respect to plasma-produced magnetic field variations. Hence, in the time interval of interest, all the electromagnetic quantities just outside such a perfectly conducting sheet are unaffected by variations of plasma currents or geometry. Such changes however modify the magnetic field in the inner region to the wall surface. As a result, the jump of $\mathbf{B}$ across the wall is equal to the difference between the actual and the initial values of $\mathbf{B}$ at the inner page of the wall:

$$\delta\mathbf{B} = \mathbf{B}_{in} - \mathbf{B}_{out} = \mathbf{B}(t) - \mathbf{B}(t_0). \tag{4.1}$$

Our interest is devoted to the surface force density $\mathbf{f}_w$, defined as the line integral across the wall:

$$\mathbf{f}_w = \int_{wall} \mathbf{j} \times \mathbf{B} \mathrm{d}l_\perp = \int_{wall} \left(-\frac{\nabla \mathbf{B}^2}{2\mu_0} + \frac{\mathbf{B}}{\mu_0} \cdot \nabla \mathbf{B} \right) \mathrm{d}l_\perp. \tag{4.2}$$

where in the last equality we used Ampere's law, and standard vector identities, see Equation (3.89). We can introduce a coordinate system local to each point of the wall mean surface, such that

$$\nabla = \hat{\mathbf{n}}_{\mathbf{w}} \frac{\partial}{\partial \ell_\perp} + \nabla_\parallel \tag{4.3}$$

As long as wall currents are tangent to the wall, we have $\nabla_\parallel \times \mathbf{B} = 0$, and the surface force density (4.2) gets simplified to

$$\mathbf{f}_{\mathbf{w}} = -\frac{B^2}{2\mu_0}\bigg|_{in}^{out} \hat{\mathbf{n}}_{\mathbf{w}} + \frac{\hat{\mathbf{n}}_{\mathbf{w}} \cdot \mathbf{B}}{\mu_0} \mathbf{B}|_{in}^{out} \tag{4.4}$$

The last term in Equation (4.4) is tangential to the wall, due to the solenoidality of $\mathbf{B}$ and the thin wall approximation, which imply the continuity for the normal component of $\mathbf{B}$ across the surface. This term was discarded in the analysis presented in [149]. Therefore the model presented there describes exclusively the surface force density normal to the wall, due to the jump of magnetic pressure,

$$p_m = \frac{\mathbf{B}^2}{2\mu_0}. \tag{4.5}$$

In *CarMa0NL* computations, both contributions to (4.4) are taken into account, and revealed the importance of the tangential force density contribution [127]. Finally such tangential forces were reintegrated in the analytical model presented later in [147]. As we shall see, a *magnetic tension* term is present whenever the magnetic flux density has a normal component to the wall. In this respect, the former model presented in [149] can be considered as the particular case of the one presented in [147], where the pre-disruption plasma position is such that the wall is a flux surface, *i.e.* $\Delta_b = \Delta_{iw}$. Indeed, in the ideal wall approximation, the normal component of $\mathbf{B}$ is frozen at the wall surface, hence the wall keeps to be a flux surface if it is such before the disruption takes place.

(a) The magnetic pressure

Equation (4.4) is still quite general, the only hypothesis up to now is that the wall is geometrically thin. From the hypothesis of axisymmetry, we may express $\mathbf{B}$, in terms of the "polodail flux" $\psi = rA_\varphi$ and the *poloidal current* $I = rB_\varphi/\mu_0$ per radian defined by (3.34) and (3.35) respectively. Thanks to the orthogonality of poloidal and toroidal magnetic fields, the overall magnetic pressure can be regarded as the sum of the separate contributions provided by each magnetic field component:

$$p_m = p_m^\psi + p_m^I \tag{4.6}$$

where we define the poloidal field magnetic pressure and the toroidal field magnetic pressure as

$$\begin{aligned} (a) \quad p_m^\psi &= \frac{|\nabla\psi|^2}{2\mu_0 r^2} \\ (b) \quad p_m^I &= \frac{\mu_0 I^2}{2r^2} \end{aligned} \tag{4.7}$$

For the study case of interest, the poloidal field magnetic pressure is easily obtained by the expression for the poloidal magnetic field provided in Equations (3.84, 3.86, 3.86). We neglect there the corrections in Δ_b/R_w and $(\Delta_b/\rho)^2$

$$p_m^\psi = p_{m,0}^\psi + p_{m,1}^\psi \cos u \tag{4.8}$$

with:

$$
\begin{aligned}
&(a)\; p^{\psi}_{m,0} = \kappa_w^2 \frac{B_J^2}{2\mu_0} \\
&(b)\; p^{\psi}_{m,1} = -2\epsilon_w \kappa_w^2 \left[\frac{B_J^2}{2\mu_0}\Lambda_w + \frac{R_w}{b}\frac{B_{\rho,1}B_J}{2\mu_0} \right]
\end{aligned}
\tag{4.9}
$$

where $\epsilon_w = b_w/R_w$ was first introduced as the wall inverse aspect ratio commenting (**??**) and we define:

$$
\Lambda_w = \Lambda + \ln\frac{b_w}{b}, \quad \kappa_w = \frac{b}{b_w} \tag{4.10}
$$

From Equation (4.9b) we see that the presence of a normal field to the wall also influences the magnetic pressure. The relative weight of that term can be understood observing from (3.86b) that

$$
\frac{B_{\rho,1}}{B_J} = \frac{b}{b_w}\frac{\Delta_b - \Delta_{iw}}{b_w} \tag{4.11}
$$

Clearly $B_{\rho,1} = 0$ whenever the wall is a flux surface.

Let us evaluate now the toroidal magnetic pressure. In our high aspect ratio assumption, the toroidal magnetic field in the plasma-wall gap can be expressed as in (3.99). In complete analogy with the discussion which lead us to (3.101), we can set up the pressure balance equation for the plasma-wall gap, where $\langle p\rangle_{\Omega_{gap}} = 0$, which reads

$$
\frac{\left\langle B_\varphi^2\right\rangle_{\Omega_{gap}}}{2\mu_0} S_{gap} = \frac{\langle B_\varphi\rangle^2_{\partial V_w}}{2\mu_0} S_w - \frac{\langle B_\varphi\rangle^2_{\partial V_{pl}}}{2\mu_0} S_{pl} + \frac{B_{u,0}^2}{2\mu_0} S_w - \frac{B_J^2}{2\mu_0} S_{pl} \tag{4.12}
$$

Scaling (3.101) by the plasma cross-sectional area S_{pl} and summing (4.12) we get

$$
\frac{\left\langle B_\varphi^2\right\rangle_{\Omega_w}}{2\mu_0} - \frac{\langle B_\varphi\rangle^2_{\partial V_w}}{2\mu_0} = -\kappa_w^2 \left[\langle p\rangle_{\Omega_{pl}} - \frac{B_J^2}{2\mu_0} \right] \tag{4.13}
$$

where we defined $\kappa_w = b_w/b$ in Equation (4.10) and the square of such a quantity appears here essentially as the ratio between the cross-sectional areas of the plasma and of the wall. Now, in the ideal wall limit, the toroidal magnetic energy cannot escape the wall, and in general the low magnitude of poloidal plasma currents prevents the conversion of the toroidal magnetic energy into thermal or dissipated energy, as discussed in [35] and later in next

Section. Hence, the variation of toroidal magnetic pressure in the plasma-wall gap, in the ideal wall approximation, is given by:

$$\delta\left(\frac{B_0^2}{2\mu_0}\right) = \delta\left[\kappa_w^2\left(\langle p\rangle_{\Omega_{pl}} - \frac{B_J^2}{2\mu_0}\right)\right] \tag{4.14}$$

where we used the fact that $\langle B_\varphi\rangle_{\partial V_w} = B_0$. Equation (4.14) contains all the information to evaluate the toroidal magnetic pressure jump at the ideal wall,

$$\delta p_m^I = \delta\left(\frac{B_0^2}{2\mu_0}\right)(1 + 2\epsilon_w \cos u) \tag{4.15}$$

We notice explicitly that Equation (4.14) can be generalized to the non-ideal wall case, or to an arbitrary $\rho = \rho^*$ surface within the plasma-wall gap as long as the fluxes of toroidal magnetic energy can be computed and this energy is not converted to other forms.

Resuming our results, we sum up the magnetic pressure jump across the wall due to toroidal and poloidal eddy currents into a single term:

$$\delta p_m = \delta p_{m,0} + \delta p_{m1} \cos u \tag{4.16}$$

where

$$\begin{aligned} &(a) \quad \delta p_{m,0} = \delta\left(k_w^2 \langle p\rangle_{\Omega_{pl}}\right) = \delta\left[k_w^2 \frac{B_J^2}{2\mu_0}\beta_p\right] \\ &(b) \quad \delta p_{m,1} = -2\epsilon_w \delta\left[k_w^2 \frac{B_J^2}{2\mu_0}\left(\frac{\ell_w}{2}\right) + \frac{R_w}{b}\,\frac{B_{\rho,1}B_J}{2\mu_0}\right] \end{aligned} \tag{4.17}$$

In (4.17) we used the equilibrium relation $\Lambda = \beta_p + \ell_i/2 - 1$, derived in (3.103) and we introduced the internal inductance up to the wall

$$\ell_w = \ell_i + 2\ln\frac{b_w}{b} \tag{4.18}$$

(b) The magnetic tension

The circumstance that the wall is not a flux surface before the transient determines $B_\rho \neq 0$ at the wall, which determines of course also $B_{\rho,1} \neq 0$ which affects the anti-symmetric magnetic pressure (4.9b)-(4.17), and is responsible for a tangential force to the wall (4.4). As hinted, the continuity of the normal component of $\mathbf{B}$ across the wall implies that $\delta\mathbf{B}$ is tangent to the wall surface, and the wall force density for the general case where $\mathbf{B} \cdot \hat{\mathbf{n}} \neq 0$ at the wall, can be written as

$$\mathbf{f_w} = \delta p_m \hat{\mathbf{n}}_\mathbf{w} + \delta\pi_u \hat{\mathbf{i}}_\mathbf{u} + \delta\pi_\varphi \hat{\mathbf{i}}_\varphi \tag{4.19}$$

where we defined the poloidal and toroidal magnetic tensions on the wall as

$$\begin{aligned} (a) \quad \delta\pi_u &= -\frac{B_\rho \delta B_u}{\mu_0} \\ (b) \quad \delta\pi_\varphi &= -\frac{B_\rho \delta B_\varphi}{\mu_0} \end{aligned} \tag{4.20}$$

In particular, using Equations (3.86)-(3.87), we get for the poloidal magnetic tension

$$\delta\pi_u = -\underbrace{\frac{B_J}{\mu_0}\frac{b}{b_w}\left(\frac{\Delta_b - \Delta_{iw}}{b_w}\right)}_{B_{\rho,1}} \delta\left[B_J\left(\frac{b}{b_w}\right)\right]\sin u \tag{4.21}$$

We explicitly remark that in the in the ideal wall approximation the normal component of the magnetic flux density is constant at the wall surface, and indeed $B_{\rho,1}$ scales like $J\left(\Delta_b - \Delta_{iw}\right)$. The latter quantity has to be constant in the ideal wall limit, as commented when studying the evolution equation for wall currents in Equation (3.75). Hence, a poloidal magnetic tension raises exclusively in reason of plasma current variations, as expressed in (4.21).

In order to evaluate the toroidal magnetic tension $\delta\pi_\varphi$, we need instead some expression for the jump of toroidal magnetic flux density across the wall, $\delta B_\varphi \simeq \delta\langle B_\varphi\rangle_{\partial V_w}\left(1 + \epsilon_w \cos u\right)$. Such a jump of toroidal field is solely related to the the net poloidal current in the wall. In tokamak devices the plasma produced toroidal field, hence the reaction toroidal field produced by eddy currents, is in general much smaller than the toroidal field imposed by external active coils, *i.e.* $\langle B_{\varphi,act}\rangle_{\partial V_w} \gg \langle B_{\varphi,w}\rangle_{\partial V_w}$. Under this assumption, Equation (4.14) is well approximated by

$$\delta\langle B_\varphi\rangle_{\partial V_w} = \frac{1}{2\langle B_{\varphi,act}\rangle_{\partial V_w}}\delta\left[k_w^2 B_J^2\left(\beta_p - 1\right)\right] \tag{4.22}$$

Hence, the toroidal magnetic tension (4.20) readily transforms to:

$$\delta\pi_\varphi = -\frac{B_{\rho,1}}{\langle B_{\varphi,act}\rangle_{\partial V_w}}\delta\left[k_w^2 \frac{B_J^2}{2\mu_0}\left(\beta_p - 1\right)\right]\sin u \tag{4.23}$$

It is worth noting that the average jump in toroidal field is clearly related to the net poloidal current in the wall:

$$I_{pol,w} = 2\pi R_w \delta \langle B_\varphi \rangle_{\partial V_w} \tag{4.24}$$

This net poloidal current is responsible on the other hand for the toroidal flux:

$$\phi_{tor,w} = \frac{\mu_0 I_{pol,w}}{2\pi R_w} \pi b_w^2 \tag{4.25}$$

which, not by coincidence, is exactly opposite to the variation of the toroidal flux due to plasma currents in the hypothesis $B_{\varphi,pl} \ll B_{\varphi,act}$, *i.e.* the flux conservation is satisfied consistently with the ideal wall assumption.

(b) The integral radial force

As significant figure of merit to quantify the mechanical stress on the wall, it is convenient to define the following integral radial force [146, 149, 128, 127, 147]

$$F_r = \int_{\partial V_w} \mathbf{f_w} \cdot \mathbf{i_r} \, \mathrm{d}\mathbf{r} \tag{4.26}$$

Besides in our axisymmetric conditions the net force is indeed zero along the radial direction, F_r quantifies the stress which tends to either compress or stretch the torus along its major radius. To get an operative expression in terms of plasma parameters, it is sufficient to consider the various contributions to the force density described in Equation (4.19) and their definitions. Clearly the toroidal magnetic tension does not contribute to the integral radial force, being $\hat{\mathbf{i}}_\varphi \cdot \hat{\mathbf{i}}_\mathbf{r} = 0$. Moreover, as observed in [147], the contributions to F_r due to a non-null normal component of the magnetic field at the wall, $B_{\rho,1} \neq 0$, compensate each other in the integration,

$$2\pi \int_{\Gamma_w} -\frac{B_{\rho,1}}{\mu_0} \delta \left[\frac{b}{b_w} B_J \right] \cdot \underbrace{\left[\cos u \left(\hat{\mathbf{n}} \cdot \hat{\mathbf{i}}_\mathbf{r} \right) + \sin u \left(\hat{\mathbf{i}}_\mathbf{u} \cdot \hat{\mathbf{i}}_\mathbf{r} \right) \right]}_{=\cos 2u} \mathrm{d}\ell = 0 \tag{4.27}$$

Hence the estimations of integral radial force already provided in [149] keep to be valid also for the more generic case where $\Delta_b \neq \Delta_{iw}$ before the disruption [147],

$$F_r = \frac{1}{2} S_w \epsilon_w \delta \left[k_w^2 \frac{B_J^2}{2\mu_0} \left(\beta_p + \ell_w \right) \right] \tag{4.28}$$

4.1.2 A test case

Following the discussion in [127], we compare the analytical formulas provided in previous Section with numerical computations of force and force densities implemented by the code *CarMa0NL*. In order to fit the high-aspect ratio hypothesis of the analytical model and not deviate too much from typical parameters of a tokamak device, we consider a circular tokamak of major radius $R_w = 1\ m$ and minor radius $b_w = 0.25\ m$, for an overall inverse aspect ratio $\epsilon_w = 4$. The wall is $1\ cm$ thick, and numerically represented by a single layer of elements, in order to force the current to be always tangent to the mean surface of the wall, as substantially happens in a sheet. We take the resistivity of the vessel to be the one of Inconel 625 at $300 \deg C$. A summary of the essential information for our wall is in Table 4.1. With these choices, the numerically computed slower time constant for the wall is about $3.24\ ms$, in fairly good agreement with the predicted τ_w^0, as defined in (3.79).

R_0	b_{fw}	b_w	d_w	$\eta_w = 1/\sigma_w$
1 m	0.2 m	0.25 m	1 cm	$1.33 \cdot 10^{-6}\ \Omega \cdot \mathrm{m}$

Table 4.1: Vessel geometry and resistivity.

The first wall implemented in *CarMa0NL* has a circular trace in the poloidal plane, with the same major radius as the wall and minor radius $b_{fw} = 0.2\ m$. The first wall bounds the domain where we can actually find the plasma, the MHD computational domain extends few mm outwards in correspondence of a suitable Coupling Surface.

We consider here the equilibrium configuration synthetically described in Table 4.2, which is also the slightly *inward-shifted* configuration described in [127]. The input parameters β_p, ℓ_i, Δ_b and b for the analytical model will be provided by CarMa0NL simulation results. *CarMa0NL* standard routines use a slightly different definition for the internal inductance and the poloidal beta, computing the average energies in the volume, rather than in the cross-sectional surface. Anyway in the high-aspect ratio limit the problem is easily circumvented accounting for the plasma-wall major radii ratio, *i.e.* $\ell_i = (R_w/R_{pl}) \cdot \ell_i^{CarMa}$, and $\beta_p = (R_w/R_{pl}) \cdot \beta_p^{CarMa}$ [127]. Hence, in Table 4.2 we show the classical poloidal beta and internal inductance, as defined in (3.103). In the same table we report the variations of main plasma quantities during two different simulations, namely a *Thermal Quench* (TQ) and a *Current Quench* (CQ). For each simulation we compare the forces, calculated with and without the account of the net poloidal current in the wall, and considering

Event	J [MA]	β_p	ℓ_i	Δ_b [cm]	Δ_{iw} [cm]
Initial	1.700	0.108	1.114	-1.43	1.14
after 0.01 ms TQ	1.700	0.081	1.114	-1.47	1.11
after 0.01 ms CQ	1.690	0.110	1.114	-1.44	1.14

Table 4.2: Global parameters for inward-shifted and low β_p plasma simulations. The further input parameters are kept constant ($\alpha_m = 0.85$, $\alpha_n = 1.15$)

	$B_\rho = 0$	$B_\rho \neq 0$	CarMa0NL
δp_{m0} [bar]	-0.204	-0.204	-0.175
δp_{m1} [bar]	-0.006	-0.006	0.004
π_{u1} [bar]	0	~ 0	0.001
$\pi_{\varphi,1}$ [bar]	0	-0.006	-0.005
F_r [kN]	-22.326	-22.326	-25.325
δp^{Ψ}_{m0} [bar]	~ 0	~ 0	$+0.006$
δp^{Ψ}_{m1} [bar]	0.096	0.096	0.096
F^{Ψ}_r [kN]	-47.433	-47.433	-47.370

Table 4.3: Forces generated during the TQ described in table 4.2

or discarding the contribution due to the normal component of the magnetic field.

In order to simulate the TQ, we impose a linear decay of the coefficient β_0 of our current parametrization (3.114). Notice that for changes of β_0 in the range $[0, 1]$ we can essentially tune the dominant contribution to the toroidal current density between $dp/d\psi$ and $fdf/d\psi$. In general β_0 is proportional to the poloidal β_p. The larger the aspect ratio the more accurate is the linear scaling between these quantities. During the TQ simulation, the plasma current is kept constant together with all the other profile parameters αs. Results for this case are illustrated synthetically in Table 4.3 and Figure 4.1. The numerical results are obtained by proper projections of the volumetric forces computed in CarMa0NL, transformation into the Fourier space along the poloidal angle, and scaling by the wall thickness.

Notice that during the *Thermal Quench*, the dominant contribution to the magnetic pressure jump is related essentially to $\delta p_{m,0}$ (4.17a), since the pressure is significantly varying within the plasma column, while $\delta p_{m,1}$ (4.17b) is much smaller, since the *wall* internal inductance ℓ_w does not vary greatly, and the plasma current is held fixed. Correspondingly $\delta \pi_u$ is essentially null while

	$B_\rho = 0$	$B_\rho \neq 0$	CarMa0NL
δp_{m0} [bar]	~ 0	~ 0	-0.004
δp_{m1} [bar]	0.034	0.027	0.024
π_{u1} [bar]	0	-0.009	-0.009
$\pi_{\varphi,1}$ [bar]	0	0.002	0.002
F_r [kN]	-17.000	-17.000	-16.831
δp_{m0}^{Ψ} [bar]	-0.087	-0.087	-0.084
δp_{m1}^{Ψ} [bar]	-0.009	-0.016	-0.017
F_r^{Ψ} [kN]	-6.267	-6.267	-7.007

Table 4.4: Forces generated during CQ described in table 4.2.

$\delta\pi_\varphi$ can still be significant. Neglecting the poloidal current both in the analytical and the numerical model we can get an astonishing agreement, indicating that there might be still some possible corrections in modelling the pressure jump due to poloidal currents. However, in all of the cases, the agreement is qualitatively good and indicates that the electromagnetic force will tend to shrink the wall towards the plasma.

For the CQ, we impose a linear decay of the plasma current of $1\ MA/ms$, and in order to keep the mean pressure almost constant during the simulation we increase β_0 correspondingly as

$$\frac{\beta_0(t)}{\beta_0(t_0)} = \left[\frac{J(t_0)}{J(t)}\right]^2. \tag{4.29}$$

A resume of the results obtained for our inward-shifted low-β_p plasma is reported in Table 4.4 and Figure 4.2. In this case the prevalent contribution on the magnetic pressure jump is $\delta p_{m,1}$, and the accordance between the numerical calculation and the analytical prediction improves greatly accounting for the normal field to the wall. Also the prediction on the magnetic tension are perfectly in agreement. Again, neglecting the poloidal current in the model we would find totally different results, confirming its important role in the task.

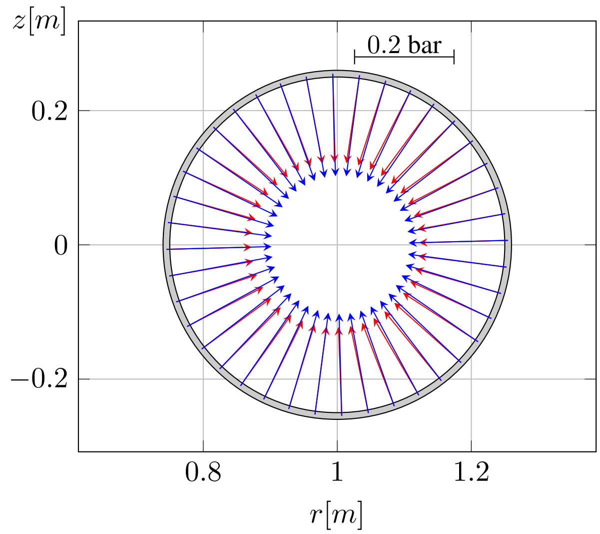

(a) with net poloidal current.

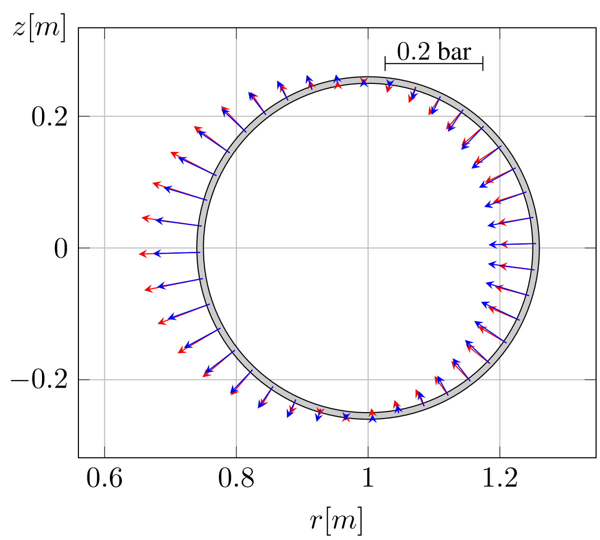

(b) without net poloidal current.

Figure 4.1: Analytical (blue) and Numerical (red) volume force density distribution during Thermal Quench scenario presented in Table 4.2, taking into account (a) and neglecting (b) the poloidal current in the wall. Corresponding quantitative results are reported in table 4.3

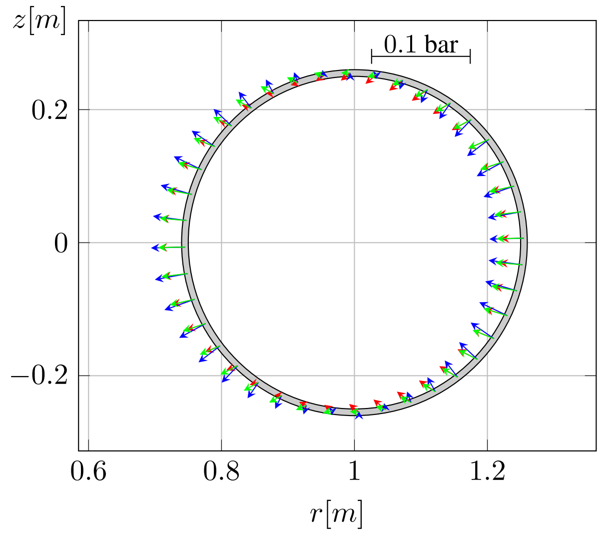

(a) with net poloidal current.

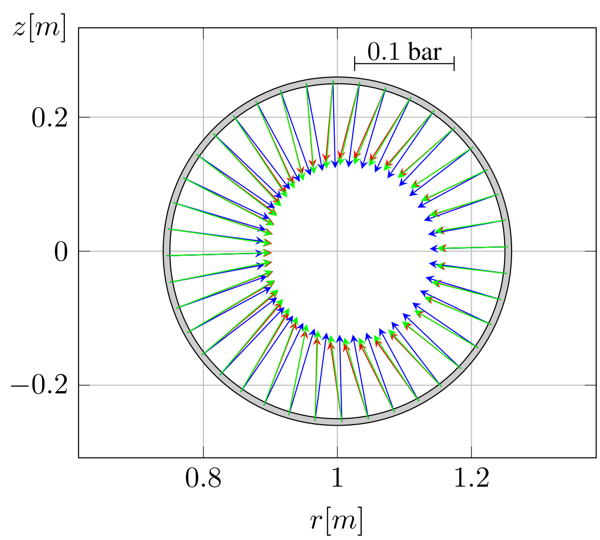

(b) without net poloidal current.

Figure 4.2: Analytical assuming $B_\rho = 0$ at the wall (blue), Analytical accounting for $B_\rho \neq 0$ (green), and Numerical (red) force density distribution during the CQ scenario described in table 4.2. Corresponding quantitative results are reported in table 4.4

4.2 Energy Balance

A second, and not less important, threat to the integrity of a tokamak during disruptions concerns heat loads on the structures surrounding the ionised gas. As hinted, in ITER, the major concern will be related to the dissipated energy during the TQ, and the eventual localized energy deposition during the CQ, due to the very likely formation of runaway electrons [44]. Nonetheless, the overall estimation of plasma losses remain an important task on itself, even during normal plasma operation. In general detailed plasma models [150, 151] are necessary to estimate the heat flux on plasma facing components, and thermal models are then necessary to finally estimate the thermal stress on each of them [152]. These approaches do not allow anyway for a simple and comprehensive understanding of the overall energy fluxes across the plasma domain, hence cross-validation between the different models. In [35] a critical review of the energy balance for a disruptive plasma was presented. Here we focus on some critical results of that study and slightly extend that discussion. In subsection 4.2.1 we will come back to the energy balance Equations describe in Section 1.5, finding the integral consequences of those relations. In subsection 4.2.2 we show how evolutionary equilibrium models, with relatively little physical details, can be employed to provide global estimates of plasma losses. This will require the hypothesis of small kinetic energy of the plasma, as compared to the thermal and magnetic energies. The same approach illustrated for the estimation of plasma losses can be used, the other way around, to test the validity of simulations against experimental estimates of radiated power and heat fluxes, although this is left as future work. In subsection 4.2.3 we comment in particular the role of the toroidal magnetic energy in the task, which turns out to be a sort of independent energy tank, not greatly involved in exchanges with other forms of energy. Finally in subsection 4.2.4 we will show by *CarMa0NL* simulations that the energy dissipated during the CQ is essentially related to the poloidal magnetic energy within the wall, and eventually the one drained from outside. This observation will motivate us to derive a simple analytical model for plasma losses as function of few plasma internal parameters. The model will clearly show that the amount of poloidal magnetic energy converted to heat depends on the overall CQ duration as compared to the time constant of the surrounding wall.

4.2.1 General considerations

In the framework of *Magneto-Hydro-Dynamics* the relevant energy reservoirs are generally retained to be the magnetic, barycentric kinetic and internal energy of the gas, as widely discussed in Section 1.5. For a certain volume V we define these overall energy tanks as

$$\begin{aligned} (a) \quad & W_m = \int_V \frac{B^2}{2\mu_0} \, \mathrm{d}\mathbf{r} \\ (b) \quad & K = \int_V \frac{1}{2} \rho v^2 \, \mathrm{d}\mathbf{r} \\ (c) \quad & U = \int_V \rho u \, \mathrm{d}\mathbf{r} \end{aligned} \tag{4.30}$$

In the general case where large currents at very low plasma densities occur, even the kinetic energy associated to the diffusion of electrons and ions respect to the *barycentric* fluid becomes important, *i.e.* the kinetic energy of electrons becomes an energy reservoir of comparable importance to kinetic energy of ions. This is certainly the case in presence of runaway electrons beams [145]. We observed also that it may be important to distinguish between the kinetic energy of neutrals and of the ionised part of the gas.

Here we do not include runaway electrons in the task, and more generally we exclude that the kinetic energy of diffusion can play a role. The internal energy remains defined by difference of the total energy and the electromagnetic and "barycentric" kinetic energy. The relevant separate energy balances were provided already in Equations (1.54), (1.56) and (1.61). Here we consider those balance Equations in their integral form, first taking an arbitrary volume $\mathbf{V}$, whose boundary eventually moves at the velocity $\mathbf{v_b}$,

$$
\begin{aligned}
&(a)\ \frac{\mathrm{d}W_m}{\mathrm{d}t} = -\int_{+\partial V} \frac{\mathbf{E}\times\mathbf{B}}{\mu_0}\,\mathrm{d}\mathbf{r} + \int_{+\partial V} \frac{B^2}{2\mu_0}\mathbf{v_b}\cdot\hat{\mathbf{n}}\,\mathrm{d}\mathbf{r} - \int_V \mathbf{E}\cdot\mathbf{i}\,\mathrm{d}\mathbf{r}\\
&(b)\ \frac{\mathrm{d}K}{\mathrm{d}t} = -\int_{+\partial V} \frac{1}{2}\rho v^2\left(\mathbf{v}-\mathbf{v_b}\right)\cdot\hat{\mathbf{n}}\,\mathrm{d}\mathbf{r} - \int_{+\partial V} p\mathbf{v}\cdot\hat{\mathbf{n}}\,\mathrm{d}\mathbf{r}\\
&\quad + \int_V p\nabla\cdot\mathbf{v}\,\mathrm{d}\mathbf{r} - \int_V \left(\mathbf{v}\times\mathbf{B}\right)\cdot\mathbf{i}\,\mathrm{d}\mathbf{r}\\
&(c)\ \frac{\mathrm{d}U}{\mathrm{d}t} = -\int_{+\partial V} \rho u\left(\mathbf{v}-\mathbf{v_b}\right)\cdot\hat{\mathbf{n}}\,\mathrm{d}\mathbf{r} - \int_{+\partial V} \mathbf{K_q}\cdot\hat{\mathbf{n}}\,\mathrm{d}\mathbf{r}\\
&\quad + \int_{V_{fw}} S_{rad}\,\mathrm{d}\mathbf{r}\\
&\quad - \int_V p\nabla\cdot\mathbf{v}\,\mathrm{d}\mathbf{r} + \int_V \left(\mathbf{E}+\mathbf{v}\times\mathbf{B}\right)\cdot\mathbf{i}\,\mathrm{d}\mathbf{r}
\end{aligned}
$$

In order to focus the attention on the key aspects we already considered a locally neutral gas, *i.e.* $q = 0$ and neglected viscous phenomena $\underline{\mathbf{P}} = p\underline{\mathbf{I}}$, considering our ionised gas as an ideal simple fluid, where $\rho u = (3/2)p$. Moreover we considered an eventual energy production term in Equation (4.31c), so to account for those energy drained outside via radiation or other phenomena not described within our thermodynamic frame. The possible volumes of interest to apply (4.31) are essentially:

- The volume occupied by the plasma, *i.e.* $V = V_{pl}$. In this case the velocity of the boundary exactly equals the fluid velocity, and we come back to a Lagrangian picture, with the null convective terms in (4.31b)-(4.31c). On the other hand, since the electromagnetic energy is not linked to the plasma mass, In Equation (4.31a) the term $\int_{+\partial V_{pl}} \frac{B^2}{2\mu_0} v_n\,\mathrm{d}\mathbf{r}$ essentially accounts for the magnetic energy incorporated in the plasma volume due to its motion.

- The volume where the plasma can live, *i.e.* the volume enclosed by the first wall surface $V = V_{fw}$. In this case certainly $\mathbf{v_b} = \mathbf{0}$, as the first wall surface is not allowed to move.

Since we are interested to take the perspective of structures, we choose the second option and consider $V = V_{fw}$. As discussed, we admit that the wall cannot absorb or emit mass towards the plasma side, which leads to consider $\rho\mathbf{v}\cdot\hat{\mathbf{n}} = 0$. Hence, the energy balance Equations take the simplified form

$$\begin{aligned}
(a)\ \frac{\mathrm{d}W_m}{\mathrm{d}t} &= -\int_{+\partial V}\frac{\mathbf{E}\times\mathbf{B}}{\mu_0}\cdot\hat{\mathbf{n}}\,\mathrm{d}\mathbf{r}-\int_V \mathbf{E}\cdot\mathbf{i}\,\mathrm{d}\mathbf{r}\\
(b)\ \frac{\mathrm{d}K}{\mathrm{d}t} &= +\int_V p\nabla\cdot\mathbf{v}\,\mathrm{d}\mathbf{r}-\int_V(\mathbf{v}\times\mathbf{B})\cdot\mathbf{i}\,\mathrm{d}\mathbf{r}\\
(c)\ \frac{\mathrm{d}U}{\mathrm{d}t} &= -\int_{+\partial V}\mathbf{K_q}+\rho u\mathbf{v}\cdot\hat{\mathbf{n}}\,\mathrm{d}\mathbf{r}+\int_{V_{fw}}S_{rad}\,\mathrm{d}\mathbf{r}\\
&\quad-\int_V p\nabla\cdot\mathbf{v}\,\mathrm{d}\mathbf{r}+\int_V(\mathbf{E}+\mathbf{v}\times\mathbf{B})\cdot\mathbf{i}\,\mathrm{d}\mathbf{r}
\end{aligned}\tag{4.31}$$

In this context the local energy exchange terms are clear: the electromagnetic energy converted to other forms is given by the term $\mathbf{E}\cdot\mathbf{i}$. The portion $(\mathbf{E}+\mathbf{v}\times\mathbf{B})\cdot\mathbf{i}$ is the electromagnetic energy spent in order to keep the electric current flowing besides collisions and dissipative phenomena within the fluid element. Indeed the electric field felt by a small volume element in its motion at the fluid velocity equals $\mathbf{E}+\mathbf{v}\times\mathbf{B}$. Notice as this interpretation does not need any assumption on the actual constitutive relation for the electric current density. The remainder portion $(\mathbf{i}\times\mathbf{B})\cdot\mathbf{v}$ is spent to accelerate the fluid itself, *i.e.* reflects into a kinetic energy variation. Even in absence of viscous phenomena related to plasma motion, the deformation work can still provide an energy exchange mechanism between kinetic and internal energy, as for any classical ideal gas,

$$P_{\rho u,w_{kin}}=\int_{V_{pl}}p\nabla\cdot\mathbf{v}\,\mathrm{d}\mathbf{r}\tag{4.32}$$

All the other terms in the energy balance equations (4.31) are related to energy fluxes across the boundary of the domain. In particular we define the flux of the Poynting vector:

$$\Phi_S=\int_{+\partial V_{fw}}\frac{\mathbf{E}\times\mathbf{B}}{\mu_0}\cdot\hat{\mathbf{n}}\,\mathrm{d}\mathbf{r}\tag{4.33}$$

Moreover, we lump the heat flux and the eventual production/absorption terms of internal energy related to radiative phenomena in a single term which we define as *plasma power losses*,

$$\frac{\mathrm{d}Q}{\mathrm{d}t}=\int_{+\partial V_{fw}}(\mathbf{K_q}+\rho u\mathbf{v})\cdot\hat{\mathbf{n}}\,\mathrm{d}\mathbf{r}+\int_{V_{fw}}S_{rad}\,\mathrm{d}\mathbf{r}\tag{4.34}$$

Finally, the *plasma power losses* can be expressed as

$$\frac{\mathrm{d}Q}{\mathrm{d}t} = -\Phi_S - \frac{\mathrm{d}W_m}{\mathrm{d}t} - \frac{\mathrm{d}K}{\mathrm{d}t} - \frac{\mathrm{d}U}{\mathrm{d}t} \tag{4.35}$$

4.2.2 Predicting plasma losses

An important assumption can be now introduced, concerning the relative weight of the various energy tanks. We may consider the typical tokamak plasma parameters reported in table 4.5, to provide some simple estimates.

J	R_{pl}	R_{pl}/b	n	T
$2\,MA$	$3\,m$	3	$10^{19}\,m^{-3}$	$17\,10^6\,K$

Table 4.5: Typical tokamak experiments plasma parameters.

For the parameters in Table 4.5, the reference poloidal magnetic field can be considered to be $B_J = \mu_0 J/2\pi b \simeq 0.4\;T$. Moreover the atomic mass of deuterium is $m_i = 3.34 \cdot 10^{-27} kg$, leading to an Alvén velocity $\nu_A \simeq 2\;km/ms$. This is the velocity of propagation for small perturbations within the plasma. However, as widely discussed in Section 3.1, when the reaction force exerted by the surrounding passive conductors on the plasma is strong enough, the macroscopic plasma motion will generally happen on the electromagnetic time scale of external conductors, which is generally in the order of tens of ms, even larger for ITER. Motion at the Alfvénic speed will be limited to local oscillations, not contributing significantly to the kinetic reservoir. Using parameters in table 4.5, and assuming the macroscopic plasma motion is indeed on the electromagnetic time-scale, *e.g.* $v \leq 1\;km/s$, the resulting kinetic energy density per unit volume is about $\lessapprox 16\;mJ/m^3$. Correspondingly the magnetic energy density is about $570\;kJ/m^3$, with about six orders of magnitude of difference. Also the thermal energy density in this example is about $3.5\;kJ/m^3$. Essentially, if we exclude that the magnetic energy can be suddenly converted to kinetic, a fairly reasonable in presence of external conductors, the kinetic energy tank is irrelevant to the task, and we can set $K = 0$.

If we neglect the kinetic energy completely, we contextually admit that all of the electromagnetic power density which was converting electromagnetic to kinetic energy, $\mathbf{i} \times \mathbf{B} \cdot \mathbf{v}$, is now instantaneously converted to deformation power density $p\nabla \cdot \mathbf{v}$. Hence all of the $\mathbf{E} \cdot \mathbf{i}$ power density in (4.31a) becomes an exchange term between magnetic and internal energy. From the energy balance Equations (4.31), in the assumption of negligible kinetic energy, the plasma power losses finally take the form

$$\frac{\mathrm{d}Q}{\mathrm{d}t} = -\Phi_S - \frac{\mathrm{d}W_m}{\mathrm{d}t} - \frac{\mathrm{d}U}{\mathrm{d}t} \tag{4.36}$$

All of the terms at the *r.h.s.* of (4.36) are readily computable as post-processed quantities of evolutionary-equilibrium simulations. In the case of *CarMa0NL*, the magnetic field is known in the MHD computational domain up to the Coupling Surface. Hence, the flux of Poynting vector (4.33) and the magnetic energy inside the first wall (4.30a) are simple integrals of known quantities. Moreover, we assumed the plasma to be a classical ideal gas, hence the energy per unit volume is directly related to the kinetic pressure $\rho u = (3/2)p$. The distribution of kinetic pressure within the plasma can be reconstructed from (3.114), since the poloidal flux map $\psi(r, z)$ is computed at each time instant, together with ψ_a, ψ_b and λ, while β_0, $\alpha_{m,p}$, $\alpha_{n,p}$ are input parameters to the model.

4.2.3 Toroidal magnetic energy

A great simplification of the actual study of the energy flows during a transient is provided by the different role poloidal and toroidal magnetic fields play in tokamak experiments. It is convenient to define separately the poloidal and toroidal magnetic energies:

$$\begin{aligned}(a)\; W_{m,pol} &= \int_{V_{fw}} \frac{B_{pol}^2}{2\mu_0}\,\mathrm{d}\mathbf{r} \\ (b)\; W_{m,tor} &= \int_{V_{fw}} \frac{B_{\varphi}^2}{2\mu_0}\,\mathrm{d}\mathbf{r}\end{aligned} \tag{4.37}$$

The flow of poloidal and toroidal magnetic energy are defined correspondingly:

$$\begin{aligned}(a)\; \Phi_{S,pol} &= \int_{+\partial V_{fw}} \frac{\mathbf{E}_{\varphi} \times \mathbf{B_{pol}}}{\mu_0} \cdot \hat{\mathbf{n}}\,\mathrm{d}\mathbf{r} \\ (b)\; \Phi_{S,tor} &= \int_{+\partial V_{fw}} \frac{\mathbf{E_{pol}} \times \mathbf{B}_{\varphi}}{\mu_0} \cdot \hat{\mathbf{n}}\,\mathrm{d}\mathbf{r}\end{aligned} \tag{4.38}$$

Let us consider an axisymmetric first wall. Moreover, we consider an axisymmetric case, where

$$B_\varphi = \frac{\mu_0 I_{pol}(r,z)}{2\pi r} \tag{4.39}$$

If there are no halo currents crossing the first wall surface the flux of toroidal magnetic energy gets the simple circuit form:

$$\Phi_{S,tor} = -I_{pol,ext}\frac{\mathrm{d}\Psi_{tor,fw}}{\mathrm{d}t} \tag{4.40}$$

where $\Psi_{tor,fw}$ is the toroidal flux across the first wall poloidal cross section and $I_{pol,ext}$ is the net poloidal current circulating in external conductors, both active coils and passive structures. Formula (4.40) complicates slightly in presence of halo currents, where additional terms related to the halo current injection and to the voltage difference between points of the first wall would appear. We proceed our study in the hypothesis of absence of halo currents, and we find in particular that

$$\frac{\mathrm{d}W_{m,tor}}{\mathrm{d}t} + \Phi_{S,tor} = \frac{\mathrm{d}}{\mathrm{d}t}\left[\frac{1}{2}\frac{\mu_0}{2\pi}\int_{S_{fw}} \frac{I_{pol}^2(r,z) - 2I_{pol,ext}\cdot I_{pol}(r,z)}{r}\,\mathrm{d}\mathbf{r}\right] \tag{4.41}$$

In tokamak devices the net poloidal current circulating in TF coils overwhelms in general the net poloidal plasma current. As the net poloidal current in passive structures is eventually induced by plasma toroidal flux variations, also the net poloidal current in the wall is in general far smaller than the net current in TF coils. Hence, we are safely in the assumption:

$$I_{pol,act} \gg I_{pol,w},\ I_{pol,pl}(r,z) \quad \forall(r,z)\in V_{pl} \tag{4.42}$$

The net poloidal current in TF coils is generally kept constant, even during fast plasma transients. Hence approximation (4.42) transforms (4.41) into:

$$\frac{\mathrm{d}W_{m,tor}}{\mathrm{d}t} + \Phi_{S,tor} \simeq 0 \tag{4.43}$$

This means that the toroidal magnetic energy represent an energy tank on its own, which does not transform to other forms, hence allowing a great simplification of our energy balance (4.36):

$$\frac{\mathrm{d}Q}{\mathrm{d}t} = -\Phi_{S,pol} - \frac{\mathrm{d}W_{m,pol}}{\mathrm{d}t} - \frac{\mathrm{d}U}{\mathrm{d}t} \tag{4.44}$$

The identification of plasma losses starts to become clear. The amount of losses is given by some contributions:

- drop of the internal energy
- drop of the poloidal magnetic energy
- influx of poloidal magnetic energy

Moreover, since $I_{pol,act} \gg I_{pol,w}$, we can consider in general the plasma toroidal flux variations as a forcing term for the induced voltages in structures, without care about the reciprocal interaction between toroidal flux and net poloidal current in the wall. This is indeed one of the assumptions adopted in the *CarMa0NL* evolutionary equilibrium model. Let us clarify this point, the toroidal flux due to plasma currents should be calculated in few steps:

- The relation $I_{pol}^2 = I_{pol}^2(\psi)$ is calculated integrating the input function $\mathrm{d}I_{pol}^2/\,\mathrm{d}\psi$ with the initial condition $I_{pol}^2|_{\partial V_{pl}} = (I_{pol,act} + I_{pol,w})^2$
- We consider the square root of such quantity $I_{pol}(\psi) = \sqrt{I_{pol}^2(\psi)}$
- The plasma poloidal current is obtained eliminating the contribution from external conductors, $I_{pol,pl}(\psi) = I_{pol}(\psi) - I_{pol,act} - I_{pol,w}$
- Finally the plasma-produced toroidal field is known and we are ready to compute its flux across the poloidal cross section of the plasma

Hence, it is quite clear that the actual value of plasma-produced toroidal flux depends on the net poloidal current $I_{pol,w}$ in principle. Anyway, since the active poloidal current is far greater than the net poloidal current in the wall, we can take

$$I_{pol,pl}(\psi) \simeq \sqrt{I_{pol,act}^2 + \int_{\psi_B}^{\psi} \frac{\mathrm{d}I_{pol}^2}{\mathrm{d}\psi}\,\mathrm{d}\psi} - I_{pol,act} \tag{4.45}$$

In this approximation, the plasma-produced toroidal flux is independent of the net poloidal current induced in the wall, and the toroidal flux time variations are essentially a forcing term in the study of eddy currents. This is the assumption adopted within the *CarMa0NL* model.

$J[MA]$	β_p	ℓ_i	Δ_{iw} [cm]	$\Delta_b[cm]$
1.5	0.586	1.125	1.48	0.25

Table 4.6: Reference MHD Equilibrium for circular high-aspect-ratio tokamak.

4.2.4 A test case

In this subsection we apply previous considerations to the estimation of plasma losses in a disruptive high-aspect-ratio tokamak device of circular cross section, using the evolutionary equilibrium model *CarMa0NL*. The initial MHD equilibrium configuration for this test case is synthetically described in table 4.6. The tokamak geometry is the same as described in previous Section, see table 4.1.

We simulate the disruption as a *Thermal Quench* followed by a *Current Quench*. The TQ is simulated bringing the the poloidal beta to zero in 0.1 ms. After that a CQ is forced with a decay rate of 1 MA/ms. We will show the results obtained for a slower CQ at 100 kA/ms later in the discussion. The actual choice of the current density profile parameters, the αs in our parametrization (3.114), determines a small drop in the internal inductance during the TQ, while this keeps to be constant during the simulation of the CQ. The excursion of the internal inductance value is within few percent points. In the considered study case hence we do not explicitly consider large internal inductance variations, which may be caused for example by the onset of runaway electron beams (e.g. $\Delta\ell_i \simeq 3\ell_i(t_0)$ [145]). An overview of the evolution of main parameters is provided in Figure 4.3.

We show the essential results of our energy losses estimation in Figure 4.4, where the various terms involved in the power balance (4.44) are integrated in time, and variations of the various energy terms are portrayed since the initial disruption time instant. Various conclusions can be drawn from here. First, during the TQ the poloidal magnetic energy does not experience large variations and contextually the poloidal magnetic energy influx is very small. On the other hand the plasma-produced toroidal flux undergoes a sudden variation which modifies eventually the toroidal magnetic energy within the first wall. This variation is however fully compensated by the Poynting flux contribution $\Phi_{S,tor}$, as commented in (4.43). Hence during this preliminary phase of the disruption the plasma loss is solely related to variations of the internal energy,

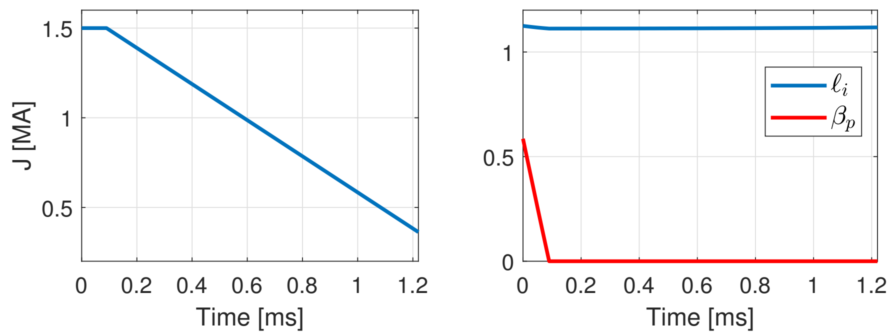

Figure 4.3: Evolution of (a) the net plasma toroidal current, and (b) the poloidal beta β_p and internal inductance ℓ_i

$$\Delta Q_{TQ} \simeq -\Delta U \tag{4.46}$$

Further, during the *Current Quench*, by assumption all of the internal energy is already lost. The plasma energy losses can be estimated as

$$\Delta Q_{CQ} \simeq -\Delta W_{m,pol} - \int_{t_0}^{t} \Phi_{S,pol}(\tau)\,\mathrm{d}\tau \tag{4.47}$$

The plasma losses during the CQ depends solely on the consumption of poloidal magnetic energy. This is both the energy contained within the first wall, and the poloidal magnetic energy coming from outside due to the corresponding Poynting vector influx.

In order to be confident that the toroidal magnetic energy is indeed not important in the task in a wide parameter range, we compare similar simulations where we force a different value for the toroidal magnetic field enforced by active coils. The maximum difference between toroidal magnetic energy variations and toroidal magnetic energy outflow should be expected during the TQ, since the plasma poloidal currents change considerably during this transient, as demonstrated by the pressure balance (3.101). Hence we define the l.h.s. of (4.43) as "uncompensated" toroidal magnetic energy and evaluate the relative weight of this term as compared to the overall toroidal magnetic energy variation within the first wall during the TQ in Table 4.7. We see that toroidal magnetic energy variation is almost perfectly compensated for very high values of the externally applied toroidal magnetic field. For lower values, the actual exchange of toroidal magnetic energy with thermal energy can be appreciable

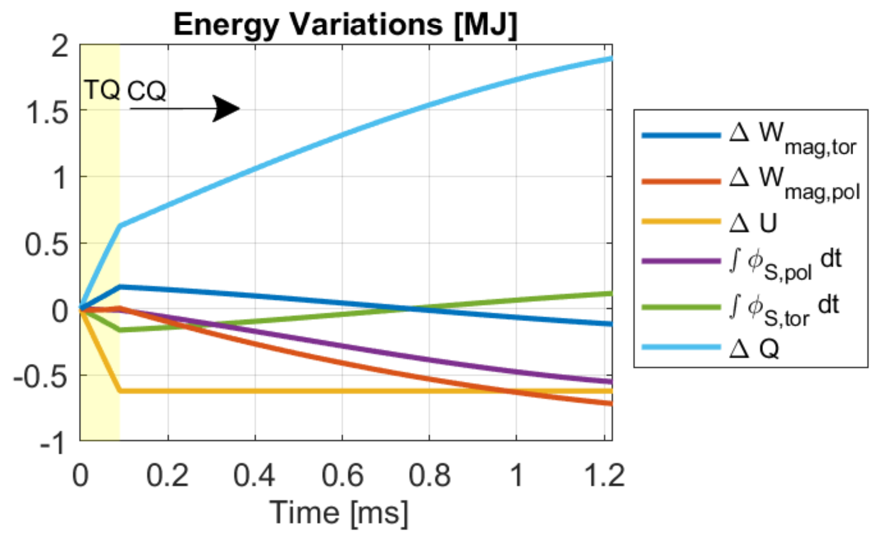

Figure 4.4: Main contributions to the energy balance (4.44) for the study case under exam, described in Figure 4.3 and table 4.6.

$B_{\varphi,act}\|_{r=R_w}$ $[T]$	14.6	4.87	2.00
$\frac{\Delta U_{tor}(t_{TQ},t_{CQ})}{\Delta W_{m,tor}(t_{TQ},t_{CQ})}$ $[\%]$	2.36	17.0	50.0

Table 4.7: "Uncompensated" toroidal magnetic energy during the TQ, for different values of the applied toroidal field.

in the TQ phase, we illustrate the correspondingly different plasma losses in Figure 4.5. You can see that in the case of relatively low applied toroidal magnetic field some of the internal energy is transferred to the toroidal magnetic energy reservoir during the TQ and released in later phases of the disruption. Nonetheless the effect of the poloidal magnetic energy consumption remain dominant on the losses.

4.2.5 The circular high-aspect ratio analytical model

As a result of previous subsection we found that the actual plasma losses during the *Current Quench* are related to the poloidal magnetic energy variation within the first wall and the corresponding influx $\Phi_{S,pol}$. In this subsection,

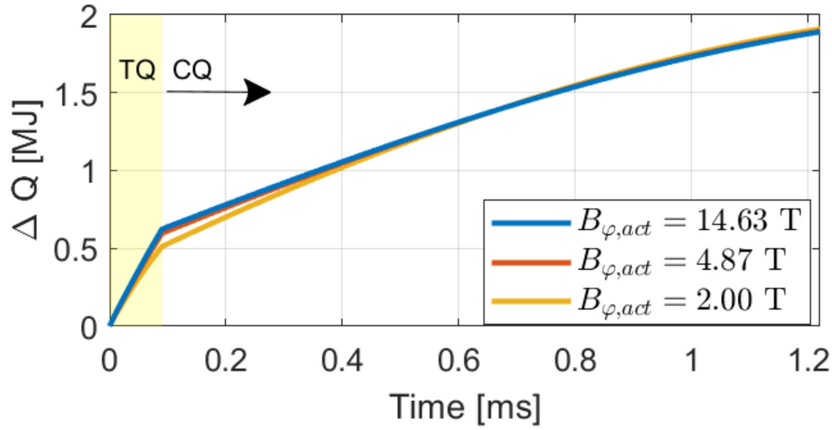

Figure 4.5: Estimation of plasma losses for different toroidal field enforced by active coils at $r = R_w$.

we provide some simple formulas for the estimation of *plasma power losses* during the CQ of our circular high-aspect-ratio tokamak. We want to find the actual dependence of dQ/dt (4.44) on global parameters, as the net toroidal current J, the poloidal beta β_p and the internal inductance ℓ_i, besides of geometrical parameters like the plasma minor radius b and shift Δ_b.

In order to do this we need to estimate the poloidal magnetic energy stored in the plasma, in the plasma-first wall gap and the flux of poloidal magnetic energy through the first wall. It is worth noticing immediately that in the cylindrical limit a shift Δ_b of the plasma column correspond to a shift of the poloidal flux map in general, hence corrections in the poloidal magnetic energy stored within the first wall and in the poloidal magnetic energy flux will appear as corrections of order i$O(\Delta_b/b_{fw})^2$. First order corrections in the plasma shift, will hence appear exclusively also as toroidal corrections to the cylindrical-limit case. In general corrections of order $o(\Delta_b/R_w)$ may be accounted in the modelling task, but they do not add great information [35]. Hence, in our derivation we will consider exclusively first order toroidal corrections ($o(b_{fw}/R_w)$) and second order cylindrical corrections in the plasma shift ($o(\Delta_b/b_{fw})^2$). In this Section, we provide the general formulas and we can use to evaluate the poloidal magnetic energy in the plasma-first wall gap and the corresponding Poynting vector flux across the first wall.

Poloidal Energy in the plasma

The poloidal magnetic energy within the plasma volume can be estimated via the internal inductance definition:

$$W_{m,pol,pl} = \frac{1}{2}\left[\mu_0 R_w \frac{\ell_i}{2}\left(1+\frac{\Delta_b}{R_w}\right)\right] J^2 \to \frac{1}{2}\mu_0 R_w \frac{\ell_i}{2} J^2 \tag{4.48}$$

Here we adopted the standard definition of internal inductance provided in (3.103), where the internal inductance is the average poloidal magnetic energy in the cross-section normalized by $B_J^2/2\mu_0$. Hence the poloidal magnetic energy in the plasma is completely determined via the plasma current J and the internal inductance parameter ℓ_i. As hinted, we discard any correction of order Δ_b/R_w as we retain it of higher order.

Poloidal Energy in the gap

Simple manipulation of Maxwell Equations for our axisymmetric case allows to write:

$$W_{m,pol,gap} = \frac{1}{2\mu_0} 2\pi \left[\psi_b \int_{\Gamma_{pl}} \mathbf{B_p} \cdot \hat{\mathbf{i}}_\alpha \, \mathrm{d}\ell - \int_{\Gamma_w} \mathbf{B_p} \cdot \hat{\mathbf{i}}_\mathbf{u} \, \mathrm{d}\ell\right] \tag{4.49}$$

where we indicated by ψ_b the poloidal flux at the boundary. Thanks to the expansions (3.80) for the poloidal flux and (3.84) for the poloidal magnetic flux density we can immediately simplify (4.49) to

$$\begin{aligned} W_{m,pol,gap} = & \frac{1}{2} J 2\pi \left[\psi_b - \psi_0(b_{fw})\right] \\ & + \frac{1}{2\mu_0} 2\pi \cdot \pi b_{fw} \cdot \left[\psi_1(b_{fw}) \cdot B_{u,1}(b_{fw}) + \psi_2(b_{fw}) \cdot B_{u,2}(b_{fw})\right] \end{aligned} \tag{4.50}$$

The poloidal flux at the boundary can be estimated directly via the equilibrium considerations which lead us to (3.71). In particular the homogeneous flux at the plasma boundary is both due to plasma currents and the external currents. correctly expanding R_{pl} in terms of the Shafranov shift Δ_b we get

$$\begin{aligned} \psi_b = \psi_{0,a} + \tilde{L}_w J_w + & \frac{\mu_0 R_w}{2\pi}\left[\ln\frac{8R_w}{b} - 2\right] J \\ & + \frac{\Delta_b}{2R_w}\frac{\mu_0 R_w}{2\pi}\left[\ln\frac{8R_w}{b} - \Lambda - \frac{3}{2}\right] J \end{aligned} \tag{4.51}$$

Notice the factor $1/2\pi$ in the inductance-like terms is necessary since by convention we refer to poloidal fluxes per radian (*i.e.* $\psi = rA_\varphi$). Plugging now our definitions (3.81), (3.87) and (4.51) into our expression for the poloidal energy in the gap (4.50), discarding second order toroidal corrections and corrections of order Δ_b/R_w, we get finally:

$$W_{m,pol,gap} = \frac{1}{2}\left[\mu_0 R_w \ln\frac{b_{fw}}{b} - \frac{\mu_0 R_w}{2}\left(\frac{\Delta_b}{b_{fw}}\right)^2\right] J^2 \tag{4.52}$$

Considering at the same time the plasma and plasma-gap energy, we have the poloidal magnetic energy in the plasma-wall gap :

$$W_{m,pol,fw} = \frac{1}{2}\left[L_{pl,fwi} - L_{shift}\left(\frac{\Delta_b}{b_{fw}}\right)^2\right] J^2 \tag{4.53}$$

where we defined the “plasma inductance internal to the first wall” and the “plasma shift inductance” terms respectively as:

$$\begin{aligned} &(a) \quad L_{pl,fwi} = \mu_0 R_w \left[\frac{\ell_i}{2} + \ln\frac{b_{fw}}{b}\right] \\ &(b) \quad L_{shift} = \mu_0 R_w \frac{1}{2} \end{aligned} \tag{4.54}$$

Poloidal Poynting vector flux

We defined the poloidal magnetic energy flux in (4.38). There we may express, thanks to Faraday’s law for our axisymmetric problem $rE_\varphi = -\frac{\mathrm{d}\psi}{\mathrm{d}t}$. Moreover the tangential component to the first wall is such that $\hat{\mathbf{i}}_\mathbf{u} = \hat{\mathbf{n}} \times \hat{\mathbf{i}}_\varphi$. The flux of the poloidal magnetic energy across the first wall hence simplifies to

$$\Phi_{S,pol} = \frac{2\pi}{\mu_0} b_{fw} \int_0^{2\pi} B_u(b_{fw}, u) \frac{\mathrm{d}\psi(b_{fw}, u)}{\mathrm{d}t}\,\mathrm{d}u \tag{4.55}$$

which leads immediately to consider the separate contributions to the overall poloidal energy flux:

$$\Phi_{S,pol,fw} = \frac{(2\pi)^2}{\mu_0} b_{fw} \left\{ B_{u,0}\frac{\mathrm{d}\psi_0}{\mathrm{d}t} + \frac{1}{2}B_{u,1}\frac{\mathrm{d}\psi_1}{\mathrm{d}t}\right\} \tag{4.56}$$

Using again definitions (3.81) and (3.87) for the poloidal flux and magnetic field in the plasma-wall gap, and discarding higher order corrections, we get the Poynting vector flux contribution

$$\Phi_{S,pol,fw} = JL_w \frac{\mathrm{d}J_w}{\mathrm{d}t} + \frac{1}{2} L_{pl,fwe} \frac{\mathrm{d}J^2}{\mathrm{d}t} + \frac{1}{2} L_{shift} \frac{\mathrm{d}}{\mathrm{d}t} \left(J \frac{\Delta_b}{b_{fw}} \right)^2 \tag{4.57}$$

where the plasma shift inductance term was given in (4.54b) and we defined the wall inductance and the "plasma inductance external to the first wall" respectively as

$$\begin{aligned} &(a) \quad L_w = \mu_0 R_w \left[\ln \frac{8R_w}{b_w} - 2 \right] \\ &(b) \quad L_{pl,fwe} = \mu_0 R_w \left[\ln \frac{8R_w}{b_{fw}} - 2 \right] \end{aligned} \tag{4.58}$$

Dissipated Heat and Time Constants

The dissipated energy during the CQ (4.47), thanks to the expressions (4.53) for the poloidal magnetic energy and (4.57) for the Poynting vector flux, can be finally provided in terms of plasma global parameters:

$$\frac{\mathrm{d}Q_{CQ}}{\mathrm{d}t} = -\frac{1}{2} \frac{\mathrm{d}L_{pl} J^2}{\mathrm{d}t} - L_w J \frac{\mathrm{d}J_w}{\mathrm{d}t} \tag{4.59}$$

where we defined the *plasma inductance*

$$L_{pl} = \mu_0 R_w \left[\frac{\ell_i}{2} + \ln \frac{8R_w}{b} - 2 \right] \tag{4.60}$$

Notice that the cylindrical plasma-shift corrections in $(\Delta_b/b_{fw})^2$, which we evaluated both for the poloidal energy and for the Poynting vector flux, cancel each other and do not enter in the estimation of plasma losses. Two important limits of (4.59) can be identified based on the overall CQ duration as compared to the electromagnetic time constant of the wall. Consider indeed the evolution Equation for the net current in the wall (3.69a).In the limit of fast CQ, *i.e.* $\Delta t_{CQ} \ll \tau_{0,w}$, a variation of the net plasma current is immediately compensated by a variation of the wall net toroidal current, so to preserve the poloidal flux outside. Hence in this case $\mathrm{d}J_w/\mathrm{d}t = -\mathrm{d}J/\mathrm{d}t$ and the dissipated heat takes the very simple form

$$\frac{\mathrm{d}Q_{CQ}^{fast}}{\mathrm{d}t} = -\frac{\mathrm{d}\left(L_{pl,wi}J^2\right)}{\mathrm{d}t} \tag{4.61}$$

where we defined the *plasma inductance internal to the wall*

$$L_{pl,wi} = \mu_0 R_w \left[\frac{\ell_i}{2} + \ln\frac{b_w}{b}\right] \tag{4.62}$$

Equation (4.61) is susceptible of a very simple interpretation. Whenever the plasma CQ is fast compared to the electromagnetic time constants there is not enough time for the poloidal magnetic energy to penetrate the wall. Hence the poloidal magnetic energy available for conversion to heat is solely the one contained within the first wall itself. In particular all of the consumed poloidal magnetic energy inside the wall is necessarily dissipated towards the external world by other forms than electromagnetic. Indeed, in the ideal wall approximation, a finite $\Phi_{S,pol}$ at the first wall is solely associated to a variation of the poloidal magnetic energy in the first wall - vacuum vessel gap.

Let us examine the diametrically opposite case, *i.e.* the no-wall limit. In this case the wall current ideally does not vary, always being null and we can set $\mathrm{d}J_w/\,\mathrm{d}t = 0$ in Equation (4.59), leading to

$$\frac{\mathrm{d}Q_{CQ}^{slow}}{\mathrm{d}t} = -\frac{1}{2}\frac{\mathrm{d}\left(L_{pl}J^2\right)}{\mathrm{d}t} \tag{4.63}$$

Virtually all of the poloidal magnetic energy inside the wall and all of the poloidal mangetic energy outside the wall (excluded the magnetic energy of PF coils) can be converted to heat! This limit finds practical application in case the CQ is much longer than the electromagnetic time constants $\Delta t_{CQ} \gg \tau_{0,w}$. In particular, consider a linear decay for the plasma net current, so that $\mathrm{d}J/\,\mathrm{d}t = \mathrm{const}$. After few electromagnetic time constants, the induced wall current will reach its steady value $J_w = \tau_{0,w}\,\mathrm{d}J/\,\mathrm{d}t$, and we can take indeed $\mathrm{d}J_w/\,\mathrm{d}t \simeq 0$.

During the CQ the plasma behaves exactly as a heater, converting poloidal magnetic energy into dissipated heat. The actual amount of magnetic energy available for conversion is regulated by the actual duration of the CQ as compared to the wall electromagnetic time constant. Besides more energy is available for conversion heat during a slow CQ, it is nonetheless true that a slower dissipation of a higher quantitative of energy can lead of course to power losses. In this respect what remains important is the power dissipation. Moreover the faster the CQ, the more severe will be the magnetic pressure

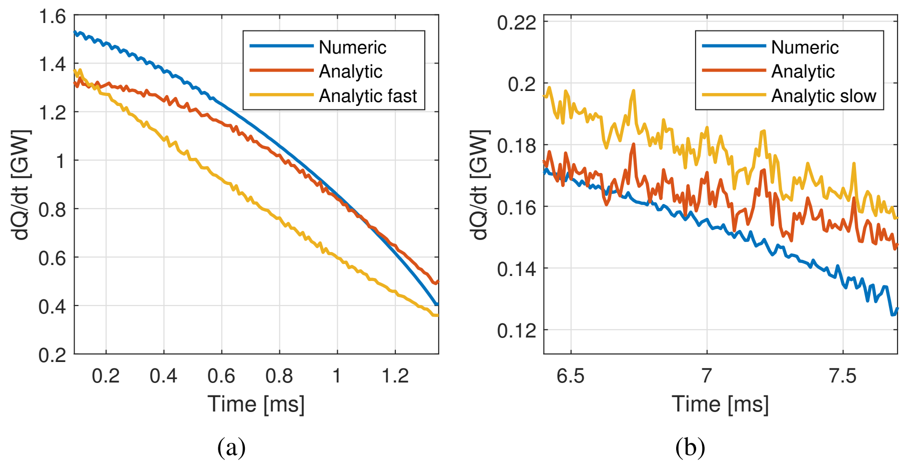

Figure 4.6: Plasma power losses during (a) a fast CQ of 1 MA/ms and (b) a slow CQ of 100 kA/ms.

differences across wall structures during the CQ, hence the greater will be the mechanical stress. These opposite trends make the design of tokamak experiments particularly delicate.

The time constant for our study case is about $\tau_{0,w} \simeq 3.5\, ms$. A verification of the "exact" analytical formula for the dissipated heat during the CQ (4.59), together with its fast CQ (4.61) and slow CQ (4.63) limits, is provided in Figure 4.6. In the left panel, we consider the relatively fast CQ of 1 MA/ms already discussed. It is evident as in the first time instants of CQ the "fast" approximation essentially matches the "exact" analytical formula, since the magnetic field has still to diffuse across the wall. Results for a slower CQ of $100kA/ms$ are shown in the right panel. In this case, we notice a good match after the net wall current is close to its steady state value, *i.e.* since a time instant $\sim 2\tau_{0,w}$ after the start of the CQ. The noise of such power losses estimations is related to the computation of the time derivatives via finite differences during the post-processing. Nonetheless, we prefer here to provide power rather than energy estimations to get rid of the cumulative error we would integrate at each time step.

4.3 JET Vertical Displacement

The Joint European Torus (JET), with its major radius $R_w \simeq 2.96\ m$, is the largest tokamak device operated up to now [1]. IN JET currents up to 3 MA and toroidal fields up to 3.45 T were achieved. With these incredibly large currents and magnetic fields, JET represents certainly the main reference for extrapolations to ITER [153]. In 2011, after some years of shut-down, the first wall materials were even replaced to install an "ITER-like" wall and study the fundamental physics interaction of the Beryllium and Tungsten divertor with the hot plasma [154, 155]. The only similarly-sized tokamak, with even larger plasma volume, is JT60-SA, which is presently in its commissioning phase and hopefully will be soon operated [156].

In subsection 4.3.1 we explain how to deal with JET magnetic iron core within an evolutionary equilibrium simulation, especially with focus on the particular case of deep magnetic saturation of the iron core. There, we also show standard procedures to set up the initial conditions for a *CarMa0NL* simulation, which requires the definition of the initial poloidal flux map in the plasma domain. In subsection 4.3.2 we describe some of the magnetic diagnostics installed, and how we set up comparison of their measurements with *CarMa0NL* simulations. Finally in subsection 4.3.3 we describe a real JET experiment and we analyse it by a CarMa0NL simulation.

4.3.1 The magnetic iron core

In order to provide sufficient flux excursion to guarantee long-lasting experiments, JET includes a large iron core [157] which slightly complicates the set up of an evolutionary equilibrium simulation. Indeed, in principle one has to couple the non-linear model of the magnetic core to the Evolutionary Equilibrium model, which is of course far from trivial.

Nonetheless, when steady state MHD Equilibrium conditions are achieved, we may assume that the iron core is deeply saturated. In the following we will assume that even during the fast plasma current transient the iron core is still saturated. In this assumption we may regard the magnetic core as a fixed source of poloidal flux for what concerns the plasma MHD Equilibrium problem. Moreover there will be no induced voltages on structures due to variations of the magnetization. This is clearly an arbitrary assumption, especially for later phases of the disruption, and future work for a more accurate

[1] and the most long-lived, considering the first plasma at JET was achieved in 1983.

description of the iron core is recommended.

Contextually to the identification of an initial flux map to initialize the simulation, we need to identify the actual poloidal flux produced at the *Coupling Surface* both by the active coil currents $\hat{\psi}_a$ and by the magnetization in the iron core $\hat{\psi}_m$. These poloidal fluxes will be retained constant throughout the whole simulation. In this respect the boundary conditions for the free-boundary MHD Equilibrium problem at each time step will be given by

$$\psi\big|_{\partial V_{CS}} = \hat{\psi}_a + \hat{\psi}_m + \hat{\psi}_I + \hat{\psi}_{pl} \tag{4.64}$$

where $\hat{\psi}_a$ and $\hat{\psi}_m$ are calculated once for all at the initial MHD equilibrium time instant. If variations of the active currents needs to be accounted, these can conveniently included as current variations of the currents in the coils implemented in the $3D$ description of external conductors.

We stress as the initial MHD Equilibrium flux map should be calculated correctly considering the presence of the iron core. In order to find such a flux map we use the CREATE-L tool [115], which include a 2D Equivalent model of the iron-core [158, 159]. The inherent advantage in using CREATE-L in this pre-processing stage is that it allows to use exactly the same discretization of the MHD computational domain within the Coupling Surface Ω_{in}. The initial poloidal flux map is found through an iterative Newton-Raphson scheme, imposing exactly the poloidal flux due to active coils via standard axisymmetric Green functions and self-consistently determining the poloidal flux due to plasma currents and iron core magnetization at each Newton iteration. Starting from a proper qualified guess[2], the solution is generally found after few Newton iterations. Clearly, we find a solution only if the input parameters provided for the set up of the toroidal plasma current profile, *i.e.* J, β_0, and the α-type parameters, can reproduce indeed a realistic current distribution in equilibrium with the external field provided by active conductors and mangetic core. We decided to compare the MHD Equilibrium found in this way directly with the magnetic measurements.

In Figure 4.7 we show the reference MHD Equilibrium configuration for the JET shot $\#71985$, calculated at the time instant $t_0 = 67.3s$, calculated with the procedure described above. Some important parameters defining the MHD Equilibrium are provided in tables 4.8 and 4.9.

[2]e.g. previously computed MHD equilibria or poloidal fluxes produced by toroidal filaments within Ω_{in}

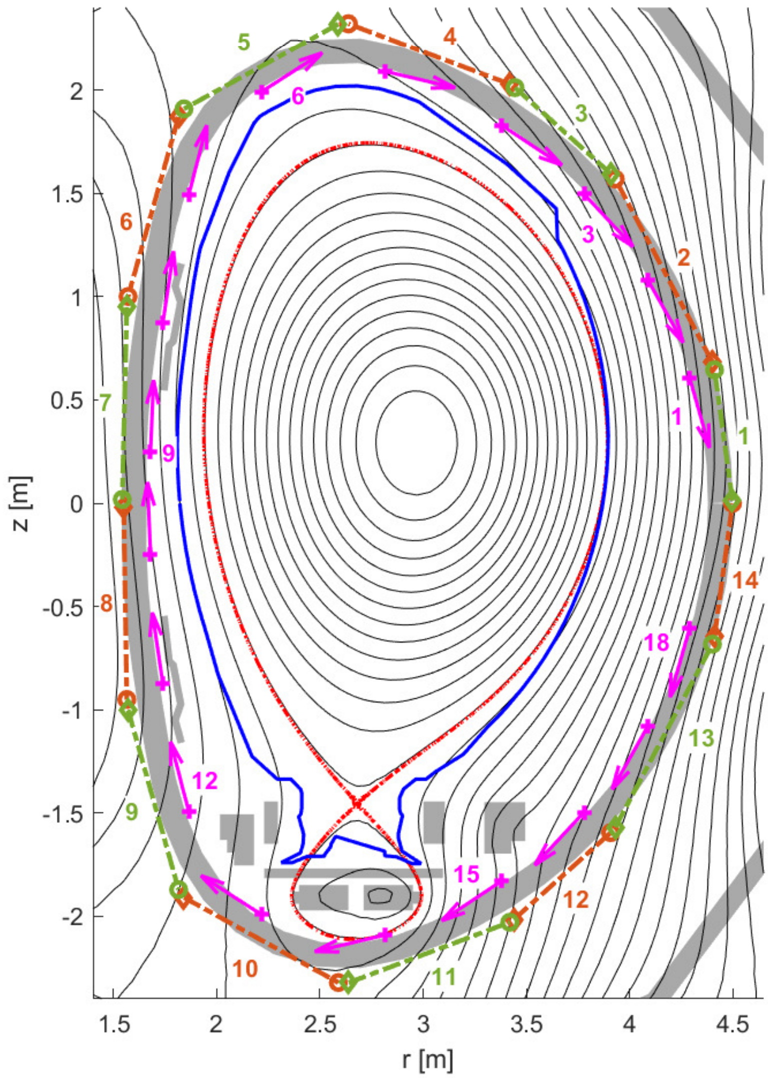

Figure 4.7: Poloidal flux surfaces for the MHD Equilibrium configuration of the JET experiment $\#71985$ at $t_0 = 67.3\ s$, computed by CREATE-L. The plasma boundary is depicted in red, the first wall in blue, the vacuum vessel and some conductors are in grey. In magenta we show the position and orientation of the 18 in-vessel Internal Discrete Coils. Green and orange dashed lines schematically show the 14 ex-vessel Saddle Loops.

β_0	$\alpha_{m,p}$	$\alpha_{n,p}$	$\alpha_{m,f}$	$\alpha_{n,f}$	λ	$\psi_a\ \left[\frac{Wb}{rad}\right]$	$\psi_b\ \left[\frac{Wb}{rad}\right]$
0.014	0.997	1.036	0.877	1.289	1.967	−0.038	−0.207

Table 4.8: Input parameters and further toroidal current profile parameters for MHD Equilibrium setting of JET shot $\#71985$ at $t_0 = 67.3\ s$.

R_{pl}	A_{pl}	J	β_p'	ℓ_i'	q_{95}
$2.92\ m$	$4.55\ m^2$	$2.146\ MA$	0.017	1.067	2.4

Table 4.9: Plasma parameters for MHD Equilibrium of JET shot $\#71985$ at $t_0 = 67.3\ s$, as computed by CREATE-L. β_p and ℓ_i are presented according to the CarMa0NL definition (*i.e.* in terms of volume averages).

4.3.2 The magnetic diagnostics

Several magnetic diagnostics are installed in JET. Inside the first wall there are pick-up coils to measure the magnetic flux density at several poloidal locations, and replicated at 4 different toroidal angles (*i.e.* in 4 of the 8 octants which constitute the JET structures) [160]. We will focus in particular on the *Internal Discrete Coils*, whose location and orientation in a single poloidal plane is given in Figure 4.7.

Similarly, several loops are present to measure the ex-vessel magnetic fluxes. In Figure 4.7 we show in particular the ideal location of the standard *Saddle Loops*. Ideally, these would be intended to measure the actual poloidal flux difference between two distinct poloidal locations. Anyway the presence of bellows and ports, besides the installation tolerances, generally requires to modify the ideal path and reduce the area linked to each coil. For example, the large horizontal port significantly reduce the toroidal span of Saddle Loops 1 and 14. This effect is simple to account rescaling the real measurement by the ratio of ideal and real toroidal span of the loops. Anyway the large port openings (both the horizontal and the vertical ones) require to significantly break the axisymmetry in case of Saddles Loops 2, 3, 4 and 11, 12, 13. Within the JET database, raw measurements are always re-scaled to virtually simulate a complete toroidal span of each Saddle Loop. A further correction factor is applied in post-processing to account for the loss of flux due to bellows and non-axisymmetric paths of the diagnostics. The locations in Figure 4.7 hence provide the *ideally axisymmetric* toroidal connections which should best fit the real, non-axisymmetric, Saddle Loops measurements.

In order to check the MHD Equilibrium we found is satisfactory, we compare the simulated Internal Discrete Coils and Saddle Loops measurements, with real ones. The experimental measurements are processed to eliminate the spurious effect due the non-perfect poloidal alignment of the diagnostics, which may link some toroidal magnetic field. Compensation coefficients are computed from the last available dry run, considering the reading of diagnostics measurements when only Toroidal Field coils are in operation. Moreover, we read the signals from all the available replica at different toroidal locations, subsequently considering the average of measurements along the toroidal angle. The standard deviation for the same measurement at different toroidal angles is generally small as compared with the average, indicating the robustness of the axisymmetry hypothesis adopted for the plasma during the experiment.

For the sake of comparison of simulated and real diagnostics measurements it is useful to introduce some reference quantities. Notice the Internal Discrete Coils are approximately tangent to the inner page of the first wall. Following some earlier discussion on the circular tokamak, we may take the average measurement as reference quantity, which would scale like $\sim B_{u,0}$. Anyway, to be more general, we consider the following effective value of the tangent field along the poloidal angle:

$$B_{ref} = \sqrt{\frac{1}{2\pi}\sum_{k=1}^{18} B_{exp,k}^2 \Delta\theta_{IDC,k}} \tag{4.65}$$

The average of saddle loops measurements would be zero in the ideal limit of perfect coverage of the torus via the loops. In this case it is especially useful to use an effective value as reference quantity:

$$\psi_{ref} = \sqrt{\frac{1}{2\pi}\sum_{k=1}^{14} \psi_{exp,k}^2 \Delta\theta_{SL,k}} \tag{4.66}$$

The relative errors for the MHD Equilibrium described in Figure 4.7 are given in Figure 4.8.

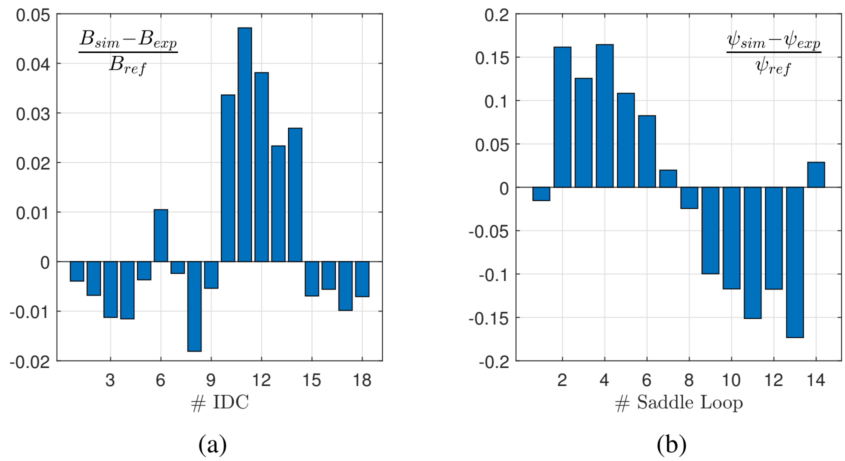

Figure 4.8: Relative error for (a) Internal Discrete Coils and (b) Saddle Loops measurements, expressed in per unit respect to the reference quantities $B_{ref} \simeq 378.8\ mT$ (4.65) and $\psi_{ref} \simeq 1.226\ Wb$ (4.66).

4.3.3 Experiment #71985

Starting from the MHD equilibrium configuration found for the JET shot #71985, we try to simulate the actual experiment. In this case a voltage kick is purposely applied to the *Fast Radial Field Circuit*, used in JET for the control of the vertical position, generating a VDE. The plasma hits the wall, and contextually loses thermal energy, up to the point when a CQ starts. The evolution of experimentally found quantities is reported in Figures which follow, together with the simulations results. In order to fit the actual electromagnetic evolution of the experiment there is a number of knobs which we can manipulate:

- The electric current in active conductors, especially the *Fast Radial Field Circuit*;
- The profile parameter β_0, which allows to drive the internal energy variations;
- The net toroidal plasma current, which is the fundamental quantity driving the poloidal magnetic energy exchanges;
- The α-type profile parameters, which we can use to modify the actual

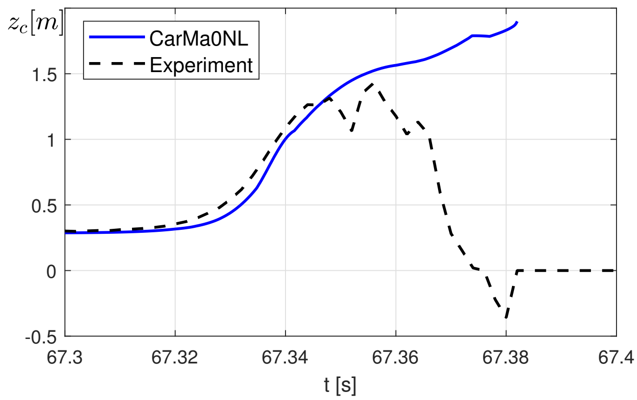

Figure 4.9: Plasma current centroid vertical position during JET experiment #71985.

steepness of the current density distribution about its current centroid, allowing to fit the internal inductance evolution

- The growth of the halo width related after the first time of plasma-wall contact

In the following simulation we model the conducting vacuum vessel by a simplified axisymmetric model, where the thickness and resistivity are adapted to account for the presence of bellows and of the JET double-shell [148]. Nonetheless, the presence of ports is discarded completely and even the bellows are not described as geometrically concentrated at a given toroidal location, *i.e.* we take a toroidally uniform resistivity. These simplifications may lead to an overestimate of the growth rate as compared to the experiment, as observed in [148]. Moreover our estimation of the initial MHD Equilibrium is subject to a small error, as evidenced in Figure 4.8, adding uncertainty in the calculated growth rate for the vertical instability. These considerations indicate clearly that a more accurate description of conducting structures and finer tuning of the initial MHD equilibrium would be necessary to accurately fit the experiment. In particular, the application of the experimental voltage kick leads to unacceptably fast vertical displacement, not observed in reality.

Nonetheless, the available knobs at our disposal allow to stimulate a Vertical Displacement in our *CarMa0NL* simulation which does not differ much from the one we observe experimentally, up to the point when the plasma hits the wall. We achieve this by proper re-scaling the applied voltage kick to the *fast radial field circuit*. This expedient, besides not fully consistent, allow us to correctly reproduce the time instant of first plasma-wall contact. From that time instant onwards, the actual dynamics of the plasma column change completely, and also the growth rate of the vertical instability gradually lose of importance. In Figure 4.9 we compare the evolution of the current centroid vertical position as evaluated by *CarMa0NL* and as found in the experiment according to the definition suggested in Reference [160]. The quite fair agreement of the vertical displacement, up to the first time of plasma-wall contact ($t_{hit} = 67.328\ s$), motivate the possibility of describing later stages of the experiment, even before more accurate models for structures and initial equilibrium are available.

We compare the net toroidal plasma current against the experimental one in Figure 4.10a. Contextually we show the CarMa0NL estimation for the poloidal plasma current in Figure 4.10b. Notice that we impose a linear decay of β_p from its nominal value 0.017 to zero, since the time instant of plasma-wall contact and lasting $1\ ms$. About the same time, *e-fit* predicts an increase of the poloidal beta and suddenly stops converging. It is worth noticing that we predict a quite lower β_p as compared to the *e-fit* reconstruction ($\beta_{efit} \simeq 4\beta_{CarMa}$). The time step adopted in the simulation is $0.2\ ms$, enough smaller than structures time constants. Since the first time of plasma-wall contact, we account for the existence of an halo layer. In particular we manually tune the flux difference between the plasma boundary and the core boundary magnetic surfaces to be a given fraction of the flux difference between the plasma boundary and the magnetic axis poloidal fluxes, *i.e.* we tune the parameter $H(t)$ of the following relation:

$$\psi_b - \psi_L = H(t)\,(\psi_a - \psi_b) \tag{4.67}$$

The label “L”, clearly indicates the limiter point, *i.e.* the boundary of the core plasma. The simulated pick-up coils measurement are very sensitive to different choices of $H(t)$, indicating that appropriate account of the halo width is necessary to correctly simulate the plasma evolution. The parametrization of the toroidal current density (3.114), remains defined up to the plasma boundary, *i.e.* includes the halo region. From Figure 4.10a we see that a significant portion of the toroidal current is carried by the plasma in the halo region.

During the current spike, slightly before the *Current Quench* takes place, the current density distribution within the plasma flattens significantly. It is important to describe this feature in order to correctly account for the poloidal

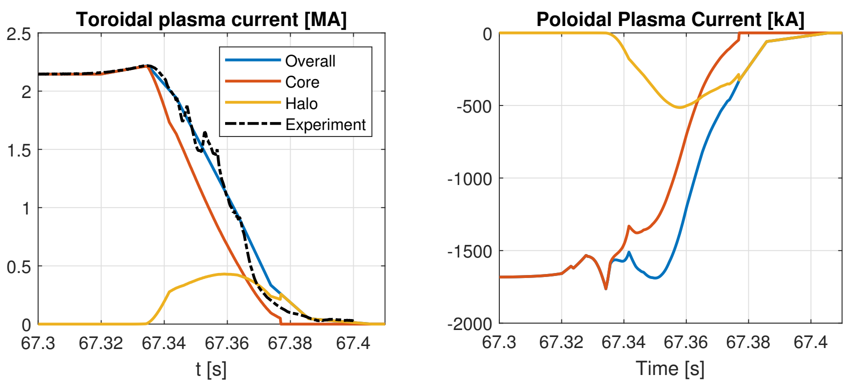

Figure 4.10: Evolution for net plasma currents during JET experiment #71985

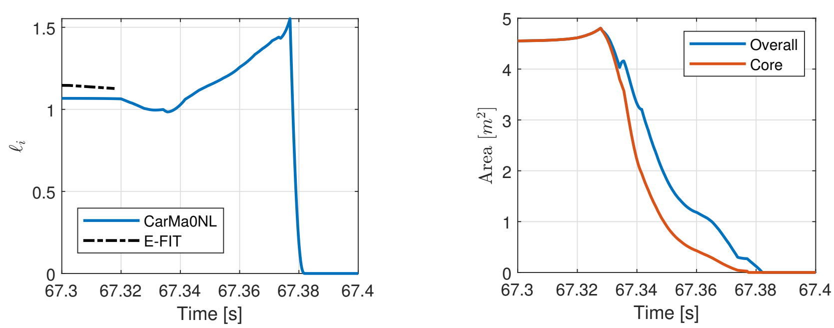

Figure 4.11: (a) Plasma internal inductance and (b) cross-sectional area during JET experiment #71985, as evaluated in *CarMa0NL* simulation.

magnetic energy variations and fluxes. Indeed a raise of the plasma current without a corresponding decrease in the internal inductance, would lead in general to an eventually non-physical increase in the poloidal magnetic energy within the first wall. We show in Figure 4.11a the internal inductance variations we find in simulation, after a detailed tuning of the $\alpha(t)$-type current profile parameters.

For completeness, we provide the actual plasma toroidal current density distribution at a later time instant of the simulation in Figure 4.12a. From this picture, the actual relatively large cross-sectional area of the halo layer is evident. In the same Figure, we show the corresponding eddy currents. The injection of halo currents into structures is not performed at this stage, as the actual toroidal field is not retained important indeed on the actual plasma evo-

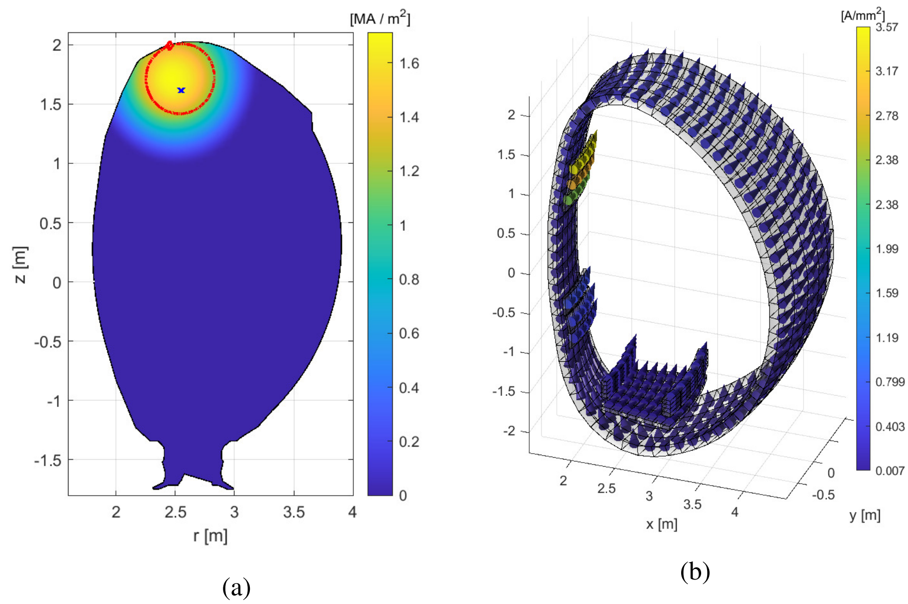

Figure 4.12: Simulated (a) toroidal plasma current density distribution and (b) eddy currents in passive structures during JET experiment $\#71985$ at $t = 67.366\ s$, *i.e.* during the *Current Quench* and beyond the instant of plasma-wall contact. The overall toroidal plasma current is $792\ kA$.

lution, as motivated in previous Sections. The actual way we compute the plasma toroidal flux variations is consistent with a surface current sheet located at the inner page of the Coupling Surface, which makes close the plasma current paths, as discussed in Section 2.7. Notice that most of the stabilizing current and toroidal current due to the plasma *Current Quench* is carried by the restraining rings, with a relatively low eddy current in the surrounding vacuum vessel. There you may also notice the net poloidal current, resulting from the toroidal flux variations.

Some of the simulated measurements for Internal Discrete Coils and Saddle Loops are compared against experimental measurements in Figures 4.13c. In particular we subtract from the signals the initial value at $t_0 = 67.3\ s$, in order to focus the attention on the efficacy of our dynamic description, rather than on the error on the initial MHD Equilibrium flux map. The agreement is quantitatively satisfactory for measurement on the top part of the machine, while large deviations are found for simulated IDC measurements placed on

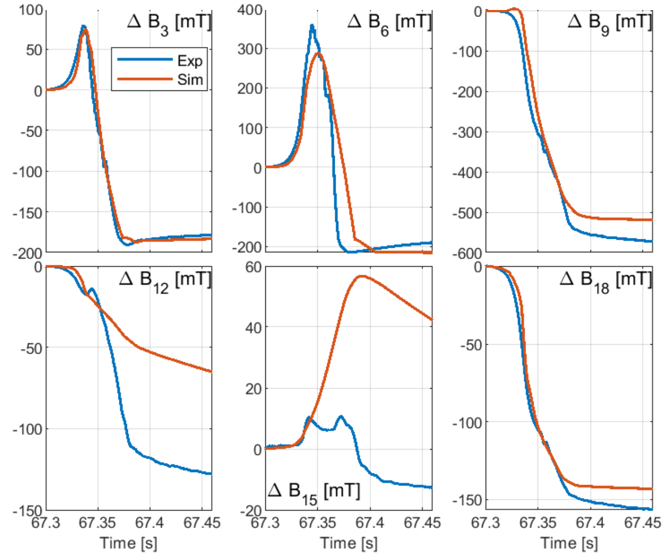

(a) Internal Discrete Coils

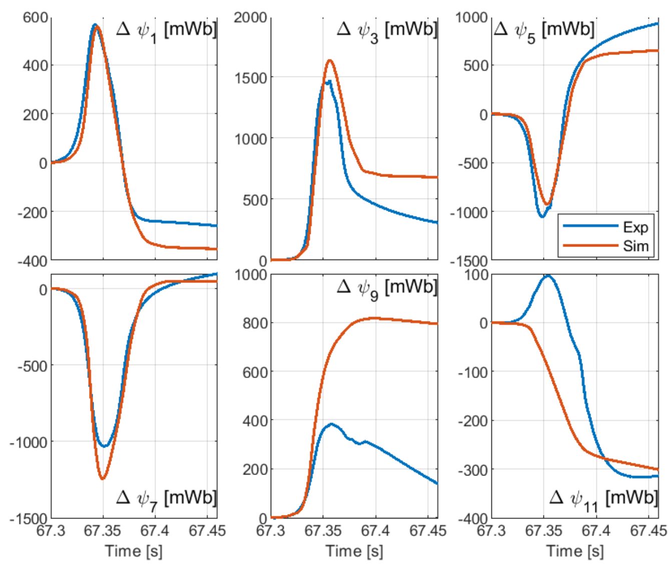

(b) Saddle Loops

(c) Summary of the comparison between simulated and experimental (a) Internal Discrete Coils and (b) Saddle Loops measurements. Variations of the signals respect to the initial time instant $t_0 = 67.3\ s$ are reported.

the bottom, at least in late time instants of the simulation. As the plasma is moving upwards, and the current centroid is clearly located at the top of the device, the mismatch is probably related to a still inaccurate description of eddy currents in the divertor structures. It is worth moreover to notice in this respect that here we are not considering the actual supply of all of the PF coils, besides the applied voltages to PF coils are instead varied during the experiment (although on a slower time scale then the fast radial field coils).

4.4 Disruption Trajectories in TCV

In this Section we collect the results of a recent experimental and simulation campaign carried out at the *Tokamak á Configuration Variable* (TCV), focused on the prediction of disruption trajectories [129]. TCV is a medium size tokamak ($R_w = 0.88\,m$, $B < 1.54\,T$), characterized by great shaping flexibility of the steady state plasma at MHD Equilibrium, thanks to its set set of 16 Poloidal Field Coils [161]. The campaign under exam was motivated by the recent idea of installing sacrificial limiters in the next generation tokamak DEMO [162]. The effectiveness of this solution relies on the capability of predicting and controlling the the target location where the plasma is hitting the wall, in consequence of a disruption. The experimental campaign [129] revealed that the actual radial motion of the plasma column is very correlated to the pre-disruption MHD Equilibrium configuration, hence in last analysis to the shaping external magnetic fields. This feature can be observed for example in Figure 4.14, where LIUQE reconstructions for different Vertical Displacement Events are presented, all triggered by a Voltage Kick and contextual shut-down of the vertical control system.

From the LIUQE reconstructions, it is quite evident that the plasma with original positive triangularity tends to move inward, while the plasma with negative triangularity move outwards. Plasmas with almost null triangularity, also defined as “drop-like” tends to stay centred in the vacuum chamber during their vertical motion. This behaviour was observed during the experimental campaign also for different disruption triggers:

- increasing the density above the Troyon density limit, via gas puff in the vacuum chamber;

- increasing the toroidal plasma current until reaching $q_{edge} = 2$, properly varying the applied homogeneous poloidal flux

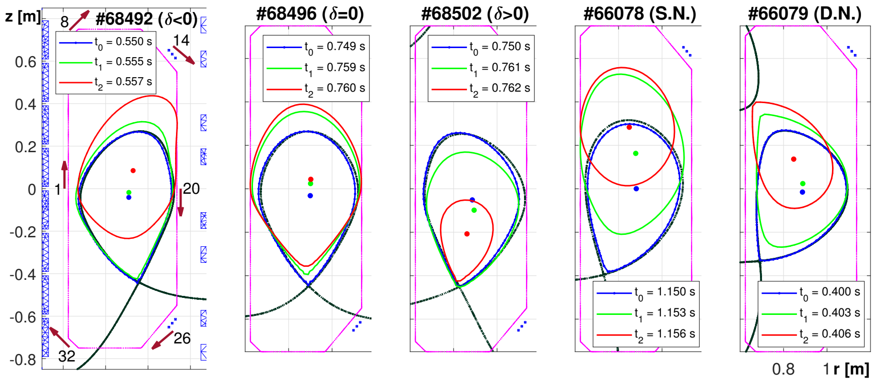

Figure 4.14: Each panel reports the LIUQE reconstruction of the plasma boundary for a TCV shot. The plasma boundaries depicted in blue are taken at a time instant prior to the disruption trigger t_0, where the plasma can be considered in static equilibrium. In all of the above experiments the disruption trigger is a Voltage Kick, and contextual shut-down of the vertical control system.

Similar plasma shapes, with different cross-sectional areas, were also triggered in the same way to examine whether the growth rate of the vertical instability influences the trajectory. It was found that the actual time-scale of the vertical motion does not influence substantially the trajectory of the current centroid in the poloidal plane [129].

The trajectories observed in experiments are substantially confirmed in *CarMa0NL* simulations. In Figure 4.14 the black solid lines represent the plasma boundary as found in CREATE-L, before the disruption trigger. There we indicate with t_0 the pre-disruption time instant where we compute the MHD equilibrium. We provide some details on these MHD equilibrium configurations, which we use to initialize *CarMa0NL* simulations, in Table 4.10.

The Vertical Displacement Events are triggered in simulation by standard voltage kicks which lead to the correct vertical motion of the plasma column. A wide variety of simulations is performed varying different plasma internal parameters during the simulation. The most significant results to the study of disruption trajectory are illustrated in Figure 4.15. The general tendency of positive triangularity plasmas to move towards the high field side, and that of negative triangularity plasmas to move towards the low field side, is confirmed.

#shot	$J\ [kA]$	β_p	ℓ_i	$\Delta_b\ [cm]$	$A_{pl}\ [m^2]$	k	δ
66078	209.2	0.391	1.087	-0.9	0.236	1.584	0.367
66079	207.2	0.298	0.989	$+0.5$	0.193	1.427	0.651
68492	251.7	0.322	0.821	$+2.2$	0.216	1.608	-0.266
68496	190.2	0.478	0.984	$+1.6$	0.218	1.586	0.020
68502	250.6	0.193	0.935	$+1.8$	0.225	1.523	0.285

Table 4.10: Summary of the pre-disruption TCV equilibria considered. The plasma profile parameters are computed by CREATE-L. The reference major radius for TCV is $R_w = 0.88\ m$.

It is noticeable as the net toroidal plasma current variations accentuate this behaviour. The sudden beta drop instead leads always to a sharp displacement of the plasma column towards the high-field side. This "inward" motion is nonetheless always over-compensated by the dynamics induced from the voltage kick and the net toroidal plasma current variations.

Both the effect of the net plasma current variation and of the poloidal beta drop on the disruption trajectory could still be explained by the simple high-aspect-ratio evolutionary equilibrium theory introduced in Section 3.2. In the ideall-wall limit, according to (3.75), the following quantity should be conserved:

$$J\,(\Delta_b - \Delta_{iw}) = \text{const} \tag{4.68}$$

where J is the plasma toroidal current, Δ_b is the shift of the plasma column respect to the wall geometrical center, and Δ_{iw} is the plasma shift which makes the wall a flux surface. For a circular high-aspect-ratio tokamak we find that for $\Delta_b < \Delta_{iw}$ the plasma should move inwards during the CQ, vice-versa we expect an outward moving plasma column when $\Delta_b > \Delta_{iw}$. The generalization of this picture to our shaped, small aspect-ratio case is of course non-trivial. A position of the plasma column which makes the wall a flux surface, for given shape, area and current distribution within the boundary, does not even exist in general. A suitable generalization of Δ_{iw} likely involves some moment of the magnetic field distribution at the wall. The real physical requirement is that the motion will try to keep B_n frozen at all the wall points, although the wall is not ideal and the magnetic field slowly diffuse through the vessel. Nonetheless, simulations and experiments suggests to frame the observed trajectories into the analytical picture claiming that $\Delta_b > \Delta_{iw}$ for plasmas with positive triangularity, and $\Delta_b < \Delta_{iw}$ in the opposite case.

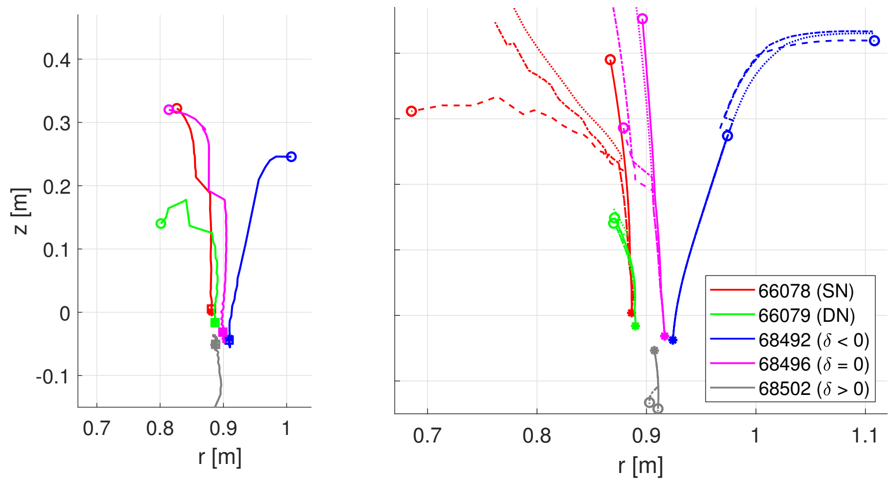

(a) LIUQE (b) CarMa0NL

Figure 4.15: Trajectories of the disruptions triggered by Voltage Kick, and reported in Figure 4.14: (a) LIUQE Reconstruction of the experiment; (b) CarMa0NL simulations: the solid lines are obtained for constant plasma current and β_p; dashed lines are found imposing a β_p drop, followed by a current overshoot and quench ($200kA/ms$); dotted lines account for a constant β_p and plasma current evolving as in the real experiment; dash-dotted lines combine the experimental plasma current evolution with a β_p drop.

This overall trend is confirmed in Figure 4.15, even from the small current overshoots occurring in shots #66078 and #66079, both with positive triangularity. The dotted lines represent simulated trajectories obtained keeping constant the poloidal beta, and varying the toroidal current as in the experiment. At some point of these trajectories you may notice a sharp outward motion, precisely related to the current spike.

Concerning the behaviour observed at the Thermal Quench, the analysis is even more simple. A drop in the poloidal beta is likely responsible for a reduction in the *ideal wall Shafranov shift*, see Equation (3.77). For a constant plasma current, Δ_b would just follow the motion of the ideal shift Δ_{iw}, so to leave the distance $\Delta_b - \Delta_{iw}$ unaltered in the ideal wall limit.

Finally we examine in greater detail the shot #66078, for which we find a good quantitative agreement between simulated and experimental measurements. In this case we force the current in active Poloidal Field coils to equal

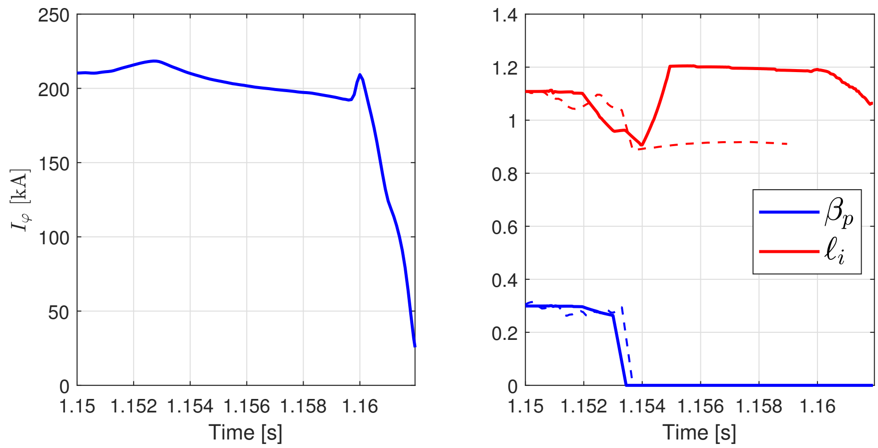

Figure 4.16: Toroidal plasma current, poloidal beta and internal inductance evolution during TCV experiment #66078.

the experimental one at each time step. As a consequence the effect of the real "Voltage Kick" is completely accounted, since the magnetic field imposed by active conductors is reproduced exactly in the simulation. An overview of the evolution of the plasma current and main internal plasma parameters is given in Figure 4.16. We report the motion of the magnetic axis in the poloidal plane as reconstructed by LIUQE and as computed in the *CarMa0NL* simulation in Figure 4.17. The simulated radial motion match quite well the reconstruction, while the simulated vertical motion differs considerably after some ms from the application of the Voltage Kick. Again notice that a radial displacement towards the low field side occurs when the plasma current overshoots without variations of β_p, *i.e.* at the time instant $t \simeq 1.16s$.

The CarMa0NL computed evolution match quite well the real magnetic measurements, as shown in Figure 4.18 for the pick-up coils whose location and orientation was illustrated in Figure 4.14. The mismatch between real and simulated measurement does not vary much during the time evolution, indicating the effectiveness of our description. Again, in order to fit the experiment, we forced the plasma current to equal the experimental one. The thermal energy was regulated similarly to what reconstructed by LIUQE via the parameter β_0. Moreover the $\alpha(t)$-type parameters were set up in such a way to determine a current flattening before the TQ, as you can notice form the internal inductance evolution in Figure 4.16b. Compared to the JET simu-

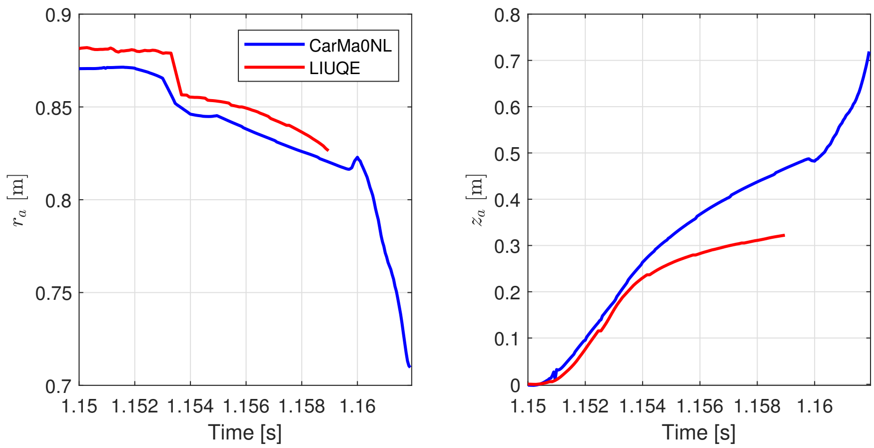

Figure 4.17: Evolution of the magnetic axis poloidal location during TCV experiment #66078.

lation of previous Section, here we don't have any halo layer, and the plasma currents are always taken within the Last Closed Flux Surface.

The results of our benchmark with experiments support the possibility of using evolutionary equilibrium tools for the analysis of disruption experiments. Nonetheless, the validity of evolutionary equilibrium models to predict the tokamak plasma evolution is still subject to different hypothesis and to the correct set-up of some input parameters, which are eventually evolving in time. Let us recollect the underlying hypothesis making an evolutionary equilibrium model valid:

- Equilibrium, hence evolutionary equilibrium, models generally assume a well defined topology for the magnetic flux surfaces. The eventual break of magnetic topology is hence neglected or assumed to not influence considerably the overall tokamak plasma evolution, except for what results from the sudden loss of thermal energy;

- The natural mechanical macroscopic motion needs to be limited to the electromagnetic time-scale by the presence of passive conductors. An Alfvénic motion cannot be captured from the model. The verification of this hypothesis can be performed at least for what concerns the rigid vertical motion of the plasma column, evaluating the *stability margin* of the planned reference equilibrium configuration. Nonetheless, it is a matter of fact that the stabilizing effect of passive conductors on the vertical motion is less and less efficient as the plasma current decreases. In this respect the vertical instability may become Alfvénic during the CQ, although this cannot be determined in advance and likely depends on the effect of halo currents on the plasma evolution.

- In order to use a tool as *CarMa0NL* one should retain reasonably satisfied the hypothesis of axisymmetric plasma. Any 3D plasma effect cannot be captured by this description.

Even when the mass-less approximation and the axisymmetric hypothesis are retained accurate, the possibility of using axisymmetric evolutionary equilibrium models for predicting the plasma evolution during disruptions of future experiments is subject to the knowledge of several physical features:

- Plasma current evolution
- Initial perturbation driving the evolution/disruption, and eventually the equivalent quasi-static trigger;
- Thermal Quench duration;
- Evolution of the current density profile parameters, *i.e.* the α-type parameters of the *CarMa0NL* representation (more generally the relation between plasma boundary geometry and B_{tan});
- Active currents evolution (which eventually requires to model the control system);
- Halo width evolution;

For example, the prediction of the net plasma current could be implemented providing information on joule losses and on the deformation power [62]. More generally, the free-functions appearing in the Grad-Shafranov equation may be evaluated by simplified diffusion models, and coupled self-consistently to the MHD equilibrium problem [163]. Anyway the actual value and evolution of diffusion coefficients may be subject to even larger uncertainties than the one we have for the input parameters listed above. When some objective is identified, a simulation scan can be conveniently set-up, varying for example the plasma current decay-rates, the evolution of the current profile parameters, or the way in which the active coils are fed. This allows for useful engineering estimations. The most classical example is given probably by

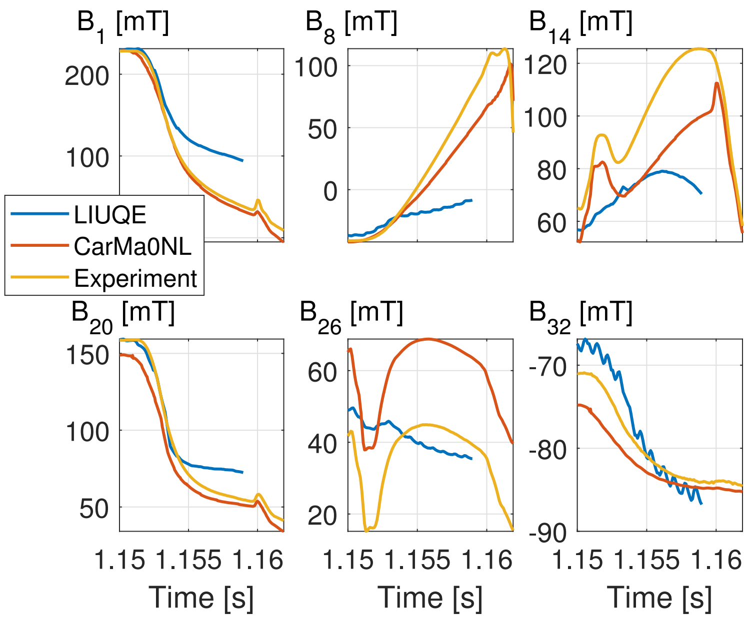

Figure 4.18: Comparison of simulated, reconstructed and raw measurements for some of the pick-up coils during TCV experiment #66078.

the estimation of the mechanical stress on passive structures during expected disruption scenarios of tokamaks actually in their design phase [128, 85]. Vast simulation-campaigns can be performed to investigate the expected forces and the mechanical stress on the tokamak wall and eventual plasma facing components. The apparent freedom in the choice of the free functions and other input parameters can be checked for energetic consistency by the considerations of Section 4.2.

Conclusions

The modelling and simulation of tokamak plasmas on the macroscopic length-scale is fundamental for the understanding of present experiments and for the design of future devices. The passive conducting structures themselves can be considered on their own a fundamental ingredient of a working tokamak, slowing down to the electromagnetic time scale otherwise Alfvénic plasma motions. The present Thesis was largely motivated by the problem of the self-consistent description of the plasma evolution under the passive feedback of the conducting structures nearby. Several questions motivated efforts in different directions, let us resume briefly what we achieved to answer and what is still largely missing.

Halo currents are among the less understood electromagnetic phenomena taking place in a tokamak device, and this work certainly does not propose a definitive interpretation. Anyway, the initial driver which motivated the thermodynamics study of Chapter 1 was, surprisingly, the study of halo currents. The discussion of Section 1.10 highlights clearly the recombination of ions and electrons at the solid interface and the ionization of the neutral gas within the bulk plasma as key features of a steady state shared current between plasma and wall. This fact makes advisable to model our fluid mixture as a *partially* ionised gas, if we want to describe operational regimes where there is significant plasma-wall contact. Hence, we devoted our initial effort in providing a simple but thermodynamically coherent description of the ionization/recombination phenomena within the context of *Magneto-Hydro-Dynamics*. The correct tool to pursue this objective was identified to be the general framework of Non-Equilibrium Thermodynamics, which allowed us to set up a constitutive relation for the ionization-recombination rate and recover *Saha Equation* in conditions of thermodynamic equilibrium. Besides the variety of extended MHD models available in the literature, only a few describe the neutral gas within the fluid mixture, and in most cases it is hard to verify whether the reference conditions of Thermodynamic equilibrium are correctly described or not. This path proposes to the MHD community the possibility of accounting for chemical reactions at the macroscopic, thermodynamic level.

As a side-effect, we had the opportunity to review in a unitary framework all of the closure relations to the MHD model generally postulated on a phenomenological basis. The discussion revealed in particular how the actual structure of constitutive relations is constrained first by a positive-definite entropy production and further by the fundamental symmetry principle of *Curie* and the reciprocal relations of *Onsager*. The anisotropy of the system introduced by the presence of a strong magnetic field was fully accounted in this context, with some interesting consequences of the magnetic field being a pseudo-vector. In particular, we found that even order thermodynamic fluxes, are only generated by even order thermodynamic forces, and the same holds for odd order quantities. The coordinate-independent form of the constitutive Equations was also a natural consequence of this discussion. We believe that this completely-macroscopic framework may be beneficial on the one hand for understanding and on the other hand to check that all the ad hoc modifications of extended-MHD models are thermodynamically consistent.

Later, we examined the problem of the electromagnetic interaction rather from the conducting structures perspective. A variety of extended-MHD models is available in the literature, and some of them include also conducting structures within the model [59, 60]. Anyway a numerical model which describes both 3D volumetric structures and 3D non-linear MHD models is still missing. The underlying question of Chapter 2 is clear: How can we develop such a tool? A review of the mathematical formulation of the extended-MHD codes M3D-C1 [39, 41] and JOREK [40, 54, 61], allowed to identify the tangent component of the magnetic field to the MHD computational boundary as the key boundary condition to set up in order to account for the effect of currents in external conductors. The Magneto-Quasi-Static problem in the outer domain to the Coupling Surface needs to be implicitly solved at each time step of the MHD simulation, accounting clearly for passive currents.

We hence explored different possible interaction schemes, all in the frame of *Boundary Element Methods*. In particular the indirect scheme based on the *Virtual Casing Principle* was described for its application to the JOREK-CARIDDI coupling. Preliminary results are satisfactory, but further work is still necessary before realistic halo current patterns can possibly be simulated. Further we explored two possible *direct* formulations [63], with the objective of avoiding the discretization of the JOREK boundary via CARIDDI elements. In this respect the *direct-A* formulation presents some gauge problems, except in the axisymmetric case, $n = 0$. Anyway its discussion revealed how to correctly account for plasma induced voltages in conducting structure, solely in terms of the tangent component of magnetic field and vector potential at the MHD computational boundary. The *direct-B* formulation, also thanks to the previous considerations on plasma-induced voltages, looks finally suitable for implementation. The resulting boundary integral equation first revealed to be non-invertible. We showed this is related to the topological singularity of the *Coupling Surface*, and how to overcome this situation. Moreover, thanks to the axisymmetry of the computational domain, we were able to attribute the singularity of our integral equation essentially to the $n = 0$ poloidal magnetic field component of the problem. In principle, for axisymmetric Coupling Surfaces, one can hence formulate an hybrid *direct-AB* coupling scheme, where the boundary condition for the $n = 0$ component of the poloidal magnetic field is provided by the means of the vector potential formulation, and all other modes are computed via the magnetic field formulation.

Our survey reveals some possible directions to take. In particular the JOREK-CARIDDI coupling via the *Virtual Casing Principle* needs to be further developed, with the aim of studying realistic halo current patterns. The main limitation of the resulting plasma-structures integrated model will be probably related to the axisymmetry of the Coupling Surface, which does not allow to simulate plasma currents in eventual toroidal gaps along the first wall or in between Plasma Facing Components. Work in this direction may be important, as only few models for simulating these currents exist at the present [164]. Moreover, complications on the boundary conditions in presence of halo currents may raise, since the correct inclusion of sheath physics effects to limit the current to its ion saturation value is not trivial [50].

The lack of a detailed 3D plasma-structures modelling tool, does not mean that we don't have other possibilities to examine the consequences of the plasma-wall electromagnetic interaction. Which electromagnetic force is generated on the wall during a disruption? What energy fluxes shall we expect? How wide is the halo layer generated due to the plasma-wall contact? Can we estimate the plasma trajectory during fast transients? In order to answer these questions we can use more synthetic descriptions, rather than a full extended MHD simulation. In this respect Chapter 3 has to be regarded as a preparatory Section for the subsequent applications. Former studies on Vertical Displacement Events [108] identified the *stability margin* as key parameter to discriminate whether the plasma motion evolves on the electromagnetic or on the Alfvénic time scale. We review those considerations with the aim of justifying quasi-static evolution tools as robust. Further studies are needed in this direction, to verify whether the quasi-static assumption is mathematically rigorous also for non-rigid motions. Following, we examine the consequences of the mass-less approximation on a circular high-aspect-ratio tokamak, providing this way the main ingredients of the evolutionary equilibrium theory [114]. In the final Section the numerical model *CarMa0NL* is reviewed, in view of its applications in the final Chapter.

Then, finally, what force shall we expect on the tokamak wall during a disruption? Studying numerically the sound analytical findings for a circular tokamak presented in [146, 149], we confirmed the key role of the net poloidal current in the task and we pointed out as the magnetic pressure jump is not necessarily the only important electromagnetic force raised during a disruption [127]. The numerical observation of a significant tangential force was later shown to be consistent with the analytical framework [147]. We review this scientific discussion in the first Section of Chapter 4. Additionally, we show here the presence of a magnetic toroidal tension on the wall, eventually present both in the TQ and the CQ. The cross-validation of the numerical and analytical model suggests that we can use *CarMa0NL* for studying disruption forces, at least as long as the plasma evolution can be retained substantially axisymmetric and the plasma motion is not Alfvénic. Further, the analytical formulas can be used as rough order of magnitude estimates also during the design phase of tokamaks [128].

In the work [35], and in Section 4.2, we comment on the energy fluxes between the plasma and the external environment. Sometimes this task is hard, due to the different models employed to study the different physics processes involved in a tokamak. We propose a procedure to estimate at least the integral plasma losses via evolutionary equilibrium simulations. The method, besides simple, is new to the literature at the best of our knowledge. The main ansatz concerns the energy reservoirs included in the task: we consider solely the internal energy of the plasma and the magnetic energy as important, neglecting the kinetic energy of the fluid or eventually of the different fluid species considered separately. All the essential ingredients to a complete energy balance are then already set up within the evolutionary equilibrium model, provided the Equation of State for an ideal gas $\rho u = \frac{3}{2}p$. We find that for large externally applied toroidal magnetic fields the internal energy is converted completely to heat during the TQ. For lower values a really small fraction of internal energy can be pumped to toroidal magnetic energy and released in later phases of the disruption. The latter effect is anyway negligible during the CQ if compared to the heat dissipated due to the poloidal magnetic energy consumption. We set up simple analytical formulas to show that the actual amount of poloidal energy converted to heat within the plasma depends on the duration of the CQ as compared to the electromagnetic time constant of the surrounding wall.

Comparing JET experiment #71985 with *CarMa0NL* simulations, in Section 4.3, we found that the actual width of the halo layer is a crucial parameter to correctly reproduce the magnetic diagnostics measurements. A proper fit of the growth of the halo layer, together with the other plasma current profile parameters, allowed to find a reasonably good reproduction of the plasma electromagnetic features in our simulation. This provides at least with the indication that evolutionary equilibrium models may still be used in circumstances of significant plasma-wall contact. Much work is anyway still missing for a detailed reproduction of the experiment: firstly more detailed descriptions for the structures shall be used [148], and the iron core should be included in the task, relaxing the deep saturation hypothesis.

The analysis of TCV experiments, in particular the quantitative match found for the TCV shot #66078, provide further support to the efficacy of evolutionary equilibrium models in the description of disruptions. The numerical analysis substantially confirmed the experimental finding that positive triangularity plasmas tend to move towards the high-field side, while negative triangularity plasmas generally displace outward during the disruption. We claim a simple interpretation of this behaviour also by the means of the simple high-aspect-ratio model.

Clearly, we addressed only a very tiny fraction of the possible theoretical and practical questions raising in the framework of the plasma-wall electromagnetic interaction. As immediate future work to accomplish we plan to continue the efforts in the JOREK-CARIDDI coupling, since it would be a very useful tool in the study of halo currents. In the near future, we will apply the energy balance scheme already described to real experiments, to check the energetic consistency of evolutionary equilibrium simulations. Further it will be extremely interesting to extend our JET analysis with further details of the structures and a proper model of the iron-core. Also, the analysis of TCV experiments should be complemented by analytical studies, to interpret clearly the observed correlation between pre-disruption plasma shape and radial motion. We add moreover some open questions, which probably need a somewhat longer time-scale:

- Is it convenient to implement the thermodynamic ionization/recombination description given in Chapter 1 in exented-MHD models?

- Can the inclusion of electron inertia be significant in the frequent situations of high electric current and small mass density? Is it possible to model the runaway electrons within the thermodynamic theory discussed in Chapter 1? How Ohm's law changes in the special relativistic case?

- How can we properly describe the ion saturation current at the plasma-wall interface? Can we couple an electromangetic model of the sheath, in the stream of the one presented in Section 1.10, to the extended MHD and conducting structures models?

- Is it possible to allow present tokamak-oriented extended-MHD models for a fully 3D computational domain?

- How can we set up the width of the halo layer in an evolutionary simulation, in order to make it predictive?

Appendices

A Invariant Tensor Functions

The full orthogonal group of the three-dimensional Euclidean space $O(3)$, is the group of all those T_1^1 tensors Q with non-null determinant, such that $Q^{-1} = Q^T$, *i.e.* the group of all the proper an improper rotations of the Euclidean space. The constitutive equations are clearly tensor-valued functions of tensors, which we take to be linear in the framework of *Non-Equilibrium Thermodynamics*. Let $F(T_1, \cdots, T_n)$ be an arbitrary tensor function of n tensors of arbitrary order. The orthogonal transformation Q is defined as a symmetry transformation for the tensor function $F(T_1, \cdots, T_n)$ if and only if the Q-transformation of the input tensors just determine a corresponding Q-transformation of the output tensor,

$$F(\langle Q\rangle T_1, \cdots, \langle Q\rangle T_n) = \langle Q\rangle F(T_1, \cdots, T_n) \tag{69}$$

Here the symbol $\langle Q\rangle$ is just a shorthand for the operator which acts on an arbitrary tensor, transforming all the contravariant components via the tensor Q and all the covariant components via the tensor Q^T. We remember in particular that any orthogonal transformation has no effect on scalars, hence the operator $\langle Q\rangle$ has no effect on scalars. Given the tensor function $F(T_k)$, the set of all symmetry transformations constitutes a subgroup S of the full orthogonal group $O(3)$, defined as *symmetry group* for the tensor function $F(T_k)$.

The problem of establishing constitutive relations in a coordinate-independent form is essentially a problem of representation of tensor functions by invariants [165, 37, 36, 26]. Indeed we are concerned with the problem of finding a set of tensors $\{F_1, \cdots, F_m\}$ invariant for transformations in the symmetry group S, such that a tensor function $F(T_1, \cdots, T_n)$ may be represented as,

$$F(T_1, \cdots, T_n) = f_1 F_1 + \cdots f_m F_m \tag{70}$$

where the coefficients f_k are functions of the scalar invariants of the input tensors. When the form-invariants $\{F_k\}$ are linearly independent, the representation is defined as irreducible. Moreover if the set $\{F_k\}$ is sufficient for the representation of any tensor function with the same tensor order value, the representation is defined as complete. *Hilbert's Theorem* [165, 26] guarantees that in the three-dimensional Euclidean space, for any compact symmetry group, there exists a finite set of scalar invariants of the input tensors. Hence the problem of representation of a constitutive equation by a finite set of form-invariants is meaningful.

The *point group* S is characterized by the set of tensors $\{\xi_1, \cdots, \xi_n\}$ when

$$[Q \in S] \iff [\langle Q \rangle \xi_1 = \xi_1, \cdots, \langle Q \rangle \xi_n = \xi_n] \tag{71}$$

the tensors $\{\xi_1, \cdots, \xi_n\}$ are also defined as *structural tensors*. Any point group that can be characterized by a finite set of structural tensors is compact, and any compact point group may be characterized even by a single structural tensor. These results allow to formulate the isotropization theorem [37] in the convenient form [26]: *An anisotropic tensor function in the three-dimensional Euclidean space of any finite number of input tensors is expressible as an isotropic tensor function of the original input tensors and the structural tensors*.

Since the structural tensor for our symmetry group is the second-order skew-symmetric tensor $\tilde{B}$, and due to the validity of the isotropicization theorem [37], we may investigate the irreducible and complete representation for our constitutive relations, considering the irreducible and complete representations for isotropic functions of the original input tensors and the tensor characterizing the symmetry, *i.e.* a second-order skew-symmetric tensor $\tilde{W}$. We report the relevant results [26] in Tables 11-12. The scalar and form invariants for a function of several input tensors are also given by the scalar and form invariants of each single input tensor.

Table 11: Scalar invariants in the three-dimensional Euclidean space in isotropic conditions. As a convention, $\mathbf{v}$ is a polar vector, $\mathbf{A}$ is a second-order symmetric tensor, $\tilde{W}$ is a second-order skew-symmetric tensor.

Input Tensors	Scalar Invariants
$\mathbf{v}$	$\mathbf{v} \cdot \mathbf{v}$
$\mathbf{A}$	$\mathrm{tr}\,\mathbf{A},\ \mathrm{tr}\,\mathbf{A}^2, \mathrm{tr}\,\mathbf{A}^3$
$\tilde{W}$	$\mathrm{tr}\,\tilde{W}^2$
$\mathbf{v},\ \tilde{W}$	$\mathbf{v} \cdot \tilde{W}^2 \mathbf{v}$
$\mathbf{A},\ \tilde{W}$	$\mathrm{tr}\,\mathbf{A}\tilde{W}^2,\ \mathrm{tr}\,\mathbf{A}^2\tilde{W}^2,\ \mathrm{tr}\,\mathbf{A}^2\tilde{W}^2\mathbf{A}\tilde{W}$

Table 12: Form invariants in the three-dimensional Euclidean space in isotropic conditions. Same conventions of Table 11 are adopted. The suffix *S* denotes symmetric part of the corresponding tensor.

Input Tensors	Form Invariants
	Second-Order Symmetric Tensor Valued
-	1
$\mathbf{v}$	$\mathbf{v} \otimes \mathbf{v}$
$\mathbf{A}$	$\mathbf{A}, \mathbf{A}^2$
$\tilde{W}$	$\tilde{W}^2$
$\mathbf{v},\ \tilde{W}$	$\left(\mathbf{v} \otimes \tilde{W}\mathbf{v}\right)_S,\ \tilde{W}\mathbf{v} \otimes \tilde{W}\mathbf{v},$ $\left(\tilde{W}\mathbf{v} \otimes \tilde{W}^2\mathbf{v}\right)_S$
$\mathbf{A},\ \tilde{W}$	$\mathbf{A}\tilde{W} - \tilde{W}\mathbf{A},\ \mathbf{A}\tilde{W}^2 + \tilde{W}^2\mathbf{A},$ $\tilde{W}\mathbf{A}\tilde{W}^2 - \tilde{W}^2\mathbf{A}\tilde{W}, \mathbf{A}^2\tilde{W} - \tilde{W}\mathbf{A}^2$
	Vector valued
-	-
$\mathbf{v}$	$\mathbf{v}$
$\mathbf{A}$	-
$\tilde{W}$	-
$\mathbf{v},\ \tilde{W}$	$\tilde{W}\mathbf{v},\ \tilde{W}^2\mathbf{v}$
$\mathbf{A},\ \tilde{W}$	-

B List of Operators

In the following table we define in cylindrical coordinates of the operators sometimes used in Chapter 2.

Symbol	Expression	Comments
$\nabla_\perp f$	$\frac{\partial f}{\partial r}\hat{\mathbf{i}}_\mathbf{r} + \frac{\partial f}{\partial z}\hat{\mathbf{i}}_\mathbf{z}$	Gradient in the poloidal plane
$\nabla_\perp \cdot \mathbf{v}$	$\frac{1}{r}\left[\frac{\partial}{\partial r}(rv_r) + \frac{\partial}{\partial z}(rv_z)\right]$	Divergence in the poloidal plane
$\nabla_\perp \times \mathbf{w}$	$\frac{1}{r}\left[\frac{\partial w_z}{\partial r} - \frac{\partial w_r}{\partial z}\right]\hat{\mathbf{i}}_\varphi$	Curl in the poloidal plane
$\Delta^* f$	$r^2\nabla_\perp \cdot \left(\frac{\nabla_\perp f}{\mu_0 r^2}\right)$	
$L^* f$	$-\frac{1}{r}\Delta^* f$	Shafranov operator
(f, g)	$\nabla_\perp f \cdot \nabla_\perp g$	
$\{f, g\}$	$\nabla_\perp f \times \nabla_\perp g \cdot \nabla\varphi$	Poisson Brackets

C Proof of Stratton's Formula

We start from Equation (2.80), and we use immediately Green's vector identity (2.23), to wirte:

$$\begin{aligned}&\mathbf{A}^*_{\mathbf{in}} + \nabla\chi_{in} = \\ &\frac{1}{4\pi}\int_{+\partial V_{in}} \left[-G\left(\hat{\mathbf{n}}'\cdot\nabla'\mathbf{A}'\right) + \left(\hat{\mathbf{n}}'\cdot\nabla' G\right)\mathbf{A}' + G\left(\nabla'\cdot\mathbf{A}'\right)\hat{\mathbf{n}}'\right]\mathrm{d}\mathbf{r}'\end{aligned} \tag{72}$$

We use $\nabla\cdot G\mathbf{v} = G\nabla\cdot\mathbf{v} + \mathbf{v}\cdot\nabla G$ to get

$$\begin{aligned}\mathbf{A}^*_{\mathbf{in}} + \nabla\chi_{in} = \frac{1}{4\pi}\int_{+\partial V_{in}} \Big[&- G\left(\hat{\mathbf{n}}'\cdot\nabla'\mathbf{A}'\right) + \left(\hat{\mathbf{n}}'\cdot\nabla' G\right)\mathbf{A}' \\ &+ \left(\nabla'\cdot G\mathbf{A}'\right)\hat{\mathbf{n}}' - \left(\mathbf{A}'\cdot\nabla' G\right)\hat{\mathbf{n}}'\Big]\mathrm{d}\mathbf{r}'\end{aligned} \tag{73}$$

Since ∂V_{in} is a bounded surface without contour, it is possible to show that

$$\int_{+\partial V_{in}} \nabla'\cdot\left(G\mathbf{A}'\right)\hat{\mathbf{n}}'\,\mathrm{d}\mathbf{r} = \int_{+\partial V_{in}} \nabla'\left(G\mathbf{A}'\right)\cdot\hat{\mathbf{n}}'\,\mathrm{d}\mathbf{r} \tag{74}$$

This result is obtained indeed using the vector identies:

$$(a) \qquad \nabla\cdot(\mathbf{A}\otimes\hat{\mathbf{n}}) = (\nabla\cdot\mathbf{A})\hat{\mathbf{n}} + \hat{\mathbf{n}}\cdot\nabla\mathbf{A} \tag{75}$$

$$(b) \qquad \textstyle\int_S \nabla\cdot\underline{\mathbf{T}}\,\mathrm{d}\mathbf{r} = \int_{\partial S}\hat{\mathbf{n}}_{\partial\mathbf{S}}\cdot\underline{\mathbf{T}}\,\mathrm{d}\mathbf{r} \tag{76}$$

$$(c) \qquad \hat{\mathbf{n}}\times\nabla\times\mathbf{A} = (\nabla\mathbf{A})\cdot\hat{\mathbf{n}} - (\hat{\mathbf{n}}\cdot\nabla)\,\mathbf{A} \tag{77}$$

$$(d) \qquad \textstyle\int_S \hat{\mathbf{n}}\times\nabla\times\mathbf{v}\,\mathrm{d}\mathbf{r} = \int_{\partial S}\hat{\mathbf{t}}_{\partial\mathbf{S}}\times\mathbf{v}\,\mathrm{d}\mathbf{r} \tag{78}$$

The vector identity (74) allows to rewrite (73) in the form:

$$\begin{aligned}\mathbf{A}^*_{\mathbf{in}} + \nabla\chi_{in} = \frac{1}{4\pi}\int_{+\partial V_{in}} \Big[&- G\left(\hat{\mathbf{n}}'\cdot\nabla'\mathbf{A}'\right) + \left(\hat{\mathbf{n}}'\cdot\nabla' G\right)\mathbf{A}' \\ &+ \nabla'\left(G\mathbf{A}'\right)\cdot\hat{\mathbf{n}}' - \left(\mathbf{A}'\cdot\nabla' G\right)\hat{\mathbf{n}}'\Big]\mathrm{d}\mathbf{r}'\end{aligned} \tag{79}$$

which we further transform, by $\nabla\left(G\mathbf{v}\right) = G\nabla\mathbf{v} + \nabla G\otimes\mathbf{v}$, into

$$\begin{aligned}\mathbf{A}^*_{\mathbf{in}}\nabla\chi_{in} = \frac{1}{4\pi}\int_{+\partial V_{in}} \Big[&- G\left(\hat{\mathbf{n}}'\cdot\nabla'\mathbf{A}'\right) + \left(\hat{\mathbf{n}}'\cdot\nabla' G\right)\mathbf{A}' \\ &+ G\left(\nabla'\mathbf{A}'\right)\cdot\hat{\mathbf{n}}' + \left(\mathbf{A}'\cdot\hat{\mathbf{n}}'\right)\nabla' g \\ &- \left(\mathbf{A}'\cdot\nabla' g\right)\hat{\mathbf{n}}'\Big]\mathrm{d}\mathbf{r}'\end{aligned} \tag{80}$$

Now we exploit the vector identities:

$$\begin{aligned} &(a) \quad \hat{\mathbf{n}} \times \nabla \times \mathbf{A} = (\nabla \mathbf{A}) \cdot \hat{\mathbf{n}} - (\hat{\mathbf{n}} \cdot \nabla) \, \mathbf{A} \\ &(b) \quad (\mathbf{A} \times \mathbf{n}) \times \nabla G = \hat{\mathbf{n}} \, (\mathbf{A} \cdot \nabla G) - \mathbf{A} \, (\hat{\mathbf{n}} \cdot \nabla G) \end{aligned} \tag{81}$$

which, considering $\nabla \times \mathbf{A} = \mathbf{B}$, allow us to rewrite (80) as

$$\begin{aligned} &\mathbf{A}^*_{\mathbf{in}} + \nabla \chi_{in} = \\ &\frac{1}{4\pi} \int_{+\partial V_{in}} \left[-G \left(\mathbf{B}' \times \hat{\mathbf{n}}' \right) - \left(\mathbf{A}' \times \hat{\mathbf{n}}' \right) \times \nabla' G + \left(\mathbf{A}' \cdot \hat{\mathbf{n}}' \right) \nabla' G \right] \mathrm{d}\mathbf{r}' \end{aligned} \tag{82}$$

Notice that Stratton's book [99] uses the opposite convention for the normal to the domain.

Bibliography

[1] Francesco Romanelli. A roadmap to realisation of fusion energy. *Euro-Fusion*, 2012.

[2] Jeffrey P. Freidberg. *Plasma Physics and Fusion Energy*, chapter Fusion Power, pages 1,36. Cambridge University Press, 2007.

[3] I. Langmuir. Oscillations in Ionized Gases. *Proceedings of the National Academy of Sciences*, 14(8):627–637, aug 1928.

[4] J E Allen. The plasma–sheath boundary: its history and langmuir's definition of the sheath edge. *Plasma Sources Science and Technology*, 18(1):014004, nov 2008.

[5] Peter Stott Garry McCracken. *Fusion: The Energy of the Universe*. Academic Press, June 2012.

[6] A. Cardinali, C. Castaldo, R. Cesario, L. Amicucci, A. Galli, F. Napoli, L. Panaccione, C. Riccardi, F. Santini, G. Schettini, and A. A. Tuccillo. Radio-frequency current drive for thermonuclear fusion reactors. *Scientific Reports*, 8(1), jul 2018.

[7] C.E Kessel. Bootstrap current in a tokamak. *Nuclear Fusion*, 34(9):1221–1238, sep 1994.

[8] Hannes Alfvén. Existence of electromagnetic-hydrodynamic waves. *Nature*, 150:405–406, 1942.

[9] Harold Grad. General fluid equations. Technical Report NYO-6486-I, Courant Institute of Mathematical Sciences, New York University, August 1956.

[10] Jeffrey P. Freidberg. *A self-consistent two-fluid model*, pages 223–244. Cambridge University Press, 2007.

[11] Francis F. Chen. *Plasmas as Fluids*, pages 51–74. Springer International Publishing, Cham, 2016.

[12] S. Chapman and T.G. Cowling. *The Mathematical Theory of Non-uniform Gases*. Cambridge Mathematical Library, 1970.

[13] Harold Grad. On the kinetic theory of rarefied gases. *Communications on Pure and Applied Mathematics*, 2(4):331–407, dec 1949.

[14] Harold Grad. *Principles of the Kinetic Theory of Gases*, pages 205–294. Springer Berlin Heidelberg, Berlin, Heidelberg, 1958.

[15] Ignace I. Kolodner. Moment description of gas mixtures. Technical Report NYO-7980-I, Courant Institute of Mathematical Sciences, New York University, September 1957.

[16] S.I. Braginskii. *Reviews of Plasma Physics*, chapter Transport processes in a plasma. Consultants Bureau, New York, 1965.

[17] Y. Klimontovich. Chapter 6 - Hydrodynamic description of processes in a plasma. In D. Ter Haar and Yu.L. Klimontovich, editors, *The Statistical Theory of Non-Equilibrium Processes in a Plasma*, volume 9 of *International Series in Natural Philosophy*, pages 243 – 276. Pergamon, 1967.

[18] Nicholas A. Krall and Alvin W. Trivelpiece. *Principles of Plasma Physics*. McGraw-Hill Book Company, 1973.

[19] Viktor Evgen'evich Golant, Alekseĭ Petrovich Zhilinskiĭ, and Igor Evgen'evich Sakharov. *Fondamenti di Fisica dei Plasmi*. Edizioni MIR, 1983.

[20] Jeffrey P. Freidberg. The ideal MHD model. In *Ideal MHD*, pages 18–19. Cambridge University Press, 1987.

[21] C. R. Garibotti and G. Spiga. Boltzmann equation for inelastic scattering. *Journal of Physics A: Mathematical and General*, 27(8):2709–2717, apr 1994.

[22] M. Groppi and G. Spiga. Kinetic approach to chemical reactions and inelastic transitions in a rarefied gas. *Journal of Mathematical Chemistry*, 26(1/3):197–219, 1999.

[23] S. De Groot and P. Mazur. *Non-equilibrium Thermodynamics*. Dover Publications (2013 Edition), 1984.

[24] Georgy Lebon and David Jou. *Understanding Non-equilibrium Thermodynamics*. Number ISBN: 978-3-540-74252-4. Springer-Verlag Berlin Heidelberg, 2008.

[25] John G. Kirkwood and Jr. Bryce Crawford. The macroscopic equations of transport. *Journal of Physical Chemistry*, 56(9):1048–1051, September 1952.

[26] Q.-S. Zheng. Theory of representations for tensor functions - a unified invariant approach to constitutive equations. *Applied Mechanics Reviews*, 47(11):545–587, 11 1994.

[27] Harold Grad. Ohm's law. Technical Report NYO-6486-IV, Courant Institute of Mathematical Sciences, New York University, August 1956.

[28] S. Rice. The kinetic theory applied to chemical reactions in solutions. In *Diffusion-limited Reactions*, volume 25 of *Comprehensive Chemical Kinetics*, chapter 12, pages 339–359. Elsevier, 1985.

[29] Carlo Cercignani. *The Boltzmann Equation*, pages 40–103. Springer New York, New York, NY, 1988.

[30] Ingo MÃ¼ller and Tommaso Ruggeri. *Extended Thermodynamics*. Springer US, 1993.

[31] Peter Atkins, Julio Depaula, James Keeler, and Julio de Paula. *Atkins' Physical Chemistry*, chapter 17, Statistical Thermodynamics 2: Applications. Oxford University Press, 2018.

[32] Howard Reiss. *Methods of Thermodynamics*, chapter Some General Concepts, pages 1–19. Dover Publications, 1996.

[33] P. Stangeby. *The Plasma Boundary of Magnetic Fusion Devices*. CRC Press, jan 2000.

[34] Charles Kittel. *Elementary Statistical Physics*, chapter 12 - Thermodynamic Functions for the Canonical Ensemble. Dover books on Physics. Courier Corporation, 2008.

[35] N Isernia, V Scalera, C Serpico, and F Villone. Energy balance during disruptions. *Plasma Physics and Controlled Fusion*, 62(9):095024, aug 2020.

[36] J. Betten, J.P. Boehler, and A.J.M. Spencer. *Application of Tensor Functions in Solid Mechanics*. Springer-Verlag, 1987.

[37] Liu I-Shih. On representations of anisotropic invariants. *International Journal of Engineering Science*, 20(10):1099 – 1109, 1982.

[38] P. Kapitza. The change of electrical conductivity in strong magnetic fields. part i. experimental results. *Proceedings of the Royal Society of London. Series A, Containing Papers of a Mathematical and Physical Character*, 123(791):292–341, 1929.

[39] J. Breslau, N. Ferraro, and S. Jardin. Some properties of the M3D-C1 form of the three-dimensional magnetohydrodynamics equations. *Physics of Plasmas*, 16(9):092503, 2009.

[40] J. W. Haverkort, H. J. de Blank, G. T. A. Huysmans, J. Pratt, and B. Koren. Implementation of the full viscoresistive magnetohydrodynamic equations in a nonlinear finite element code. *Journal of Computational Physics*, 316:281–302, jul 2016.

[41] S. C. Jardin, J. Breslau, and N. Ferraro. A high-order implicit finite element method for integrating the two-fluid magnetohydrodynamic equations in two dimensions. *Journal of Computational Physics*, 226(2):2146–2174, oct 2007.

[42] Allen H. Boozer. Tokamak halo currents. *Physics of Plasmas*, 20(8):082510, aug 2013.

[43] Allen H. Boozer. Characteristic time for halo current growth and rotation. *Physics of Plasmas*, 22(10):102511, oct 2015.

[44] T. C. Hender, J. C. Wesley, J. Bialek, A. Bondeson, A. H. Boozer, R. J. Buttery, A. Garofalo, T. P. Goodman, R. S. Granetz, Y. Gribov, O. Gruber, M. Gryaznevich, G. Giruzzi, S. Günter, N. Hayashi, P. Helander, C. C. Hegna, D. F. Howell, D. A. Humphreys, G. T. A. Huysmans, A. W. Hyatt, A. Isayama, S. C. Jardin, Y. Kawano, A. Kellman, C. Kessel, H. R. Koslowski, R. J. La Haye, E. Lazzaro, Y. Q. Liu, V. Lukash, J. Manickam, S. Medvedev, V. Mertens, S. V. Mirnov, Y. Nakamura,

G. Navratil, M. Okabayashi, T. Ozeki, R. Paccagnella, G. Pautasso, F. Porcelli, V. D. Pustovitov, V. Riccardo, M. Sato, O. Sauter, M. J. Schaffer, M. Shimada, P. Sonato, E. J. Strait, M. Sugihara, M. Takechi, A. D. Turnbull, E. Westerhof, D. G. Whyte, R. Yoshino, H. Zohm, Disruption the ITPA MHD, and Magnet Group. Chapter 3: MHD stability, operational limits and disruptions. *Nuclear Fusion*, 47(6):128,202, June 2007.

[45] Raoul N. Franklin. *Plasma phenomena in gas discharges*, chapter Effects of Space Charge, pages 51,80. Oxford University Press, 1976.

[46] K. U. Riemann. The Bohm criterion and sheath formation. *Journal of Physics D: Applied Physics*, 24(4):493–518, apr 1991.

[47] A.H. Boozer. Bohm stability criterion and the MHD theory of plasma flow into an absorbing wall. Technical report, aug 1975.

[48] P. C. Stangeby and J. E. Allen. Plasma boundary as a Mach surface. *Journal of Physics A: General Physics*, 3(3):304–308, may 1970.

[49] Karl-Birger Persson. Inertia-Controlled Ambipolar Diffusion. *Physics of Fluids*, 5(12):1625, 1962.

[50] F J Artola, A Loarte, E Matveeva, J Havlicek, T Markovic, J Adamek, J Cavalier, L Kripner, G T A Huijsmans, M Lehnen, M Hoelzl, and R Panek. Simulations of COMPASS vertical displacement events with a self-consistent model for halo currents including neutrals and sheath boundary conditions. *Plasma Physics and Controlled Fusion*, 63(6):064004, apr 2021.

[51] R. Chodura. Plasma–wall transition in an oblique magnetic field. *Physics of Fluids*, 25(9):1628, 1982.

[52] P. C. Stangeby. The bohm–chodura plasma sheath criterion. *Physics of Plasmas*, 2(3):702–706, mar 1995.

[53] S. C. Jardin. A triangular finite element with first-derivative continuity applied to fusion MHD applications. *Journal of Computational Physics*, 200(1):133–152, oct 2004.

[54] Olivier Czarny and Guido Huysmans. Bézier surfaces and finite elements for MHD simulations. *Journal of Computational Physics*, 227(16):7423–7445, aug 2008.

[55] G. T. A. Huysmans and O. Czarny. MHD stability in X-point geometry: simulation of ELMs. *Nuclear Fusion*, 47(7):659–666, jun 2007.

[56] M. Hoelzl, G. T. A. Huijsmans, S. J. P. Pamela, M. Bécoulet, E. Nardon, F. J. Artola, B. Nkonga, C. V. Atanasiu, V. Bandaru, A. Bhole, D. Bonfiglio, A. Cathey, O. Czarny, A. Dvornova, T. Fehér, A. Fil, E. Franck, S. Futatani, M. Gruca, H. Guillard, J. W. Haverkort, I. Holod, D. Hu, S. K. Kim, S. Q. Korving, L. Kos, I. Krebs, L. Kripner, G. Latu, F. Liu, P. Merkel, D. Meshcheriakov, V. Mitterauer, S. Mochalskyy, J. A. Morales, R. Nies, N. Nikulsin, F. Orain, J. Pratt, R. Ramasamy, P. Ramet, C. Reux, K. Särkimäki, N. Schwarz, P. Singh Verma, S. F. Smith, C. Sommariva, E. Strumberger, D. C. van Vugt, M. Verbeek, E. Westerhof, F. Wieschollek, and J. Zielinski. The JOREK non-linear extended MHD code and applications to large-scale instabilities and their control in magnetically confined fusion plasmas. *Nuclear Fusion*, 61(6):065001, may 2021.

[57] R. Albanese and G. Rubinacci. Finite Element Methods for the solution of 3D eddy current problems. volume 102 of *Advances in Imaging and Electron Physics*, pages 1,86. Elsevier, 1997.

[58] Blaise Faugeras and Holger Heumann. FEM-BEM coupling methods for tokamak plasma axisymmetric free-boundary equilibrium computations in unbounded domains. *Journal of Computational Physics*, 343:201–216, aug 2017.

[59] N. M. Ferraro, S. C. Jardin, L. L. Lao, M. S. Shephard, and F. Zhang. Multi-region approach to free-boundary three-dimensional tokamak equilibria and resistive wall instabilities. *Physics of Plasmas*, 23(5):056114, may 2016.

[60] M. Hoelzl, P. Merkel, G. T. A. Huysmans, E. Nardon, E. Strumberger, R. McAdams, I. Chapman, S. Günter, and K. Lackner. Coupling JOREK and STARWALL codes for non-linear resistive-wall simulations. *Journal of Physics: Conference Series*, 401:012010, dec 2012.

[61] F. J. Artola. *Free-boundary simulations of MHD plasma instabilities in tokamaks*. PhD thesis, UniversitÃ¨ Aix-Marseille, 2018.

[62] F. Villone, L. Barbato, S. Mastrostefano, and S. Ventre. Coupling of nonlinear axisymmetric plasma evolution with three-dimensional

volumetric conductors. *Plasma Physics and Controlled Fusion*, 55(9):095008, 2013.

[63] F. Brezzi and C. Johnson. On the coupling of boundary integral and finite element methods. *Calcolo*, 16(2):189–201, jun 1979.

[64] Claes Johnson and J.-Claude Nédélec. On the coupling of boundary integral and finite element methods. *Mathematics of Computation*, 35(152):1063–1079, 1980.

[65] H.R. Strauss, A. Pletzer, W. Park, S. Jardin, J. Breslau, and L. Sugiyama. MHD simulations with resistive wall and magnetic separatrix. *Computer Physics Communications*, 164(1-3):40–45, dec 2004.

[66] S C Jardin, N Ferraro, J Breslau, and J Chen. Multiple timescale calculations of sawteeth and other global macroscopic dynamics of tokamak plasmas. *Computational Science & Discovery*, 5(1):014002, may 2012.

[67] S. C. Jardin. Review of implicit methods for the magnetohydrodynamic description of magnetically confined plasmas. *Journal of Computational Physics*, 231(3):822–838, feb 2012.

[68] C. Reux, G. Huysmans, J. Bucalossi, and M. Becoulet. Non-linear simulations of disruption mitigation using massive gas injection on tore supra. In *38th European Physical Society Conf. on Plasma Physics (EPS)*, 2011.

[69] D. Hu, E. Nardon, M. Lehnen, G. T. A. Huijsmans, and D. C. van Vugt. 3D non-linear MHD simulation of the MHD response and density increase as a result of shattered pellet injection. *Nuclear Fusion*, 58(12):126025, oct 2018.

[70] M. Hoelzl, D. Hu, E. Nardon, G. T. A. Huijsmans, and and. First predictive simulations for deuterium shattered pellet injection in ASDEX upgrade. *Physics of Plasmas*, 27(2):022510, feb 2020.

[71] V. Bandaru, M. Hoelzl, F. J. Artola, G. Papp, and G. T. A. Huijsmans. Simulating the nonlinear interaction of relativistic electrons and tokamak plasma instabilities: Implementation and validation of a fluid model. *Physical Review E*, 99(6):063317, jun 2019.

[72] V. Bandaru, M. Hoelzl, C. Reux, O. Ficker, S. Silburn, M. Lehnen, N. Eidietis, and J. O. R. E. K. Team. Magnetohydrodynamic simulations of runaway electron beam termination in JET. *Plasma Physics and Controlled Fusion*, 63(3):035024, jan 2021.

[73] Stanislas Pamela. *Simulation Magnéto-Hydro-Dynamiques des Edge-Localised-Modes dans un Tokamak*. PhD thesis, UniversitÃ¨ de Provence, 2010.

[74] Emmanuel Franck, Matthias HÃ¶lzl, Alexander Lessig, and Eric SonnendrÃ¼cker. Energy conservation and numerical stability for the reduced MHD models of the non-linear JOREK code. *ESAIM: Mathematical Modelling and Numerical Analysis*, 49(5):1331–1365, aug 2015.

[75] S. J. P. Pamela, A. Bhole, G. T. A. Huijsmans, B. Nkonga, M. Hoelzl, I. Krebs, and E. Strumberger. Extended full-MHD simulation of non-linear instabilities in tokamak plasmas. *Physics of Plasmas*, 27(10):102510, oct 2020.

[76] R. Albanese and G. Rubinacci. Integral formulation for 3d eddy-current computation using edge elements. *IEE Proceedings A Physical Science, Measurement and Instrumentation, Management and Education, Reviews*, 135(7):457, 1988.

[77] R. Albanese and G. Rubinacci. Formulation of the eddy-current problem. *IEE Proceedings A (Physical Science, Measurement and Instrumentation, Management and Education)*, 137(1):16–22, jan 1990.

[78] R. Albanese, R. Martone, G. Miano, and G. Rubinacci. A T formulation for 3D finite element eddy current computation. *IEEE Transactions on Magnetics*, 21(6):2299–2302, nov 1985.

[79] G. Rubinacci, A. Tamburrino, and F. Villone. Circuits/fields coupling and multiply connected domains in integral formulations. *IEEE Transactions on Magnetics*, 38(2):581–584, mar 2002.

[80] E. Strumberger, P. Merkel, M. Sempf, and S. GÃ¼nter. On fully three-dimensional resistive wall mode and feedback stabilization computations. *Physics of Plasmas*, 15(5):056110, may 2008.

[81] P. Merkel and E. Strumberger. Linear MHD stability studies with the STARWALL code. August 2015.

[82] L.R. Turner. Electromagnetic computations for fusion devices. *IEEE Transactions on Magnetics*, 26(2):847–852, mar 1990.

[83] R. Albanese, R. Fresa, G. Rubinacci, and F. Villone. Time evolution of tokamak plasmas in the presence of 3D conducting structures. *IEEE Transactions on Magnetics*, 36(4):1804–1807, jul 2000.

[84] S.L. Chen, F. Villone, Y.W. Sun, G. Rubinacci, S. Ventre, B.J. Xiao, Z.P. Luo, Y. Guo, H.H. Wang, T.H. Shi, D.L. Chen, L. Liu, and Y. Huang. Disruptive plasma simulations in EAST including 3d effects. *Nuclear Fusion*, 59(10):106039, sep 2019.

[85] V. V. Yanovskiy, N. Isernia, V. D. Pustovitov, V. Scalera, F. Villone, J. Hromadka, M. Imrisek, J. Havlicek, M. Hron, and R. Panek. Global forces on the COMPASS-U wall during plasma disruptions. *Nuclear Fusion*, 61(9):096016, August 2021.

[86] Guglielmo Rubinacci, Antonello Tamburrino, Salvatore Ventre, and Fabio Villone. Application of n-fold rotational symmetries to eddy currents integral model in the time domain. *IEEE Transactions on Magnetics*, 56(1):1–4, jan 2020.

[87] Paolo Bettini, Nicolò Marconato, Maurizio Furno Palumbo, Simone Peruzzo, Ruben Specogna, Raffaele Albanese, Guglielmo Rubinacci, Salvatore Ventre, and Fabio Villone. Numerical modeling of 3d halo current path in ITER structures. *Fusion Engineering and Design*, 88(6-8):529–532, oct 2013.

[88] S. Jardin, F. Villone, C. Clauser, N. Ferraroand N. Isernia, G. Rubinacci, and et al. ITER disruption simulations with realistic plasma and conductors modelling. In *47th EPS Conference on Plasma Physics*, 2021.

[89] C.J. Carpenter. Comparison of alternative formulations of 3-dimensional magnetic-field and eddy-current problems at power frequencies. *Proceedings of the Institution of Electrical Engineers*, 124(11):1026, 1977.

[90] M. L. Brown. Calculation of 3-dimensional eddy currents at power frequencies. *IEE Proceedings A Physical Science, Measurement and Instrumentation, Management and Education, Reviews*, 129(1):46, 1982.

[91] A. Bossavit. A rationale for 'edge-elements' in 3-D fields computations. *IEEE Transactions on Magnetics*, 24(1):74–79, 1988.

[92] R. Albanese and G. Rubinacci. Treatment of multiply connected regions in two-component electric vector potentials formulations. *IEEE Transactions on Magnetics*, 26(2):650–653, mar 1990.

[93] Guglielmo Rubinacci and Antonello Tamburrino. Automatic treatment of multiply connected regions in integral formulations. *IEEE Transactions on Magnetics*, 46(8):2791–2794, aug 2010.

[94] V. D. Shafranov and L. E. Zakharov. Use of the virtual-casing principle in calculating the containing magnetic field in toroidal plasma systems. *Nuclear Fusion*, 12(5):599–601, sep 1972.

[95] L. E. Zakharov. Numerical methods for solving some problems of the theory of plasma equilibrium in toroidal configurations. *Nuclear Fusion*, 13(4):595–602, aug 1973.

[96] B. J. Braams. The interpretation of tokamak magnetic diagnostics. *Plasma Physics and Controlled Fusion*, 33(7):715–748, jul 1991.

[97] V. D. Pustovitov. Magnetic diagnostics: General principles and the problem of reconstruction of plasma current and pressure profiles in toroidal systems. *Nuclear Fusion*, 41(6):721–730, jun 2001.

[98] J. L. Luxon and B. B. Brown. Magnetic analysis of non-circular cross-section tokamaks. *Nuclear Fusion*, 22(6):813–821, jun 1982.

[99] Julius Adams Stratton. *Electromagnetic Theory*. McGra-Hill Book Company, 1941.

[100] V. D. Pustovitov. Decoupling in the problem of tokamak plasma response to asymmetric magnetic perturbations. *Plasma Physics and Controlled Fusion*, 50(10):105001, aug 2008.

[101] R. S. Granetz, I. H. Hutchinson, J. Sorci, J. H. Irby, B. LaBombard, and D. Gwinn. Disruptions and halo currents in Alcator C-mod. *Nuclear Fusion*, 36(5):545–556, may 1996.

[102] Y. Neyatani, R. Yoshino, Y. Nakamura, and S. Sakurai. Characteristics of halo currents in JT-60U. *Nuclear Fusion*, 39(4):559–567, apr 1999.

[103] G. Pautasso, Y. Zhang, B. Reiter, L. Giannone, O. Gruber, A. Herrmann, O. Kardaun, K. K. Khayrutdinov, V. E. Lukash, M. Maraschek, A. Mlynek, Y. Nakamura, W. Schneider, G. Sias, and M. Sugihara. Contribution of ASDEX Upgrade to disruption studies for ITER. *Nuclear Fusion*, 51(10):103009, aug 2011.

[104] Vadim Yanovskiy, Nicola Isernia, Vladimir D. Pustovitov, Valentino Scalera, Fabio Villone, Josef Havlicek, Ales Havranek, Martin Hron, Michael Komm, Jaroslav Krbec, Tomas Markovic, Ekaterina Matveeva, Radomir Panek, and David Tskhakaya. Poloidal currents in COMPASS vacuum vessel during disruptions: diamagnetic measurements and comparison with Carma0NL modeling. In *APS Division of Plasma Physics Meeting 2019*, 2019.

[105] D.C. Robinson and A.J. Wootton. An experimental study of tokamak plasmas with vertically elongated cross-sections. *Nuclear Fusion*, 18(11):1555–1567, nov 1978.

[106] A. Pironti and M. Walker. Fusion, tokamaks, and plasma control: an introduction and tutorial. *IEEE Control Systems*, 25(5):30–43, oct 2005.

[107] V. S. Mukhovatov and V. D. Shafranov. Plasma equilibrium in a Tokamak. *Nuclear Fusion*, 11(6):605–633, dec 1971.

[108] E. A. Lazarus, J. B. Lister, and G. H. Neilson. Control of the vertical instability in tokamaks. *Nuclear Fusion*, 30(1):111–141, jan 1990.

[109] R. Albanese, E. Coccorese, R. Martone, and G. Rubinacci. Analysis of vertical instabilities in air core tokamaks in the presence of three-dimensional conducting structures. *IEEE Transactions on Magnetics*, 26(2):853–856, mar 1990.

[110] Alfredo Portone. The stability margin of elongated plasmas. *Nuclear Fusion*, 45(8):926–932, aug 2005.

[111] S. C. Jardin and D. A. Larrabee. Feedback stabilization of rigid axisymmetric modes in tokamaks. *Nuclear Fusion*, 22(8):1095–1098, aug 1982.

[112] V. D. Pustovitov. General formulation of the resistive wall mode coupling equations. *Physics of Plasmas*, 15(7):072501, 2008.

[113] V. D. Pustovitov. Reaction of the toroidal resistive wall on the magnetic field variations in tokamak-like systems. *Physics of Plasmas*, 25(6):062510, 2018.

[114] V. D. Pustovitov. Extension of shafranov's equilibrium theory to the description of current quenches affected by resistive wall dissipation in tokamaks. *Plasma Physics Reports*, 45(12):1114–1127, dec 2019.

[115] R. Albanese and F. Villone. The linearized CREATE-L plasma response model for the control of current, position and shape in tokamaks. *Nuclear Fusion*, 38(5):723–738, may 1998.

[116] D. A. Wells. Application of the Lagrangian Equations to Electrical Circuits. *Journal of Applied Physics*, 9(312):312–320, 1938.

[117] Allen H. Boozer. Halo currents and vertical displacements after ITER disruptions. *Physics of Plasmas*, 26(11):114501, nov 2019.

[118] Mark H. Holmes. *Introduction to Perturbation Methods*, chapter Multiple Scales, pages 139,221. Springer, New York, NY, 2013.

[119] Ferdinand Verhulst. *Methods and Applications of Singular Perturbations*, chapter Boundary Layers in Time, pages 93,120. Springer, New York, NY, 2005.

[120] Shigeo Hamada. Hydromagnetic equilibria and their proper coordinates. *Nuclear Fusion*, 2(1-2):23–37, jan 1962.

[121] Allen H. Boozer. Evaluation of the structure of ergodic fields. *Physics of Fluids*, 26(5):1288, 1983.

[122] V. D. Pustovitov. Determination of plasma shift in a stellarator from magnetic measurements. *Nuclear Fusion*, 30(8):1523–1531, aug 1990.

[123] V. D. Shafranov. Plasma Equilibrium in a Magnetic Field. In M. A. Leontovich, editor, *Reviews of Plasma Physics*, volume 2, chapter 2, pages 103–152. Consultants Bureau, Oxford, 1966.

[124] John Wesson. *Tokamaks*, chapter Equilibrium, pages 101,142. Oxford University Press, fourth (2011) edition, 1987.

[125] K. Lackner. Computation of ideal MHD equilibria. *Computer Physics Communications*, 12(1):33–44, sep 1976.

[126] V. D. Pustovitov, G. Rubinacci, and F. Villone. On the computation of the disruption forces in tokamaks. *Nuclear Fusion*, 57(12):126038, oct 2017.

[127] N. Isernia, V. D. Pustovitov, F. Villone, and V. Yanovskiy. Cross-validation of analytical models for computation of disruption forces in tokamaks. *Plasma Physics and Controlled Fusion*, 61(11):115003, sep 2019.

[128] V. V. Yanovskiy, N. Isernia, V. D. Pustovitov, F. Villone, D. Abate, P. Bettini, S. L. Chen, J. Havlicek, A. Herrmann, J. Hromadka, M. Hron, M. Imrisek, M. Komm, R. Paccagnella, R. Panek, G. Pautasso, S. Peruzzo, D. Sestak, M. Teschke, and I. Zammuto. Comparison of approaches to the electromagnetic analysis of COMPASS-U vacuum vessel during fast transients. *Fusion Engineering and Design*, 146:2338–2342, sep 2019.

[129] F. Villone, S. Coda, N. Isernia, G. Rubinacci, Team TCV, and Team EUROFusion MST1. Disruption trajectory studies on TCV: experiments and modelling. In *47th EPS Conference on Plasma Physics*, 2021.

[130] V. D. Shafranov. *Equilibrium in Certain Practical Systems*, chapter Plasma Equilibrium in a Magnetic Field, pages 103–153. Consultants Bureau, 1966.

[131] R. Albanese, Blum J., and O. Barbieri. On the solution of the magnetic flux equation in an infinite domain. In *8th EPS Conference on Computing in Plasma Physics*, 1986.

[132] J. A. Wesson, R. D. Gill, M. Hugon, F. C. SchÃ¼ller, J. A. Snipes, D. J. Ward, D. V. Bartlett, D. J. Campbell, P. A. Duperrex, A. W. Edwards, R. S. Granetz, N. A. O. Gottardi, T. C. Hender, E. Lazzaro, P. J. Lomas, N. Lopes Cardozo, K. F. Mast, M. F. F. Nave, N. A. Salmon, P. Smeulders, P. R. Thomas, B. J. D. Tubbing, M. F. Turner, and A. Weller. Disruptions in JET. *Nuclear Fusion*, 29(4):641–666, apr 1989.

[133] P. C. de Vries, M. F. Johnson, B. Alper, P. Buratti, T. C. Hender, H. R. Koslowski, and V. Riccardo. Survey of disruption causes at JET. *Nuclear Fusion*, 51(5):053018, apr 2011.

[134] S. N. Gerasimov, P. Abreu, G. Artaserse, M. Baruzzo, P. Buratti, I. S. Carvalho, I. H. Coffey, E. De La Luna, T. C. Hender, R. B. Henriques,

R. Felton, S. Jachmich, U. Kruezi, P. J. Lomas, P. McCullen, M. Maslov, E. Matveeva, S. Moradi, L. Piron, F. G. Rimini, W. Schippers, C. Stuart, G. Szepesi, M. Tsalas, D. Valcarcel, and L. E. Zakharov. Overview of disruptions with JET-ILW. *Nuclear Fusion*, 60(6):066028, may 2020.

[135] E. Matveeva, O. Ficker, J. Havlícek, A. Havránek, O. Hronova, V. Weinzettl, V. Yanovskiy, and Team COMPASS. Statistical Analysis of Disruptions in COMPASS. In *WDS'18 Proceedings of Contributed Papers - Physics*, pages 105,111, 2018.

[136] ITER Physics Expert Group on Disruptions, Plasma Control, MHD and Editors ITER Physics Basis. Chapter 3: MHD stability, operational limits and disruptions. *Nuclear Fusion*, 39(12):2251–2389, dec 1999.

[137] F Troyon, A Roy, W A Cooper, F Yasseen, and A Turnbull. Beta limit in tokamaks. experimental and computational status. *Plasma Physics and Controlled Fusion*, 30(11):1597–1609, oct 1988.

[138] M. Greenwald, J. L. Terry, S. M. Wolfe, S. Ejima, M. G. Bell, S. M. Kaye, and G. H. Neilson. A new look at density limits in tokamaks. *Nuclear Fusion*, 28(12):2199–2207, dec 1988.

[139] J. P. Freidberg. *Ideal MHD*, chapter Stability: one-dimensional configurations, pages 428,569. Cambridge University Press, 2014.

[140] N. Commaux, L. R. Baylor, T. C. Jernigan, E. M. Hollmann, P. B. Parks, D. A. Humphreys, J. C. Wesley, and J. H. Yu. Demonstration of rapid shutdown using large shattered deuterium pellet injection in DIII-D. *Nuclear Fusion*, 50(11):112001, sep 2010.

[141] M. Lehnen, A. Alonso, G. Arnoux, N. Baumgarten, S. A. Bozhenkov, S. Brezinsek, M. Brix, T. Eich, S. N. Gerasimov, A. Huber, S. Jachmich, U. Kruezi, P. D. Morgan, V. V. Plyusnin, C. Reux, V. Riccardo, G. Sergienko, and M. F. Stamp. Disruption mitigation by massive gas injection in JET. *Nuclear Fusion*, 51(12):123010, nov 2011.

[142] M. Lehnen, K. Aleynikova, P. B. Aleynikov, D. J. Campbell, P. Drewelow, N. W. Eidietis, Yu. Gasparyan, R. S. Granetz, Y. Gribov, N. Hartmann, E. M. Hollmann, V. A. Izzo, S. Jachmich, S.-H. Kim, M. Kočan, H. R. Koslowski, D. Kovalenko, U. Kruezi, A. Loarte, S. Maruyama, G. F. Matthews, P. B. Parks, G. Pautasso, R. A. Pitts,

C. Reux, V. Riccardo, R. Roccella, J. A. Snipes, A. J. Thornton, and P. C. de Vries. Disruptions in ITER and strategies for their control and mitigation. *Journal of Nuclear Materials*, 463:39–48, aug 2015.

[143] A.W. Hyatt, R.L. Lee, Cuthberston J.W., D.A. Humphreys, A.G. Kellman, C.J. Lasnier, P.L. Taylor, and Team DIII-D. Magnetic and thermal energy flow during disruptions in DIII-D. Technical Report GA 3466, General Atomics, 1996.

[144] J. I. Paley, P. Andrew, S. C. Cowley, W. Fundamenski, A. Huber, and Contributors JET EFDA. Energy flow during disruptions in JET. *Journal of Nuclear Materials*, 337-339:702–706, mar 2005.

[145] A. Loarte, V. Riccardo, J.R. Martín-Solís, J. Paley, A. Huber, and M. Lehnen and. Magnetic energy flows during the current quench and termination of disruptions with runaway current plateau formation in JET and implications for ITER. *Nuclear Fusion*, 51(7):073004, may 2011.

[146] V. D. Pustovitov. Disruption forces on the tokamak wall with and without poloidal currents. *Plasma Physics and Controlled Fusion*, 59(5):055008, 2017.

[147] V. D. Pustovitov. Dependence of disruption forces on the plasma position inside the vacuum vessel in tokamaks. *Plasma Physics and Controlled Fusion*, 62(6):065003, apr 2020.

[148] R. Albanese, M. Mattei, and F. Villone. Prediction of the growth rates of VDEs in JET. *Nuclear Fusion*, 44(9):999–1007, aug 2004.

[149] V. D. Pustovitov and D. I. Kiramov. Local and integral disruption forces on the tokamak wall. *Plasma Physics and Controlled Fusion*, 60(4):045011, 2018.

[150] M. Sugihara, M. Shimada, H. Fujieda, Yu Gribov, K. Ioki, Y. Kawano, R. Khayrutdinov, V. Lukash, and J. Ohmori. Disruption scenarios, their mitigation and operation window in ITER. *Nuclear Fusion*, 47(4):337–352, mar 2007.

[151] H. Strauss, E. Joffrin, V. Riccardo, J. Breslau, and R. Paccagnella. Comparison of JET AVDE disruption data with M3D simulations and implications for ITER. *Physics of Plasmas*, 24(10):102512, oct 2017.

[152] F. Maviglia, R. Albanese, R. Ambrosino, W. Arter, C. Bachmann, T. Barrett, G. Federici, M. Firdaous, J. Gerardin, M. Kovari, V. Loschiavo, M. Mattei, F. Villone, and R. Wenninger. Wall protection strategies for DEMO plasma transients. *Fusion Engineering and Design*, 136:410–414, nov 2018.

[153] J. Paméla, Emilia R. Solano, and Contributors JET EFDA. Overview of JET results. *Nuclear Fusion*, 43(12):1540–1554, dec 2003.

[154] V. Philipps, Ph. Mertens, G. F. Matthews, and H. Maier. Overview of the JET ITER-like Wall Project. *Fusion Engineering and Design*, 85(7-9):1581–1586, dec 2010.

[155] F. Romanelli and contributors JET EFDA. Overview of the JET results with the ITER-like wall. *Nuclear Fusion*, 53(10):104002, sep 2013.

[156] press F4E. Europe and Japan complete JT-60SA, the most powerful tokamak in the world!, June 2020. https://fusionforenergy.europa.eu/news/europe-and-japan-complete-jt-60sa-the-most-powerful-tokamak-in-the-world/.

[157] Andrea Gaetano Chiariello, Francesco Ledda, Raffaele Martone, Andrea Murari, Francesco Pizzo, and Fernanda Rimini. A 3D electromagnetic model of the iron core in JET. *Fusion Engineering and Design*, 123:527–531, nov 2017.

[158] A. Khalafallah. An equivalent 2D model for the JET transformer. *JET Technical Note JTN/E 68, JET Joint Undertaking*, 1976.

[159] Raffaele Albanese, G. Calabrò, M. Mattei, and F. Villone. Plasma response models for current, shape and position control in JET. *Fusion Engineering and Design*, 66-68:715–718, sep 2003.

[160] S. N. Gerasimov, T. C. Hender, J. Morris, V. Riccardo, and L. E. Zakharov. Plasma current asymmetries during disruptions in JET. *Nuclear Fusion*, 54(7):073009, apr 2014.

[161] T. P. Goodman, S. M. Ahmed, S. Alberti, Y. Andrèbe, C. Angioni, K. Appert, G. Arnoux, R. Behn, P. Blanchard, P. Bosshard, Y. Camenen, R. Chavan, S. Coda, I. Condrea, A. Degeling, B. P. Duval, P. Etienne,

D. Fasel, A. Fasoli, J.-Y. Favez, I. Furno, M. Henderson, F. Hofmann, J.-P. Hogge, J. Horacek, P. Isoz, B. Joye, A. Karpushov, I. Klimanov, P. Lavanchy, J. B. Lister, X. Llobet, J.-C. Magnin, A. Manini, B. Marlétaz, P. Marmillod, Y. Martin, An Martynov, J.-M. Mayor, J. Mlynar, J.-M. Moret, E. Nelson-Melby, P. Nikkola, P. J. Paris, A. Perez, Y. Peysson, R. A. Pitts, A. Pochelon, L. Porte, D. Raju, H. Reimerdes, O. Sauter, A. Scarabosio, E. Scavino, S. H. Seo, U. Siravo, A. Sushkov, G. Tonetti, M. Q. Tran, H. Weisen, M. Wischmeier, A. Zabolotsky, and G. Zhuang. An overview of results from the TCV tokamak. *Nuclear Fusion*, 43(12):1619–1631, dec 2003.

[162] Francesco Maviglia, Christian Bachmann, Gianfranco Federici, Thomas Franke, Mattia Siccinio, Christian Vorpahl, Raffaele Albanese, Roberto Ambrosino, Emiliano Fable, Mehdi Firdaouss, Jonathan Gerardin, Vincenzo Paolo Loschiavo, Massimiliano Mattei, Francesco Palermo, Maria Lorena Richiusa, Fabio Villone, and Zsolt Vizvary. Impact of plasma thermal transients on the design of the EU DEMO first wall protection. *Fusion Engineering and Design*, 158:111713, sep 2020.

[163] J. Blum, J. Le Foll, and B. Thooris. The self-consistent equilibrium and diffusion code sced. *Computer Physics Communications*, 24(3-4):235–254, dec 1981.

[164] R. Roccella, M. Roccella, V. Riccardo, and S. Chiocchio. Asymmetric toroidal eddy currents (ATEC) to explain sideways forces at JET. *Nuclear Fusion*, 56(10):106010, aug 2016.

[165] A.J.M. Spencer. *Continuum Physics*, volume 1, chapter Theory of Invariants, pages 239–353. Academic Press, 1971.